NOTICE

The quality of this microform is heavily dependent upon the quality of the original thesis submitted for microfilming. Every effort has been made to ensure the highest quality of reproduction possible.

If pages are missing, contact the university which granted the degree

Some pages may have indistinct print especially if the original pages were typed with a poor typewriter ribbon or if the university sent us an inferior photocopy.

Reproduction in full or in part of this microform is governed by the Canadian Copyright Act, R.S.C. 1970, c. C-30, and subsequent amendments.

AVIS

La qualité de cette microforme dépend grandement de la qualité de la thèse soumise au microfilmage Nous avons tout fait pour assurer une qualité supérieure de reproduction.

S'il manque des pages, veuillez communiquer avec l'université qui a conféré le grade

La qualité d'impression de certaines pages peut laisser à désirer, surtout si les pages originales ont été dactylographiées à l'aide d'un ruban usé ou si l'université nous a fait parvenir une photocopie de qualité inférieure

La reproduction, même partielle, de cette microforme est soumise à la Loi canadienne sur le droit d'auteur, SRC 1970, c C-30, et ses amendements subséquents

BANDWIDTH-EFFICIENT CODED-MODULATION TECHNIQUES FOR FADING CHANNELS

Seyed Hamidreza Jamali

A Thesis
in
The Department
of
Electrical and Computer Engineering

Presented in Partial Fulfillment of the Requirements
for the Degree of Doctor of Philosophy at
Concordia University
Montreal, Quebec, Canada

November 1991

ISBN 0 315-73662-3

ABSTRACT

BANDWIDTH-EFFICIENT CODED-MODULATION TECHNIQUES FOR FADING CHANNELS

Seyed Hamidreza Jamali, Ph. D.

Concordia University, 1991

Coded-modulation techniques have recently become a popular signaling method over bandwidth-limited channels. They provide coding gain on the Additive White Gaussian Noise (AWGN) channel without sacrificing the bandwidth. This is accomplished by coding onto an expanded signal constellation so that the minimum Euclidean distance between coded sequences is maximized. Maximizing the minimum Euclidean distance improves the coding gain on the AWGN channel. However, the performance of these schemes on fading channels is dominated by other factors. On fading channels the *length of the shortest error event path* (time diversity) as well as the *squared product distances* along this path are considered as primary code design criteria. The minimum Euclidean distance has secondary importance on fading channels. Thus, coded-modulation schemes designed to be strong for the AWGN channel can be quite poor for fading channel and conversely suboptimal designs for AWGN can become superior choices for fading channels.

In this research we introduce coded-modulation schemes constructed based on the design criteria for fading channels. In this study both Trellis-Coded Modulation (TCM) and Block-Coded Modulation (BCM) schemes are considered.

Construction of a TCM scheme for fading channels is addressed by initiating design rules. These rules are introduced to avoid the exhaustive computer search. It is shown that the introduced code outperforms TCM schemes with the same number of trellis

states, because of its higher time diversity and minimum product distance.

To construct BCM schemes, Reed-Solomon (RS) codes are combined with Multi-Phase Shift Keying (MPSK) signaling. These nonbinary codes are of particular interest because they make highly efficient use of the redundancy and their block lengths and character sizes can be readily adjusted to match with the appropriate MPSK signaling.

The performance of the introduced schemes is evaluated on a Rayleigh fading channel, for different decoding strategies, by means of the error bound analysis and computer simulations. The potential coding gains compared to the uncoded schemes are reported. Different soft-decision decoding techniques for the RS coded schemes are addressed.

We also evaluate the performance of the introduced schemes on a shadowed Rician fading channel using parameters suitable for the Canadian Mobile Satellite (MSAT) Communication channel. The effect of fading bandwidth on the performance degradation of both TCM and BCM coded schemes is studied.

To my Parents

ACKNOWLEDGEMENTS

I would like to express my most sincere gratitude towards my friend and advisor Dr. T. Le-Ngoc for his guidance, encouragement and constructive criticism throughout the course of this work.

I would like also to thank Dr. A. Benyamin-Seeyar, Dr. A. K. Elhakeem, Dr. P. K. M. Ho, Dr. J. Opatrny and Dr. E. I. Plotkin for reading this thesis and serving on the doctoral committee.

Special thanks to my friend Dr. M. R. Soleymani for many enlightening discussions and suggestions. I wish to express my special appreciations to all my fellow graduate students for their sincere encouragements and help from time to time.

I would like also to acknowledge the financial support provided by Canada NSERC Grants STR01011312, 00322671, OGP0005987 and Quebec FCAR Grant 92ER0106.

Outside the technical realm, I am deeply indebted to my parents for starting me towards a career of advanced studies.

TABLE OF CONTENTS

LIST OF ABBREVIATIONS

AWGN	Additive White Gaussian Noise
BCM	Block-Coded Modulation
BPSK	Binary Phase Shift Keying
CPM	Continuous Phase Modulation
CSI	Channel State Information
DMC	Discrete Memoryless Channel
EED	Errors-and-Erasures Decoding
EOD	Errors-Only Decoding
FEC	Forward Error Correcting
GMD	Generalized Minimum-Distance Decoding
GRV	Gaussian Random Variable
HF	High Frequency
MDS	Maximum-Distance-Separable
ML	Maximum Likelihood
MLD	Maximum Likelihood Decoding
MPSK	Multi-Phase Shift Keying
MTCM	Multiple Trellis-Coded Modulation
pdf	probability density function
PSK	Phase Shift Keying
QAM	Quadrature Amplitude Modulation
QPSK	Quadrature Phase Shift Keying
RS	Reed-Solomon
SED	Successive Erasure Decoding
SEMDD	Successive Erasure Minimum Distance Decoding
SNR	Signal-to-Noise Ratio
TCM	Trellis-Coded Modulation
UEP	Uniform Error Property
VA	Viterbi Algorithm
WSS	Wide-Sense Stationary

LIST OF SYMBOLS

$\mathbf{A}$	MPSK Signal Set
$\mathbf{A}_i$	A Subset of MPSK Signal Set in the Set Partitioning Process
a	Fading Amplitude
$\mathbf{a}$	Fading Amplitude Vector
$a(t) = a_i(t) + ja(t)$	Complex Multiplicative Fading
$a(\mathbf{s},\hat{\mathbf{s}})$	Number of Errors Between the Correct Sequence s and the Erroneous sequence $\hat{\mathbf{s}}$
a_T	Fading Threshold for Errors-and-Erasures Decoding with CSI
$a(\beta_l^2)$	Average Number of Sequences at Squared Product Euclidean Distance β_l^2 (Squared Product Distance Multiplicity)
$\mathbf{b}$	Sequence of the TCM Encoder Input Bits
B_D	Fading Bandwidth or Doppler Spread
$\mathbf{c}$	Sequence of the TCM Encoder Output
$C(\mathbf{s}, \hat{\mathbf{s}},\lambda)$	Chernoff Bound between Code Words s and $\hat{\mathbf{s}}$
$C(s, \hat{s},\lambda)$	Chernoff Factor of Signals s and $\hat{s}$
d_E	Euclidean Distance
d_e	Minimum Euclidean Distance
d_H	Hamming Distance
d_h	Minimum Hamming Distance
$\mathbf{e}$	Error Sequence
E_b	Average Energy per Bit
E_s	Average Energy per Symbol
$E[.]$	Statistical Averaging Operator
g	Coding Gain
g_∞	Asymptotic Coding Gain
$H(f, t)$	Equivalent Low-Pass Transfer Function of a Fading Channel
$h(\tau, t)$	Equivalent Low-Pass Impulse Response of a Fading Channel
K	Rician Fading Channel Parameter
k	Number of Information Bits in a Block Code
L	Shortest Error Event Path length (Time Diversity)

M	Number of Signal Points (Code Words) in a Signal Space
m	Symbol Size of an MPSK Signal Set with $M = 2^m$
$\hat{m}$	Number of Uncoded Input Bits in a TCM Encoder
m_γ	The Average Value of the Lognormal Process in a Shadowed Rician Fading Channel
$m(\mathbf{r}, \mathbf{s})$	Metric for the Received Signal Vector **r** and Transmitted one **s** in a Fading Channel without CSI
$m(\mathbf{r}, \mathbf{s}, \mathbf{a})$	Metric for the Received Signal Vector **r** and Transmitted one **s** in a Fading Channel with CSI
N	Dimension of a Signal Space
N_0	Single-Sided Power Spectral Density of the AWGN
$N(d_\epsilon)$	Average Number of Sequences at Minimum Euclidean Distance d_e (Minimum Distance Multiplicity)
n	Block Code Word Length
$\mathbf{n}$	Additive Noise Vector in a Vector Channel
$n(t)$	Additive Noise Process in a Waveform Channel
P_{av}	Average Signal Power
P_b	Probability of Bit Error
P_e	Probability of Error Event
P_{BC}	Probability of Bit Error of RS Coded Schemes
P_{BM}	Probability of Bit Error of RS MPSK Signal Set
P_{Blc}	Probability of Block Error of RS Coded Schemes
P_{EM}	Probability of an Unreliable (Erased) MPSK Symbol
$P_{\bar{E}M}$	Probability of a Reliable (Not Erased) MPSK Symbol
P_{SC}	Probability of Symbol Error of RS Coded Schemes
P_{SM}	Probability of Symbol Error of MPSK Signal Set
$P_{SM\|E}$	Probability of an Unreliable MPSK Symbol Being in Error
$P_{SM\|\bar{E}}$	Probability of a Reliable MPSK Symbol Being in Error
$P_2(\mathbf{s},\hat{\mathbf{s}})$	Pairwise Error Probability of the Sequences **s** and $\hat{\mathbf{s}}$
$P_2(\mathbf{s},\hat{\mathbf{s}}\|\mathbf{a})$	Conditional Pairwise Error Probability of the Sequences **s** and $\hat{\mathbf{s}}$ Conditioned on the Fading Vector **a**
p_l	Probability of Transmitting the lth Symbol
$p_A(a)$	Probability Density Function of the Fading Amplitude a

$p_{\Phi}(\phi)$	Probability Density Function of the Fading Phase ϕ
Q_i^E	Probability of Correct Decision of a Reliable MPSK Symbol
q_{lh}	Probability of Transmitting lth Symbol and receiving hth Symbol
R	Code Rate
R_0	Cut-Off Rate
$\mathbf{r}$	Output of the Vector Channel (Received Vector)
$r(t)$	Output of the Waveform Channel (Received Waveform)
S_n	State of a Trellis Code at n th Time Interval
$\mathbf{s}$	Input of a Vector Channel (Transmitted Vector)
$s(t)$	Input of a Waveform Channel (Transmitted Waveform)
s_i	i th Symbol of an MPSK Signal Set
T_M	Fading Channel Time Spread Parameter
$T(D), T(D, I)$	Generating Function of a Trellis Code
α	Reliability Vector
β_L^2	Squared Product Distances along the Shortest Error Event Path (Minimum Product Distance)
$\gamma_b \equiv E_b/N_0$	Bit Energy Signal-to-Noise Ratio
$\gamma_s \equiv E_s/N_0$	Symbol Energy Signal-to-Noise Ratio
Δ_i	Minimum Euclidean Distance between Signals of a Signal Set in i th Partitioning
δ	Euclidean Distance between Signals of MPSK Signal Set
θ_i	Angular Representation of the i th MPSK Signal
Λ_e	Erasure Region
Λ_i	i th MPSK Symbol Decision Region
λ, λ_{opt}	Chernoff Parameter
ν	Number of Memories in a TCM Encoder
ρ_T	Radius of the Erasure Region in Errors-and-Erasures Decoding without CSI
ρ_{T_n}	Normalized Radius of the Erasure Region in Errors-and-Erasures Decoding without CSI
σ	Standard Deviation Parameter
ϕ	Fading Phase

LIST OF FIGURES

LIST OF TABLES

CHAPTER 1

INTRODUCTION

1.1. MOTIVATION

In many important radio applications the channel characteristics are often time-varying, as evidenced by *signal fading*. This characterization serves as a model for transmission over many radio channels such as short-wave ionospheric radio communication in the 3- to 30-MHz frequency band (HF), tropospheric scattering (beyond -the -horizon), radio communication in the 300- to 3,000-MHz frequency band (UHF), 3,000- to 30,000-MHz frequency band (SHF), and ionospheric forward scatter in the 30- to 300-MHz frequency band (VHF) [1]. These channels have randomly time-variant impulse responses. The time-variant impulse responses of these channels are consequences of the constantly changing physical characteristics of the media. The physical characteristics of such channels results from the multipath nature of the propagation medium. The meaning of multipath is implicit in its name; the propagation medium consists of several distinguishable *paths* connecting the transmitter to the receiver.

In a multipath fading environment the received signal can be viewed as a sum of several complex waveforms arriving via different individual paths. If the number of paths is large, then applying the central limit theorem will lead to the conclusion that both in phase and quadrature components of the received signal are approximately Gaussian [2]. Therefore, in such a fading channel the amplitude of the received signal is *Rayleigh distributed.* Fading that fits to this channel is generally called *Rayleigh fading*. When there is a single dominant, nonfading component in the received signal along with a fading

process, the signal amplitude is *Rician distributed* [3]. Such a channel is called *Rician fading* channel. The experimental evidences confirm that envelope statistics on different kind of fading channels fit to a Rayleigh or Rician distribution [4]-[7].

In fading channels, errors occur in burst. Conventional digital modulation and detection schemes provide poor performance over such channels. For instance, for binary orthogonal signaling on a Rayleigh fading channel, it is shown that the error probability is given by [2, p. 533]

$$P_b = \frac{1}{2 + E_s/N_0}, \tag{1.1}$$

where E_s is the mean value of the received signal energy and E_s/N_0 is the channel symbol Signal-to-Noise Ratio (SNR). Equation (1.1) states that, the error probability decreases inversely with E_s/N_0. This is in contrast to the Additive White Gaussian Noise (AWGN) case in which the error probability decreases exponentially with E_s/N_0 [2, p. 250]. In order to reduce the error probability on a Rayleigh fading channel, the high error probability of a deep fade on a single transmission must be circumvented. This is accomplished by means of *diversity transmission* [1]-[3]. One form of diversity transmission, called, *time diversity*, involves sending a symbol L_t times, in the hope that not all of the transmission will be subjected to deep fades. In other words, by transmitting the same information signal over independently fading channels, the probability that all the signal components will fade simultaneously is reduced considerably. In this technique the receiver performs some averaging to achieve an error performance that decreases exponentially with E_s/N_0 [2, p. 550]

$$P_b < e^{-0.149\, L_t\, (E_s/N_0)} \quad . \tag{1.2}$$

From a coding point of view the time diversity technique can be regarded as a repetition (block) code of rate $1/L_t$. Since a repetition code is a simple form of coding, one might expect that selection of more efficient types of codes maintains the benefit of

the time diversity technique. The order of time diversity provided by a code can be related to its minimum Hamming distance if maximum likelihood soft-decision decoding is considered (see Chapters 3 and 6).

Retransmitting the same signal L_t times or using a code with redundancy involves bandwidth expansion which is not tolerable in *bandwidth-limited channels*, e.g., mobile channels. To achieve the benefit of coding without bandwidth expansion, one might consider the recently developed bandwidth-efficient coded-modulation schemes [8]-[52]. These schemes are the integration of a bandwidth-efficient modulation scheme with some form of coding which are suitable for the channels in which both power and bandwidth are limited.

Trellis-Coded Modulation (TCM) schemes, as one of the coded-modulation techniques, were originally developed for the AWGN channel by Ungerboeck [9]. In his pioneering paper [9], Ungerboeck showed that by combining trellis codes with multilevel/phase signaling schemes, substantial coding gains (3-6 dB) can be obtained on the AWGN channels without sacrificing bandwidth efficiency. He also pointed out that to get benefit of coding with no bandwidth expansion, the coded schemes should be designed based on maximizing the *minimum Euclidean distance* between the channel coded sequences rather than the *minimum Hamming distance*. Following his idea many authors [12]-[45] contributed in this area by searching for new TCM schemes and in formalizing the theory. Calderbank and Mazo in [3] gave a new description of the trellis-coded modulation schemes and showed that asymmetric one-dimensional TCM schemes provide more coding gain than symmetric ones. Extension of Ungerboeck's two-dimensional TCM to multidimensional schemes was performed by Calderbank and Sloane [14]-[16] and Wei [17]. Some trellis codes were constructed in [25]-[26] by Divsalar *et al.* using two-dimensional as well as one-dimensional asymmetric signal sets. Multiple Trellis-Coded Modulation (MTCM) schemes were introduced by Divsalar and Simon [22]-[24] as an extension of multidimensional schemes using Multi-Phase Shift

Keying (MPSK) signaling. The rotationally invariant TCM schemes were presented by Wei [27]-[28] and one of these schemes with coding gain of 4 dB was adopted by CCITT [29] for use in new high-speed voiceband modems in 1984.

Although it was originally developed for the AWGN channel, there has been considerable interest in recent years [31]-[45] in applying TCM to fading channels. The principle advantage is that, when combined with interleaving of sufficient depth, TCM provides a form of *time diversity,* allowing the error rate to decrease with signal-to-noise ratio faster than the inverse dependence commonly found on Rayleigh fading channels. In [34] Divsalar and Simon show that the performance of the TCM schemes depends mainly on the *shortest error event path length* (time diversity) and the *squared product of the Euclidean distances along the shortest error event path* (minimum product distance). The minimum Euclidean distance of the TCM schemes is considered as a secondary parameter on fading channels. Thus, for fading channels the ability of TCM schemes to provide time diversity is more important than the minimum Euclidean distance. Fortunately it is possible to achieve both coding gain (i.e., an increase in minimum Euclidean distance) and time diversity from the same TCM scheme. However, when two schemes are compared, the one that yields the best coding gain may not yield the best time diversity. Hence, to develop a suitable coded modulation scheme for fading channels, these schemes must be designed based on fading channel criteria.

1.2. THESIS OUTLINE

The primary objective of this research is to introduce a new class of coded-modulation schemes, designed based on fading channel criteria. The channel of interest is the Rayleigh fading channel. However, the obtained results will be applied to a mobile fading channel as an application example.

In Chapter 2, the characteristics of multipath fading are reviewed. Statistical models for Rayleigh and Rician fading channels are considered. A general coded communication system for fading channel is briefly described. Then, the random coding bound for an

ensemble of coded schemes is calculated. We discuss the cut-off rate for different signal constellations and decoding strategies. This general discussion reveals the potential gains of coded-modulation schemes on bandwidth-limited fading channels.

Chapter 3 is devoted to a background on the development of the trellis-coded modulation schemes. These schemes are reviewed for the AWGN channel. The performance of these schemes, then, is evaluated over fading channels. The parameters which dominate the performance of the coded schemes over fading channels are extracted from this evaluation. This leads to the observation that the *time diversity* and *minimum product distance* of the coded schemes are main design criteria for fading channels. This motivates us to construct coded schemes for fading channels based on these criteria.

In chapter 4 we construct a new TCM scheme based on the design criteria obtained in the preceding chapter. This scheme is designed to maximize the time diversity as well as the minimum product distance of the coded scheme. The construction of the code is performed by introducing some design rules rather than exhaustive computer search. The error bounds for this scheme as well as other analogous schemes are derived and compared. The simulation is carried out to confirm the analytical results.

The construction of block-coded schemes as a counterpart to the trellis-coded ones is discussed in Chapter 5. We combine Reed-Solomon (RS) codes defined over $GF(2^m)$ with Multilevel Phase Shift Keying (MPSK) signals. In this combination, the symbol size of the RS codes is chosen as a multiple of MPSK symbol size with the hope that the combined scheme provides a time diversity equal to that of the RS code. The lower bounds of the post decoding bit error probability for these schemes over a Rayleigh fading channel are derived for two decoding strategies, namely, errors-only and errors-and-erasures decoding techniques. For errors-and-erasures decoding these bounds are evaluated for different erasure generation strategies based on the existence or the lack of the Channel State Information (CSI). The simulation results are provided to examine the tightness of the error bounds.

The results of Chapter 2 show that the reduction in SNR due to the soft-decision decoding in fading channel is much more than the one in the AWGN channel. Applying this decoding technique for block-coded schemes, hence, is of great importance on fading channels. In chapter 6, the issue of soft-decision decoding of RS-coded schemes is considered. This decoding technique is implemented by the Viterbi Algorithm (VA) for short RS codes. For the longer low rate RS coded schemes the Successive Erasure Minimum Distance Decoding (SEMDD) is discussed. The performance of these decoding strategies are evaluated and compared with the other techniques.

Chapter 7 represents the application of the trellis- and RS-coded schemes on a shadowed Rician fading channel. The fading model used is based on the one developed for the Canadian Mobile Satellite (MSAT) program. The performance of these coded schemes is evaluated for an ideally-interleaved channel. The effect of imperfect interleaving on the performance of the coded schemes is also investigated. A comparison between trellis-coded and RS-coded schemes is carried out based on the obtained results.

Finally, in Chapter 8 we summarize the contents of the thesis, and identify future research problems that can be derived from this thesis.

CHAPTER 2

DIGITAL TRANSMISSION VIA FADING CHANNELS

Our objective in this chapter is to show the potential gains of bandwidth-efficient coded-modulation schemes on bandwidth-limited fading channels. The treatment of this problem is general and does not include any specific coded scheme. With this objective in mind, after a brief introduction about the physical behavior, we will develop a statistical model of the fading channel. This model and its related parameters will be used throughout the thesis. Then a general coded transmission system over fading channels will be described. To study the performance of the coded signaling schemes over fading channels the random coding bounding technique will be employed. In this approach the error bound is evaluated for an ensemble of coded signaling schemes rather than a specific one. This yields an appropriate parameter, namely *cut-off rate*, which can be used for comparing different signaling schemes over a *Discrete Memoryless Channel* (DMC). We will evaluate this parameter for some two-dimensional signaling schemes, for different decoding strategies, on a Rayleigh fading channel and discuss the results. We will conclude this discussion by showing that the potential coding gains for bandwidth-efficient coded-modulation schemes over a Rayleigh fading channel is much more than that of the Additive White Gaussian Noise (AWGN) one.

2.1. FADING CHANNEL MODEL

There are numerous causes of fading. Among them a few will be addressed in this introductory section. One common cause of fading is the multipath nature of the propaga-

tion media. In this case, the transmitted signal arrives at the receiver from different paths frequently with time and/ or frequency varying relative phase differences. These individual paths cannot be distinguished at the receiver and in some fashion all of them are added. Thus, the received signal becomes a replica of the transmitted one with randomly amplitude and phase. This kind of fading occurs in ground-to-ground radio communication, and tropospheric and ionospheric scatter communication [3], [7].

The second kind of fading which is most common in ionospheric High Frequency (HF) radio propagation is the electron density variation versus altitude in the ionospheric layers. This occurs in HF radio communication which uses ionospheric layers as reflectors to communicate between two points which are not in line-of-sight or are too far apart for ground wave propagation. As the height of the ionosphere varies (due to the day-night changes or son spot activity, among the other causes), the length of the transmission path varies, and the received signal experiences random variations in both amplitude and phase.

Another significant cause of fading is the relative motion of the transmitter and receiver in a static multipath environment. In mobile radio systems, the propagation between the transmitting antenna and the mobile unit antenna is over several paths, namely, the line-of-sight path and the path due to the scattering caused by reflections from and diffractions around obstacles. These interfering signals produce a complex standing-wave pattern of varying field strength, with minima and maxima being of the order of a quarter wavelength apart. As a result of the vehicle movement through this standing-wave pattern, the amplitude and phase variations are induced in the received signal.

Two kinds of fading, namely, *short-term* and *long-term* fading are often considered in fading channels. In short-term fading the changes in channel characteristics occur within a time scale that ranges from fractions of a second to several seconds. While in long-term fading the variations of the channel characteristics are in the range of minutes,

tens of minutes, hours or even more. These variations often related to solar or meteorological influences [3]. Both kinds of variations are of course continually in process. However, the distinction between them is extremely useful for engineering because, for most fading channels, only the short-term fading variation affects the details of the received waveform structure and the inter-relationships of errors within a message; while the long-term variations determine in effect the *availability* of the channel.

A widely used model for channels that suffer from short-term fading is the *linear time-varying* filter model [3]. Representing the complex envelope of the input signal to such a channel by $s(t)$, the complex envelope of the output signal $r(t)$ can be shown as

$$r(t) = \int_{-\infty}^{\infty} h(\tau, t) \, . \, s(t-\tau) \, . \, d\tau + n(t), \qquad (2.1.1)$$

where $n(t)$ is the complex additive white Gaussian noise. Also, $h(\tau, t)$ shows the complex equivalent low-pass impulse response of the channel. The parameter τ in $h(\tau, t)$, represents the usual filter response variable, while the t-dependence indicates that the very structure of the impulse response changes with time. The corresponding equivalent low-pass transfer function of the channel can be obtained as

$$H(f, t) = \int_{0}^{\infty} h(\tau, t) \, . \, e^{-j 2\pi f \tau} \, . \, d\tau, \qquad (2.1.2)$$

which is the Fourier transform of $h(\tau, t)$ relative to its τ-dependence.

Considering $H(f, t)$ as a complex Wide-Sense Stationary (WSS) process [3], it is characterized by its covariance function defined as

$$R(\Delta f, \Delta t) = \frac{1}{2} E[\, H(f, t) \, . \, H^{*}(f + \Delta f, t + \Delta t) \,]. \qquad (2.1.3)$$

If $R(\Delta f, \Delta t)$ is negligible for $|\Delta t| > T_M$ and $|\Delta f| > B_D$, the channel is said to have *fading bandwidth (Doppler spread)*, B_D, *time spread*, T_M, and *coherence bandwidth* $1/T_M$ [1].

[1] A much more detailed discussion about these parameters can be found in [3] and [1, chap 7]

The selectivity of fading is characterized by the coherence bandwidth. If the coherence bandwidth of the fading channel is smaller than the signal bandwidth, the signal components with frequency separation greater than the coherence bandwidth are affected differently by the channel. In this case the fading is called to be *frequency-selective* fading. On the other hand for signals with bandwidth much smaller than $1/T_M$ all signal components fade together and $H(f, t)$, in effect, is an all-pass filter (for that bandwidth) with a varying amplitude and gains that applies to all the signal spectral lines. This is called *frequency-nonselective* or *flat* fading channel since the channel treats all the frequency components of the signal in the same way. This kind of fading channel is considered throughout the thesis and whenever we refer to the fading channel the flat fading is assumed.

The flat fading channel imposes a multiplicative distortion $h(\tau, t)$ on the signal, with

$$h(\tau, t) = \delta(\tau) \cdot a(t), \tag{2.1.4a}$$

where

$$a(t) = a_i(t) + j a_q(t). \tag{2.1.4b}$$

Using (2.1.1) and (2.1.4b) the output of the channel $r(t)$ is related to its input $s(t)$ as

$$r(t) = a(t) \cdot s(t) + n(t). \tag{2.1.5}$$

Because of this multiplicative distortion the flat fading channel has also been called *multiplicative* fading channel.

Central limit theorem arguments lead to the conclusion that [2], [3] the in-phase $a_i(t)$ and quadrature $a_q(t)$ components of $a(t)$ are two statistically independent Gaussian random processes and are characterized by their autocorrelation functions or by their power spectra, $P(f)$, with bandwidth B_D. In fading channels with only a diffused multipath signal, these Gaussian processes have zero mean and the fading envelope, defined as

$$a \equiv \sqrt{a_i^2 + a_q^2}, \tag{2.1.6a}$$

has a *Rayleigh* distribution with a probability density function (pdf)

$$p_A(a) = \frac{a}{\sigma_a^2} \cdot e^{-\frac{a^2}{2\sigma_a^2}}, \tag{2.1.6b}$$

where σ_a^2 represents the variance of the Gaussian random processes. The average energy of the fading envelope is related to σ_a^2 as

$$E[\,a^2\,] = 2\sigma_a^2. \tag{2.1.6c}$$

The fading phase defined as

$$\phi = \tan^{-1} \frac{a_q}{a_i}, \tag{2.1.7a}$$

is a uniformly distributed random process with a pdf of

$$p_\Phi(\phi) = \frac{1}{2\pi}; \qquad 0 \le \phi < 2\pi. \tag{2.1.7b}$$

When there is a single dominant, nonfading component in the received signal along with a diffused multipath fading process, $a(t)$ can no longer be modeled as having a zero mean. This occurs when there are fixed scatterers or signal reflectors in the medium, in addition to randomly moving scatterers. In such a case the fading envelope is *Rician* distributed, having a pdf

$$p_A(a) = 2a \,.\, (1+K) \,.\, e^{-(K + a^2(1+K))} \,.\, I_0(2a\sqrt{K(K+1)}), \tag{2.1.8}$$

where $I_0(\,.\,)$ is the zero-order modified Bessel function of the first kind, and K is the ratio of the energy of direct component to the energy of the diffused multipath one. In this case the phase is no longer uniformly distributed, but rather is more concentrated around that of the nonfading component. Note that for $K = 0$, (2.1.8) reduces to (2.1.6b).

2.2. CODED COMMUNICATION ON FADING CHANNELS

The basic elements of a coded communication system are shown by the general block diagram in Fig. 2.1. A sequence of digital information is produced by the data source. The channel encoder adds some redundancy to the incoming bits and delivers the encoded message to the modulator at a rate of R bits/sec. The modulator transforms the encoded bits to a waveform that is compatible with the channel characteristics. In its general form the modulator transmits m bits at a time by using $q = 2^m$ distinct waveforms $s_i(t)$, $i = 0,1,...,q-1$, one waveform for each of the 2^m possible m-bit sequences. This is called q-ary modulation. The transmitted waveforms are subjected to channel noise and distortion. In an additive white Gaussian noise channel, only Gaussian-distributed white noise is added, while in a multiplicative fading channel the amplitude and phase of the transmitted waveforms will be distorted as well.

At the receiver the demodulator processes the corrupted signals and reduces each of them to a number that represents an estimate of the q-ary transmitted symbol. In such a case we say that the demodulator has *quantized* the received signal to q levels and has made a *hard decision*. As an alternative, the demodulator may make Q-ary decision, where $Q > q$. In this case it is said to make *soft decision*. In its extreme case, $Q = \infty$, no quantization is performed. Based on the quantized or unquantized information furnished by the demodulator, the decoder attempts to reconstruct the original transmitted message from the knowledge of the code used by the encoder and the redundancy contained in the received data.

From the analysis point of view, the function of the encoder-modulator can be divided into separate discrete-time and continuous-time operations. The justification for this separation lies in the *Gram-Schmidt orthogonalization* procedure [2]. This procedure permits us to expand any one of the M finite-energy time functions $s_i(t)$, $i = 0,1, ..., M-1$, as linear combinations of $N \leq M$ *orthonormal basis functions* over the finite time interval $0 \leq t \leq T$, i.e.,

$$s_i(t) = \sum_{n=1}^{N} s_{in} \cdot \phi_n(t); \qquad i = 0,1, ..., M-1, \tag{2.2.1a}$$

where $\phi_n(t)$, $n = 0,1, ..., N-1$, are N set of orthonormal functions

$$\int_0^T \phi_l(t) \cdot \phi_j(t) \cdot dt = \delta_{lj} = \begin{cases} 1 & l = j \\ 0 & l \neq j, \end{cases} \tag{2.2.1b}$$

and the coefficient s_{in} shows the projection of $s_i(t)$ onto the function $\phi_n(t)$ over the time interval $0 \leq t \leq T$, i.e.,

$$s_{in} = \int_0^T s_i(t) \cdot \phi_n(t)\, dt. \tag{2.2.1c}$$

The orthogonalization procedure provides us a tool to represent the waveforms $\{s_i(t)\}$ as the points of an *N-dimensional signal space* formed by the orthonormal basis, $\{\phi_i(t)\}$. The idea of signal space is of fundamental importance, for it visualizes the design of the communication systems from an abstract point of view using the language of geometry. Each of the waveforms $s_i(t)$, $i = 0,1, \cdots, M-1$, are completely determined by the vector of their coefficients

$$\mathbf{s}_i = (s_{i0}, s_{i1}, ..., s_{i(N-1)}); \qquad i = 0,1, ..., M-1, \tag{2.2.2a}$$

and their energies are interpretated as the norms of the corresponding vectors as

$$E_s \equiv \int_0^T |s_i(t)|^2 \cdot dt = \sum_{n=1}^{N} |s_{in}|^2 \equiv |\mathbf{s}_i|^2. \tag{2.2.2b}$$

The distance between two signal waveforms $s_i(t)$ and $s_j(t)$ can be viewed as the *Euclidean distance* between the corresponding signal points in N-dimensional signal space as

$$d_E^2 = \int_0^T |s_i(t) - s_j(t)|^2 \cdot dt = |\mathbf{s}_i - \mathbf{s}_j|^2. \tag{2.2.3}$$

At the receiver, to recover the transmitted vectors from the received waveforms the virtue of the orthonormality of the $\{\phi_i(t)\}$ is used. This is done by multiplying the received signal by each of the orthonormal basis and integrating over the interval $0 \le t \le T$.

In general, the input to the receiver is a random process expressed as

$$r(t) = a(t) \cdot s_i(t) + n(t); \qquad 0 \le t \le T, \tag{2.2.4}$$

for a multiplicative fading channel. In (2.2.4) $n(t)$ is the additive white Gaussian noise with a two sided spectral density of $N_0/2$ and $a(t)$ is the fading process. Assume that $a(t)$ is slow enough that it has a constant envelope a and a constant phase[2] ϕ over the interval $0 \le t \le T$. In this case the integrator outputs, say

$$r_j \equiv \int_0^T r(t) \cdot \phi_j(t) \cdot dt; \qquad j = 0, 1, ..., N-1, \tag{2.2.5a}$$

are random variables which constitute the components of a random vector

$$\mathbf{r} \equiv (r_{i0}, r_{i1}, ..., r_{i(N-1)}). \tag{2.2.5b}$$

Considering (2.2.4) we have

$$\mathbf{r} = a \cdot \mathbf{s}_i + \mathbf{n}, \tag{2.2.6}$$

where

$$\mathbf{n} \equiv (n_{i0}, n_{i1}, ..., n_{i(N-1)}), \tag{2.2.7a}$$

is a random vector whose components

$$n_j \equiv \int_0^T n(t) \cdot \phi_j(t) \cdot dt; \qquad j = 0, 1, ..., N-1, \tag{2.2.7b}$$

---

[2] It is assumed that the phase ϕ is known at the receiver, and the receiver compensate the phase variations of the received signal by multiplying it by $exp(-j\phi)$. This kind of receiver is called *coherent receiver* and is considered in this thesis. Also we assume that the fading envelopes are independent random variables. This is achieved by using theoretically infinite size interleaver and de-interleaver in the coded communication system.

are independent zero mean Gaussian variables with variances $N_0/2$ [2]. Assuming that $n(t)$, hence $\mathbf{n}$, is statistically independent of $\mathbf{s}_i$, it is clear that the vector $\mathbf{r}$, is a random vector whose components, $\{r_j\}$, are statistically independent Gaussian random variables with mean

$$E[r_j] = a \cdot s_{ij}, \tag{2.2.8}$$

and variances $N_0/2$. It follows that the conditional density of $\mathbf{r}$ given the fading envelope a and the transmitted vector $\mathbf{s}_i$

$$p_N(\mathbf{r} \mid a, \mathbf{s}_i) = \prod_{j=0}^{N-1} p(r_j \mid a, s_{ij}) = \prod_{j=0}^{N-1} \frac{e^{-|r_j - a \cdot s_{ij}|^2/N_0}}{\sqrt{\pi N_0}}. \tag{2.2.9a}$$

This expression can be modified as

$$p_N(\mathbf{r} \mid a, \mathbf{s}_i) = \prod_{j=0}^{N-1} p(r_j \mid a, s_{ij}) = \prod_{j=0}^{N-1} \frac{e^{-|r_j - a \cdot s_{ij}|^2 \cdot E_s/N_0}}{\sqrt{\pi N_0/E_s}}, \tag{2.2.9b}$$

by assuming that the output of the integrators at the receiver is divided by $\sqrt{E_s}$. This operation normalized the average energy of the received signal components to one and the variance of the Gaussian noise to $N_0/2E_s$.

We may summarize the results of this section by saying that, from the analysis point of view, the effect of the modulator, the waveform channel, and the demodulator can be considered as a *random mapping* which maps the points of an N-dimensional signal space to an N-dimensional real vector space. This random mapping, which is called *vector or discrete channel* is characterized by the conditional (or transition) probability density of (2.2.9).

2.3. ERROR BOUND AND CUT-OFF RATE

In a digital communication system the function of the demodulator-decoder pair is to estimate the transmitted message from the received noisy waveforms. Such an estimation must be based on some desirable criterion. The most reasonable criterion for this

purpose is to minimize the *probability of error* of this estimation. A communication system, hence, is judged by its ability in communicating a stream of data between a source and a destination with a low probability of error.

To evaluate the error performance of a specific coded system, the knowledge of the specific code and signal set is required. Exact expressions for the probability of error, in general, involve multidimensional integrals, which are complex to calculate. Upper bounds are hence developed [2], [53], which are applicable to any signal set. However, evaluation of these bounds for a specific signal set, other than a few simple cases, is essentially cumbersome. This becomes particularly prohibitive as the size of the signal set M and the dimensionality N, become large.

These difficulties can be circumvented by bounding the probability of error for an ensemble of coded systems, rather than a specific one. Strangely enough, it is much easier to find the error bounds not for just one communication system, but rather a whole collection of communication systems, each consisting of an encoder, vector channel, and decoder. Since such an upper bound is the average of the probability of error over the entire ensemble of coded systems, it is obvious that at least one coded system must have a probability of error which is no greater than the ensemble average. Hence, the ensemble average is an upper bound of the probability of error for the optimum coded system with signal set of M signals of dimensionality N. This technique was first introduced by Shannon [54] and now is referred as *random coding* bounding in information theory [53].

Using this technique Wozencraft and Jacobs show that the average error probability for an ensemble of the block coded systems over a discrete memoryless channel is upper bounded as [2, p. 392]

$$\overline{P(\varepsilon)} < 2^{-N[R_0 - R]}, \tag{2.3.1}$$

where N is the number of times that the channel is used in the transmission of a coded word, and R is the information rate in bits per channel use. The parameter R_0 is called

the *cut-off rate* and is derived as [2, p. 396]

$$R_0 = -\log_2 \sum_{h=0}^{Q-1} [\sum_{l=0}^{q-1} p_l \sqrt{q_{lh}}]^2, \qquad (2.3.2)$$

where q and Q denote the number of the transmitter alphabet and the receiver quantization levels, respectively. Also, p_l shows the probability of transmitting the l-th symbol, s_l, and $\{q_{lh}\}$ represent the set of the channel transition probabilities. We will use (2.3.2) to evaluate the cut-off rates of some known two-dimensional signaling schemes over fading channels which employ hard-decision or erasure decoding techniques. In the following we extend the above results to the fading channels with soft decision decoding. The cut-off rate for such a case is derived in a manner similar to [2] for an ensemble of block coded systems.

Consider an ensemble of block codes with block length of N and symbols chosen from a signal alphabet $\{s_i\}$ with cardinality of q. We assume that the code words of this ensemble are pairwise statistically independent, i.e.,

$$P(\mathbf{s}_i, \mathbf{s}_k) = P(\mathbf{s}_i) \cdot P(\mathbf{s}_k); \qquad all \quad i, k \neq i, \qquad (2.3.3a)$$

and furthermore, the constituent components of each code word have the same property[3], i.e.,

$$P(\mathbf{s}_i) = \prod_{j=0}^{N-1} P(s_{ij}); \qquad i = 0, 1, ..., M-1, \qquad (2.3.3b)$$

where M is the total number of the code words in the ensemble.

To derive the bound of (2.3.1) for such an ensemble of codes we start with union bound. Assume that the i-th message, m_i, is transmitted, then the probability of erroneous detection of this message is upper bounded by invoking the union bound as,

$$P(\varepsilon | m_i) \leq \sum_{k=0, i \neq k}^{M-1} P_2(\mathbf{s}_i, \mathbf{s}_k), \qquad (2.3.4)$$

[3] In [2, chap. 6] it is proved that these assumptions are true for an ensemble of parity check codes

where $P_2(\mathbf{s}_i, \mathbf{s}_k)$ is called *pairwise error probability* and represents the probability of error when the two code words $\mathbf{s}_i$ and $\mathbf{s}_k$ are used to communicate one of the two equally likely messages. By virtue of (2.3.3) the statistical average of $P_2(\mathbf{s}_i, \mathbf{s}_k)$ over the ensemble of coded systems is independent of subscripts i and k. Hence,

$$\overline{P_2(\mathbf{s}_i, \mathbf{s}_k)} = \overline{P_2(\varepsilon)}; \qquad all \ \ i, k \neq i, \tag{2.3.5a}$$

and

$$\overline{P(\varepsilon)} = \overline{P(\varepsilon | m_i)} < M \ \overline{P_2(\varepsilon)}, \tag{2.3.5b}$$

where the bar sign denotes the averaging operation over all codes in the ensemble. The number of code words in the ensemble, M, is related to R as

$$M = 2^{NR}. \tag{2.3.6}$$

Substituting (2.3.6) into (2.3.5b) results in

$$\overline{P(\varepsilon)} < 2^{NR} \ . \overline{P_2(\varepsilon)}. \tag{2.3.7a}$$

Hence, we need only to show that

$$\overline{P_2(\varepsilon)} \leq 2^{-NR_0}, \tag{2.3.7b}$$

to obtain the desired bound of (2.3.1).

2.3.1. Calculation of the Pairwise Error Probability

In fading channels, the decoding process uses a metric of the form $m(\mathbf{r}, \mathbf{s}, \mathbf{a})$ if an estimate of fading amplitude, $\mathbf{a}$, is available at the receiver, and $m(\mathbf{r}, \mathbf{s})$ if not. The estimate of the fading amplitude is called Channel State Information (CSI) [32]. Whatever the metric is used, it is desirable from the view point of simplifying the decoding process that it have an additive property, namely, that the total metric for a code word is the sum of metrics for the constituent components, i.e.,

$$m(\mathbf{r}, \mathbf{s}) = \sum_{n=0}^{N-1} m(r_n, s_n). \tag{2.3.8}$$

If we consider the Maximum Likelihood (ML) criterion for the optimum decoder, then the ML metric is defined as

$$m(\mathbf{r}, \mathbf{s}) = \ln P_N(\mathbf{r} \mid \mathbf{s}, \mathbf{a}), \tag{2.3.9a}$$

when CSI is available, and

$$m(\mathbf{r}, \mathbf{s}) = \ln P_N(\mathbf{r} \mid \mathbf{s}), \tag{2.3.9b}$$

if not. Note that for memoryless channels the ML metric of (2.3.9) satisfies the requirement in (2.3.8).

Assuming that $\mathbf{s}$ is transmitted and $\mathbf{r}$ is received. Between the two sequences $\mathbf{s}$ and $\hat{\mathbf{s}}$ the optimum decoder incorrectly decides $\hat{\mathbf{s}}$ if and only if[4]

$$m(\mathbf{r}, \hat{\mathbf{s}}) \geq m(\mathbf{r}, \mathbf{s}), \tag{2.3.10a}$$

or equivalently

$$\sum_{n=0}^{N-1} m(r_n, \hat{s}_n) \geq \sum_{n=0}^{N-1} m(r_n, s_n). \tag{2.3.10b}$$

Then the pairwise error probability is given by

$$P_2(\mathbf{s}, \hat{\mathbf{s}}) = E_{\mathbf{a}}[\, P_2(\mathbf{s}, \hat{\mathbf{s}} \mid \mathbf{a}) \,], \tag{2.3.11a}$$

where

$$P_2(\mathbf{s}, \hat{\mathbf{s}} \mid \mathbf{a}) = Pr\left[\, m(\mathbf{r}, \hat{\mathbf{s}}) \geq m(\mathbf{r}, \mathbf{s}) \mid \mathbf{s}, \mathbf{a} \,\right], \tag{2.3.11b}$$

is the conditional pairwise error probability conditioned on the fading amplitude vector $\mathbf{a}$, and E shows the statistical expectation operation. The conditional probability of (2.3.11b) is upper bounded using the Chernoff bound techniques [2], [55] as

$$P_2(\mathbf{s}, \hat{\mathbf{s}} \mid \mathbf{a}) \leq E_{\mathbf{r}|\mathbf{s}}[\, \exp(\lambda[m(\mathbf{r}, \hat{\mathbf{s}}) - m(\mathbf{r}, \mathbf{s})]) \,], \tag{2.3.12a}$$

[4] We drop subscripts i and k and use $\mathbf{s}$ and $\hat{\mathbf{s}}$ instead of $\mathbf{s}_i$ and $\mathbf{s}_k$ to show the fact that the pairwise error probability is independent of subscripts i and k.

where $\lambda \geq 0$ is the Chernoff parameter to be optimized to tighten the bound. Substituting (2.3.12a) into (2.3.11a) yields

$$P_2(\mathbf{s}, \hat{\mathbf{s}}) \leq E_{\mathbf{a}} \left[E_{\mathbf{r}|\mathbf{s}} \left[\exp(\lambda[m(\mathbf{r}, \hat{\mathbf{s}}) - m(\mathbf{r}, \mathbf{s})]) \right] \right]. \tag{2.3.12b}$$

Defining the Chernoff bound between the code words $\mathbf{s}$ and $\hat{\mathbf{s}}$ as

$$C(\mathbf{s}, \hat{\mathbf{s}}, \lambda) \equiv E_{\mathbf{a}} \left[E_{\mathbf{r}|\mathbf{s}} \left[\exp(\lambda[m(\mathbf{r}, \hat{\mathbf{s}}) - m(\mathbf{r}, \mathbf{s})]) \right] \right], \tag{2.3.12c}$$

(2.3.12a) can be written as

$$P_2(\mathbf{s}, \hat{\mathbf{s}}) \leq C(\mathbf{s}, \hat{\mathbf{s}}, \lambda). \tag{2.3.12d}$$

Averaging (2.3.12d) over all codes in the ensemble and recalling (2.3.3), we obtain

$$\begin{aligned} \overline{P_2(\varepsilon)} &\leq \overline{C(\mathbf{s}, \hat{\mathbf{s}}, \lambda)}, \\ &= \prod_{n=0}^{N-1} \overline{C(s_n, \hat{s}_n, \lambda)}, \\ &= [\overline{C(s, \hat{s}, \lambda)}]^N, \end{aligned} \tag{2.3.13}$$

where $C(s, \hat{s}, \lambda)$ is called Chernoff factor of signals s and $\hat{s}$. Defining

$$R_0(\lambda) \equiv -\log_2 \overline{C(s, \hat{s}, \lambda)}, \tag{2.3.14a}$$

(2.3.13) can be written as

$$\overline{P_2(\varepsilon)} \leq 2^{-NR_0(\lambda)}; \qquad \lambda \geq 0. \tag{2.3.14b}$$

The bound in (2.3.14b) is valid for any $\lambda \geq 0$. The parameter λ should be chosen in a such a way that the bound is as tight as possible. For this optimum λ, $R_0(\lambda)$ has the largest possible value. Defining

$$R_0 \equiv \max_{\lambda} R_0(\lambda) = R_0(\lambda_{opt}), \tag{2.3.14c}$$

the desired result of (2.3.7b) is obtained.

2.3.2. Calculation of $\overline{C(s, \hat{s}, \lambda)}$

Averaging $C(s, \hat{s}, \lambda)$ over all assignments of signals s and $\hat{s}$, we obtain

$$\overline{C(s, \hat{s}, \lambda)} = \sum_{n=0}^{q-1} \sum_{m=0}^{q-1} p(s_n) \cdot p(s_m) \cdot C(s_n, s_m, \lambda). \tag{2.3.15}$$

Then (2.3.14c) becomes

$$R_0 = -\log_2 \min_{\lambda} \sum_{n=0}^{q-1} \sum_{m=0}^{q-1} p(s_n) \cdot p(s_m) \cdot C(s_n, s_m, \lambda). \tag{2.3.16a}$$

Assuming that the signals are used uniformly, i.e., $p(s_n) = p(s_m) = 1/q$, then (2.3.16a) turns out to be

$$R_0 = 2 \log_2 q - \log_2 \min_{\lambda} \sum_{n=0}^{q-1} \sum_{m=0}^{q-1} C(s_n, s_m, \lambda). \tag{2.3.16b}$$

Similar expression for cut-off rate is obtained in [44] using the ensemble of convolutional coded schemes.

2.3.3. Cut-Off Rate for Some Two-Dimensional Signal Constellations

The cut-off rate, R_0, is the appropriate criterion for comparing different modulation schemes on a discrete memoryless channel [8]. The bigger R_0 for a given signal energy-to-noise ratio the better the modulation system. In the following, we calculate the cut-off rate for some known two-dimensional signal constellations shown in Fig. 2.2, and compare them based on the R_0 criterion over a Rayleigh fading channel.

To evaluate the cut-off rate of (2.3.16) the expressions for Chernoff factors are required. The Chernoff factors for fading channels with and without channel state information have recently been evaluated in [32] with an emphasize on Multi-Phase Shift Keying (MPSK) signal sets. A procedure for evaluating these factors for general two-dimensional signal sets is included in Appendix A and the results are summarized in the following.

2.3.3.1 Fading Channel with CSI

Assuming that the channel state information is available at the receiver, the Chernoff factor of signals s and $\hat{s}$ for a Rician fading channel is derived as [see Appendix A]

$$C'(s,\hat{s}) \equiv C(s,\hat{s},\lambda_{opt})$$

$$= \frac{1+K}{1+K+E_s/4N_0|s-\hat{s}|^2}\exp\left[-\frac{KE_s/4N_0|s-\hat{s}|^2}{1+K+E_s/4N_0|s-\hat{s}|^2}\right]. \qquad (2.3.17a)$$

The Chernoff factor for a Rayleigh fading channel is obtained from (2.3.17a) by setting $K = 0$ as

$$C(s,\hat{s}) = \frac{1}{1+E_s/4N_0|s-\hat{s}|^2}. \qquad (2.3.17b)$$

Using (2.3.16) and (2.3.17), R_0 is plotted for a Rayleigh fading channel in Fig. 2.3. It is worth noting that the cut-off rate for the AWGN channel is obtained from (2.3.16) and (2.3.17) by setting $K = \infty$. The result is consistent with the findings of [2, p.317] and is shown in Fig 2.4.

From Fig.'s 2.3 and 2.4 it is apparent that at low signal-to-noise ratios the required E_s/N_0 to achieve a given R_0 in the Rayleigh fading channel is more than that of the AWGN one. For example, if we consider the required E_s/N_0 for rates around 3/4 of the saturated rate, then the Rayleigh fading channel needs 4.5-6 dB more E_s/N_0 than the AWGN one, depending on the selected signal set. However, at high signal-to-noise ratios (SNR) both channels provide the same rate.

2.3.3.2. Fading Channel without CSI

For fading channels without the channel state information the Chernoff factor of signals s and $\hat{s}$ is evaluated in Appendix A. For a Rician fading channel this factor is given by

$$C(s,\hat{s},\lambda) = \exp(\lambda\frac{E_s}{N_0}(|s|^2 - |\hat{s}|^2 + \lambda|s-\hat{s}|^2)) \cdot \frac{e^{-K}}{\pi}\int_0^{\pi}(1-\sqrt{\pi}erfc(\nu)e^{\nu^2}\nu)\,.\,d\theta, \tag{2.3.18a}$$

where

$$\nu = \frac{\lambda E_s/2N_0(|s|^2 - |\hat{s}|^2 + |s-\hat{s}|^2)}{\sqrt{1+K}} - \sqrt{K}\cos(\theta). \tag{2.3.18b}$$

The Chernoff factor for a Rayleigh fading channel ($K = 0$) simplifies to

$$C(s,\hat{s},\lambda) = \exp(\lambda\frac{E_s}{N_0}(|s|^2 - |\hat{s}|^2 + \lambda|s-\hat{s}|^2)) \cdot (1-\sqrt{\pi}erfc\left[\lambda\frac{E_s}{2N_0}(|s|^2 - |\hat{s}|^2 + |s-\hat{s}|^2)\right] \cdot \exp\left[(\lambda\frac{E_s}{2N_0}(|s|^2 - |\hat{s}|^2 + |s-\hat{s}|^2))^2\right] \cdot (\lambda\frac{E_s}{2N_0}(|s|^2 - |\hat{s}|^2 + |s-\hat{s}|^2))). \tag{2.3.19}$$

Note that for constant envelope signal sets such as MPSK, $|s|^2 = |\hat{s}|^2$ and (2.3.18) and (2.3.19) are identical to the results given in [32].

In this case, unlike the case with CSI, the cut-off rate of (2.3.16) is maximized by optimizing λ numerically. Using (2.3.19) the cut-off rate R_0 is plotted in Fig. 2.5, for a Rayleigh fading channel.

To compare the cut-off rate for Rayleigh fading channels with and without CSI the cut-off rates for these cases are replotted in Fig. 2.6. It is observed that, unlike the AWGN and fading channels with CSI, constant envelope signal sets, i.e., MPSK constellations perform much better than rectangular constellations for the fading channels without CSI. Note that the cut-off rates of the 16QAM and 32CROSS signal sets are even inferior to 4PSK. This is explained by considering the fact that in an MPSK signal set the boundary

of the optimum decision regions are radial and thus invariant to radial scaling of the received signals caused by fading [2]. This makes the MPSK signal sets a suitable choice for designing the modulator part of the coded schemes on fading channels. Furthermore, these signal sets are less sensitive to the nonlinear distortion caused by the nonlinerity of the power amplifiers in the transmitter. Thus, we restrict our attention to the constant envelope signal sets throughout the thesis.

2.3.4. Quantized Fading Channel

To complete the discussion of the cut-off rate, we now apply the analysis of R_0 to the quantized fading channels where either the number of quantized levels, Q, is the same as the transmitter alphabet size, q, (hard quantized channel) or there is one null zone besides q quantized levels (erasure channel). Since the former is a special case of the latter we begin our discussion with the erasure channel first.

2.3.4.1. Fading Channel with Erasure Zone

The cut-off rate in (2.3.2) can be written as

$$R_0 = -\log_2 \left[\sum_{h=0}^{q-1} \left[\sum_{l=0}^{q-1} p_l \sqrt{q_{lh}} \right]^2 + \left[\sum_{l=0}^{q-1} p_l \sqrt{q_{le}} \right]^2 \right], \qquad (2.3.20a)$$

where q_{le} represents the probability of the received signal being in the erasure region provided that the l-th signal is transmitted. Defining a circular erasure region for MPSK signal sets as in Fig. 2.7, q_{le} is independent of the transmitted signal and will be denoted as q_e Using the symmetry of the MPSK signal set and assuming that the signal points are uniformly used, i.e., $p_l = 1/q$, (2.3.20a) is further simplified as

$$R_0 = -\log_2 \left[\frac{1}{q} \left[\sum_{l=0}^{q-1} \sqrt{q_l} \right]^2 + q_e \right], \qquad (2.3.20b)$$

where

$$q_l = E_a \left[\int_{\Lambda_l} p(r \mid s_0, a) \, . \, dr \right]; \qquad l = 0, 1, ..., q-1. \tag{2.3.21a}$$

and

$$q_e = E_a \left[\int_{\Lambda_e} p(r \mid s_0, a) \, . \, dr \right]. \tag{2.3.21b}$$

In (2.3.21), Λ_l and Λ_e denote the decision region of the l-th signal and the erasure region, respectively.

Assume that the fading amplitude is known at the receiver. In this case a simple erasure zone is defined based on the fading amplitude. If the fading amplitude is less than a threshold value, say a_T, then the received signal is considered to be in the erasure region. Based on such definition, the probabilities q_l and q_e are evaluated in Appendix B as

$$q_l = \frac{E_s/N_0}{\pi(1 + E_s/N_0)} \left(\frac{\pi}{ME_s/N_0} e^{-E_s a_T^2/N_0} + \int_{(2l-1)\pi/M}^{(2l+1)\pi/M} d\theta \left(\int_{a_T}^{\infty} \rho^2 \frac{E_s}{N_0} \sqrt{\pi} \cos\theta \right. \right.$$

$$\left. \left. . \, e^{-E_s \rho^2/N_0 + \frac{\rho^2 (E_s/N_0)^2 \cos^2\theta}{1 + E_s/N_0}} \, erfc\left(\frac{-\rho E_s/N_0 \cos\theta}{\sqrt{1 + E_s/N_0}} \right) d\rho \right) \right), \tag{2.3.22a}$$

and

$$q_e = 1 - \sum_{l=0}^{q-1} q_l. \tag{2.3.22b}$$

In (2.3.22), we choose a_T in such a way that R_0 is maximum.

2.3.4.2. Fading Channel with Hard-Decision

By setting the threshold value $a_T = 0$ in (2.3.22), the transition probabilities for a fading channel is obtained. In this case $q_e = 0$ and (2.3.20) simplifies to

$$R_0 = \log_2 q - 2\log_2 [\sum_{l=0}^{q-1} \sqrt{q_l}\,]. \qquad (2.3.23)$$

Using (2.3.20), (2.3.22), and (2.3.23) the cut-off rates for the hard quantized and erasure channels are plotted in Fig. 2.8, for some MPSK signal sets. In this figures R_0 for soft-decision fading channels with CSI is also included. It is observed that the soft-decision decoding significantly improves the performance of the coded schemes compared to the hard-decision one. The reduction in SNR due to the soft-decision decoding at rates around 3/4 of the saturated rate is about 7.5 dB compared to the hard-decision one. Also, the erasure decoding can save about 2 dB at the same rate compared to the hard-decision decoding. It is worth noting that the reduction in SNR due to the soft-decision decoding in fading channels is much more than the one in the AWGN channel. The cut-off rates for the AWGN channel using different decoding strategies are shown in Fig. 2.9 for comparison.

2.4. DISCUSSION

The cut-off rate curves may be interpreted to show the benefit of using bandwidth-efficient coded-modulation schemes on bandwidth-limited channels. First, we investigate the potential gains of these schemes on the AWGN channel.

Consider a situation in which uncoded QPSK signal set is used to transmit a message with rate of 2 bits/symbol over the AWGN channel with an error probability not to exceed 10^{-5}. The required E_s/N_0 for such an error probability is about 12.9 dB. This points is indicated in Fig. 2.4. Now consider a coded system which transmits messages with the rate of 2 bits/symbol by using 8PSK signal set. Assuming unlimited coding and decoding effort (very large N), according to Fig. 2.4, this coded scheme can provide the same performance of uncoded QPSK with a reduction of 5.2 dB in SNR without bandwidth expansion. It is also apparent that further expansion of the signal set to more than twice may not achieve additional gain.

The same argument can be applied to the Rayleigh fading channel. In such a channel, the uncoded QPSK can provide an error probability of 10^{-5} at $E_s/N_0 = 50$ dB. This point is shown in Fig. 2.3. It is observed that if the number of channel signals is doubled, e.g., by choosing 8PSK modulation, error-free transmission of 2 bits/symbol is theoretically possible at $E_s/N_0 = 12$ dB. Hence, for Rayleigh fading channel the use of bandwidth-efficient coded modulation may result in 38 dB reduction in SNR at error probability of 10^{-5}. This is significantly more than the reduction of SNR in the AWGN channel due to the use of bandwidth-efficient signaling.

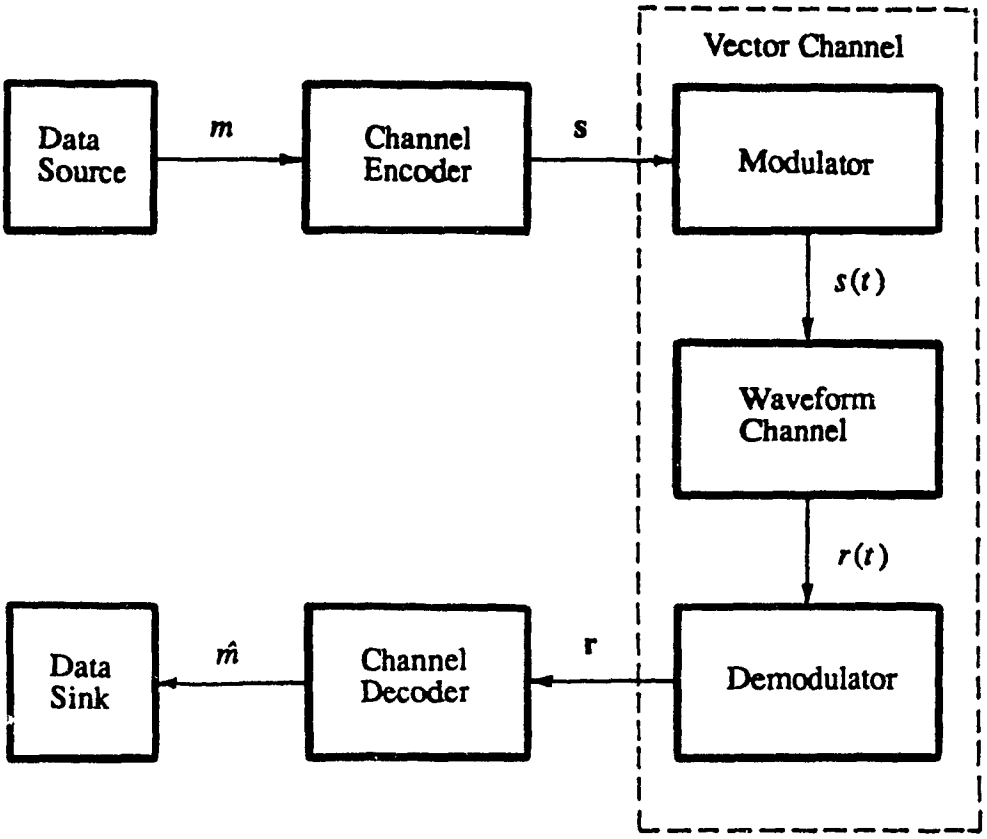

Fig. 2.1. The block diagram of a coded communication system.

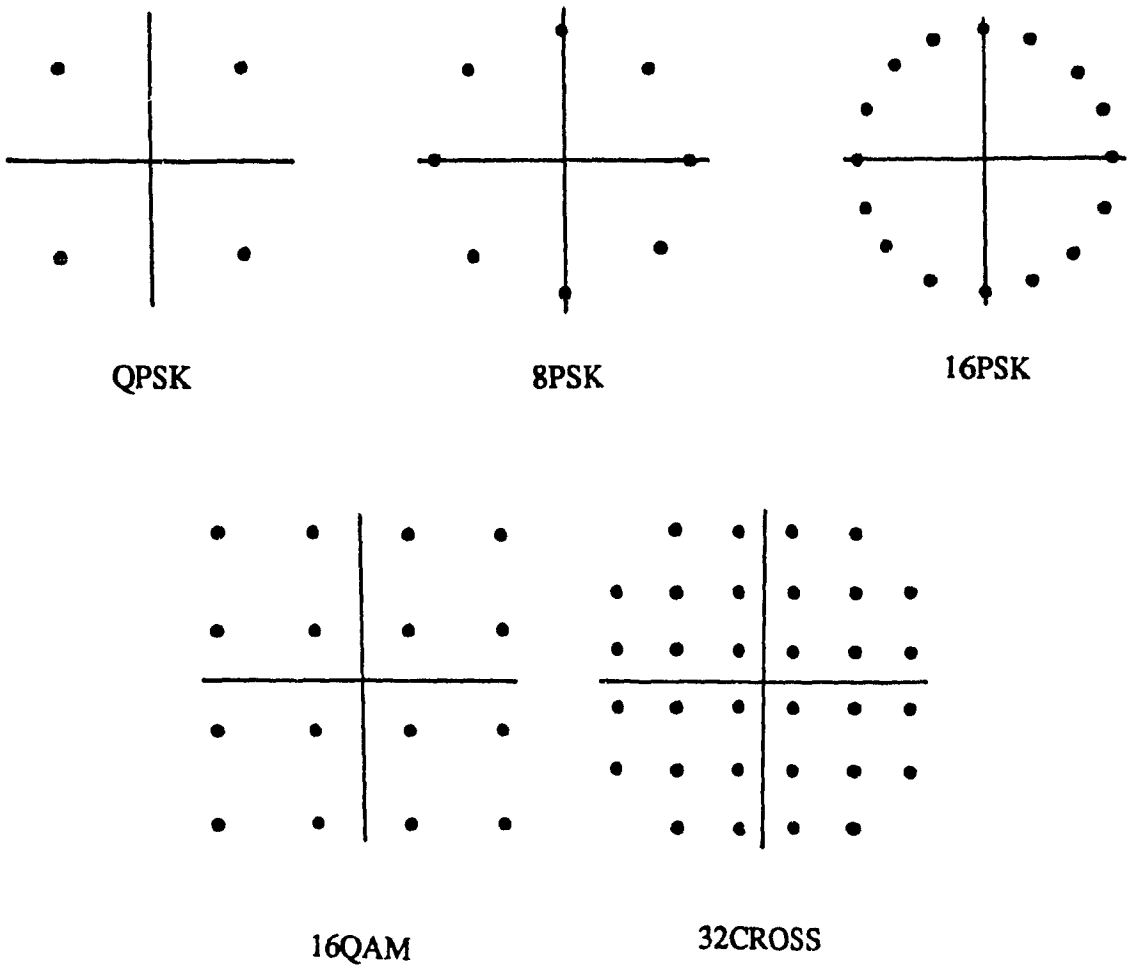

Fig. 2.2. Some two-dimensional signal constellations.

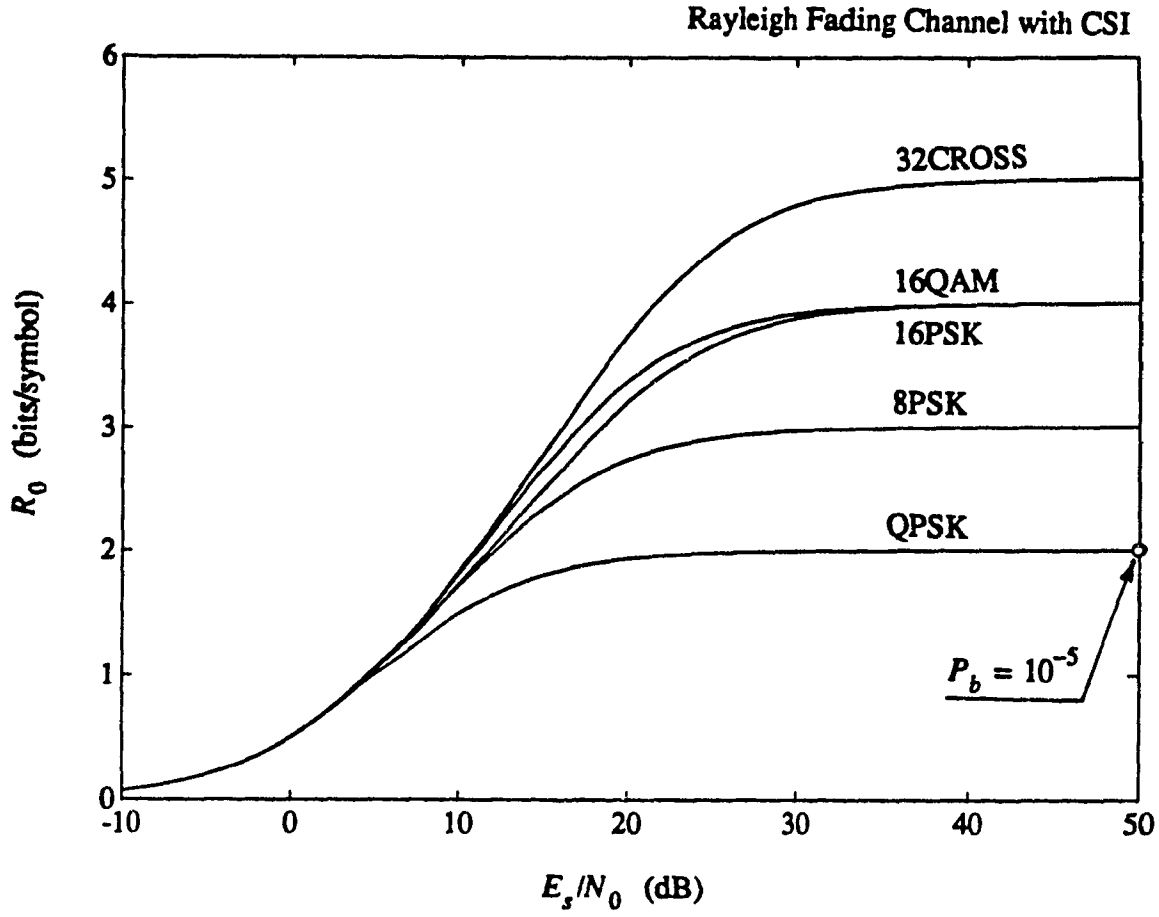

Fig. 2.3. Cut-off rates for the Rayleigh fading channel with channel state information.

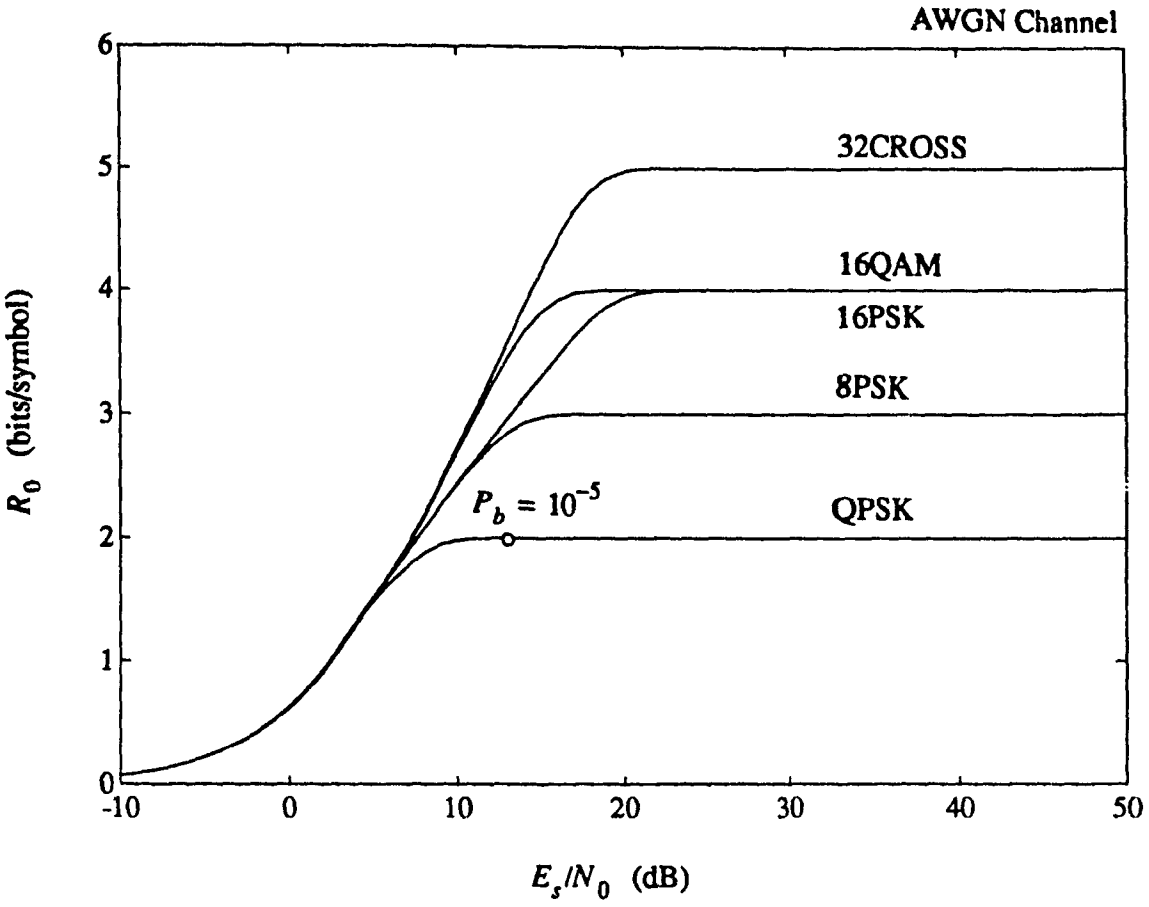

Fig. 2.4. Cut-off rates for the AWGN channel.

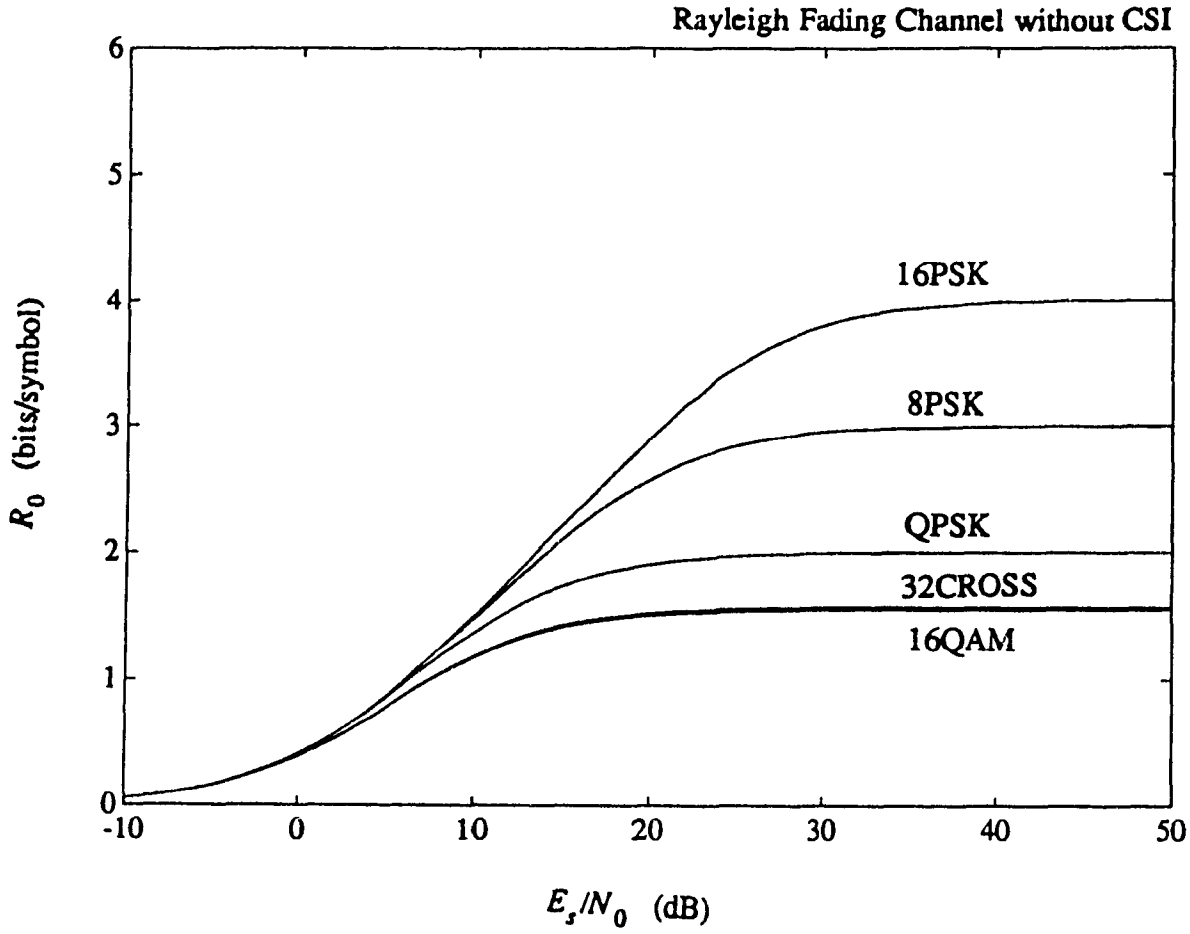

Fig. 2.5. Cut-off rates for the Rayleigh fading channel without the channel state information.

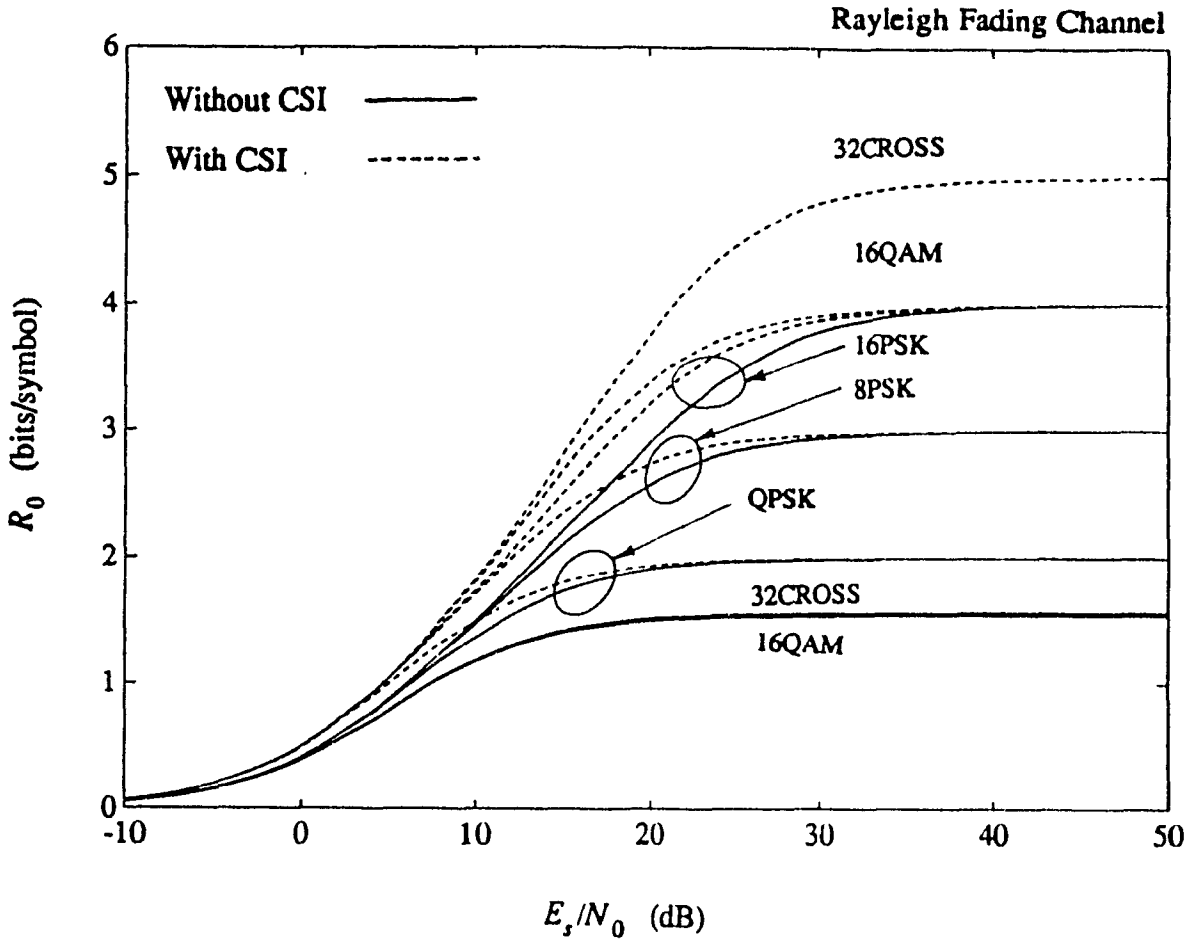

Fig. 2.6. Comparison between the cut-off rates of the Rayleigh fading channel with and without the channel state information.

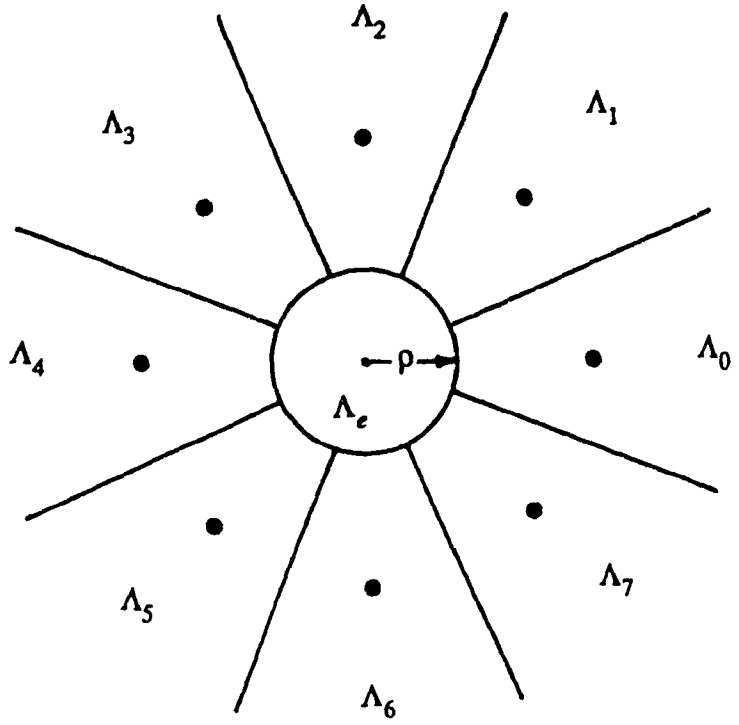

Fig. 2.7. Decision regions for an 8PSK signal set with an erasure region.

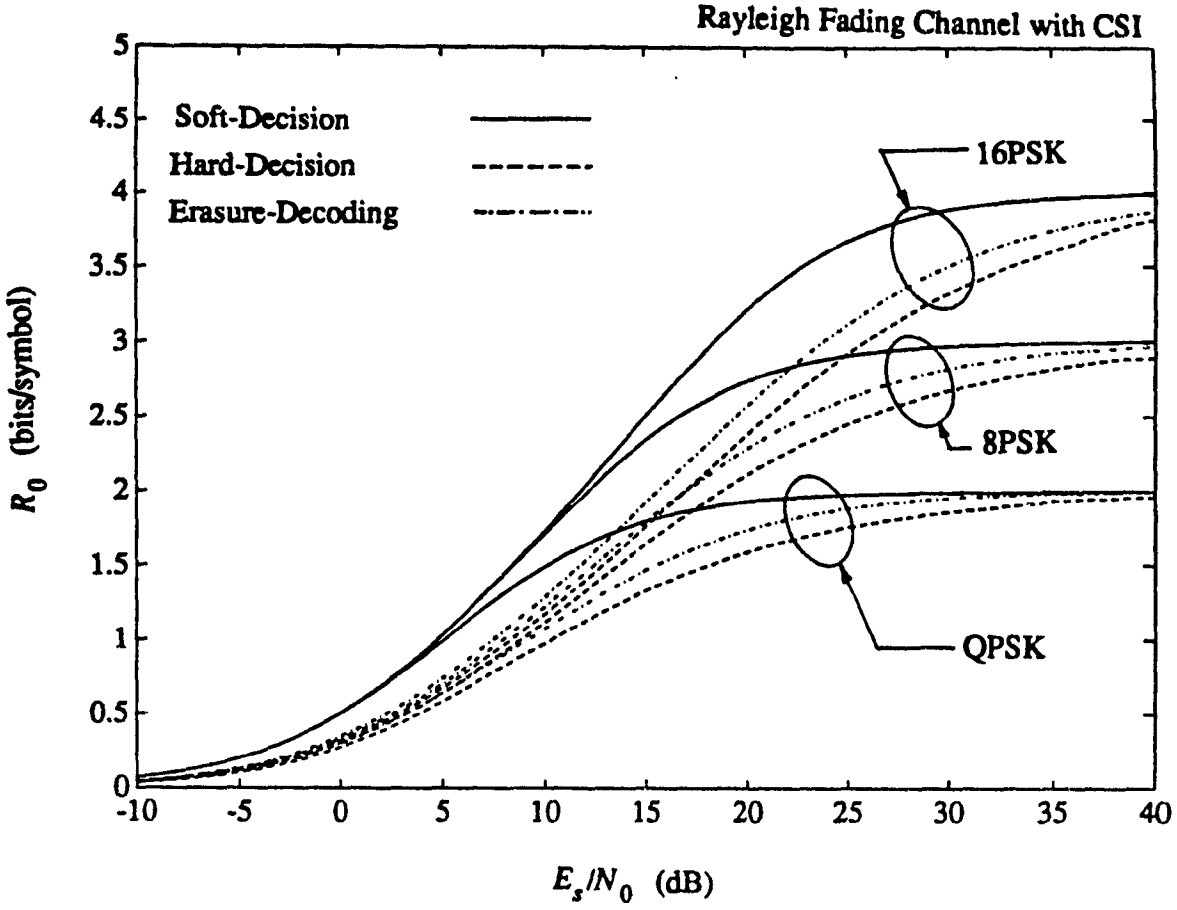

Fig. 2.8. Comparison of the cut-off rates for the Rayleigh fading channel with channel state information for some MPSK signal sets using different decoding strategies.

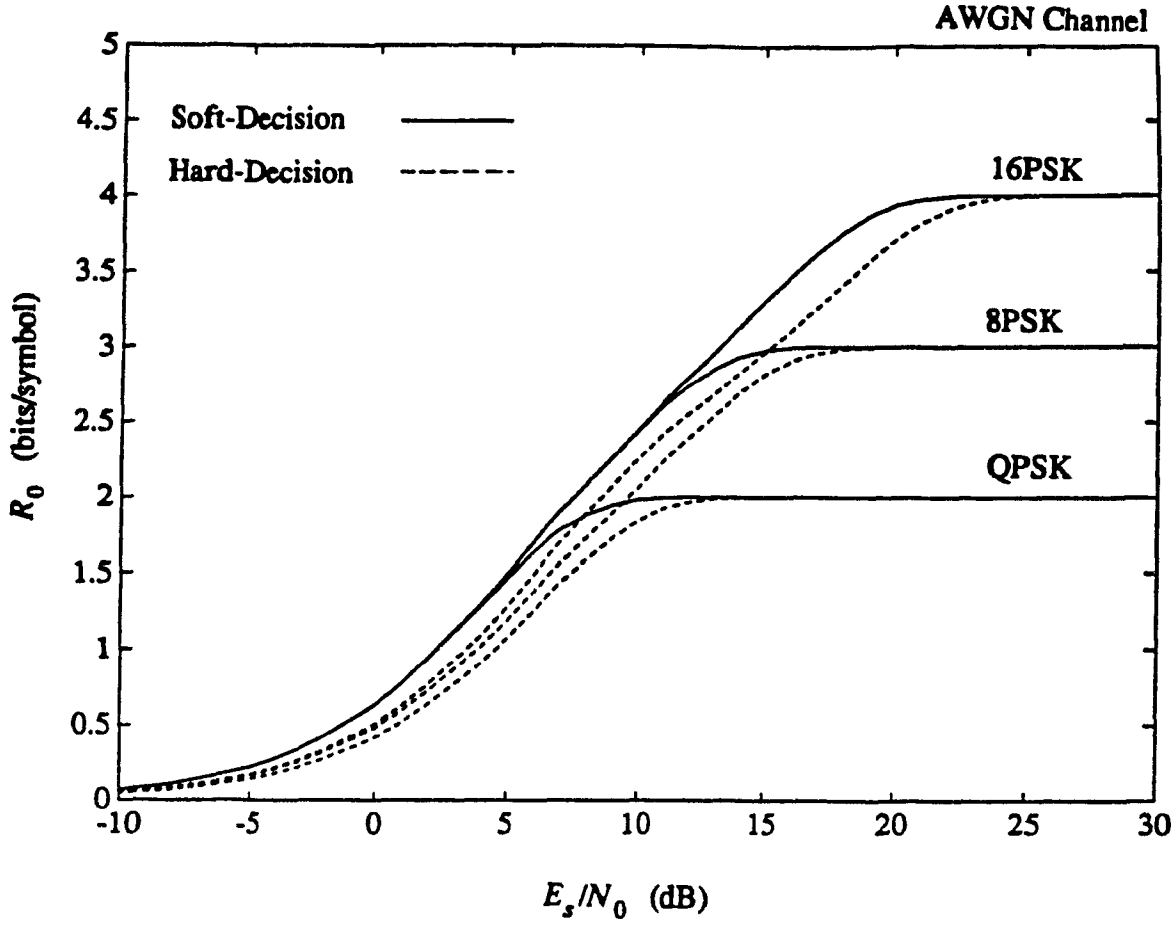

Fig. 2.9. Comparison of the cut-off rates for the AWGN channel for some MPSK signal sets using different decoding strategies.

CHAPTER 3

TRELLIS-CODED MODULATION SCHEMES

The purpose of this chapter is to give a brief background on the Trellis-Coded Modulation (TCM) schemes as the first developed bandwidth-efficient coded-modulation schemes, introduced by Ungerboeck. After giving a historical background on the development of these schemes we will explain the set-partitioning technique as a tool for designing TCM schemes. The performance measures of the TCM schemes will be briefly discussed. The rest of this chapter will be devoted to evaluating the performance of TCM schemes over fading channels. This performance analysis provides some code design criteria for fading channels, different from the AWGN one, which will be used for designing the strong coded schemes for fading channels in the following chapters.

3.1. HISTORICAL BACKGROUND

Designing a reliable communication system depends on different parameters. One of these parameters is the communication channel which is characterized by its frequency response and noise level. Some of the communication channels like telephone channels are only bandwidth-limited and signal-to-noise ratio in these channels is high enough so that the channel can support a number of bits/Hz of bandwidth. To satisfy the bandwidth limitation, one can employ bandwidth-efficient modulation techniques such as Multi-Phase Shift Keying (MPSK), Quadrature Amplitude Modulation (QAM), and the various forms of Continuous Phase Modulation (CPM) techniques. For the power-limited channels where the power is limited rather than the bandwidth, like deep-space commun-

ication channel, Forward Error Correcting (FEC) coding is usually used. Some channels like mobile satellite channels not only are bandwidth-limited but also are power-limited. In such cases usually it is not possible to achieve the desired throughput with either modulation techniques or coding techniques acting alone. Instead, what is required is the integration of a bandwidth-efficient modulation scheme with some form of FEC coding to exploit the best possible attributes of both.

Traditionally, coding and modulation have been treated as separate operations with regard to overall system design. In this traditional approach to channel coding, encoding is performed separately from modulation in the transmitter; likewise for decoding and detection in the receiver. Moreover, error control is provided by transmitting additional redundant bits, which has the effect of lowering the information bit rate per channel bandwidth. That is, bandwidth efficiency is traded for increased reliability.

In order to make a more efficient use of the available bandwidth and power, coding and modulation have to be treated as a single entity. In fact Massey [8] was among the first to show that to obtain considerable performance improvement, the modulation system must be designed based on unconventional basis. He predicted " *the coding techniques such as sequential decoding, Viterbi decoding and threshold decoding all of which employ convolutional codes and make use of the soft decision information provided by the demodulator, will then naturally suggest themselves as solution to the design of coded portion of the over-all digital communication system* [8]." Following this approach, Ungerboeck showed in the pioneering paper [9] that by combining convolutional codes with bandwidth-efficient modulation techniques considerable gains in terms of SNR can be achieved compared to the uncoded situation, sacrificing neither data rate nor bandwidth. His motivation for developing this new coding and modulation technique, called trellis-coded modulation, initially came from work on multilevel systems that employ the Viterbi Algorithm (VA) to improve signal detection in the presence of intersymbol interference [10]. This work provided him with ample evidence of the impor-

tance of the *Euclidean distance* between signal sequences. Considering this fact, he noticed that codes *should be designed based on maximizing the minimum Euclidean distance between coded sequences rather than Hamming distance*, and that *the redundancy necessary for coding would have to come from an expansion in the signal set*. By computing the capacity of channels with AWGN for the case of discrete multilevel modulation at the channel input and unquantized signal observation at the channel output he observed, *that coding gains of about 7-8 dB over conventional uncoded multilevel modulation are achievable*, and, *that an expansion of the signal set by a factor of two is sufficient for most cases* [9].

In the following we review the main aspects of the trellis-coded modulation schemes and consider the performance of these schemes on both the AWGN and fading channels. The design criteria of TCM schemes for these channels are obtained from performance analysis.

3.2. TRELLIS-CODED MODULATION FOR THE AWGN CHANNEL

In classical digital communication systems, the function of modulation and error-correction coding are separated. Modulators and demodulators convert an analog waveform channel into a discrete channel, whereas encoder and decoder correct errors that occur on the discrete channel. Conventional encoder and decoder for error correction operate on *binary*, or more generally *Q-ary*, code symbols transmitted over a discrete channel. Since the decoder receives only discrete code symbols, *Hamming distance* is the appropriate measure of distance for decoding and hence for the code design. The codes with larger minimum Hamming distance d_h provide more error correction capability and better performance. However, this can only be achieved by increasing the number of redundant symbols which causes transmission rate loss.

Generally, there exist two possibilities to compensate for the rate loss: increasing the modulation rate if the channel permits bandwidth expansion, or enlarging the signal set of the modulation system if the channel is bandwidth-limited. First approach has been

used successfully for channels constrained in energy but not in bandwidth like deep-space communication channel[1]. The latter leads to the use of non-binary modulation However, when modulation and error-correction coding are performed in the classical manner, disappointing results are obtained. Two problems contribute to this unsatisfactory situation.

One problem in the coded systems arises from the *hard amplitude or phase decisions* made in the demodulator prior to the final decoding. This causes an *irreversible* loss of information, which in the binary case is equivalent to approximately a 3 dB loss in signal-to-noise ratio [56]. The remedy for this problem is to employ *soft decision* decoding, which means that the decoder operates directly on the unquantized "soft" output samples of the channel. If the *Maximum Likelihood (ML)* criterion is applied in soft decoding of the unquantized demodulator output, then the decision rule of the optimum sequence decoder will depend on the *minimum Euclidean distance*. In other words, the optimum decoder chooses the code sequence which is closest to the received sequence in terms of the squared Euclidean distance. In this decoding scheme, the most probable error occurs between signals or signal sequences, one transmitted and the other decoded, that are closest together in terms of squared Euclidean distance. Hence, in such a case the appropriate design criterion for coded schemes is maximizing the minimum Euclidean distance between the coded sequences.

The second problem becomes apparent when the optimum sequence decisions are made based on Euclidean distances. *Mapping of code symbols of a code optimized for Hamming distance into nonbinary modulation does not guarantee that a good Euclidean distance is obtained* In general, one cannot even find a monotonic relationship between Hamming and Euclidean distances, no matter how code symbols are mapped [1] [10].

By looking at modulation and encoding as a single aspect of the signal design prob-

[1] The squared Euclidean and Hamming distances are equivalent only in the case of binary modulation or 4-PSK modulation, which merely corresponds to two orthogonal binary modulations of a carrier

lem and likewise demodulation and decoding as a single aspect of the signal detection problem, the problems encountered in classical approach of error-correction coding on bandwidth-limited channels can be easily overcome.

In *coded-modulation* techniques the modulation is considered as an integral part of encoding process and is designed in conjunction with the code to increase the *minimum Euclidean distance* between pairs of coded signals. The key to this integrated modulation and coding approach is to devise an effective method for mapping the coded bits into signal points such that the minimum Euclidean distance is maximized. Furthermore, using the maximum likelihood decoding technique based on unquantized samples (soft decision), demodulation and decoding is integrated in one step, avoiding the loss of information due to the hard decision prior to the decoding process. Such a method was developed by Ungerboeck [9], and is based on the principle of *mapping by set partitioning*.

3.2.1. Mapping by Set Partitioning

In TCM schemes in order to transmit m bits in each signaling interval a redundant 2^{m+1}-ary signal set is used. The m input bits are encoded by a rate $m/(m+1)$ trellis encoder and $m+1$ encoded bits are mapped to the signal points of the 2^{m+1}-ary signal set in such a way that the minimum Euclidean distance between channel-signal sequences is maximized. This is done by a rule called *mapping by set partitioning* [9]. This rule is based on successive partitioning of the 2^{m+1}-ary signal set into *subsets* with increasing minimum Euclidean distances $\Delta_0<\Delta_1<\Delta_2<\cdots$ between the signals of these subsets. The partitioning is repeated $\tilde{m}+1$ times ($\tilde{m} \le m$) until $\Delta_{\tilde{m}+1}$ is equal or greater than the desired minimum Euclidean distance of the TCM scheme to be designed. The set partitioning of an 8-PSK signal set is shown in Fig. 3.1 as an illustrative example.

A general structure of a TCM encoder is shown in Fig. 3.2. In this figure, at each time instant n, a block of m information bits ($b_n^m, b_n^{m-1}, \ldots, b_n^1$) enters the TCM encoder. From these m information bits, $\tilde{m} \le m$ bits are expanded by a rate $\tilde{m}/(\tilde{m}+1)$ binary

convolutional encoder into $\tilde{m}$ + 1 coded bits. The convolutional encoder can be considered as a *finite state machine,* which at each time interval n, accepts $\tilde{m}$ binary bits $(b_n^{\tilde{m}}, b_n^{\tilde{m}-1}, ..., b_n^1)$, makes a transition from its initial state S_n to one of the $2^{\tilde{m}}$ possible successor states S_{n+1} and outputs one of the $2^{\tilde{m}+1}$ $(\tilde{m}+1)$-tuples. The $(\tilde{m}+1)$-tuples are used to select one of the $2^{\tilde{m}+1}$ subsets of a 2^{m+1}-ary signal set. The remaining $m-\tilde{m}$ uncoded bits determine which of the $2^{m-\tilde{m}}$ signals in this subset to be transmitted.

It is traditional and instructive to describe a convolutional code by means of a trellis diagram. Such a diagram shows the time evolution of the coded sequences. The number of states in the trellis diagram of a TCM scheme depends on the memories in the encoder. For an encoder with ν memories the total number of states is 2^{ν}. The connection (transitions) between consecutive states in the trellis diagram depends upon the encoder. For an encoder with $m = \tilde{m}$ the states are joined by *single transitions* while for encoder with $m > \tilde{m}$, $2^{m-\tilde{m}}$ *parallel transitions* exist between states. These parallel transitions are associated with the $2^{m-\tilde{m}}$ signals of the subsets in the lowest layer of the set partitioning tree.

Denoting the minimum Euclidean distance between parallel transitions by $\Delta_{\tilde{m}+1}$ and the minimum distance between non-parallel paths in the TCM trellis diagram by $d_e(\tilde{m})$, the minimum distance of a TCM code can be expressed as [11]

$$d_e = \min [\, \Delta_{\tilde{m}+1}, d_e(\tilde{m}) \,]. \tag{3.2.1}$$

Note that in the special case of $m = \tilde{m}$, the subsets contain only one signal and the minimum distance of the TCM code is determined solely by the code trellis diagram.

Fig. 3.3 represents the encoder and the code trellis diagram of a rate 2/3 4-state 8PSK TCM. This scheme is designed [9] for coded transmission of 2 bits/T in the AWGN channel and its performance is compared with an uncoded QPSK which has the same transmission rate. Using (3.2.1) the minimum squared Euclidean distance of this TCM scheme is found to be 4, which is determined by parallel transitions. Thus, this scheme

provides a

$$g_\infty = 10 \log_{10}(4/2) = 3dB$$

asymptotic coding gain compared to uncoded QPSK without any sacrifice in bandwidth efficiency.

3.2.2. Performance Measures

The performance of a TCM scheme over the AWGN channel can be evaluated by considering different performance measures. The minimum Euclidean distance between all possible pairs of infinitely long code sequences is an important performance measure which is usually used as the code design criterion over the AWGN channel. Besides this measure, the performance of TCM schemes can be evaluated based on the different parameters considered in the following.

Number of sequences at minimum distance $N(d_e)$: For a given sequence, this parameter gives the number of neighbors at distance d_e, and hence those with which it is more likely to be confused by the receiver [10], [30]. This number is used, together with d_e, to obtain an asymptotic expression for the *error event* probability defined in the following.

Error event probability P_e: Two paths of finite length through the trellis diagram of the code form an error event if they start form the same state, merge in the same state, and do not simultaneously occupy the same state in between. Mathematically speaking, an error event of length l is defined by two coded sequences $\mathbf{s}_t$ and $\hat{\mathbf{s}}_t$ as [30]

$$\begin{aligned} \mathbf{s}_t &= (s_t, s_{t+1}, \ldots, s_{t+1+l}) \\ \hat{\mathbf{s}}_t &= (\hat{s}_t, \hat{s}_{t+1}, \ldots, \hat{s}_{t+1+l}) \end{aligned} \tag{3.2.2}$$

such that

$$\begin{aligned} &S_t = \hat{S}_t \qquad S_{t+l} = \hat{S}_{t+l} \\ &S_i \neq \hat{S}_i \qquad i = t+1, \ldots, t+l-1, \end{aligned} \tag{3.2.3}$$

where S_i and $\hat{S}_i$ denote the state of the code sequences s and ŝ at time i, respectively. The probability of an error event starting at time t, given that the decoder has estimated the correct transmitter state at that time is called error event probability or P_e.

Bit error probability P_b: This is the most important performance measure for the user and is defined as the expected number of decoded information bit errors per information bit.

Coding gain g: This parameter is defined as the difference between the values of coded and uncoded signal-to-noise ratios required to achieve the same event error (or bit error) probability:

$$g \equiv SNR\,|_{uncoded} - SNR\,|_{coded} \qquad (dB). \tag{3.2.4}$$

At high signal-to-noise ratios, it is possible to show that [30]

$$g_\infty \equiv g\,|_{SNR \to \infty} = 10 \log_{10} \frac{\left[d_e^2 / P_{av} \right]_{coded}}{\left[d_e^2 / P_{av} \right]_{uncoded}}, \tag{3.2.5}$$

where g_∞ represents the *asymptotic coding gain* and P_{av} is the average signal power. Note that (3.2.5) shows once again the importance of the minimum Euclidean distance.

3.2.3. Performance Evaluation on the AWGN Channel

The performance of the TCM schemes is evaluated by means of upper and lower bounds for the error probability. This is done based on the *generating function approach* [53], [58], which has been extensively applied in the performance evaluation of convolutional codes. This approach involves finding a generating function for the code which, when combined with a union bound, gives the upper bound on the probability of error attainable by the code.

The generating function is derived from the state diagram of the code and expresses the weight distribution of the code in closed form. This function enumerates the dis-

tance, length, and the number of errors on any incorrect path, compared to the correct one, at any step in the Viterbi decoding process. For linear codes, without loss of generality, it is assumed that the correct path is the all-zero code word. In such a case the generating function is obtained as a transfer function of a state diagram containing 2^{ν} states [58], where ν is the memory of the code.

Generally speaking, the TCM schemes are nonlinear. The Euclidean distance between any incorrect path and the correct one depends upon the correct path. In such a case the error probability bound still can be derived by the generating function approach. However, the generating function in this case is obtained as a transfer function of an expanded pair state diagram containing $2^{2\nu}$ states [53], [59], [60]. This approach is extremely general, but has a computational complexity increasing with the squared number of states in the trellis diagram of the code.

Among the TCM schemes, some of them have the *Uniform Error Property* (UEP) [30], [61]. According to [30] UEP means that every code word has the same weight distance distribution, or the same error event probability. Ungerboeck's codes [9] can be considered as a class of codes with such property [61]. The UEP permits the error bounds to be evaluated with the same approach used for linear convolutional codes with the computational complexity of 2^{ν} instead of $2^{2\nu}$ [30], [61].

3.2.3.1. Lower Bound on P_e

The error bounds will be evaluated for TCM schemes on fading channels in more details later. However, here we summarize these bound for the AWGN channel. Let assume that the sequence $\mathbf{s}$ is transmitted. The probability of selecting the sequence $\hat{\mathbf{s}}$ instead of the correct one, $\mathbf{s}$, is called the pairwise error probability. The error event probability is lower-bounded by evaluating the pairwise error probability for a sequence at minimum distance from the correct one. This lower bound is expressed [30] as

$$P_e > \frac{1}{2} erfc\left[\frac{d_e}{\sqrt{8}\,\sigma}\right], \tag{3.2.6}$$

where $\sigma^2 = N_0/2E_s$ is the variance of the noise at the output of the matched filter (see Chapter 2, Section 2.2a). This lower bound is general and is applicable to both codes with and without UEP.

3.2.3.2. Asymptotic Estimate on P_e

Considering $N(d_e)$ an asymptotic estimate of the error event probability (at high signal-to-noise ratios) is obtained [10] as

$$P_e \geq \frac{1}{2} N(d_e)\, erfc\left[\frac{d_e}{\sqrt{8}\,\sigma}\right]. \tag{3.2.7}$$

Note that the asymptotic estimate is also applicable to the codes with or without UEP provided that in the latter $N(d_e)$ to be considered as the *average* number of near neighbors at minimum distance d_e.

3.2.3.3. Upper Bounds on P_e and P_b The upper bound on the error event probability for the codes with UEP can be obtained using the generating function approach applied for linear convolutional codes. This upper bound is expressed [30] as

$$P_e \leq \frac{1}{2} N(d_e)\, erfc\left[\frac{d_e}{\sqrt{8}\,\sigma}\right] . e^{d_e^2/8\sigma^2} . T(D)\,|_{D\,=\,\exp(-1/8\sigma^2)}, \tag{3.2.8}$$

where $T(D)$ represents the generating function of the code obtained from the state digram. The probability of bit error is derived from the generating function which enumerates the distance as well as the number of bit errors on any incorrect path. Representing this generating function by $T(D, I)$ the upper bound on P_b is expressed [30] as

$$P_e \leq \frac{1}{2m} N(d_e)\, erfc\left[\frac{d_e}{\sqrt{8}\,\sigma}\right] . e^{d_e^2/8\sigma^2} . \frac{\partial T(D, I)}{\partial I}\,|_{I\,=\,1,\ D\,=\,\exp(-1/8\sigma^2)}. \tag{3.2.9}$$

It is shown [30] that the same upper bound on the error event probability and bit error

probability can be obtained for general TCM schemes, replacing $T(D)$ and $T(D, I)$ in (3.2.8) and (3.2.9), respectively, by corresponding generating functions derived from the expanded pair state diagram of the code.

3.3. ANALYTICAL DESCRIPTION OF THE TCM SCHEMES

In the previous section TCM schemes were introduced as a convolutional code and a rule (mapping by set partioning) that maps the output of this code onto a fixed signal constellation. Calderbank and Mazo in [13] combine these two steps into one and introduce a new description of these schemes, analytical rather than graphical, which express the TCM output as a series of expansion of products (of all orders) of the encoder bits. This method can be used in obtaining the performance bounds. In the following their approach is briefly described.

Assume a rate $m/(m + 1)$ TCM scheme with ν memories in its encoder. The output of this scheme (each channel symbol) depends not only on the most recent m bits, but also on the ν previous bits, i.e.,

$$s_n = f(b_n, b_{n-1}, \ldots, b_{n-(\nu+m)+1}), \tag{3.3.1}$$

where s_n is the transmitted channel symbol at time n, and b_i's are the input bits to the encoder. Dropping the time index n for convenience and assuming that the encoder input bits are represented by ±1, (3.3.1) can be written as a sum of products of b_i's [13],

$$\begin{aligned} s &= f(b_1, \ldots, b_m, b_{m+1}, \ldots, b_{\nu+m}) \\ &= d_0 + \sum_{i=1}^{\nu+m} b_i d_i + \sum_{\substack{i,j=1 \\ j>i}}^{\nu+m} b_i b_j d_{ij} + \cdots + b_1 \cdots b_{\nu+m}\ d_{1\ldots(\nu+m)}. \end{aligned} \tag{3.3.2}$$

Regarding $2^{\nu+m}$ values taken by s, by a column vector **s**, and also each product of the variables b_i as $2^{\nu+m}$-length vector $\mathbf{d} = (d_0, d_1, \cdots, d_{1\ldots(\nu+m)})$, the above equation can be written as

$$\mathbf{s} = \mathbf{B}_{II} \cdot \mathbf{d}, \tag{3.3.3}$$

where $\mathbf{B}_{II}$ is a $2^{\nu+m} \times 2^{\nu+m}$ matrix, whose each row represents the $2^{\nu+m}$ values taken by all products of the b_i's called for in (3.3.2) for each sequence $b_1, b_2, ..., b_m$. If $\boldsymbol{\beta}$ is a vector corresponding to a particular product of the b_i's (i.e., a column of $\mathbf{B}_H$), then as shown in [62], the corresponding coefficient of that product in the expansion of (3.3.2) is simply obtained from

$$d = \frac{1}{2^{(\nu+m)}} \cdot \boldsymbol{\beta}^T \cdot \mathbf{s}, \tag{3.3.4}$$

where the "T" superscript denotes the transpose operation.

Knowing the modulator output corresponding to the all possible input sequence of length $m+1$, the coefficients $\{d_i\}$ can be determined from (3.3.4). This completes the description of the TCM codes, analytically.

3.4. PERFORMANCE OF THE TCM SCHEMES OVER FADING CHANNELS

TCM schemes can be used for transmission of reliable digital information over bandwidth limited fading channels. It is shown that [34], [37] when combined with interleaving/de-interleaving of sufficient depth, these schemes can provide significant coding gains compared to the uncoded ones, provided that some new designing criteria are utilized in designing the code. To obtain these criteria we first evaluate the performance of the trellis coded MPSK schemes over a Rician fading channel as an illustrative example.

A general block diagram of a TCM system on a fading channel is shown in Fig. 3.4. Input bits are encoded by a trellis encoder. The encoded digits are interleaved and mapped to an MPSK symbol. Transmitted signal is faded and corrupted by AWGN in passing through the fading channel. At the receiver the in-phase and quadrature components of the received signal are demodulated, quantized for soft decision, and de-interleaved. Using these quantized components, the Viterbi decoder detects the

transmitted sequence based on maximum likelihood estimation. To improve the performance of the system, the Channel State Information (CSI) may be used in the decoding process. This is shown by thee dashed line.

The Performance analysis of the system under consideration depends upon different parameters such as the type of the demodulation, the decoding metric, the presence or absence of the CSI. Assume that coherent detection with ideal interleaving/de-interleaving, and the ML decoding metric defined by (2.3.9) is used. Then using the union bound technique, the average bit error probability is upper bounded as

$$P_b \le \sum_{\mathbf{s},\hat{\mathbf{s}} \in C} \sum a(\mathbf{s}, \hat{\mathbf{s}}) \cdot p(\mathbf{s}) \cdot P_2(\mathbf{s}, \hat{\mathbf{s}}), \tag{3.4.1}$$

where $a(\mathbf{s}, \hat{\mathbf{s}})$ enumerates the number of bit errors between the correct sequence $\mathbf{s}$ and the erroneous sequence $\hat{\mathbf{s}}$, $p(\mathbf{s})$ is *a priori* probability of transmitting $\mathbf{s}$, and C shows the set of all coded sequences. Also $P_2(\mathbf{s}, \hat{\mathbf{s}})$ represents the pairwise error probability of $\mathbf{s}$ and $\hat{\mathbf{s}}$, specified by (2.3.11). Using the results of Chapter 2, the pairwise error probability is obtained as

$$\begin{aligned} P_2(\mathbf{s}, \hat{\mathbf{s}}) &\le \min_{\lambda} C(\mathbf{s}, \hat{\mathbf{s}}, \lambda) \\ &= \min_{\lambda} \prod_{n \in \eta} C(s_n, \hat{s}_n, \lambda), \end{aligned} \tag{3.4.2}$$

where $C(s_n, \hat{s}_n, \lambda)$ is defined as the Chernoff factor of signals s_n and $\hat{s}_n$ (see Chapter 2, Section 2.3.2) and η represents the set of all n for which $s_n \neq \hat{s}_n$. This factor for a Rician fading channel with a pdf of (2.1.8), and for decoding strategies with/without CSI is obtained in Appendix A. Using the results of this appendix the bit error probability is derived in the following.

3.4.1. Decoding with CSI

Using (A.12) the pairwise error probability of (3.4.2) for the case with CSI is obtained as

$$P_2(\mathbf{s}, \hat{\mathbf{s}}) \le \prod_{n \in \eta} \frac{1+K}{1+K+(E_s/4N_0)|s_n - s_{\hat{n}}|^2} \exp\left[-\frac{K(E_s/4N_0)\,|s_n - \hat{s}_n|^2}{1+K+(E_s/4N_0)|s - \hat{s}_n|^2} \right], \quad (3.4.3)$$

which simplifies at high signal-to-noise ratios to

$$P_2(\mathbf{s}, \hat{\mathbf{s}}) \le \prod_{n \in \eta} \frac{(1+K)e^{-K}}{(E_s/4N_0)\,|s_n - s_{\hat{n}}|^2}. \quad (3.4.4)$$

Note that the pairwise error probability for a Rayleigh fading channel can be simply obtained from (3.4.3) or (3.4.4) by setting $K = 0$.

The upper bound of the bit error rate at high SNR's is obtained by substituting (3.4.4) into (3.4.1) as

$$P_b \le \sum_{\mathbf{s}, \hat{\mathbf{s}} \in C} \sum a(\mathbf{s}, \hat{\mathbf{s}}) \cdot p(\mathbf{s}) \cdot \frac{(1+K)^l e^{-lK}}{(E_s/4N_0)^l} \cdot \frac{1}{\beta_l^2}, \quad (3.4.5)$$

where l is the number of unlike symbols of the sequences $\mathbf{s}$ and $\hat{\mathbf{s}}$ (i.e., the number of elements in η) and β_l^2 is the product of the distances between these unlike symbols defined as

$$\beta_l^2 \equiv \prod_{n \in \eta} |s_n - \hat{s}_n|^2. \quad (3.4.6)$$

We postpone the extraction of any conclusion from this performance analysis until deriving the upper bound of the bit error probability for the case of decoding without CSI.

3.4.2. Decoding without CSI

The pairwise error probability in this case is obtained from (A.18) with $|s_n| = |\hat{s}_n|$ (MPSK signal set) as

$$P_2(\mathbf{s}, \hat{\mathbf{s}}) \le \min_{\lambda} \prod_{n \in \eta} \exp\left[\lambda^2 \frac{E_s}{N_0} \cdot |s_n - \hat{s}_n|^2 \right] \frac{e^{-K}}{\pi} \int_0^{\pi} (1 - \sqrt{\pi} erfc(v) e^{v^2} v) \cdot d\theta, \quad (3.4.7a)$$

where ν is defined by (A.18b) as

$$\nu = \frac{\lambda E_s/2N_0 \, |s_n - \hat{s}_n|^2}{\sqrt{1+K}} - \sqrt{K}\cos(\theta). \tag{3.4.7b}$$

The pairwise error probability of (3.4.7.a) can be simplified at high signal-to-noise ratios by noticing that the first term of (3.4.7.b) dominates and ν becomes independent of θ. In this case, the evaluation of the integral becomes trivial and after some mathematical manipulations, (3.4.7a) simplifies to [34]

$$P_2(\mathbf{s}, \hat{\mathbf{s}}) \le \frac{\exp\left[\lambda^2 \cdot E_s/N_0 \sum_{n\in\eta} |s_n - \hat{s}_n|^2\right] \cdot (1+K)^l \cdot e^{-lK}}{2^l \lambda^{2l} (E_s/2N_0)^{2l} \cdot \beta_l^2}. \tag{3.4.8}$$

Optimizing the Chernoff parameter λ provides a tighter upper bound for $P_2(\mathbf{s}, \hat{\mathbf{s}})$ [34] as

$$P_2(\mathbf{s}, \hat{\mathbf{s}}) \le \frac{(2e/l)^l}{(E_s/N_0)^l} \cdot \frac{\left[\sum_{n\in\eta} |s_n - \hat{s}_n|^2\right]^l}{\beta_l^2} \cdot (1+K)^l \cdot e^{-lK}, \tag{3.4.9a}$$

with the optimum value of λ being

$$\lambda_{opt}^2 = \frac{l}{(E_s/N_0) \sum_{n\in\eta} |s_n - \hat{s}_n|^2}. \tag{3.4.9b}$$

Substituting (3.4.9a) into (3.4.1) gives the upper bound on the bit error probability as

$$P_b \le \sum_{\mathbf{s},\hat{\mathbf{s}}\in C}\sum a(\mathbf{s}, \hat{\mathbf{s}}) \cdot p(\mathbf{s}) \cdot \frac{(2e/l)^l}{(E_s/N_0)^l} \cdot \frac{\left[\sum_{n\in\eta} |s_n - \hat{s}_n|^2\right]^l}{\beta_l^2} \cdot (1+K)^l \cdot e^{-lK}, \tag{3.4.10}$$

Some concluding remarks can be extracted from the upper bound evaluation of the bit error probability. First, it is observed that the probability of bit error depends on l, the

length of the error event path, or the number of elements in η. For high signal-to-noise ratios the upper bounds of (3.4.5) and (3.4.10) are determined by the smallest value of l which corresponds to the error event path with the smallest number of discrepancies between the correct and erroneous sequences. This path, henceforth, is called the *shortest error event path* and its length is shown by L. Therefore, at high signal-to-noise ratios the bit error probability is approximated by

$$P_b \approx \alpha \cdot \left[\frac{(1+K)e^{-K}}{E_s/N_0} \right]^L \cdot \frac{1}{\beta_L^2}, \tag{3.4.11}$$

where β_L^2 denotes the *squared product of the distances along the shortest error event path.* For simplicity this parameter will be called *minimum product distance.* In (3.4.11) the parameter α is a constant that depends on the distance structure of the code and the presence or the absence of CSI.

We observe that P_b varies inversely with L-th power of the SNR. A larger L provides a better performance for TCM schemes operating in fading channels. This effect resembles what is normally achieved with *time* or *space diversity,* the difference being that no price is paid in terms of the increase in bandwidth or complexity. The parameter L, hence, is also called the *time diversity* of the TCM schemes.

3.5. TCM SCHEMES FOR FADING CHANNELS

Most of the TCM schemes appearing in the literature have been designed based on maximizing the minimum Euclidean distance. The choice of the minimum Euclidean distance as the performance criterion is justifiable when the channel being considered is the AWGN channel. However, for fading channels, the ability of TCM schemes to provide time diversity is very important. Fortunately, it is possible to achieve both coding gain and time diversity from TCM schemes. However, when two schemes are compared, the one that yields the best coding gain may not yield the best time diversity. In other words, the codes designed to be strong for the AWGN channel, can be quite poor for fading

channels and conversely suboptimal designs for the AWGN channel may be superior choices for fading channels.

3.5.1. Maximum Time Diversity of TCM Codes

Let's consider a conventional $m/m+1$ rate TCM scheme with ν memory in its encoder. The trellis diagram of such a code has 2^{ν} states and 2^{m} branches leaving each state during each symbol interval. Parallel transitions occur if ν is less than m, or when the trellis encoder has $(m-\tilde{m})>0$ uncoded bits (Fig. 3.2). It's shown that [42], [43] the maximum achievable time diversity, $L_{\max}$, is given by

$$L_{\max} = \left\lfloor \frac{\nu}{m} \right\rfloor + 1, \tag{3.5.1}$$

where $\lfloor\ \rfloor$ denotes integer truncation. Note that the maximum time diversity of the codes with parallel branches is limited to one. Also, L will always be equal to $L_{\max}$, if the number of symbols in the signal space, M, has its maximum value $2^{\nu+m}$. However, if M is less than its maximum value then the maximum time diversity factor might not be achieved.

In Tables 3.1 and 3.2 we list the time diversity for the set of rate 2/3 8PSK and rate 3/4 16PSK trellis codes designed by Ungerboeck [9] for the AWGN channel. It is observed that some of the Ungerboeck's codes have parallel transitions and, hence, provide a time diversity of one. The 4-state rate 2/3 8PSK TCM scheme and most of rate 3/4 16PSK TCM schemes can be given as examples. Furthermore, most of the Ungerboeck's codes with no-parallel transitions do not achieve the maximum time diversities.

In order to achieve the maximum time diversity, some authors have designed new TCM codes for fading channels [37], [44], [45]. These results are included in Table 3.1 for comparison. Besides these schemes, *Multiple Trellis-Coded Modulation* (MTCM) techniques are introduced in [35] for fading channels.

3.5.2. Multiple Trellis-Coded Modulation

The maximum time diversity of the conventional TCM schemes are limited by their structure. To remove this limit and provide more time diversity one can use MTCM schemes wherein more than one channel symbol is transmitted per trellis branch [22]-[24], [35]. The principle behind this technique is to design a rate $mk/(m+1)k$ $(k = 2,3,...)$ encoder and combine it through a suitable mapping rule with a 2^{m+1}-point signal set outputting k of these signal points in each transmission interval. In this case the length of the shortest error event path is always equal to or greater than the number of branches along this path. In view of (3.4.11), the possibility of a value L greater than the length (in branches) of the shortest path is significant and what affords multiple trellis coding the opportunity of improving trellis coding performance on the fading channels.

Although these schemes may provide more time diversity, but the buffer size of the Viterbi decoder for these schemes increases with the multiplicity of the code k. This brings more decoding delay which can be considered as a drawback when the overall transmission delay is limited by the nature of the transmission system. Less decoding delay is important particularly in the channels with burst errors when the large interleaving/de-interleaving size is necessary for destroying the memory of the channel. Hence, the schemes with less decoding delay may be preferable for these channels. In the next chapter we will design a conventional TCM scheme based on maximizing both time diversity and minimum product distance and compare its performance with similar schemes (with the same complexity) on a Rayleigh fading channel.

3.6. DISCUSSION

The performance evaluation of the trellis-coded schemes on fading channels leads to the TCM code design criteria for fading channels. One can say that although the TCM schemes on the AWGN channel is solely designed based on the minimum Euclidean distance, this design criterion is considered as a secondary parameter for high SNR's on

fading channels. The primary design criteria for high SNR's on fading channels are the length of the shortest error event path (time diversity), L, and the minimum product distance β_L^2. However, for small signal-to-noise ratios the minimum Euclidean distance may be considered as the important design criterion. This is shown by evaluating the pairwise error probability of (3.4.3) at low SNR's, as an illustrative example, in the following.

Assuming low SNR's, (3.4.3) is simplified by ignoring $E_s/4N_0|s_n - \hat{s}_n|^2$ with respect to $(1 + K)$ to

$$\begin{aligned} P_2(\mathbf{s}, \hat{\mathbf{s}}) &\le \prod_{n\in\eta} \exp\left[-\frac{K}{1+K} \cdot \frac{E_s}{4N_0} \cdot |s_n - \hat{s}_n|^2\right] \\ &= \exp\left[\sum_{n\in\eta} -\frac{K}{1+K} \cdot \frac{E_s}{4N_0} \cdot |s_n - \hat{s}_n|^2\right] \\ &= \exp\left[-\frac{K}{1+K} \cdot \frac{E_s}{4N_0} \cdot d_E^2\right]. \end{aligned} \tag{3.6.1a}$$

where d_E^2 denotes the Euclidean distance defined as

$$d_E^2 = \sum_{n\in\eta} |s_n - \hat{s}_n|^2. \tag{3.6.1b}$$

This shows that at low signal-to-noise ratios the performance of the TCM scheme over fading channel depends on the Euclidean distance rather than the length of the error event path. This is not surprising and can be explained intuitively. Between the fading process and the AWGN, the latter is more effective at low signal-to-noise ratios and, hence, dominates the bit error probability. To combat the noise component, one has to increase the Euclidean distance between the coded sequences. However, at high signal-to-noise ratios the effect of the channel fading amplitude is dominant. In this case increasing the time diversity of the code has been long known [2] as a remedy.

Table 3.1. Time Diversity of the Rate 2/3 8PSK TCM Codes.

ν	No. of states 2^{ν}	AWGN-Channels [9] No. of transitions between two states $2^{m-\hat{m}}$ $\hat{m}$		L	Fading-Channels [44], [45] No. of transitions between two states $2^{m-\hat{m}}$ $\hat{m}$		L	L_{max}
2	4	1	2	1	2	1	2	2
3	8	2	1	2	2	1	2	2
4	16	2	1	3	2	1	3	3
5	32	2	1	2	2	1	3	3
6	64	2	1	3	2	1	4	4
7	128	2	1	4	2	1	4	4
8	256	2	1	3	2	1	5	5
9	512	2	1	3	2	1	5	5
10	1024	2	1	4	2	1	5	6
11	2048				2	1	6	6

Table 3.2. Time Diversity of the Rate 3/4 16PSK TCM Codes.

ν	No. of states 2^{ν}	AWGN-Channels [9] No. of transitions between two states $2^{m-\hat{m}}$ $\hat{m}$		L	L_{max}
2	4	1	4	1	1
3	8	1	4	1	2
4	16	1	4	1	2
5	32	1	4	1	2
6	64	1	4	1	3
7	128	1	4	1	3
8	256	2	2	1	3

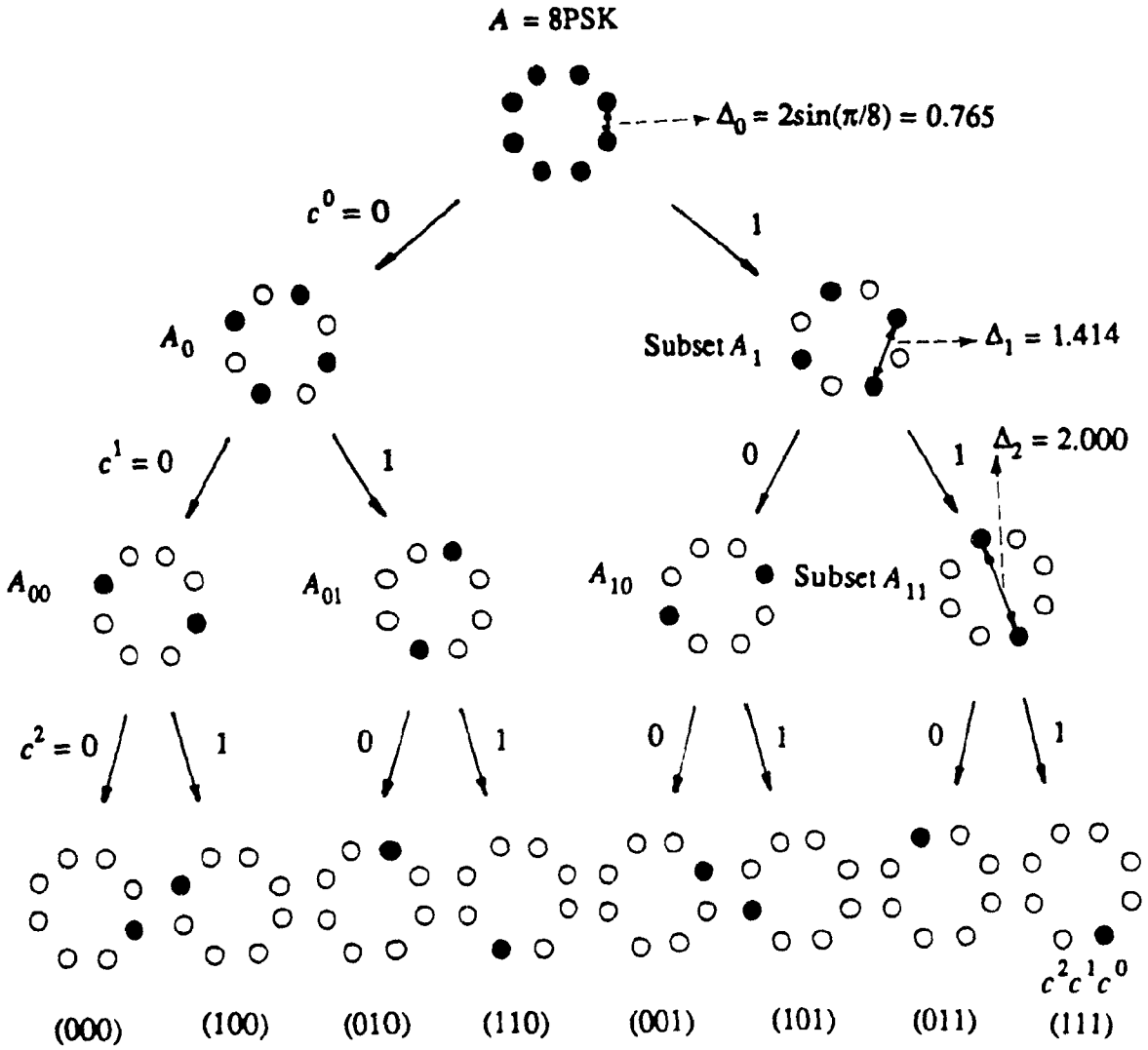

Fig. 3.1. Set partitioning of an 8PSK signal set.

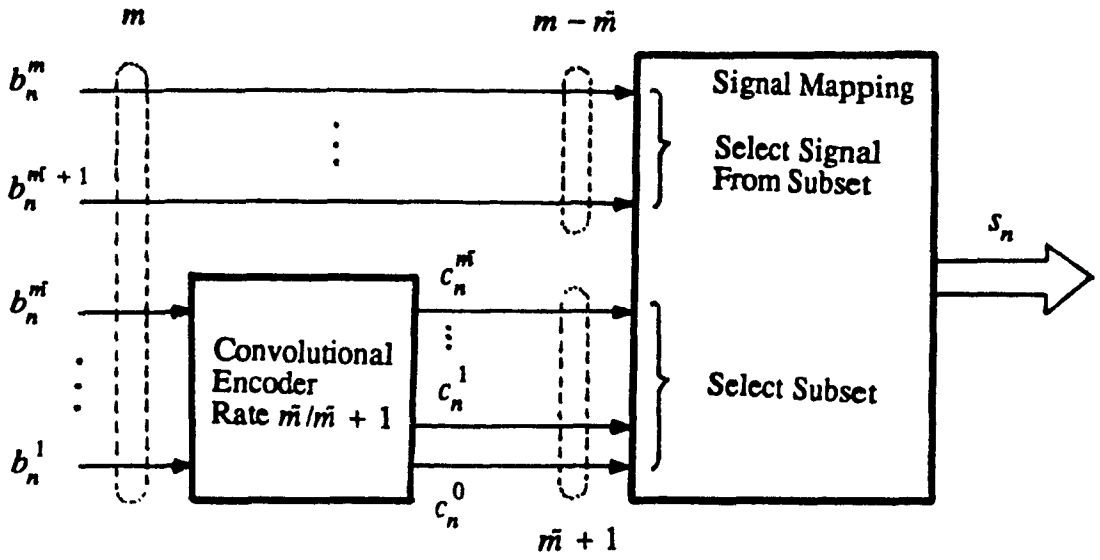

Fig. 3.2. General structure of a TCM encoder.

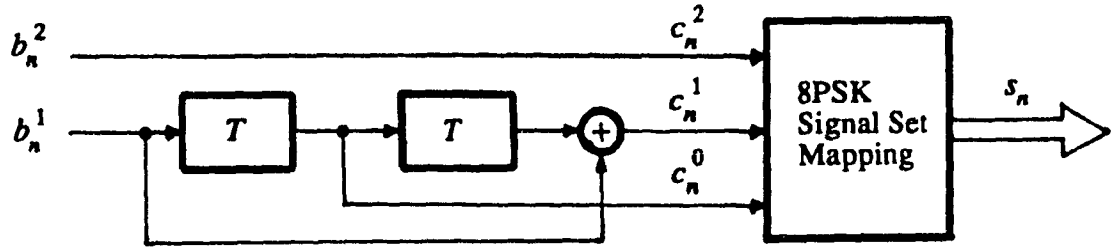

(a)

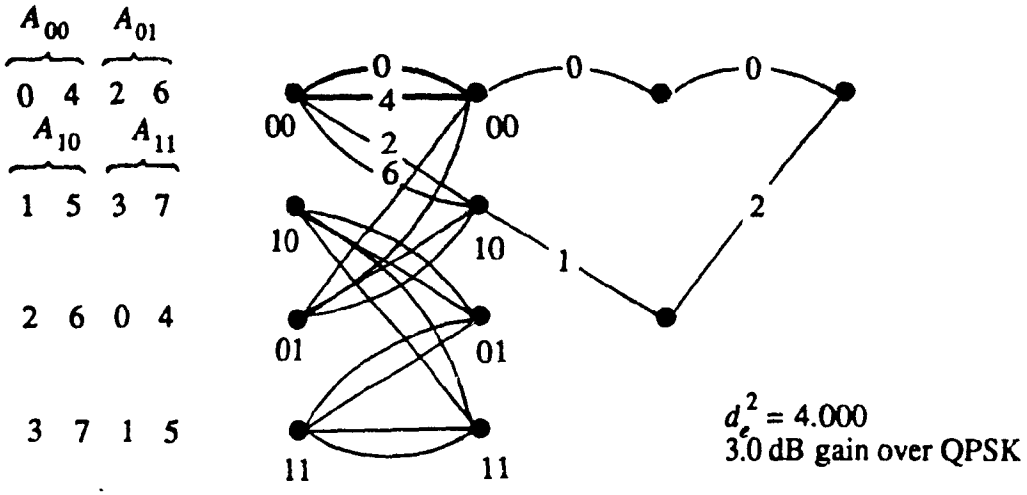

(b)

Fig. 3.3. The rate 2/3 4-state 8PSK TCM scheme [9];

(a) Encoder structure,

(b) Trellis diagram.

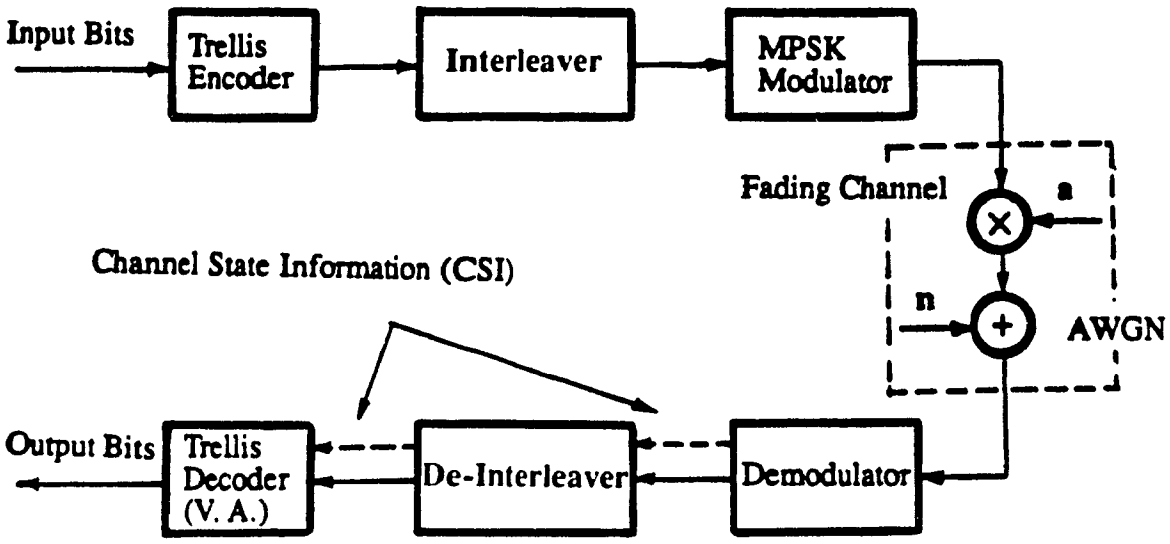

Fig. 3.4. Block diagram of TCM schemes on a fading channel.

CHAPTER 4

A TCM SCHEME FOR FADING CHANNELS

The previous chapter has described the concept and performance of trellis-coded modulation schemes operating over both the AWGN and fading channels. We observed that the design criteria for TCM in fading channels are different from that of the AWGN channel. Thus, TCM schemes designed to be strong for the AWGN channel can be quite poor for fading channels and suboptimal AWGN designs may be superior choices for fading channels. In this chapter a new 4-state rate 2/3 8PSK TCM scheme is designed based on the code design criteria for fading channels. Both the time diversity and the minimum product distance of the code are maximized. Some design rules are introduced to avoid the exhaustive computer search for designing the code. Using upper bound analysis and computer simulations we evaluate the performance of the new code and compare it with other 4-state 8PSK TCM schemes over a normalized Rayleigh fading channel. This comparison shows the superiority of the new scheme compared to the other 4-state schemes on fading channels.

4.1. 4-STATE RATE 2/3 8PSK TCM SCHEMES FOR FADING CHANNELS

The performance analysis of the TCM schemes over fading channels (Chapter 3, Section 3.4) leads to the conclusion that maximizing the shortest error event length (time diversity) and the product of the squared branch distances along that path (minimum product distance) is the main objective for the code design. A simple argument shows that maximizing the minimum product distance for codes with a small time diversity is more

effective than for codes with a large time diversity. Assume a TCM scheme with a time diversity L and a minimum product distance β_1^2. Suppose this code is redesigned to provide a minimum product distance β_2^2 with the same time diversity. Using (3.4.11), the increase in coding gain due to increasing the minimum product distance from β_1^2 to β_2^2 is obtained as

$$\Delta g_\infty \equiv SNR_1 - SNR_2|_{P_{b_1} = P_{b_2}} = (10/L) \cdot \log_{10}\left((\beta_2/\beta_1)^2 \cdot (\alpha_1/\alpha_2) \right), \qquad (4.1.1)$$

where α_1 and α_2 depend upon the distance structure of the schemes 1 and 2, respectively.

It is observed that the increase in the coding gain due to the increase in the minimum product distance is inversely proportional to the time diversity L. For instance, doubling the minimum product distance of a code with a time diversity of 2 provides 1.5 dB more coding gain (assuming the same α for both schemes), while the same increment in the minimum product distance yields only 0.75 dB more coding gain for a time diversity 4. Thus, we attempt to increase the minimum product distance for codes with small time diversities.

Ungerboeck's 4-state 8PSK TCM with 3 dB gain over uncoded QPSK on the AWGN channel was considered as an example in Chapter 3 (see Fig. 3.3). This code has been designed for the AWGN channel [9] and its trellis diagram contains parallel transitions implying that a one-step error events can occur. This limits the achievable shortest error event length to one. Thus, if this code is used over fading channels with interleaving, the asymptotic steepest rate of descent of P_b with E_s/N_0 will be inverse linear.

To increase the shortest error event length, parallel transitions must be avoided. For Rayleigh fading channels a 4-state 8PSK TCM without parallel transitions is suggested in [37]. Trellis diagram of this code is shown in Fig. 4.1. Hereafter this code is called Wilson's code. As it is seen the trellis diagram of Wilson's code is fully connected and results in shortest error event paths of length two, i.e., asymptotically the rate of descent

of P_b with E_s/N_0 follows the inverse square law. This is the maximum achievable time diversity with 4-state 8PSK TCM schemes (see (3.5.1)). The coding gain achieved by this code in the AWGN channel is 1.1 dB, which is 1.9 dB inferior to Ungerboeck's code.

This code has been designed to increase the shortest error event path length. However, the product of the squared branch distances along this path has not been optimized. Fig. 4.1 indicates that this parameter for the code is limited by $\beta^2(000,201) = \delta_1^2 \cdot \delta_2^2 = 1.172$ which is the product of the squared distances between unlike pairs of the paths (0,0,0) and (2,0,1) [1]. Note that this is an error event of actual length three but the shortest error event is of length two. In the following we shall introduce new rules to avoid such paths and shall design a new 4-state TCM based on maximizing β^2.

4.1.1. Code Design Rules

The trellis diagram of the 4-state 8PSK TCM scheme without parallel transitions is fully connected. This allows us to represent the signal associated with transitions between states of consecutive stages by a 4×4 matrix **B**, whose ij-th element is denoted by b_{ij}, representing the signal associated with the path from state i at stage k to state j at stage $k+1$ of the trellis diagram. Also, note that the elements of the i-th row indicates the associated signals with paths diverging from state i and the elements of the j-th column show the associated signals with paths remerging to state j.

Using set partitioning, the 8PSK signal set can be partitioned into two subsets $\mathbf{A}_0 = (0,2,4,6)$ and $\mathbf{A}_1 = (1,3,5,7)$ with intra-set distances δ_2 and δ_4. Signal points from either of the subsets $\mathbf{A}_0$ and $\mathbf{A}_1$ are assigned to the alternative rows of matrix **B**. To assign signal points to the elements of the matrix **B** the following rules are utilized. To express these rules we define the *"state difference"* as the *number of bits in which two states*

[1] We represent the distance between signals of an MPSK signal set by δ_i to avoid the confusion with Δ_i, defined as the minimum distance between signal points of a signal set at i-th step of set partitioning (see Chapter 3, Section 3.2.1)

differ. For instance, the *"state difference"* of the states 01 and 10 can be considered as two.

Rule 1: Elements of each row of matrix **B** are associated with signals from subsets A_0 or A_1 such that the distance between a pair of branches diverging from one state to two adjacent states with *"state differences"* two or one to be δ_2 or δ_4, respectively. This rule is shown schematically in Fig. 4.2.

This rule guarantees that the distance between each pair of diverging paths from state *i* is at least δ_2. The same rule cannot be applied for assigning the signal points to the elements in one column, since there will be at least two elements in one column whose distances differ only by δ_1. In other words, among the remerging branches to state *j* there will be at least one pair with distance δ_1 If we assign the signals with distance δ_1 to the pair of branches remerging to state *j* from the two states with a *"state difference"* of one, then the minimum product of squared branch distances of the error events of actual length two (diverging at stage *k* and remerging at stage *k*+2) will be limited to $\delta_1^2 . \delta_4^2 = 2.344$ which is greater than $\delta_1^2 . \delta_2^2 = 1.172$. Thus,

Rule 2: In assigning signal points to each column of the matrix **B**, the signals with distances δ_3 are associated with branches remerging to state *j* (column *j*) from two adjacent states with *"state difference"* of two. The pair of paths remerging to state *j* from two states with *"state difference"* of one may be associated with signals with distances δ_1 or δ_3.

By using rules 1 and 2 the minimum product of the squared distances of the error events of actual length two will be

$$\beta^2 = \min(\delta_1^2 . \delta_4^2 \ , \ \delta_2^2 . \delta_3^2) = \delta_1^2 . \delta_4^2 = 2.344 .$$

To limit β^2 to the error event path with actual length two the third rule is introduced as

Rule 3: The same signals can be used in two different columns whose associated states have *"state difference"* two. In other words, if a signal appears in column 1, it

can only be used in column 4, and the signals of column 2 can only be repeated in column 3.

This rule guarantees that the product of the squared branch distances for the shortest error events of length two and actual length three are always $\delta_2^2 . \delta_3^2 > \delta_1^2 . \delta_4^2$, since each pair of branches with like signals between stage $k+1$ and stage $k+2$ are connected to two adjacent states with *"state difference"* two and according to the second rule, remerging branches from these two adjacent states at stage $k+2$ to a state at stage $k+3$ have intra-set distance δ_3.

4.1.2. Code Design Example

Fig. 4.3 shows an example of the code design procedure in 4 steps. In the first step the signals from subset $\mathbf{A}_0$ are assigned to the first row of the matrix **B** according to rule 1. Using the third rule the elements of the third row can be obtained in step 2. For the signals of the second and the fourth rows the subset $\mathbf{A}_1$ must be used. At this stage we may use signal points 1 or 3 as the first element of the second row according to rule 2. Choosing 3, the second and the third elements of this row can be found as 7 and 1, respectively, according to rule 1 and rule 1 + rule 2. Finally, the fourth row of the matrix **B** can be obtained from the second row by using the third rule. This comp. tes the code design. The trellis diagram of this code is shown in Fig. 4.4*a*. If signal point 1 is chosen in step 2 another code will be obtained as Fig. 4.4*b*.

The minimum Euclidean distance of these code can be obtained simply by using the design rules as

$$d_e^2 = \min (\delta_1^2+\delta_4^2 , \delta_2^2+\delta_3^2 , \delta_1^2+\delta_1^2+\delta_2^2) = \delta_1^2+\delta_1^2+\delta_2^2 = 3.172,$$

which implies that the coding gain of these codes over uncoded QPSK on the AWGN channel is 2 dB which is only 1dB inferior to Ungerboeck's code. However, these new schemes provide 0.9 dB more coding gain compared to Wilson's scheme over the AWGN channel. Over fading channels the new schemes outperform Ungerboeck's code. Also,

the coding gain of the new schemes is more than that of Wilson's code over these channels. This can be justified by noting that β^2 for the new schemes is *doubled*.

4.1.3. Encoder Realization

The encoder of the new schemes may be realized using the analytical description of the TCM codes [16], [62] (see (3.2.2)). In the following the analytical description of the new scheme shown in Fig. 4.4*a* is obtained as an example. For this scheme the input and memory bits are associated with the phase of the channel input signals as follows

$$\begin{aligned}
\theta_0 &= f(1,1,1,1) = \pi/8 & \theta_4 &= f(1,1,-1,1) = 3\pi/8 \\
\theta_1 &= f(-1,1,1,1) = -7\pi/8 & \theta_5 &= f(-1,1,-1,1) = -5\pi/8 \\
\theta_2 &= f(1,-1,1,1) = 5\pi/8 & \theta_6 &= f(1,-1,-1,1) = 7\pi/8 \\
\theta_3 &= f(-1,-1,1,1) = -3\pi/8 & \theta_7 &= f(-1,-1,-1,1) = -\pi/8 \\
\theta_8 &= f(1,1,1,-1) = -7\pi/8 & \theta_{12} &= f(1,1,-1,-1) = -5\pi/8 \\
\theta_9 &= f(-1,1,1,-1) = \pi/8 & \theta_{13} &= f(-1,1,-1,-1) = 3\pi/8 \\
\theta_{10} &= f(1,-1,1,-1) = -3\pi/8 & \theta_{14} &= f(1,-1,-1,-1) = -\pi/8 \\
\theta_{11} &= f(-1,-1,1,-1) = 5\pi/8 & \theta_{15} &= f(-1,-1,-1,-1) = 7\pi/8.
\end{aligned} \tag{4.1.2}$$

Replacing (4.1.2) as a vector form ($\boldsymbol{\theta}$ instead of $\mathbf{s}$) in (3.3.4) and solving for d, the desired result is obtained as

$$\theta = (-b_3 + 4b_1b_4 - 2b_2b_3b_4)\pi/8. \tag{4.1.3}$$

The realization of the TCM encoder based on (4.1.3) is shown in Fig. 4.5*a*.

The analytical description involves multiplication, and the variables $\{b_i\}$ are not in (0, 1) form suitable for logic circuits. The Ungerboeck representation of TCM schemes (a linear convolutional encoder followed by a mapping rule), on the other hand, has a logic structure. Indeed, it is shown in [63], if the analytical expression of a rate $m/(m+1)$ TCM scheme has only $m+1$ terms (codes with minimal transmitter complexity) then a

convolutional encoder realization can be found using a simple procedure.

The scheme described by (4.1.3) is of minimal complexity and hence can be converted to the Ungerboeck representation. Assume a natural mapping is used in associating the outputs of the convolutional encoder to the signal points. Denoting the input and output bits of the convolutional encoder at time n by b_n^i $(i = 1,2)$ and c_n^j $(j = 0,1,2)$, respectively, the following associations are found

$$\begin{aligned} c_n^0 &= b_n^1 \oplus b_{n-1}^2 \qquad c_n^1 = b_n^2 \oplus b_{n-1}^1 \oplus b_{n-1}^2 \\ c_n^2 &= b_{n-1}^1, \end{aligned} \tag{4.1.4}$$

where $\oplus$ shows the modulo-2 addition. Equation (4.1.4) defines the underlying convolutional code. It is realized in Fig. 4.5*b*.

4.2. PERFORMANCE ANALYSIS

In this section the performance of the new scheme is evaluated by means of upper bound analysis and computer simulation for both the AWGN and Rayleigh fading channels. These results are compared with those of the other rate 2/3 4-state 8PSK schemes.

For upper bound analysis the generating function approach is used (see Chapter 3, Section 3.2.3). To avoid the higher computational complexity of the expanded pair state diagram some structural properties of the TCM encoder are exploited.

As it is explained in Chapter 3 TCM schemes are, in general, nonlinear and the assumption of the transmitted all-zero code word cannot be utilized in the evaluation of the error bounds. Instead, every possible code word should be considered as a transmitted one. This requires an error evaluation algorithm which has a computational complexity increasing with 2^{ν}, where ν is the memory length of the encoder.

It is shown in [61] and [64] that for a class of TCM schemes with Uniform Error Property (UEP), the error bounds can be found with a computational complexity of order 2^{ν}, the same as linear convolutional codes. According to [64] this approach can be

applied for TCM schemes with the following properties.

i) The TCM scheme consists of a binary (linear) convolutional code with a memoryless mapping from the encoder output to channel input signals.

ii) The weight profile of the signal subsets $\mathbf{A}_0$ and $\mathbf{A}_1$ (subsets of the first step of set partitioning) for a given error vector **e** is not a function of the subset under consideration.

The weight profile of a subset $\mathbf{A}_i$ for a given error vector **e** is defined as

$$F(\mathbf{A}_i, \mathbf{e}, D) = \sum a_\alpha D^\alpha, \tag{4.2.1}$$

where a_α is the number of channel signals in the subset A_i that have a squared Euclidean weight α with respect to **e**. The Euclidean weight α is defined as the squared Euclidean distance between $\mathbf{s} \in \mathbf{A}_i$ and $\mathbf{s} + \mathbf{s}_e$, where $\mathbf{s}_e$ is the channel signal corresponding to the error vector **e**. In (4.2.1) the sum is taken over all possible values of the Euclidean error weights with respect to **e**.

The second property is held for 8PSK TCM schemes which use the Ungerboeck approach in set partitioning. Consider the 8PSK signal set $\mathbf{A} = \{0, 1, ..., 7\}$ and its two subsets $\mathbf{A}_0 = \{0, 2, 4, 6\}$ and $\mathbf{A}_1 = \{1, 3, 5, 7\}$ at the first step of set partitioning. The weight profile of these subsets with respect to all possible values of **e** can be obtained using (4.2.1). Table 4.1 shows the results for both subsets $\mathbf{A}_0$ and $\mathbf{A}_1$. It is observed that these subsets have the same weight profiles with respect to **e** and thus the second condition is satisfied. In addition, condition 1 is also satisfied; see Fig. 4.5*b*.

We can now find the generating function of the new scheme using the error state diagram proposed in [64]. The branches of this diagram are labeled as $(1/2^m)\, I^r\, F(\mathbf{A}_0, \mathbf{e}, D)$ where r denotes the number of data bits corresponding to the branch error **e**. Using Table 4.1 the branch labels of the error state diagram shown in Fig. 4.6 are obtained as

$$
\begin{aligned}
t_1 &= t_9 = I\,D^{\delta_2^2} & t_{10} &= t_{12} = I\,D^{\delta_1^2} \\
t_2 &= t_4 = I\,D^{\delta_4^2} & t_{11} &= I^2 D^{\delta_1^2} \\
t_3 &= I^2 D^{\delta_2^2} & t_{13} &= D^{\delta_2^2} \\
t_5 &= t_8 = 0.5\,I\,(D^{\delta_1^2} + D^{\delta_1^2}) & t_{14} &= 0.5\,I^2\,(D^{\delta_1^2} + D^{\delta_1^2}) \\
t_6 &= 0.5\,I^2\,(D^{\delta_1^2} + D^{\delta_3^2}) & t_{15} &= D^{\delta_1^2}. \\
t_7 &= I^2
\end{aligned}
\tag{4.2.2}
$$

The encoder generator function is now obtained from the error state diagram of Fig. 4.6 by solving the nodal equations of this graph as outlined in [53]. This yields

$$T(D, I) = \xi_1 t_{13} + \xi_2 t_{14} + \xi_3 t_{15}, \tag{4.2.3a}$$

where

$$
\begin{bmatrix} \xi_1 \\ \xi_2 \\ \xi_3 \end{bmatrix} = \begin{bmatrix} 1 - t_4 & -t_{10} & -t_8 \\ -t_9 & 1 - t_5 & -t_{12} \\ -t_7 & -t_{11} & 1 - t_6 \end{bmatrix}^{-1} \cdot \begin{bmatrix} t_1 \\ t_2 \\ t_3 \end{bmatrix}. \tag{4.2.3b}
$$

After some mathematical manipulations, the transfer function $T(D, I)$ is simplified as

$$T(D, I) = \frac{A_1 I + A_2 I^2 + A_3 I^3 + A_4 I^4}{1 + B_1 I + B_2 I^2 + B_3 I^3 + B_4 I^4}, \tag{4.2.4a}$$

where

$$
\begin{aligned}
A_1 &= 1.5D^{4.000} + 0.5D^{4.586} \\
A_2 &= D^{5.414} + D^{6.586} - 0.5D^{8.586} - 0.5D^{11.414} \\
A_3 &= 0.5D^{3.172} - 0.25D^{5.172} + D^{5.414} - 0.5D^{8.000} - 0.5D^{8.828} \\
&\quad - D^{9.414} + 0.75D^{10.828}
\end{aligned}
$$

$$
\begin{aligned}
A_4 &= 0.5D^{3.172} + 0.75D^{5.172} - D^{7.172} - 1.5D^{8.000} - 0.5D^{8.828} \\
&\quad + 0.25D^{9.172} + 0.75D^{10.828} + 0.5D^{12.000} + D^{12.828} - 0.75D^{14.828} \\
B_1 &= -0.5D^{0.586} - 0.5D^{3.414} + D^{4.000} \\
B_2 &= -0.5D^{0.586} - D^{2.586} - 0.5D^{3.414} + 0.5D^{4.586} + 0.5D^{7.414} \\
B_3 &= -0.5D^{0.586} + 0.5D^{1.172} - 0.5D^{3.414} - 0.5D^{4.000} + 0.5D^{4.586} \\
&\quad + 0.25D^{6.828} + 0.5D^{7.414} \\
B_4 &= -0.75D^{1.172} + 0.5D^{3.172} + 0.5D^{4.000} - 0.25D^{5.172} + 0.25D^{6.828} \\
&\quad + 0.5D^{8.000} - 0.5D^{8.828} - 0.25D^{10.828}.
\end{aligned}
\tag{4.2.4b}
$$

The minimum Euclidean distance of the code can be obtained from the transfer function as follows [30]

$$
d_e^2 = \lim_{D \to 0} \frac{dT(D)/dD}{T(D)/D} = 3.172,
$$

which agrees with the previously obtained result.

4.2.1. Performance in the AWGN Channel

Using the transfer function $T(D, I)$, given in (4.2.4), the upper bound on the probability of bit error, $P_b(e)$, is obtained from (3.2.9). For the AWGN channel D is replaced by $e^{-1/8\sigma^2}$, where $\sigma^2 \equiv N_0/2E_s$ is the normalized variance of the AWGN (see Chapter 2, Section 2.2). The upper bound for the new 4-state scheme is plotted versus E_b/N_0 in Fig. 4.7. To compare with other 4-state schemes, the upper bound on $P_b(e)$ for Ungerboeck's code and Wilson's code are also included. To examine the tightness of the upper bounds computer simulation is performed. The results show that the upper bounds are quite tight for high signal-to-noise ratios.

The performance comparison of the 4-state schemes reveals that the new scheme outperforms Wilson's code but its performance is inferior to Ungerboeck's scheme in the AWGN channel. This is not surprising and can be explained by considering the minimum

Euclidean distance of these schemes.

4.2.2. Performance in the Rayleigh Fading Channel

For fading channels an upper bound on the bit error probability is developed in [32] as

$$P_b \le \frac{1}{m} \frac{\partial \bar{T}(D, I)}{\partial I} \Big|_{I = 1,\ D = \exp(-E_s/4N_0)}, \tag{4.2.5}$$

where $\bar{T}(D, I)$ is the transfer function of the error state diagram whose branch labels are modified from those of the no fading case as follows. In the absence of fading each branch label has a factor of $D^{\delta_i^2}$ (see (4.2.2)). For the fading case, $D^{\delta_i^2}$ is simply replaced by $E_a[\, D^{g\delta_i^2}]$ where the E_a denotes averaging over the fading amplitude and g is given as

$$g = \begin{cases} a^2 & with\ \ CSI \\ 4\lambda(a - \lambda) & without\ \ CSI. \end{cases} \tag{4.2.6}$$

In (4.2.6), a denotes the fading amplitude and λ is the Chernoff bound parameter. To perform averaging two cases are considered.

4.2.2.1. Fading Channel with CSI

In this case it is assumed that the fading amplitude is known at the receiver and the decoder uses this information in the decoding process. For a Rayleigh fading channel it is shown that [32]

$$E_a[\, D^{a^2\delta_i^2}] = \frac{1}{1 + \delta_i^2 E_s/4N_0}. \tag{4.2.7}$$

Using (4.2.5), (4.2.4) and (4.2.7) the upper bound on P_b versus E_b/N_0 is plotted in Fig. 4.8 for the new scheme along with the other 4-state TCM schemes.

4.2.2.2. Fading Channel without CSI

In the absence of the fading amplitude estimation at the receiver, it is shown that [32]

$$E_a[\,D^{4\lambda(a-\lambda)\delta_i^2}] = e^{\lambda^2\delta_i^2 E_s/N_0}\left[1-\sqrt{\pi}v\,.\,e^{-v^2}\,.\,erfc\,(v)\right], \tag{4.2.8a}$$

where

$$v \equiv \lambda\delta_i^2\frac{E_s}{2N_0}. \tag{4.2.8b}$$

The upper bound on P_b for this case is obtained by replacing $D^{\delta_i^2}$ in (4.2.2) by (4.2.8) and using (4.2.4) and (4.2.5). However, in this case the Chernoff parameter should be optimized for a tighter bound. This is done by means of numerical analysis. The upper bound for the new scheme on fading channel with CSI is compared with that of fading channel without CSI in Fig. 4.9. It is observed that the use of CSI improves the performance of the coded scheme about 1.5 dB.

4.2.3. Simulation Results

While the upper bound analysis reveals the dependency of the error rates to the code parameters, it could be very loose over the range of signal-to-noise ratios of interest. To predict the true system performance the development of computer simulation is required. Although this technique is straightforward and relatively easy to implement, but it requires an unacceptably large computer time when smaller values of error probability are needed.

The simulation in our study is based on Fig. 3.4. The channel is modeled as an additive white Gaussian noise with a time varying fading process **a**, representing the complex signal gain. The in-phase and quadrature components of the channel complex gain are generated as two independent Gaussian random variables. In such a case the fading amplitude is Rayleigh distributed. To implement the ideal interleaver/de-interleaver the samples of the fading process are generated independently.

The simulation results for the fading channels with and without CSI for three different TCM schemes are included in Fig.'s 4.7-4.10.

4.3. DISCUSSION

The results shown in Fig. 4.8 compares the performance of the three 4-state TCM schemes, namely, New scheme (4S-N), Wilson's scheme (4S-W) and Ungerboeck's code (4S-U). For error probabilities of 10^{-2} or less, the new scheme has better performance than the other two. The coding gain of this code for bit error probabilities in the area of 10^{-3}, which is important in digital speech transmission, is about 1.8 dB and 4.5 dB with respect to 4S-W and 4S-U codes, respectively. For the lower bit error probabilities, both the 4S-N and the 4S-W codes have significantly more coding gain than the 4S-U code because of their doubled time diversities. However, the performance of the 4S-N code is about 2 dB superior to that of the 4S-W code at high signal-to-noise ratios. This is because of the fact that the minimum squared product distance of the former is twice more than that of the latter.

The results of Fig. 4.10 shows the benefit of using the CSI in the decoding process for different 4-state codes. For Ungerboeck's code the use of the CSI slightly improves the performance of the scheme at low SNR's. However, its effect at high SNR's is negligible. This may be explained by considering the contribution of different error events with different lengths at low signal-to-noise ratios and the effect of the dominant error event with the shortest length at high SNR's. For this scheme the error events with length one are dominant at high signal-to-noise ratios. This means that for high SNR's the decision can be made only by observing the received signal in one signaling interval. Thus, in such a case the detection of the coded signals are similar to the detection of uncoded MPSK signals which is independent of the CSI because of their angular decision regions [2]. Based on this fact it seems that the use of CSI is more effective for the codes with higher time diversities. Fig. 4.10 shows that the improvement for 4S-W and 4S-N due to the use of CSI is about 1.5 dB

Table 4.1. Weight Profile of Subsets $\mathbf{A}_0$ and $\mathbf{A}_1$ with Respect to **e**.

Subsets of Channel Signals	**e**	Weight Profile
$\mathbf{A}_0$	0 0 0	4
$\mathbf{A}_0$	0 0 1	$4D^{\delta_1^2}$
$\mathbf{A}_0$	0 1 0	$4D^{\delta_2^2}$
$\mathbf{A}_0$	0 1 1	$2D^{\delta_1^2} + 2D^{\delta_3^2}$
$\mathbf{A}_0$	1 0 0	$4D^{\delta_4^2}$
$\mathbf{A}_0$	1 0 1	$4D^{\delta_3^2}$
$\mathbf{A}_0$	1 1 0	$4D^{\delta_2^2}$
$\mathbf{A}_0$	1 1 1	$2D^{\delta_1^2} + 2D^{\delta_3^2}$
$\mathbf{A}_1$	0 0 0	4
$\mathbf{A}_1$	0 0 1	$4D^{\delta_1^2}$
$\mathbf{A}_1$	0 1 0	$4D^{\delta_2^2}$
$\mathbf{A}_1$	0 1 1	$2D^{\delta_1^2} + 2D^{\delta_3^2}$
$\mathbf{A}_1$	1 0 0	$4D^{\delta_4^2}$
$\mathbf{A}_1$	1 0 1	$4D^{\delta_3^2}$
$\mathbf{A}_1$	1 1 0	$4D^{\delta_2^2}$
$\mathbf{A}_1$	1 1 1	$2D^{\delta_1^2} + 2D^{\delta_3^2}$

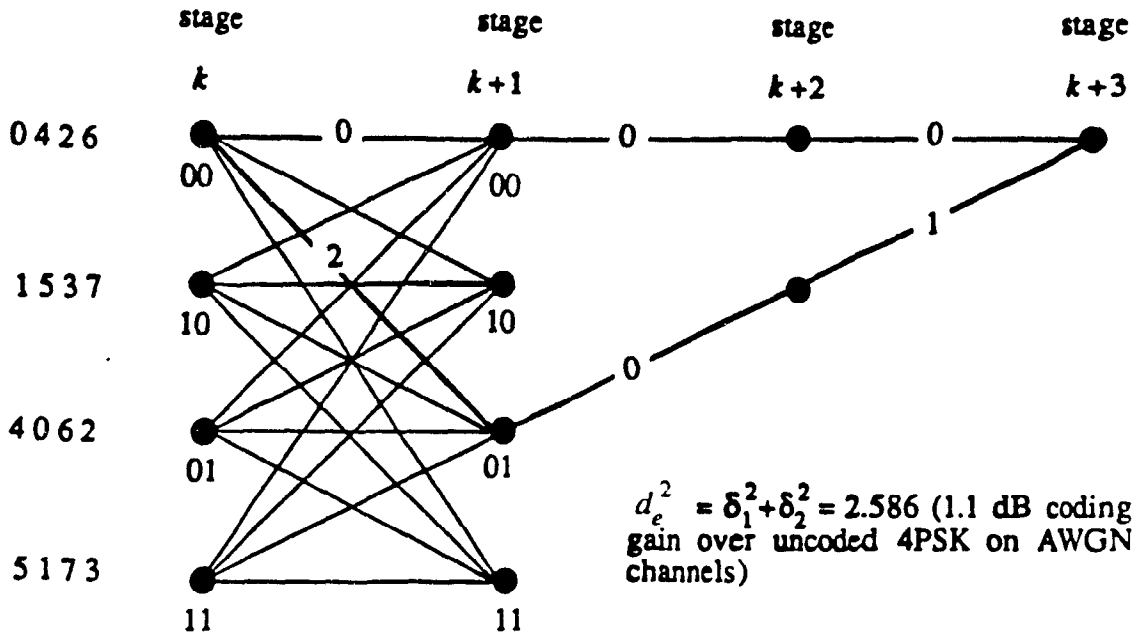

Fig. 4.1. The trellis diagram of a 4-state 8PSK TCM scheme without parallel transitions (Wilson's code).

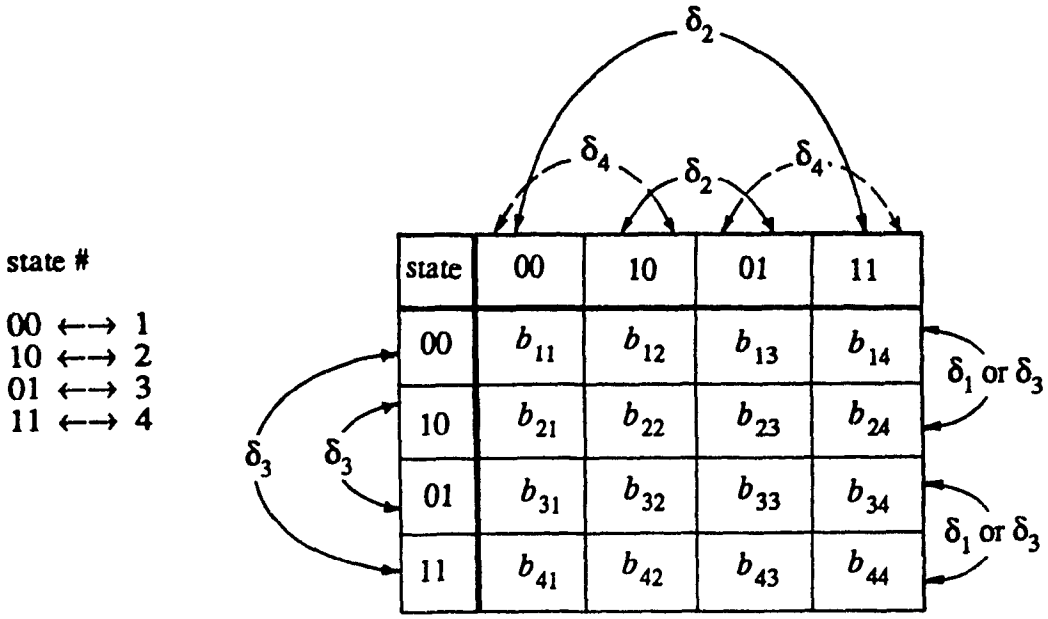

Fig. 4.2. The schematic representation of rules 1 and 2.

0 4 2 6	0 4 2 6	0 4 2 6	0 4 2 6
x x x x	x x x x	3 7 1 5	3 7 1 5
x x x x	6 2 4 0	6 2 4 0	6 2 4 0
x x x x	x x x x	x x x x	5 1 7 3
step 1	step 2	step 3	step 4

Fig. 4.3. The new 4-state 8PSK TCM code design procedure.

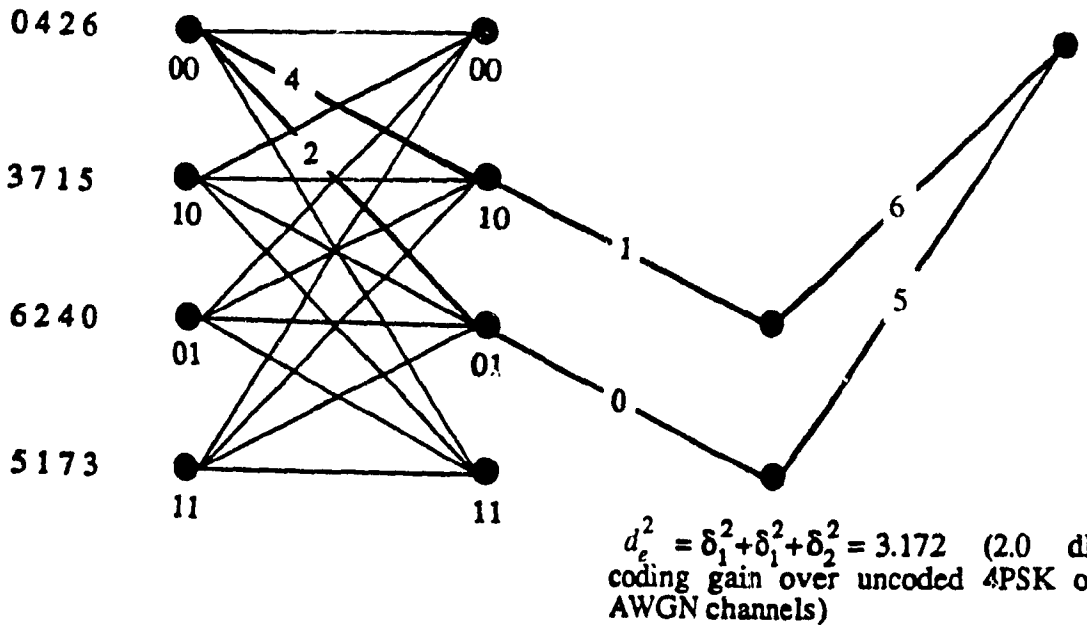

(a)

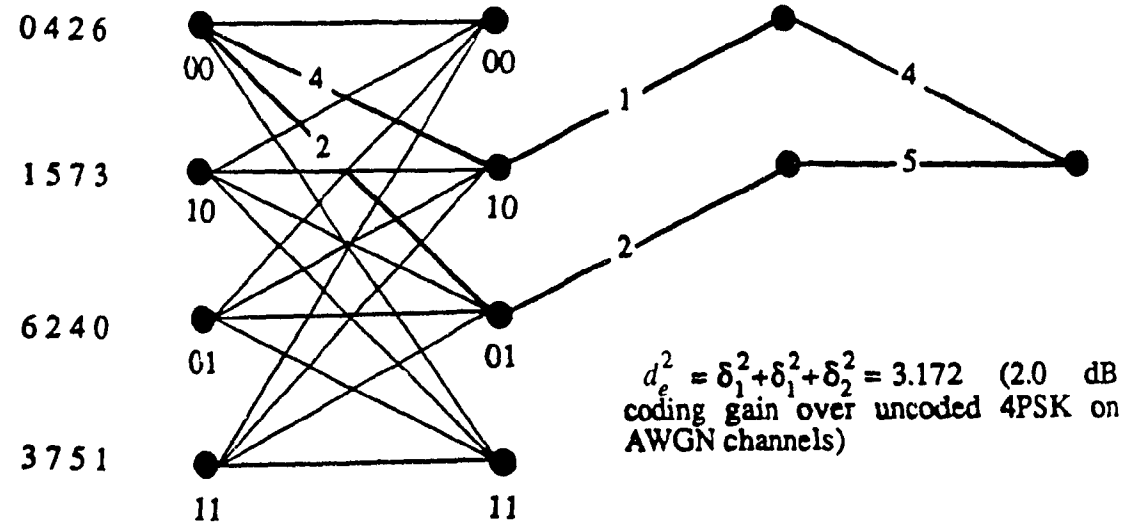

(b)

Fig. 4.4. The new 4-state 8PSK TCM codes designed for fading channels;

(a) TCM Scheme 1,

(b) TCM Scheme 2.

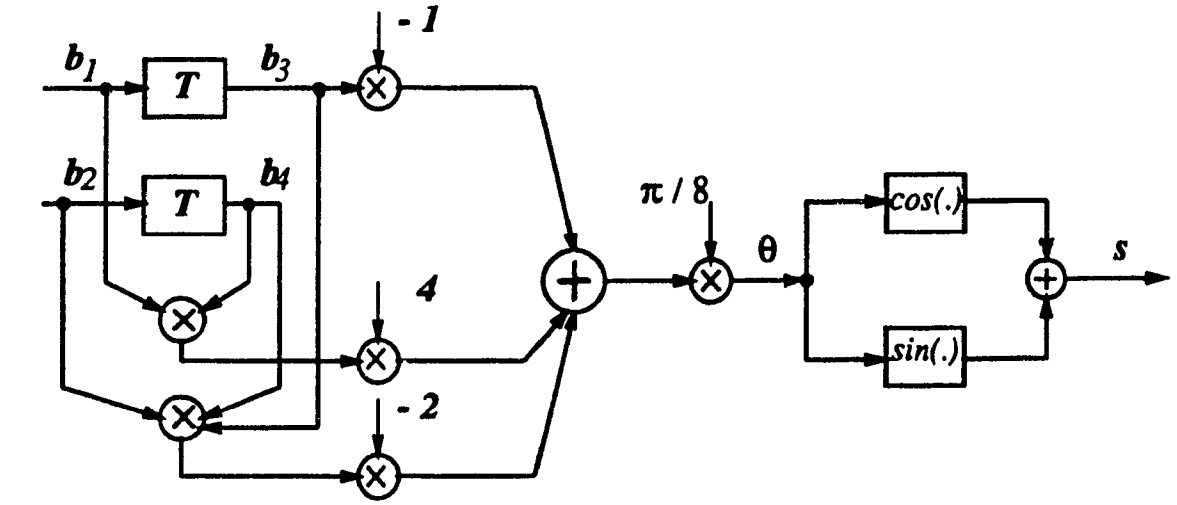

(a)

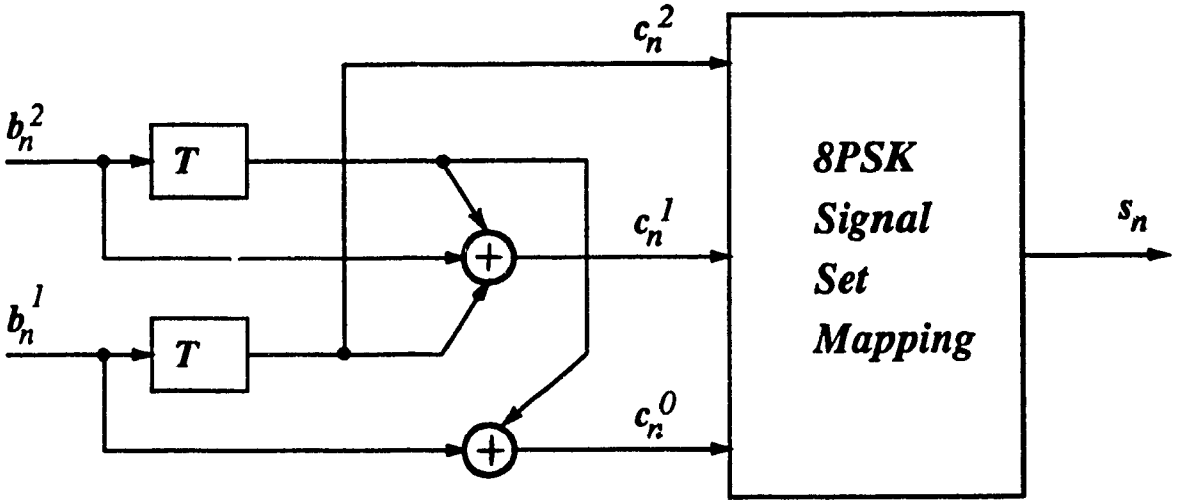

(b)

Fig. 4.5. Two different encoder realization of New TCM Scheme 1;

(a) Analytical approach,

(b) Ungerboeck's approach.

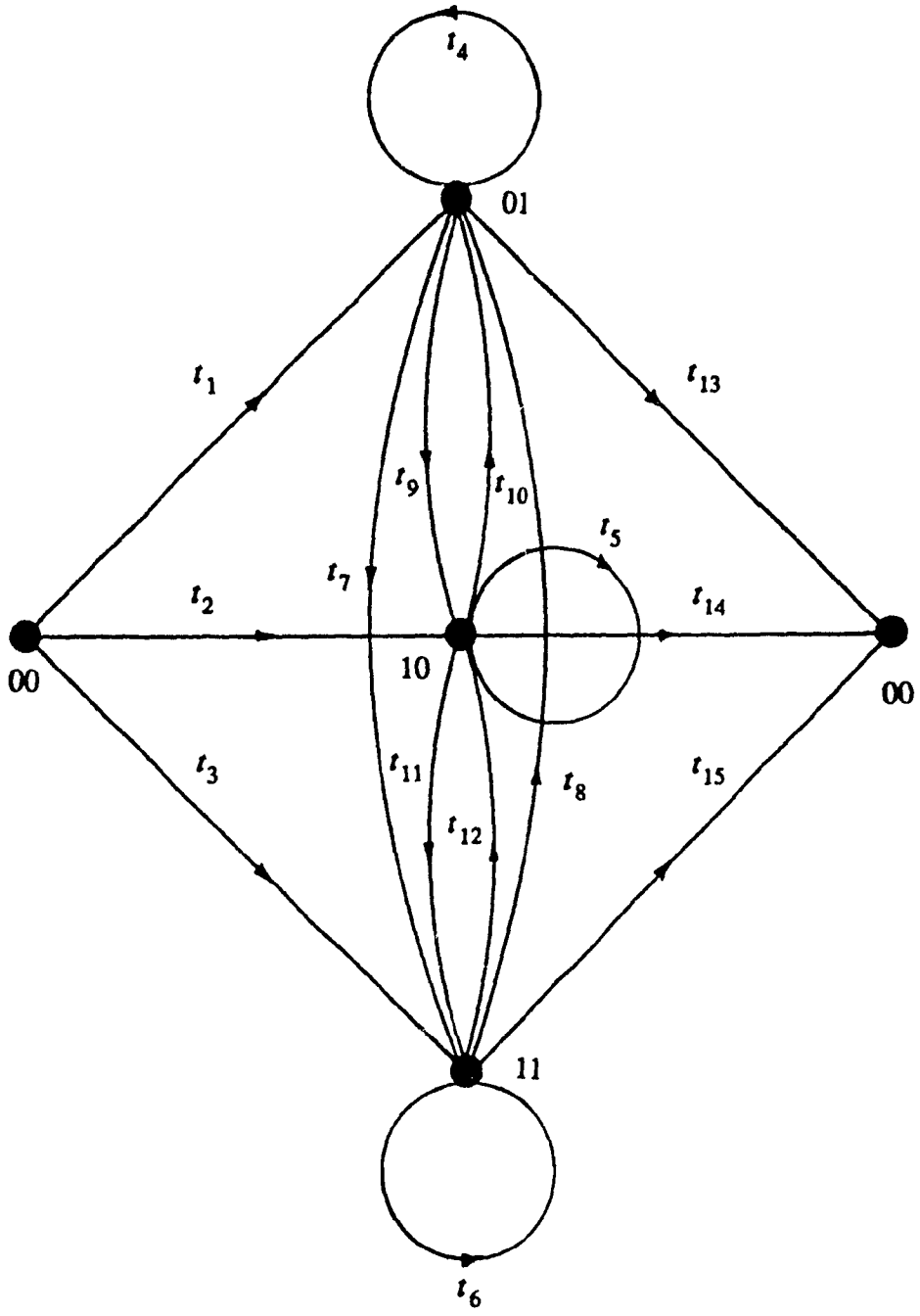

Fig. 4.6. Error state diagram of New TCM Scheme 1.

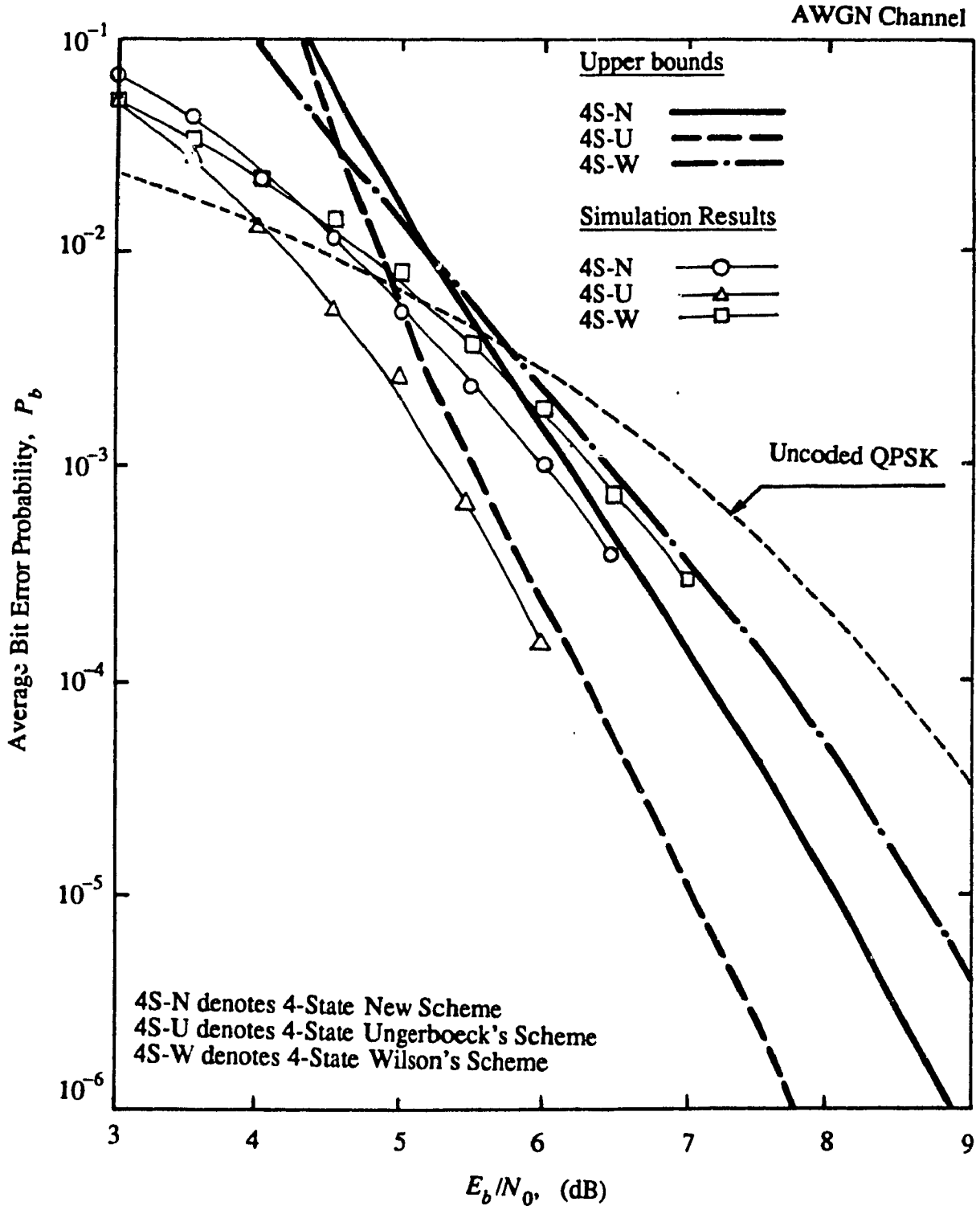

Fig. 4.7. The average bit error probability for different 4-state 8PSK schemes over the AWGN channel.

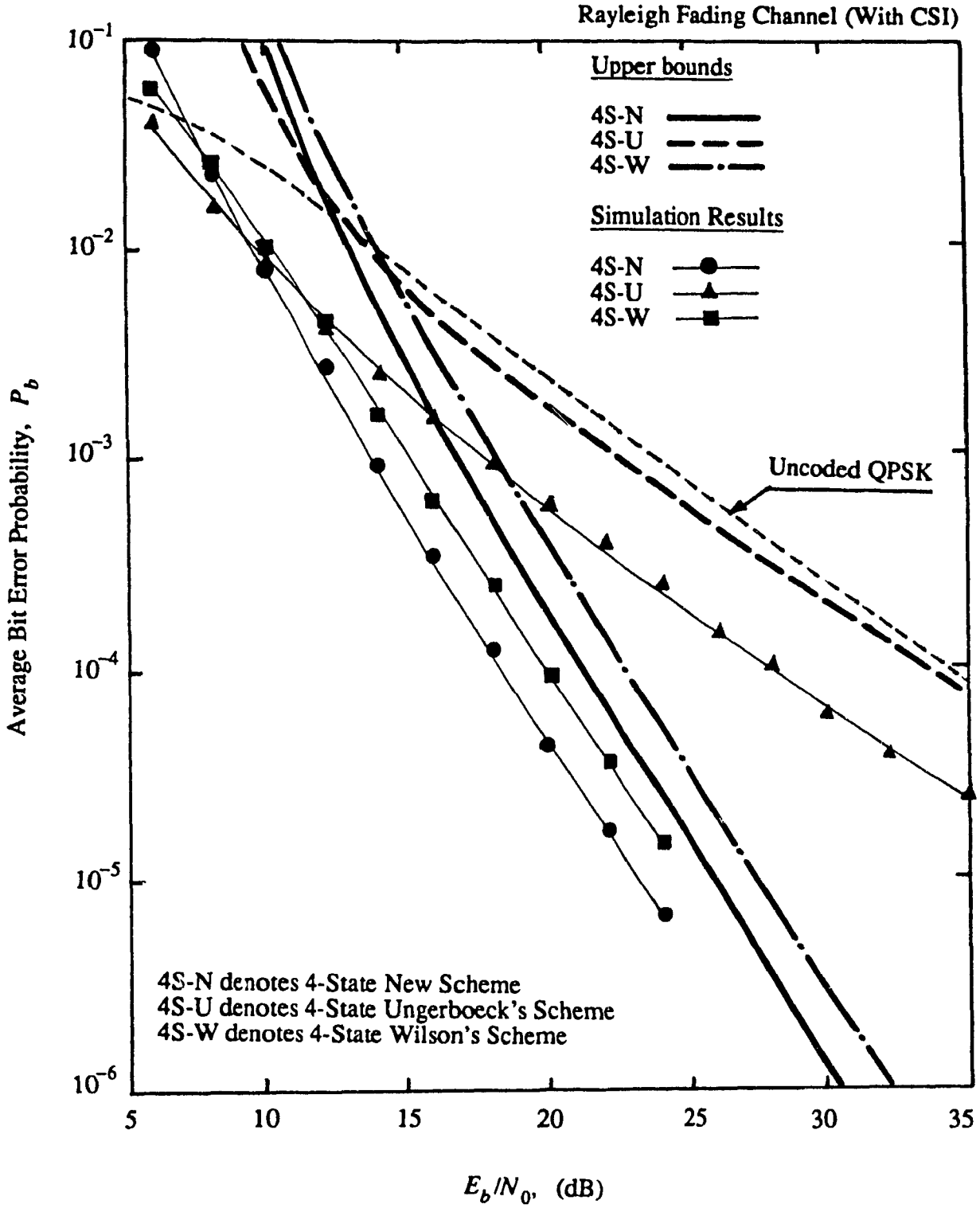

Fig. 4.8. The average bit error probability for different 4-state 8PSK schemes over the Rayleigh fading channel with use of CSI.

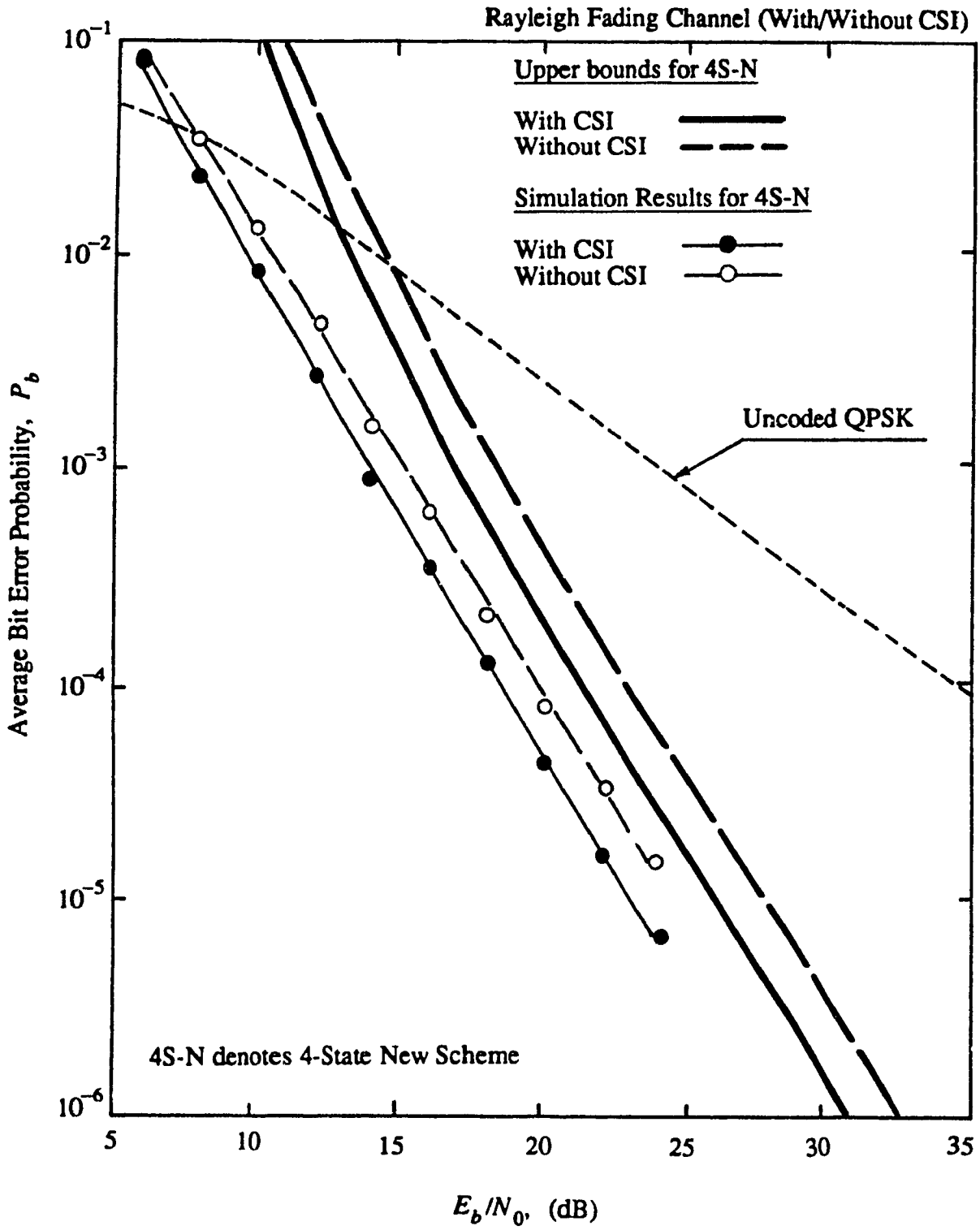

Fig. 4.9. The effect of CSI on the performance of New 4-state TCM scheme over a Rayleigh fading channel.

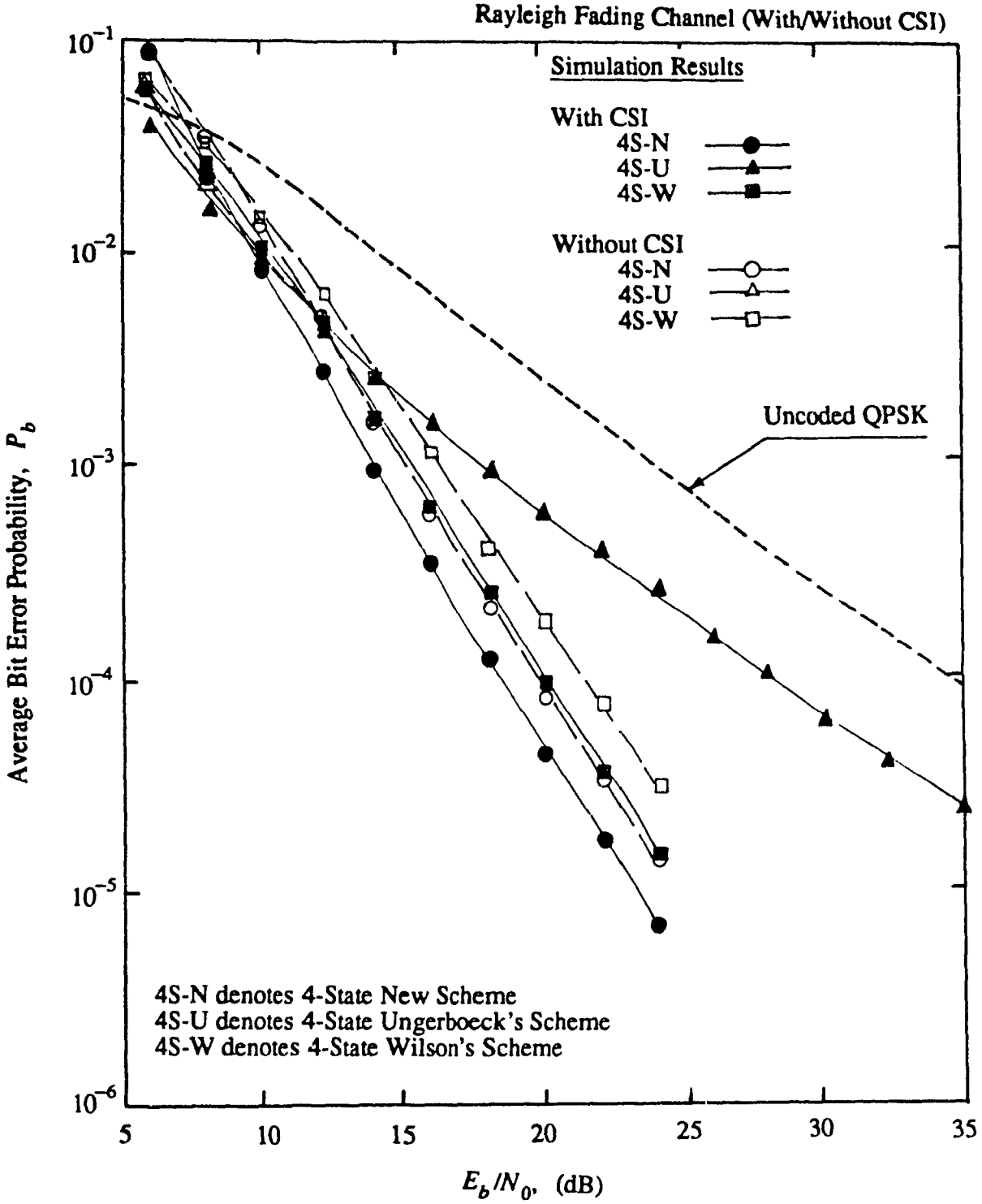

Fig. 4.10. The effect of CSI on the performance of different 4-state TCM schemes over a Rayleigh fading channel.

CHAPTER 5

BANDWIDTH EFFICIENT RS CODED MPSK SIGNALING OVER FADING CHANNELS

In the preceding chapters, the Trellis-Coded Modulation (TCM) schemes were studied based on the fading channel design criteria. In this chapter the issue of using Block-Coded Modulation (BCM) schemes, as a counterpart of trellis-coded modulation schemes, is addressed. Specifically, we combine Reed-Solomon (RS) codes with Multi-Phase Shift Keying (MPSK) schemes, as possible joint power and bandwidth-efficient BCM schemes for fading channels. The performance of these schemes over a Rayleigh fading channel is evaluated for different decoding strategies; i.e., *Errors-Only Decoding* (EOD) and *Errors-and-Erasures Decoding* (EED) techniques. The lower bounds of the post decoding bit error probability for these decoding strategies are obtained by deriving the probabilities of the channel symbol error and erasure for the MPSK signaling over the Rayleigh fading channel and developing expressions for the code symbol error and erasure. Based on the existence or the lack of the Channel State Information (CSI), two erasure generating strategies are considered. The tightness of these lower bounds are confirmed by the simulation for of three RS coded 8PSK schemes. The potential coding gain of RS coded MPSK schemes compared to the uncoded case is discussed based on the results.

5.1. RS CODED MPSK SCHEMES

Although, it is believed that [12], "generally, anything that can be achieved with a

block code can be achieved with somewhat greater simplicity with a convolutional code," the BCM schemes may challenge their counterpart for the following reason.

A feature of TCM schemes is that the transmitted symbol at any given time depends on the previous input symbol sequence. In decoding the process, hence, the decoder has to know the history of the coded sequences before being able to decode a particular symbol. Furthermore, it has to look at the subsequence history of the sequence to examine the total influence of that symbol on the transmitted sequence. Therefore, if the decoder losses or makes a mistake in the history of the sequence, *errors will propagate*. This event can be considered as a drawback in some channels such as the mobile radio channels with a slow shadowing fading. In such a case, the errors due to shadowing will affect the decoding process of the symbols in an unshadowed time and so cause long-term error propagation. In such a scenario, the block-coded modulation may be more advantageous, because, the decoding of a received code block is independent of any other blocks.

BCM schemes have been studied by several authors [12], [16], [46]-[52]. Cusack [46] was apparently the first to propose a BCM scheme based on Ungerboek's set partitioning principle. He used QAM signal constellations and Reed-Muller codes in his BCM schemes. Sayegh [47] later generalized Cusack's work by applying known binary block codes to design BCM schemes based on various QAM and MPSK signal constellations. These schemes mainly have been designed for the AWGN channel where maximizing the minimum Euclidean distance between coded channel symbols is considered as the main criterion.

Although some authors [65] have attempted to apply various known BCM schemes on fading channels, the issue of designing these schemes based on maximizing the time diversity has not been well appeared in the literature. In the following we introduce the idea of combining Reed-Solomon codes with MPSK signaling, as a *bandwidth-efficient* block-coded technique, over the *bandwidth-limited fading channels*. There are many reasons for using RS codes. Being *Maximum-Distance-Separable* (MDS) [68] codes,

they make highly efficient use of the redundancy, and the block lengths and character sizes can be readily adjusted to match the MPSK constellation. By choosing the same cardinality for the channel and code symbols, the minimum Hamming distance of the RS code will determine the time diversity of the coded scheme. RS codes also provide a wide range of code rates that can be chosen such that the coded scheme have compatible bandwidth efficiency as the reference uncoded system. Finally, the available *errors-and-erasures decoding* techniques for these codes make them a suitable choice for channels with side information.

5.2. CONSTRUCTION OF RS CODED SCHEMES FOR FADING CHANNELS

To develop an RS coded MPSK scheme we consider two approaches. First, an RS code, defined over $GF(2^m)$, is combined with an expanded 2^m-PSK signal set. In this combination the code rate is chosen such that the rate of the coded scheme is the same as the uncoded one (usually 2^{m-1}-PSK). In this case the time diversity of the coded scheme is determined by the minimum Hamming distance of the RS code. In the second approach the symbols of an RS code, defined over $GF(2^{lm})$ are mapped to the signal points of a 2^m-PSK signal set such that each symbol of RS code consists of the concatenation of l channel symbols. The following proposition indicates that the effective order of time diversity in such a mapping is at least d_h, the minimum Hamming distance of RS code.

Proposition:

> Assume a code, defined over $GF(2^{lm})$, with a minimum Hamming distance d_h. Let the symbols of this code be transmitted using a signal set with a cardinality of 2^m in such a way that each code symbol consists of the concatenation of l channel symbols. Then, the minimum Hamming distance between the coded signals is at least d_h.

Proof: Let $c_1 = (s_{11}, s_{12}, ..., s_{1l})$ and $c_2 = (s_{21}, s_{22}, ..., s_{2l})$ be two code symbols with

constituent channel symbol components $\{s_{ij}\}$. If $c_1 \neq c_2$, then *at least* one of the constituent channel symbols of c_1 differs from that of c_2. Thus, for two code words which differ in d_h code symbol positions, the corresponding channel coded sequences will differ in *at least* d_h positions. The proposition, then, follows. □

Note that the second approach allows us to enhance the order of time diversity by using powerful low rate codes. Increasing l provides more powerful codes. However, for practical purposes, such as decoding delay, we restrict ourselves to $l = 2$. In the following we consider some examples of RS coded MPSK schemes.

5.2.1. Example 1: RS (7, 5) Coded 8PSK

As the first example we construct an RS coded scheme using the 8PSK signal set. Applying the first approach the RS code is defined over $GF(2^3)$ and its rate chosen such that the overall coded 8PSK rate is comparable with that of uncoded QPSK, i.e., 2 bits/symbol. The code which comply with this requirement is the RS (7, 5) code with a minimum Hamming distance of 3.

5.2.2. Example 2: RS (15, 8) Coded 8PSK

To obtain more coding gain, the minimum Hamming distance of the coded scheme should be increased. This can be done by using longer and lower rate RS codes. However, to compensate for the rate loss, the cardinality of the MPSK signal set should be increased. As the second example we combine RS (15, 8) code, defined over $GF(2^4)$, with 16PSK signal set. This yields a coded scheme with minimum Hamming distance 8 and the overall rate $4\times8/15 = 32/15 > 2$ bits/symbol with almost the same bandwidth efficiency as uncoded QPSK.

5.2.3. Example 3: RS (63, 42) Coded 8PSK

Choosing a signal set with a larger number of signal points has a drawback when the issue of the carrier recovery is concerned. For denser MPSK signal sets it is a difficult

(if not impossible) task to maintain carrier synchronization during deep fades. An alternative is to use the second approach in constructing of these schemes. As an example of such approach, we consider the RS (63, 42) coded 8PSK scheme. The RS code is defined over $GF(2^6)$ and hence, each code symbol consists of two concatenated 8PSK symbols. The rate of the RS code is 42/63 which translates into 2 bits/symbol when combined with 8PSK signal set. The minimum Hamming distance of this coded MPSK scheme is lower bounded with that of the original RS code, i.e., 22.

5.3. PERFORMANCE EVALUATION OF RS CODED MPSK SCHEMES

The transmission model of the system under consideration over a fading channel is depicted in Fig. 5.1. A single sample per symbol is assumed in representing of this model. An RS encoder, defined over $GF(2^m)$, encodes the input bits into words of length n with alphabet size m. The code symbols are interleaved and then used to modulate an M-ary PSK waveform. The channel corrupts the transmitted signal by introducing a fading gain and an additive Gaussian noise term. It is assumed that the receiver performs *coherent detection* and hence the channel phase shift is compensated by the receiver. Also, it is assumed that ideal interleaving/de-interleaving is employed to destroy the memory of the fading channel. This allows us to consider the samples of the fading amplitude as being statistically independent.

The additive Gaussian noise is defined to have a two-sided spectral density $N_0/2$. The multiplicative gain is a random variable having a *normalized* Rayleigh fading density function as

$$p_A(a) = 2a.e^{-a^2}, \tag{5.3.1}$$

with a mean-square value of unity, i.e., $E[A^2] = 1$. We choose normalized Rayleigh density function so that the measured signal energy at the receiver represents the average *signal energy per channel symbol*, E_s.

In the case of the errors-only decoding, the MPSK detector makes a hard decision on each of the received signals according to their phases. These decisions are de-interleaved and supplied to the RS decoder. If the decoder performs errors-and-erasures decoding, the MPSK detector also provides the erasure location information to the RS decoder.

5.3.1. Uncoded MPSK Performance

The performance of MPSK signaling in the AWGN channel with an amplitude gain a AWGN is derived in [1]. At high signal-to-noise ratios the *symbol-error probability* is well approximated [1, p.169] by

$$P_{SM}(a) \approx erfc\left[a\sqrt{E_s/N_0}\sin(\pi/M)\right], \tag{5.3.2}$$

where $erfc(.)$ is the complementary error function defined as

$$erfc(x) \equiv \frac{2}{\sqrt{\pi}} \int_{x}^{\infty} e^{-t^2} . dt. \tag{5.3.3}$$

For the purpose of comparing coded systems with uncoded ones, we need to distinguish between the signal energy per channel symbol E_s, and the *energy per bit* E_b, defined as the required energy per information bits. For MPSK signaling with $M = 2^m$, each M-ary symbol represents m channel bits and therefore $E_s = mE_b$. In the case of using a rate R encoder, m channel bits carry mR information bits and the signal energy per channel symbol can be related to the energy per information bits as

$$E_s = m.R.E_b. \tag{5.3.4}$$

Substituting (5.3.4) into (5.3.2) yields

$$P_{SM}(a) \approx erfc\left[a\sqrt{mR\gamma_b}\sin(\pi/M)\right], \tag{5.3.5}$$

where $\gamma_b \equiv E_b/N_0$. Equation (5.3.5) can be considered as the conditional MPSK symbol-

error probability conditioned on the fading amplitude, a.

The symbol-error probability for MPSK signaling over a Rayleigh fading channel can be found by averaging the conditional symbol-error probability of (5.3.5) with respect to the fading amplitude a as

$$\begin{aligned} P_{SM} &= \int_0^\infty P_{SM}(a) \,.\, p_A(a) \,.\, da \\ &= \int_0^\infty 2a \,.\, erfc\left[a\sqrt{mR\gamma_b}\,\sin(\pi/M)\right] \,.\, e^{-a^2} \,.\, da \\ &= 1 - \left[\frac{mR\gamma_b \sin^2(\pi/M)}{1 + mR\gamma_b \sin^2(\pi/M)}\right]^{1/2} . \end{aligned} \tag{5.3.6}$$

The relationship between the symbol-error probability and *bit-error probability* of MPSK signals depends upon the mapping of the m-bit groups to the symbols. If one uses a *Gray code* for this purpose, in which the bit groups assigned to adjacent phases differ by only one bit, the bit-error probability is approximated by

$$P_{BM} \approx \frac{P_{SM}}{\log_2 M} = \frac{P_{SM}}{m}. \tag{5.3.7}$$

5.3.2. RS Coded MPSK Schemes Performance

5.3.2.1. Errors-Only Decoding

Consider an (n, k) RS code defined over $GF(2^m)$. The minimum Hamming distance d_h, and the error correction capability t of this code are $d_h = n-k+1$ and $t = \left\lfloor (d_h-1)/2 \right\rfloor = \lfloor (n-k)/2 \rfloor$, respectively. If the number of errors in the received signal exceeds the error correction capability of the code, the decoder cannot find the correct code word. This event is called a *decoding failure*. Summing up the all possible decoding failure probabilities, the *post decoding block error probability* can be expressed

[68] as

$$P_{Blc} = \sum_{i=t+1}^{n} \binom{n}{i} P_{SC}^{i} (1-P_{SC})^{n-i}, \tag{5.3.8}$$

where P_{SC} is the RS code symbol-error rate. Note that if the first approach in combining RS codes with MPSK signal set is used, then P_{SC} is the same as P_{SM}, given by (5.3.6). However, in the second approach where each symbol of the RS code consists of two concatenated MPSK symbols, the probability of a correct reception of each code symbol is $(1-P_{SM})^2$ and the error probability of the code symbol, P_{SC}, is derived as

$$P_{SC} = 1 - (1-P_{SM})^2. \tag{5.3.9}$$

Assuming that for every undecodable error the decoder is aware of its decoding failure, a lower bound for the *post decoding bit error probability* can be derived [69] as

$$P_b \geq \frac{1}{n} \sum_{i=t+1}^{n} \binom{n}{i} P_{SC}^{i} (1-P_{SC})^{n-i} \left(i \cdot \frac{P_{BC}}{P_{SC}}\right), \tag{5.3.10}$$

where P_{BC} indicates the mean bit error probability of a code symbol.

5.3.2.2. Errors-and-Erasures Decoding

In errors-only decoding a *hard decision* is performed at the receiver prior to decoding. In other words, the receiver decides, on the basis of the received signal, which one of the M symbols of the signal set was most likely to have been sent. Such a receiver discards a part of the channel information about the reliability of the received symbols and this results in a performance degradation. One way of improving the performance is to allow the receiver to have the option of not deciding at all when the received signal does not clearly indicate one of the transmissions as the most probable. This non-choice is called an *erasure*.

Algorithms that decode both symbol errors and symbol erasures for the RS codes, e.g., the Berlekamp-Massey decoding algorithm, are well known [68]. Using these

decoding algorithms all patterns of t symbol errors and e symbol erasures can be corrected provided that

$$e + 2t \leq d_h - 1. \tag{5.3.11}$$

To consider the performance of the RS coded schemes over fading channels with side information (errors-and-erasures decoding technique), a decision region for erasures should be defined. Depending on the existence or the lack of information about the fading amplitude, CSI, two strategies for defining the decision region for erasures are considered.

Erasure Generation with CSI. It is assumed that the value of the fading amplitude, a, is available at the receiver. In this case a simple erasure generation strategy is suggested by Hagenauer and Lutz [69], in which a threshold value, a_T is defined for the fading amplitude. If the fading amplitude is less than this threshold value then the received symbol is declared as an erasure. This definition is based solely on the value of the fading amplitude and ignores the impact of the additive noise on the channel symbol.

To evaluate the performance of the RS coded schemes with erasure decoding, it is necessary to consider the probabilities of different events. For this erasure generation strategy the following probabilities are determined.

i) The probability of an unreliable (erased) MPSK symbol is

$$P_{EM} = \int_0^{a_T} p_A(a)\,.\,da = 1 - e^{-a_T^2}. \tag{5.3.12}$$

ii) The probability of a reliable (not erased) MPSK symbol is

$$P_{\bar{E}M} = 1 - P_{EM} = e^{-a_T^2}. \tag{5.3.13}$$

iii) The probability of a reliable MPSK symbol being in error is

$$P_{SM|\bar{E}} = \frac{1}{P_{\bar{E}M}} \int_{a_T}^{\infty} P_{SM}(a) \cdot p_A(a) \cdot da$$

$$= erfc\,(a_T \cdot \Gamma_b) - \frac{e^{a_T^2} \cdot \Gamma_b}{\sqrt{1+\Gamma_b^2}}\, erfc\,(a_T \sqrt{1+\Gamma_b^2}), \qquad (5.3.14a)$$

where

$$\Gamma_b \equiv \sqrt{mRE_b/N_0}\sin(\pi/M). \qquad (5.3.14b)$$

iv) The probability of an unreliable MPSK symbol being in error is

$$P_{SM|E} = \frac{1}{P_{EM}} \int_{0}^{a_T} P_{SM}(a) \cdot p_A(a) \cdot da$$

$$= \frac{1}{P_{EM}} \left[1 - e^{-a_T^2} erfc\,(a_T \Gamma_b) - \frac{\Gamma_b}{\sqrt{1+\Gamma_b^2}} (1 - erfc\,(a_T \sqrt{1+\Gamma_b^2})) \right]. \qquad (5.3.15)$$

Erasure Generation without CSI. In the case of no channel state information a circular region with radius ρ_T in the MPSK signal space is considered for erasures [44]. This region , Λ_e, along with the angular decision regions, Λ_i, for an 8PSK signal set is shown in Fig. 2.7. A channel symbol erasure is declared if the received signal falls into the region Λ_e. Note that with this definition of the erasure region, the impact of the additive noise on the erasure declaration is taken into account in addition to that due to fading. However, at high signal-to-noise ratios the effect of the additive noise is negligible, and as it will be shown, this erasure strategy is equivalent to the previous one.

Suppose the i-th channel symbol is transmitted, then the probability that the received signal r falls into the decision region Λ_i is expressed as

$$Q_i^E = E_a\left[\int_{\Lambda_i} p(r \mid a, s_i)\, dr\right], \tag{5.3.16}$$

where E_a represents the averaging operation over the fading amplitude a. Note that Q_i^E is the probability of correct decision of a reliable MPSK symbol. Hence, the probability of a reliable MPSK symbol being in error is obtained as

$$P_{SM \mid \bar{E}} = 1 - \frac{1}{P_{\bar{E}M}} Q_i^E, \tag{5.3.17}$$

where

$$P_{\bar{E}M} = E_a\left[1 - \int_{\Lambda_i} p(r \mid a, s_i)\, dr\right]. \tag{5.3.18}$$

In general case these expressions must be evaluated numerically. As we will see, to find the lower bound of the post decoding bit error probabilities using errors-and-erasures decoding the threshold value for each signal-to-noise ratio has to be optimized. To avoid numerical evaluation of the above expressions in the optimization procedure, appropriate approximation that leads to a closed form expression is developed; see Appendix C. Using the results of Appendix C the probabilities of different events are given as

i) The probability of a reliable (not erased) MPSK symbol is

$$P_{\bar{E}M} = e^{-\rho_{T_n}^2}(1 - erfc(\sqrt{mR\gamma_b}\rho_{T_n})) + erfc(\sqrt{mR\gamma_b}\rho_{T_n}). \tag{5.3.19}$$

ii) The probability of a reliable (not erased) MPSK symbol being in error is

$$P_{SM \mid \bar{E}} = 1 - \frac{1}{P_{\bar{E}M}}\left[e^{-\rho_{T_n}^2} + \frac{\Gamma_b}{\sqrt{1+\Gamma_b^2}} erfc(\sqrt{1+\Gamma_b^2}\rho_{T_n})\right]$$

$$- e^{-\rho_{T_n}^2} erfc(\Gamma_b \rho_{T_n}). \tag{5.3.20}$$

iii) The probability of an unreliable (erased) MPSK symbol being in error is

$$P_{SM|E} = 1 - \frac{1}{1-P_{\bar{E}M}}\left[e^{-\rho_{T_n}^2} erfc(\Gamma_b \rho_{T_n}) + \frac{\Gamma_b}{\sqrt{1+\Gamma_b^2}} - e^{-\rho_{T_n}^2} - \frac{\Gamma_b}{\sqrt{1+\Gamma_b^2}} erfc(\sqrt{1+\Gamma_b^2}\rho_{T_n})\right], \tag{5.3.21}$$

where $\rho_{T_n} = \rho_T/\sqrt{E_s}$ shows the normalized erasure threshold value.

The post decoding block error probability of RS codes for the errors-and-erasures decoding technique can be computed [69] as

$$P_{Blc} = \sum_{e=0}^{d_h-1} P_{EC}(e) \sum_{t=\lceil (d_h-e)/2 \rceil}^{n-e} \binom{n-e}{t} P_{SC|\bar{E}}^{t} (1-P_{SC|\bar{E}})^{n-e-t} + \sum_{e=d_h}^{n} P_{EC}(e), \tag{5.3.22}$$

where $P_{EC}(e)$ is the probability that e code symbols being in erasure, and can be expressed as

$$P_{EC}(e) = \binom{n}{e} P_{EC}^{e} (1-P_{EC})^{n-e}. \tag{5.3.23}$$

Again, for the first approach of RS coded schemes, P_{EC} and $P_{SC|\bar{E}}$ can be replaced by P_{EM} and $P_{SM|\bar{E}}$, respectively. For the second approach, we assume that the RS code symbol is erased if either one of the two MPSK signals belonging to that symbol lies in the erasure region. In this case P_{EC} and $P_{SC|\bar{E}}$ are obtained as

$$\begin{aligned} P_{EC} &= 1 - (P_{\bar{E}M})^2, \\ P_{SC|\bar{E}} &= 1 - (1-P_{SM|\bar{E}})^2. \end{aligned} \tag{5.3.24}$$

The lower bound of the post decoding bit error probability for the errors-and-erasures decoding can be obtained by weighting the probabilities of all possible decoding

failures, given in (5.3.22), by the corresponding bit error probabilities [69] as

$$P_b \geq \frac{1}{n} \sum_{e=0}^{d_h - 1} P_{EC}(e) \sum_{t = \lceil (d_h - e)/2 \rceil}^{n-e} \binom{n-e}{t} P_{SC|\bar{E}}^{t} \cdot (1 - P_{SC|\bar{E}})^{n-e-t} \left(e P_{BC|E} + t \frac{P_{BC|\bar{E}}}{P_{SC|\bar{E}}} \right)$$

$$+ \frac{1}{n} \sum_{e=d_n}^{n} P_{EC}(e) \left(e P_{BC|E} + (n-e) P_{BC|\bar{E}} \right). \qquad (5.3.25)$$

5.4. PERFORMANCE EVALUATION OF SOME EXAMPLES OF RS CODED SCHEMES

In this section we consider the performance of three RS coded MPSK signaling schemes, constructed in Section 5.2, and compare them with a reference uncoded signaling scheme over a normalized Rayleigh fading channel. The reference scheme for all examples is uncoded QPSK.

Using (5.3.10) and (5.3.25), the lower bounds of the post decoding bit error probability of EOD and EED techniques can be obtained. These bounds for the RS (7,5) coded 8PSK, the RS (15, 8) coded 16PSK, and the RS (63, 42) coded 8PSK schemes are evaluated and shown in Fig.'s 5.2, 5.3, and 5.4, respectively. The bit error rate of uncoded QPSK over a normalized Rayleigh fading channel is included for comparison.

In evaluating the error bounds for RS (7, 5) coded 8PSK and RS (15, 8) coded 16PSK (both use the first approach in code construction), the code symbol-error rates are replaced by the MPSK symbol-error rates of Section 5.3. Assuming Gray mapping is used in the bit assignment of the code symbols, (5.3.7) can be used in relating the mean bit error probability of a code symbol to its symbol-error rate. In calculating these bounds for the RS (63,42) coded 8PSK scheme (which uses the second approach in code construction), two points are being considered. First, the code symbol-error rates are related

to the 8PSK symbol-error rates using (5.3.24). Second, a simple argument shows that the mean bit error probability of a code symbol can be approximately related to the channel symbol-error rate by multiplying the latter by $2/m$, where m is the code symbol size in bits,[1] i.e., $m = 6$.

The lower bounds for EED are evaluated for two erasure generation strategies: with and without CSI. The numerical results show that the performance of the coded schemes improves at low SNR's slightly when CSI is utilized in the erasure generation process. However, this improvement is not significant enough to be shown in Fig.'s 5.2-5.4. For high SNR's both erasure generation strategies yield the same performance.

The lower bounds of the post decoding bit error rate for the errors-and-erasures decoding techniques have been found by optimizing the fading amplitude threshold, a_T, and the erasure region radius, ρ_T, for each value of E_b/N_0, based on the existence or lack of CSI, respectively. Fig. 5.5 represents the optimized fading amplitude threshold a_T and the normalized erasure region radius ρ_{T_n} as a function of E_b/N_0 for the different schemes considered in Fig.'s 5.2-5.4. Note that at lower signal-to-noise ratios, the value of ρ_{T_n} is slightly higher than that of a_T. This is due to the fact that in erasure decoding without CSI the impact of the additive noise is considered as well as the fading amplitude. As the signal-to-noise ratio increases these values get closer.

To examine the tightness of the lower error bounds computer simulations are performed for three RS coded MPSK schemes. The results of the simulations are included in Fig.'s 5.2-5.4. The simulation results substantiate the tightness of the error bounds. For the RS (7,5) coded 8PSK scheme the bounds are tight at high SNR's while for the other two schemes the tightness of the bounds is held for the whole range of signal-to-noise ratios of interest.

[1] Assume that a Gray mapping is used in assigning the bit groups to the 8PSK symbols. If a code symbol is in error then one of the following cases might occur: 1) Only one of the two concatenated 8PSK symbols is in error 2) Both 8PSK symbols are in error. Weighting the probabilities of events (1) and (2) by $1/m$ and $2/m$, respectively, and summing them up leads to this result.

To compare the performance of the three RS coded schemes, the corresponding error bounds are redrawn in Fig. 5.6. It is observed that using longer and lower rate codes improves the performance of the coded schemes at the expense of the decoding complexity. Note that, for instance, the RS (15, 8) coded 16PSK scheme provides a 3-4.5 dB more coding gain than RS (7, 5) coded 8PSK at bit error rates around 10^{-5}. However, at low SNR's the latter scheme outperforms the former one. This can be explained as follows.

By using 16PSK signaling the signal set becomes denser and the distance between channel symbols becomes shorter. Hence, at low signal-to-noise ratios for the second scheme, more errors occur during transmission and the decoder fails to correct more erasures/errors. In other words, at low error rates the high error correction capability of this scheme cannot compensate the performance degradation due to the use of a denser signal set.

5.5 DISCUSSION

The idea of combining RS codes with MPSK signal sets is introduced in this chapter by constructing some bandwidth-efficient RS coded MPSK schemes. Both analytical and simulation results show that substantial coding gains can be obtained compared to the uncoded reference system. Using errors-only decoding, the coding gains compared to uncoded QPSK, at bit error rates around 10^{-5}, for RS (7, 5) coded 8PSK, RS (15, 8) coded 16PSK, and RS (63, 42) coded 8PSK are 17.6, 21, and 28 dB, respectively.

The use of erasure information in the decoding process enhances the coding gain by additional 2-3 dB, depending on the RS coded scheme used. Indeed, this technique is a specific example of *soft decision* decoding. Using more general unquantized soft decision decoding, more coding gain is expected for these schemes on a fading channel. The soft decision decoding of the RS codes, in general, is a formidable task. However, for short RS coded schemes, it is practical to perform soft decision decoding by introducing a trellis structure and using the Viterbi algorithm. This issue along with the other soft

decision decoding techniques for block-coded schemes will be discussed in the next chapter. Based on the results in Chapter 6, a comparison will be performed between RS coded MPSK schemes and some other BCM schemes.

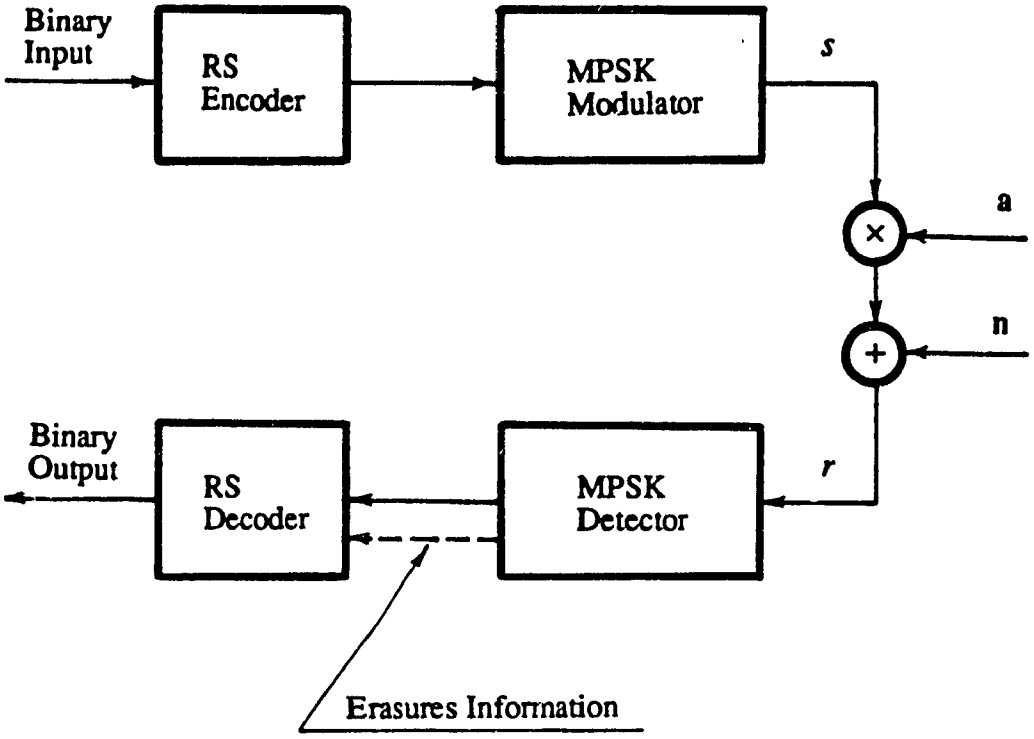

Fig. 5.1. The baseband signal transmission model for RS coded MPSK schemes on a fading channel.

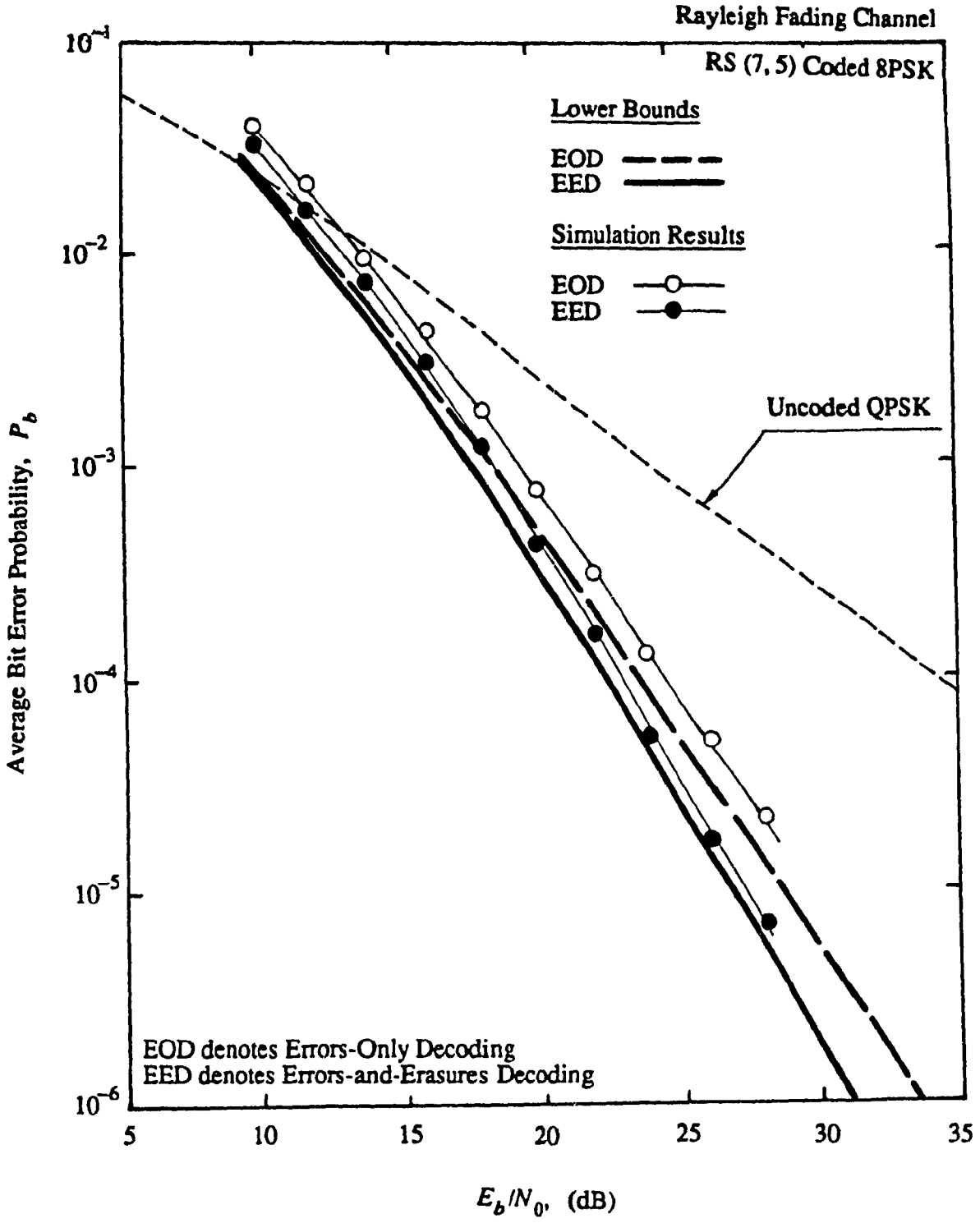

Fig. 5.2. Performance of the RS (7, 5) coded 8PSK scheme in a normalized Rayleigh fading channel.

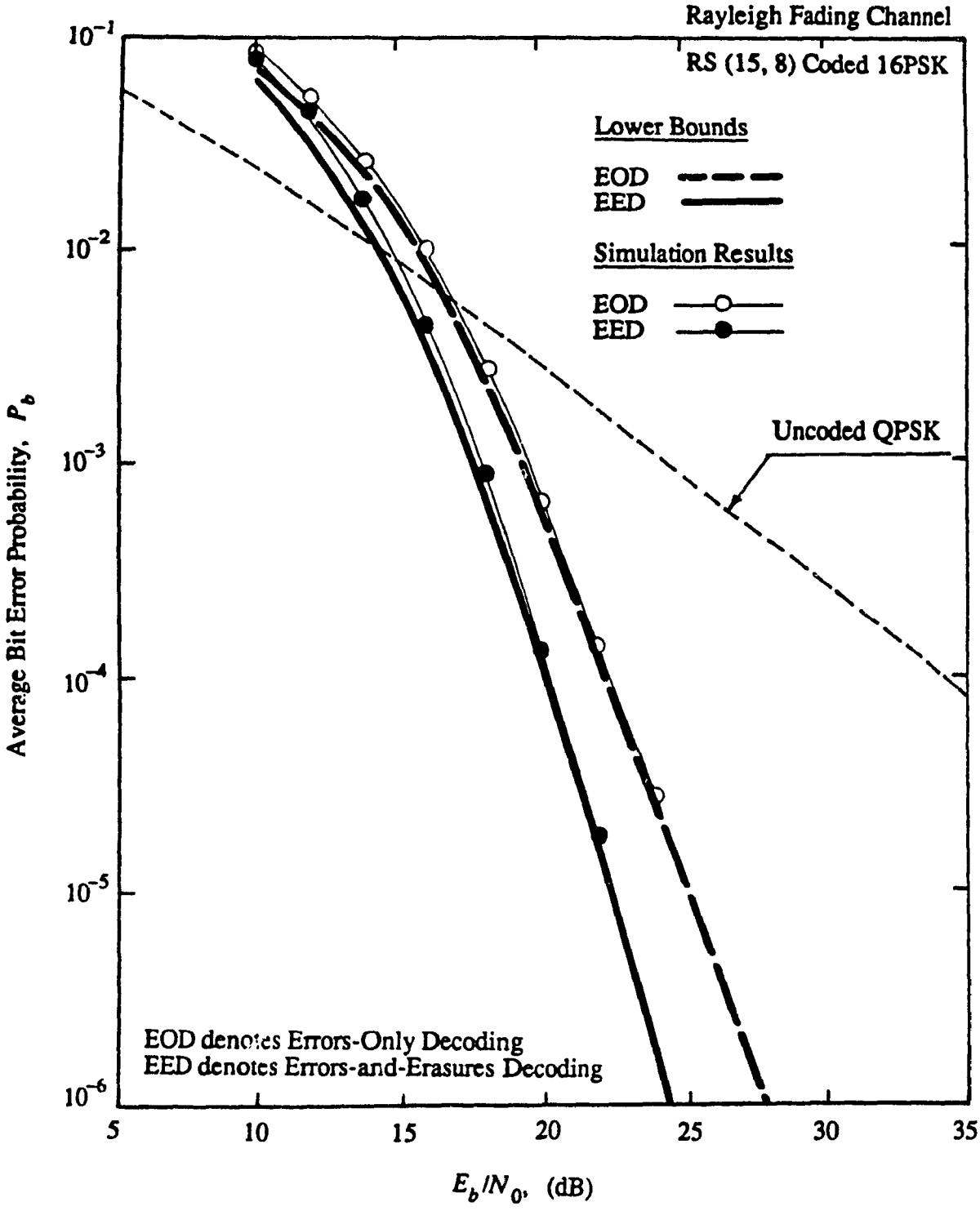

Fig. 5.3. Performance of the RS (15, 8) coded 16PSK scheme in a normalized Rayleigh fading channel.

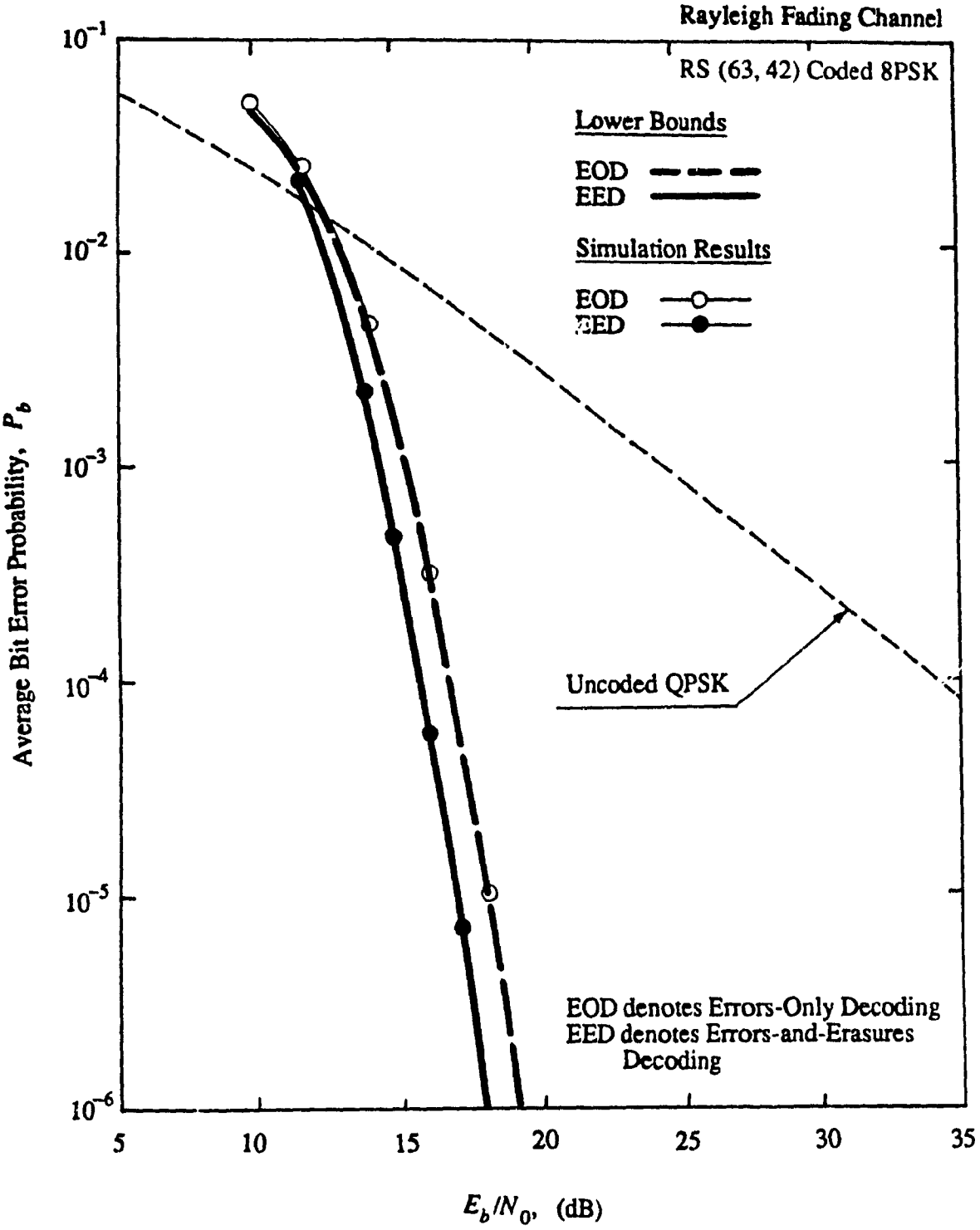

Fig. 5.4. Performance of the RS (63, 42) coded 8PSK scheme in a normalized Rayleigh fading channel.

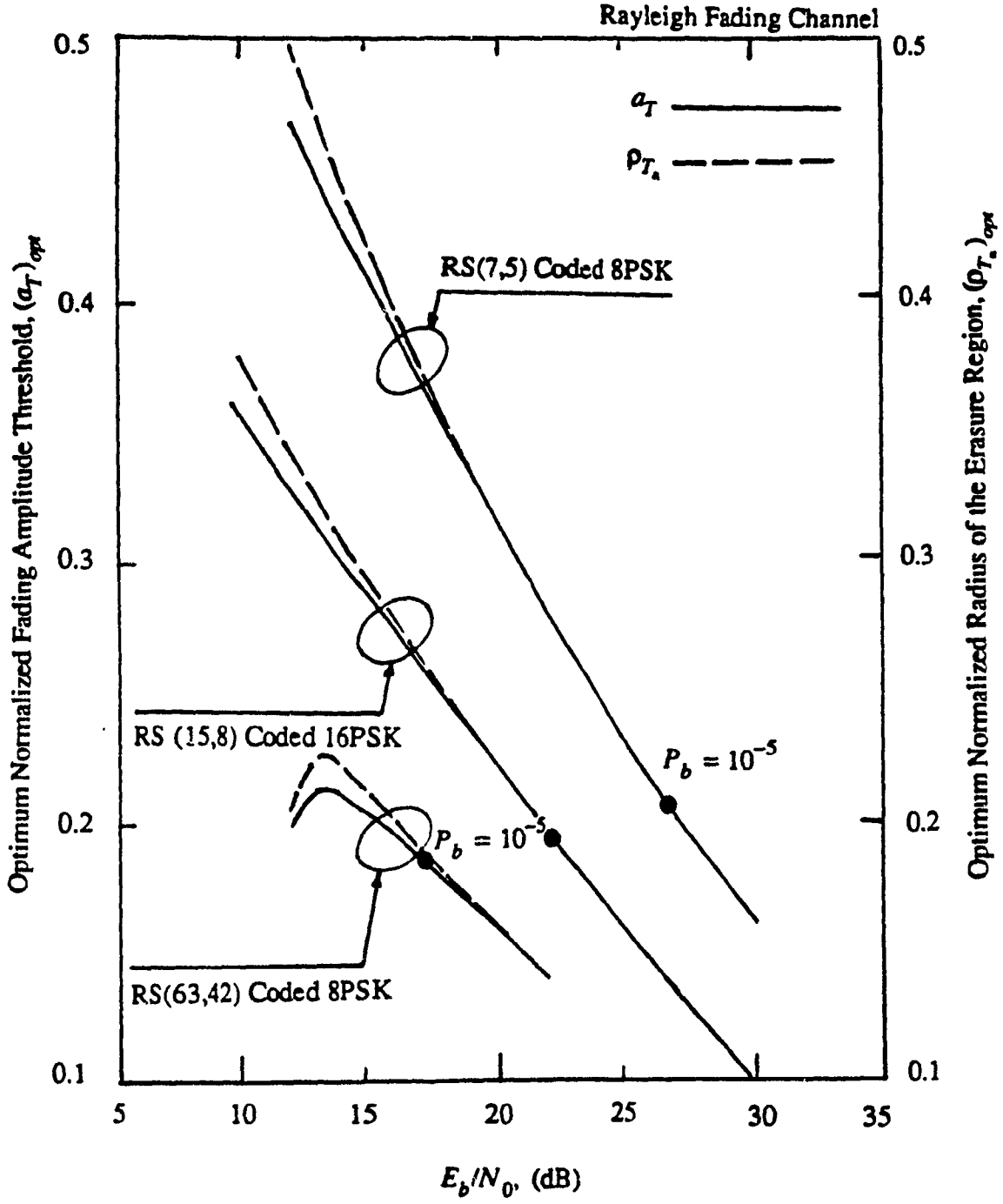

Fig. 5.5. Optimum erasure threshold (with/without CSI) of the errors-and-erasures decoding of the three RS coded MPSK schemes as a function of the average bit signal-to-noise ratio.

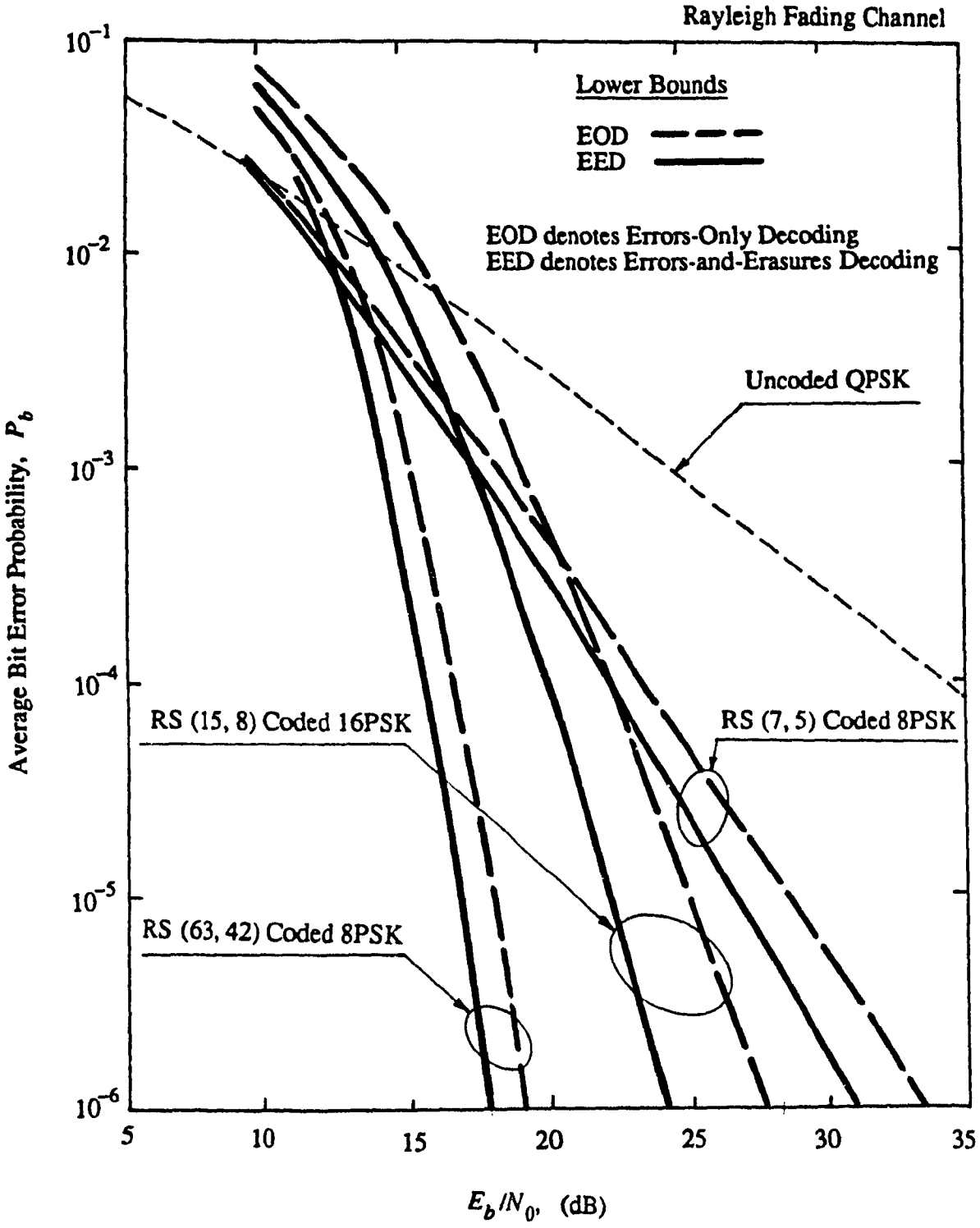

Fig. 5.6. Comparison of the performance of the three different RS coded schemes in a normalized Rayleigh fading channel.

CHAPTER 6

SOFT-DECISION DECODING OF RS CODED MPSK SCHEMES

In Chapter 5 it was shown that the RS coded MPSK schemes provide substantial coding gains compared to uncoded schemes on a Rayleigh fading channel. These coding gains were evaluated for errors-only and errors-and-erasures decoding strategies. On the other hand the cut-off rate evaluation of Chapter 2 revealed that soft-decision decoding technique on fading channels improves the performance of the coded schemes remarkably, compared to the hard-decision one. The soft-decision of the RS coded schemes is considered in this chapter. For short RS coded schemes, this decoding strategy is implemented by introducing a trellis structure and using the Viterbi Algorithm (VA). Based on this technique the upper bound analysis and simulations are carried out for two short RS coded 8PSK schemes. These results are compared with those of errors-only and errors-and-erasures decoding techniques. Because of its higher complexity the Viterbi decoding cannot be applied to the longer low rate RS coded schemes. In such cases, low complex soft-decision decoding techniques, such as *Successive Erasure Decoding* (SED), will be used instead, at the expense of performance degradation. We will apply this technique for soft-decision decoding of longer low rate RS coded schemes. The performance of this technique for different RS coded schemes will be compared with the other decoding strategies. Finally, a comparison will be carried out between RS coded schemes and some other Block-Coded Modulation (BCM) schemes.

6.1. TRELLIS DECODING OF BLOCK CODES

The soft-decision decoding for binary signaling (BPSK) asymptotically provide 3 dB improvement compared to the hard-decision decoding in the AWGN channel [2], [56]. Most of this improvement can be gained by three level quantization (errors-and-erasures decoding) and little improvement is left for quantizing to more than three levels [2]. For channels other than the AWGN channel, however, soft decision decoding may significantly improve the performance of the coded schemes (see the cut-off rate analysis of Chapter 2). For instance, in the case of independent Rayleigh fading, the improvement is equivalent to the change of a $(t + 1)$-order diversity receiving system to performance of a d_h-order diversity system [70]. This improvement increases drastically by increasing the signal-to-noise ratio.

In contrary to convolutional codes which use the Viterbi algorithm as the low complex implementation of the maximum likelihood decoding, most soft-decision algorithms for block codes are complex. To implement maximum likelihood decoding for block codes, in general, the received vector must be correlated with each of the valid code words and the closest code word to the received one must be chosen as the transmitted one. However, when the number of code words is large, implementing such a receiver is impractical. In such a case, soft-decision decoding of the block coded schemes can be implemented by employing some techniques which discard improbable code words without correlating the entire set of code words with the received one [56], [70]-[72]. One of these techniques, introduced by Wolf [71], uses the Viterbi algorithm on an equivalent trellis diagram constructed for the block code. In [71] Wolf shows that for any (n, k) linear block code defined over $GF(q)$ there is a trellis structure having no more than q^{n-k} states. For cyclic codes, this trellis is periodic.

For a linear (n, k) cyclic code over $GF(q)$, the encoder has $n-k$ storage devices for elements from $GF(q)$. It is shown that the trellis for this code can be formed by associating the trellis nodes with the $q^{(n-k)}$ possible states of the $(n-k)$ stage shift register

used for encoding. However, not all of these states are used at different depths of the trellis. The number of states at depth j is given by [71]

$$N_s = \begin{cases} q^j, & j = 1, 2, \cdots, n-k-1, \\ q^{n-k}, & j = n-k, n-k+1, \cdots, k, \\ q^{n-j}, & j = k+1, \cdots, n. \end{cases} \tag{6.1.1}$$

The trellis is repetitive for $j = n-k+1, \cdots, k$.

To interconnect nodes of the trellis a polynomial $p(x; j)$ in x of degree $(n-k-1)$ with coefficients from $GF(q)$ is associated with each node at depth j. The polynomials at depth $(j+1)$ are then formed from the polynomial at depth j in accordance with [71]

$$p_l(x; j+1) \equiv (x\, p_i(x; j) + x^{n-k}\alpha_p) \ \textit{modulo}\ g(x), \tag{6.1.2}$$

where $g(x)$ is the generator polynomial of the code. In (6.1.2) i shows the index of the starting node at depth j, l shows the index of the terminating node at depth $j+1$, and $\alpha_p \in GF(q)$ is the label of the connecting branch between these nodes.

As an example, using (6.1.1) and (6.1.2) the trellis diagram of the RS(7,5) coded 8PSK scheme is shown in Fig. 6.1. This code is defined over $GF(8)$ and its trellis diagram has $8^{(7-5)} = 8^2 = 64$ states. Using this trellis, we can apply the VA to perform soft-decision decoding for this code. In the following we drive the upper on the block error rate as well as the bit error rate for the RS coded schemes which employ the VA for soft-decision decoding.

6.1.1. UPPER BOUND ANALYSIS

To derive an upper bound, first a union bound is obtained on the *error event* probability. An error event starts where the two paths in the trellis diagram diverge and ends where they remerge. A union bound for the error event probability may be obtained by summing the probabilities of the error events of all possible lengths given a particular

transmitted sequence s and averaging this quantity over all possible correct sequences s

$$P_e \le \sum_{\mathbf{s},\hat{\mathbf{s}} \in \mathbf{C}} \sum p(\mathbf{s}) \cdot P_2(\mathbf{s}, \hat{\mathbf{s}}), \tag{6.1.3}$$

where $\hat{\mathbf{s}}$ is the incorrect decoded code word, and $\mathbf{C}$ is the set of all valid code sequences. In (6.1.3) $P_2(\mathbf{s}, \hat{\mathbf{s}})$ represents the pairwise error event probability for two code words s and $\hat{\mathbf{s}}$.

In applying the VA to the soft-decision decoding of block codes, the algorithm finds the closest code word to the transmitted one for each received block. In this case the length of the error events is limited to the block length, n, and (6.1.3) is equivalent to an upper bound on the block error probability.

To evaluate the upper bound (6.1.3), the pairwise error event probability $P_2(\mathbf{s}, \hat{\mathbf{s}})$ should be found. Using the results of Chapter 3 the pairwise error probability for a Rayleigh fading channel is obtained for cases with and without CSI by replacing $K = 0$ in (3.4.4) and (3.4.9a), respectively, as

With CSI

$$P_2(\mathbf{s}, \hat{\mathbf{s}}) \le \prod_{i \in \eta} \frac{1}{\beta_l^2 \cdot (E_s/4N_0)^l}, \tag{6.1.4a}$$

Without CSI

$$P_2(\mathbf{s}, \hat{\mathbf{s}}) \le \frac{(2e/l)^l}{(\bar{E}_s/N_0)^l} \cdot \frac{\left[\sum_{n \in \eta} |s_n - \hat{s}_n|^2\right]^2}{\beta_l^2}, \tag{6.1.4b}$$

where η is the set of all i for which $s_i \neq \hat{s}_i$, l shows the length of the error event, and β_l^2 is the squared product of the distances defined as (3.4.6). Substituting (6.1.4) into (6.1.3) gives the upper bound on the block error probability as

With CSI

$$P_{blc} \le \sum_{s,\hat{s}\in C}\sum p(s)\cdot \prod_{i\in\eta}\frac{1}{\beta_l^2\cdot(E_s/4N_0)^l},$$

$$\le \sum_{l=d_h}\sum_{\beta_l^2}\frac{a(\beta_l^2)}{\beta_l^2}\cdot\left(\frac{1}{E_s/4N_0}\right)^l, \tag{6.1.5a}$$

where d_h is the minimum Hamming distance of the code and $a(\beta_l^2)$ is the average number of code words with a Hamming distance of l and a squared product of branch distances of β_l^2 from the transmitted code word.

If no CSI is used in the decoding process, we have

Without CSI

$$P_{blc} \le \sum_{s,\hat{s}\in C}\sum p(s)\cdot\frac{(2e/l)^l}{(E_s/N_0)^l}\cdot\frac{\left[\sum_{n\in\eta}|s_n-\hat{s}_n|^2\right]^2}{\beta_l^2},$$

$$\le \sum_{l=d_h}\sum_{\beta_l^2} a(\beta_l^2)\cdot\frac{(2e/l)^l}{(E_s/N_0)^l}\cdot\frac{(d_E^2(\beta_l))^l}{\beta_l^2}, \tag{6.1.5b}$$

where

$$d_E^2(\beta_l) = \sum_{i\in\eta}|s_i-\hat{s}_i|^2, \tag{6.1.5c}$$

is the squared Euclidean distance between the two unmerged paths with a squared product distance of β_l^2 and a length of l. In deriving (6.1.5b) it is assumed that all error events of length l with the squared product distance of β_l^2 have the same Euclidean distance.

To derive the bit error probability we use the upper bounds of (6.1.5). Assuming that *Gray mapping* is used in assigning the bits to the 2^m- ary PSK signal points, the bit error probability can be related to the probability of the symbol error by dividing the latter by m (see (5.3.7)). To find the symbol error rate, we can weight the terms corresponding to the error events of length l by l/n. For, two paths with l unmerged branches have l different symbols. Thus, the probability of the bit error can be upper bounded as

With CSI

$$P_b \le \sum_{l=d_h} \sum_{\beta_l^2} \frac{l}{mn} \cdot \frac{a(\beta_l^2)}{\beta_l^2} \cdot \left(\frac{1}{E_s/4N_0}\right)^l, \tag{6.1.6a}$$

Without CSI

$$P_b \le \sum_{l=d_h} \sum_{\beta_l^2} \frac{l}{mn} \cdot a(\beta_l^2) \cdot \frac{(2e/l)^l}{(E_s/N_0)^l} \cdot \frac{(d_E^2(\beta_l)^l}{\beta_l^2}. \tag{6.1.6b}$$

For high signal-to-noise ratios these upper bounds can be simplified by considering only the terms corresponding to the shortest error event paths (the path with minimum Hamming distance d_h) as

With CSI

$$P_b \le \sum_{\beta_{d_h}^2} \frac{d_h}{mn} \cdot \frac{a(\beta_{d_h}^2)}{\beta_{d_h}^2} \cdot \left(\frac{1}{E_s/4N_0}\right)^{d_h}, \tag{6.1.7a}$$

Without CSI

$$P_b \le \sum_{\beta_{d_h}^2} \frac{d_h}{mn} \cdot a(\beta_{d_h}^2) \cdot \frac{(2e/d_h)^{d_h}}{(E_s/N_0)^{d_h}} \cdot \frac{(d_E^2(\beta_{d_h}))^{d_h}}{\beta_{d_h}^2}. \tag{6.1.7b}$$

As an illustrative example the upper bounds in (6.1.7) are evaluated for the RS (7, 5) coded 8PSK and the shortened RS (6, 4) coded 8PSK schemes. To find the distance weight distribution of these schemes an exhaustive computer search is performed. Fig.'s 6.2 and 6.3 show the multiplicity of $\beta_{d_h}^2$ for the code words with minimum Hamming distance of 3. Using (6.1.7) the bit error rate upper bounds of the RS (7, 5) coded 8PSK and the shortened RS (6, 4) coded 8PSK schemes are shown in Fig. 6.4 and 6.5, respectively, for the cases with and without CSI.

6.1.2. Simulation Results

In this section the performance of two short RS coded schemes; namely, RS (7, 5) coded 8PSK and its shortened code RS (6, 4) coded 8PSK is evaluated via computer simulation. The soft-decision decoding of these schemes was implemented using the Viterbi algorithm for cases with and without CSI. The simulation results for the the RS (7, 5) coded 8PSK and the RS (6, 4) coded 8PSK schemes are included in Fig.'s 6.4-6.5. In order to compare with the errors-only and the errors-and-erasures decoding techniques, the results for the RS (7, 5) coded 8PSK scheme from Chapter 5 are redrawn in Fig. 6.6. It is observed that by using soft-decision decoding, about 8.5 dB and 6.5 dB coding gain can be obtained at a bit error probability of 10^{-5} compared to errors-only and errors-and-erasures decoding techniques, respectively. The use of CSI improves this gain by 1 dB additional coding gain.

6.2. SUCCESSIVE-ERASURE DECODING

The trellis decoding is applicable for the short codes with a small number of redundancy. For longer low rate codes this technique is impractical because of its high complexity. In this section we consider another soft-decision decoding approach which is applicable to all RS coded schemes. Such approach, termed successive-erasure decoding, was introduced by G. D. Forney [72] in connection with *Generalized Minimum-Distance Decoding* (GMD). For binary signaling, this technique yields asymptotically the same

performance as the maximum likelihood decoding (MLD) [56]. However, its performance for nonbinary codes with multi level/phase signaling is inferior to that of MLD [73]. We begin our discussion by reviewing GMD briefly.

6.2.1. Generalized Minimum-Distance Decoding

Let $\mathbf{s} = (s_0, s_1, ..., s_{n-1})$ be a transmitted code word with symbols from $GF(q)$, and $\mathbf{r} = (r_0, r_1, ..., r_{n-1})$ be the corresponding output from an unquantized channel. Assume that the receiver consists of a detector and a decoder. The detector constructs two components corresponding to each received signal r_i, an estimate of s_i denoted by $\hat{s}_i$, and a weight α_i, $0 \le \alpha_i \le 1$, indicating the reliability of that estimate. The output of the detector will then be a sequence of n estimates $\hat{s}_i$ with their n corresponding weights α_i. Defining

$$f(\hat{s}, s) = \begin{cases} +1 & \text{if} \quad s = \hat{s}; \\ -1 & \text{if} \quad s \neq \hat{s}, \end{cases} \tag{6.2.1}$$

we are able to develop the following theorem.

Theorem [Forney]:

> Consider a code of length n and minimum Hamming distance d_h. Assume a received vector $\mathbf{r}$ with a corresponding estimate vector $\hat{\mathbf{s}}$ and a reliability vector $\boldsymbol{\alpha}$. Then there exists at most one code word $\mathbf{s}_j$ for which
>
> $$\boldsymbol{\alpha} \cdot \mathbf{s}_j \equiv \sum_{i=1}^{n} \alpha_i \cdot f(\hat{s}_i, s_{ji}) > n - d_h, \tag{6.2.2}$$
>
> where $0 \le \alpha_i \le 1$.

Proof : See [72].

This theorem shows that it is possible to modify the errors-and-erasures decoding technique to utilize the channel side information (soft-decision). It is shown that [72] using an errors-and-erasures decoding algorithm by no more than $(d_h + 1)/2$ trials the

unique code word satisfied in (6.2.2) can be decoded, if there is one. This decoding algorithm can be explained as follows.

First we start by applying the errors-and-erasures decoding to the hard-decision component of the received vector $\hat{\mathbf{s}}$. The decoded code word is then examined by applying (6.2.2). If this code word satisfies the condition then it is the estimate of the transmitted code word and we are done. Otherwise we erase the two symbols in $\hat{\mathbf{s}}$ with the least reliability weights and repeat the errors-and-erasures decoding process. Again, the decoded code word is tested by the condition of (6.2.2). If it satisfies this condition the decoding ends otherwise we erase the four symbols with the smallest values of reliabilities, and continue the errors-and-erasures decoding. This procedure is continued up to erasing $d_h - 1$ symbols, successively. The GMD procedure decodes successfully whenever any of the successive decoder outputs satisfies (6.2.2), otherwise a decoding failure is declared. When successful, it will produce a unique code word.

6.2.2. Choice of Reliability Weight

The performance of GMD depends on the choice of the reliability weight, α. A way of obtaining an expression for the α_i's is by optimizing the error probability bound for GMD at high SNR. This can be done by applying the Chernoff bound technique to the condition (6.2.2) as follows [72].

The probability of not decoding correctly for GMD is obtained by considering the condition (6.2.2) as

$$P(ndc) = \sum_{\mathbf{r},\, \mathbf{s}_j} P(\mathbf{r}, \mathbf{s}_j) \, . \, Pr\left[\sum_{i=0}^{n-1} \alpha(r_i) \, . \, f(\hat{s}(r_i), s_{ji}) \le n - d_h \right]. \qquad (6.2.3)$$

Using the Chernoff bound, for an ensemble of codes, it is shown that [72]

$$P(ndc) \le \exp\left[-n(\lambda d_h - \mu(\lambda)) \right], \qquad (6.2.4a)$$

where $\mu(\lambda) = \ln[g(\lambda)]$ and

$$g(\lambda) = E\left[\exp\left[\lambda(1-\alpha(r)) \cdot f(\hat{s}(r), s)\right]\right]. \qquad (6.2.4b)$$

Note that in (6.2.4) the subscripts i and j have been deleted for simplicity. The upper bound (6.2.4a) can be tightened by choosing an appropriate reliability weight α and optimizing the Chernoff bound parameter λ. To choose $\alpha(r)$, $g(\gamma)$ can be evaluated as

$$g(\gamma) = \frac{1}{q}\int[P(r \mid \hat{s}(r)) \cdot exp(\lambda(1-\alpha(r)) + \sum_{s \neq \hat{s}} P(r \mid s) \cdot exp(\lambda(1+\alpha(r))]dr. \qquad (6.2.5)$$

To minimize the error bound, we minimize $g(\lambda)$ over $\alpha(r)$. By differentiating (6.2.5) with respect to $\alpha(r)$, we find that the $\alpha(r)$ which minimizes $g(\lambda)$ is

$$\alpha(r) = \frac{1}{2\lambda} \ln \frac{P(r \mid \hat{s}(r))}{\sum_{s \neq \hat{s}} P(r \mid s)} = \frac{1}{2\lambda} L. \qquad (6.2.6)$$

Since $0 \leq \alpha \leq 1$, we must set $\alpha = 1$ if $L \geq 2\lambda$ or $\alpha = 0$ if $L \leq 0$. Thus

$$\alpha(r) = \begin{cases} 1 & \text{if} \quad L \geq 2\lambda \\ L/2\lambda & \text{if} \quad 0 \leq L \leq 2\lambda \\ 0 & \text{if} \quad L \leq 0, \end{cases} \qquad (6.2.7a)$$

where

$$L = \ln \frac{P(r \mid \hat{s}(r))}{\sum_{s \neq \hat{s}} P(r \mid s)}. \qquad (6.2.7b)$$

6.2.3. SEMDD Algorithm

In GMD the decoder usually does not utilize the full error-correcting capability of the code since many correctable error patterns, in general, fall outside the error-correcting radius. In such a case a decoding failure is announced. To improve the performance of this decoding algorithm a decoding scheme closely related to GMD [72] is used as the following. Let the decoder be a full likelihood detector and it store a complete

likelihood packet for each reception r_i, i.e., $P(r_i \mid s_j)$ for all j. Based on this information the detector also provides an estimate $\hat{s}_i$, for each received signal r_i, for which $P(r_i \mid s_j)$ is greatest. Define the estimate log likelihood ratio as

$$L(\hat{s}_i) = \ln \frac{P(r_i \mid \hat{s}_i(r_i))}{\sum_{s_j \neq \hat{s}_i} P(r_i \mid s_j)}. \tag{6.2.8}$$

Note that this parameter is the same as the reliability weight, used in GMD, except that it is not bounded. Now, the same decoding procedure, as explained for GMD, can be applied by successive erasing pairs of unreliable symbols and utilizing errors-and-erasures decoding. In each step of this process an estimate of the transmitted code word is obtained and is stored. Up to $(d_h + 1)/2$ estimated code words may result. The decoder, then, chooses that one for which $P(\mathbf{r} \mid \hat{\mathbf{s}}_j)$ is the greatest, i.e., the one closest to the received vector $\mathbf{r}$ in likelihood distance. For the AWGN channel this is equivalent to choosing an estimated code word with minimum Euclidean distance form the received vector. This decoding algorithm is named, *Successive-Erasure Minimum Distance Decoding* (SEMDD) [73]. Note that the set of estimated code words generated in this algorithm is the same as those generated by GMD; the difference is the choice between them is made by the likelihood measure rather than testing the condition (6.2.2).

Also SEMDD algorithm forces the decoder to always make a decision. Although it is difficult to obtain analytical results for SEMDD it can be said that the performance of this decoding technique is superior to GMD. This follows from the fact that whenever GMD decodes correctly so does SEMDD, but converse is not true. Since the complexity of these decoding algorithms are almost the same, SEMDD is preferred because of its superior performance.

6.2.4. Simulation Results

For GMD, the probability of not decoding correctly can be evaluated for the

AWGN channel using BPSK signaling [56] and MPSK signaling [73]. Indeed, the condition (6.2.2) provides a basis for this evaluation. However, the performance of SEMDD is hard to analyze, particularly when the fading channel is concerned. Hence, the performance of this decoding technique for different RS coded MPSK schemes are evaluated using computer simulations.

In our simulation we consider a normalized Rayleigh fading channel for the cases when CSI is available at the receiver and when it is not. Depending on the existence or the lack of channel state information, the reliability function of (6.2.8) is

With CSI

$$L(\hat{s}_i) = \ln \frac{(M-1) \cdot exp(-|r_i - a \cdot \hat{s}_i|^2/N_0)}{\sum_{s_j \neq \hat{s}_i} \exp(-|r_i - a \cdot s_j|^2/N_0)}, \tag{6.2.9a}$$

Without CSI

$$L(\hat{s}_i) = \ln \frac{(M-1) \cdot exp(-|r_i - \hat{s}_i|^2/N_0)}{\sum_{s_j \neq \hat{s}_i} \exp(-|r_i - s_j|^2/N_0)}, \tag{6.2.9b}$$

where a shows the fading amplitude. In (6.2.9) the factor $(M-1)$ in the denominator ensures that the reliability function always will be positive.

In the successive-erasure decoding process, we start deleting 1, 3, ..., $d_h - 1$ symbols successively when d_h is even, while for odd d_h's, 2, 4, ..., $d_h - 1$ symbols are deleted in each decoding step. This ensures that the full erasure-correcting capability of the code will be employed.

Fig. 6.6 shows the results of the simulation for the RS (7, 5) coded 8PSK scheme with and without CSI. It is observed that using SEMDD without CSI for a $P_b = 10^{-5}$, about 3.5-6 dB coding gain is obtained compared to errors-only decoding and errors-and-erasures decoding, respectively. This coding gain is improved by an additional 0.7

dB when channel state information is used. Comparing the results of SEMDD with those of the Viterbi decoding reveals that the performance of the latter is superior to that of the former.

The simulation results for the RS (15, 8) coded 16PSK and the RS (63, 42) coded 8PSK schemes are shown in Fig. 6.7 and Fig. 6.8, respectively. For these schemes, the use of SEMDD improves the performance compared to hard-decision decoding. However, this improvement is less than that of the RS (7, 5) coded 8PSK scheme.

6.3. PERFORMANCE COMPARISON OF RS CODED MPSK SCHEMES WITH SOME OTHER BCM SCHEMES

In this section we compare the performance of RS coded schemes with other block-coded 8PSK schemes [65]. These block-coded schemes were designed based on the set-partitioning approach and consists of three binary codes (n, k_1, d_{h1}), (n, k_2, d_{h2}) and (n, k_3, d_{h3}). A general structure of these schemes is shown in Fig. 6.9. The information bits length, k_i, for each code is chosen subject to the condition [47]

$$k_1 + k_2 + k_3 = 3Rn, \tag{6.3.1}$$

where R denotes the code rate. In this case the minimum Euclidean distance of block-coded 8PSK scheme can be obtained as [47]

$$d_e^2 \geq \min(0.586d_{h1}, 2d_{h2}, 4d_{h3}). \tag{6.3.2}$$

In [47]-[51] some BCM schemes are designed for the AWGN channel based on maximizing the minimum Euclidean distance of (6.3.2). Most of these schemes utilize the known binary codes as the components of the BCM schemes.

Some BCM schemes are constructed for fading channels [65] based on the time diversity parameter. We choose three BCM schemes [65] with time diversities 2 or 3 and compare their performances with that of RS (7, 5) coded 8PSK on a Rayleigh fading channel. These codes are denoted by BCM1, BCM2 and BCM3 for our reference. The

parameters of these codes are given in Table 6.1.

Fig. 6.10 shows the average bit error probability of BCM1, BCM2 and BCM3 along with that of the RS (7, 5) coded 8PSK scheme. The Performance of the latter is shown in this figure for different decoding strategies. The performance of RS (7, 5) coded 8PSK, using hard-decision decoding techniques, is comparable with BCM codes with a time diversity of 2. For this coded scheme provides a time diversity of 2 when errors-only or errors-and-erasures decoding techniques is employed. It is seen that in this case the performance is almost the same as that of BCM2. However, it outperforms BCM1.

Comparing the performance of the RS (7, 5) coded 8PSK scheme, using the VA, with that of BCM3 reveals that the performance of the former is superior to the latter in spite of their same decoding complexities. Recalling that (see Table 6.1) the bandwidth efficiency of BCM3 (1.7334 bits/Hz/sec) is less than that of RS (7, 5) coded 8PSK (2.1428 bits/Hz/sec), one can conclude that the latter provides more coding gain and more bandwidth efficiency with no decoding complexity price.

6.4. DISCUSSION

The use of soft-decision information in the decoding process of coded modulation systems provides a remarkable coding gain over hard-decision decoding in Rayleigh fading channels. This gain in general, is much larger than that achieved in the AWGN channel, due to the increase in time diversity of the coded schemes when soft-decision decoding is employed.

The implementation of maximum likelihood decoding is realized by introducing a trellis structure for RS codes and utilizing the VA. A measure of the complexity for this decoding technique is the number of states in the trellis diagram. This number for RS codes is q^{n-k} which grows exponentially with the number of redundant symbols. This decoding technique, hence, is only applicable to codes with small symbol size, q, and small number of redundancy.

Another implementation of the soft-decision decoding for RS codes is the SEMDD algorithm. Although SEMDD is asymptotically optimum for binary codes with antipodal signaling [56], its performance for nonbinary codes with multiphase signaling is inferior to that of MLD. The results of Section 6.2 confirms this statement.

Indeed, this decoding procedure bridges part of the gap between hard-decision decoding and MLD, but not the whole gap. For RS (7, 5) coded 8PSK at a $P_b = 10^{-5}$ almost 2/3 of the MLD performance is obtained by SEMDD. Due to the lack of the results for the other codes such comparison cannot be done properly. But it is observed that by increasing the symbol size, SEMDD becomes less effective. This can be explained as follows.

For the nonbinary case the scalar reliability function (6.2.9) does not contain information about reliability in exactly the same way as in the binary case. In the binary case, there are only two signal points and one decision border. The reliability weight in this case determines exactly the closeness of each of the signal points to the decision border. However, in the nonbinary case there are more than one decision border and a small reliability function does not determine which of these decision borders the received signal is closer to. In other words, it reveals that the hard-decided signal point is unreliable but does not say which one of the other signal points are more likely to be transmitted one. A way to improve this decoding algorithm, hence, is to use a reliability vector, rather than a reliability scalar, for each received signal and to produce more decoded code word candidates than that of the SED procedure. This may improve the performance at the expense of more complexity.

A complexity measure for the SED algorithms is the minimum Hamming distance d_h. Since no more than $(d_h + 1)/2$ successive decoding steps are required for such a decoding process then the number of an errors-and-erasures decoder needed for SED is proportional to d_h. Recalling that the complexity of the errors-and-erasures decoding (the Berlekamp-Massey Algorithm) is proportional to d_h^2 [68], the SED procedure can be

performed with a complexity proportional to d_h^3.

As a final comment the effect of using the channel state information (CSI) in the decoding process can be considered. The results of Chapter 5 showed that the use of CSI in the errors-and-erasures decoding process has no effect on the performance at high SNR. While the results for soft-decision decoding reveals that the use of such information improves the performance of the coded schemes. The effect of CSI for MLD is more than SED.

Table 6.1. Some Block-Coded 8PSK Schemes [65].

Code	L	d_e^2	No. of States	Component Codes C_{b3}	C_{b2}	C_{b1}	n	R (bits/Hz/sec)
BCM1	2	4	4	P_8	P_8	(8,8)	8	2
BCM2	2	4	8	P_{15}^d	P_{15}	P_{15}	15	1.9334
BCM3	3	6	64	P_{15}^d	H_{15}	P_{15}	15	1.7334

P_n: The Overall Parity-Check Code

P_n^d: Dual Code of P_n

H_n: $(2^k - 1, 2^k - k - 1)$ Hamming Code

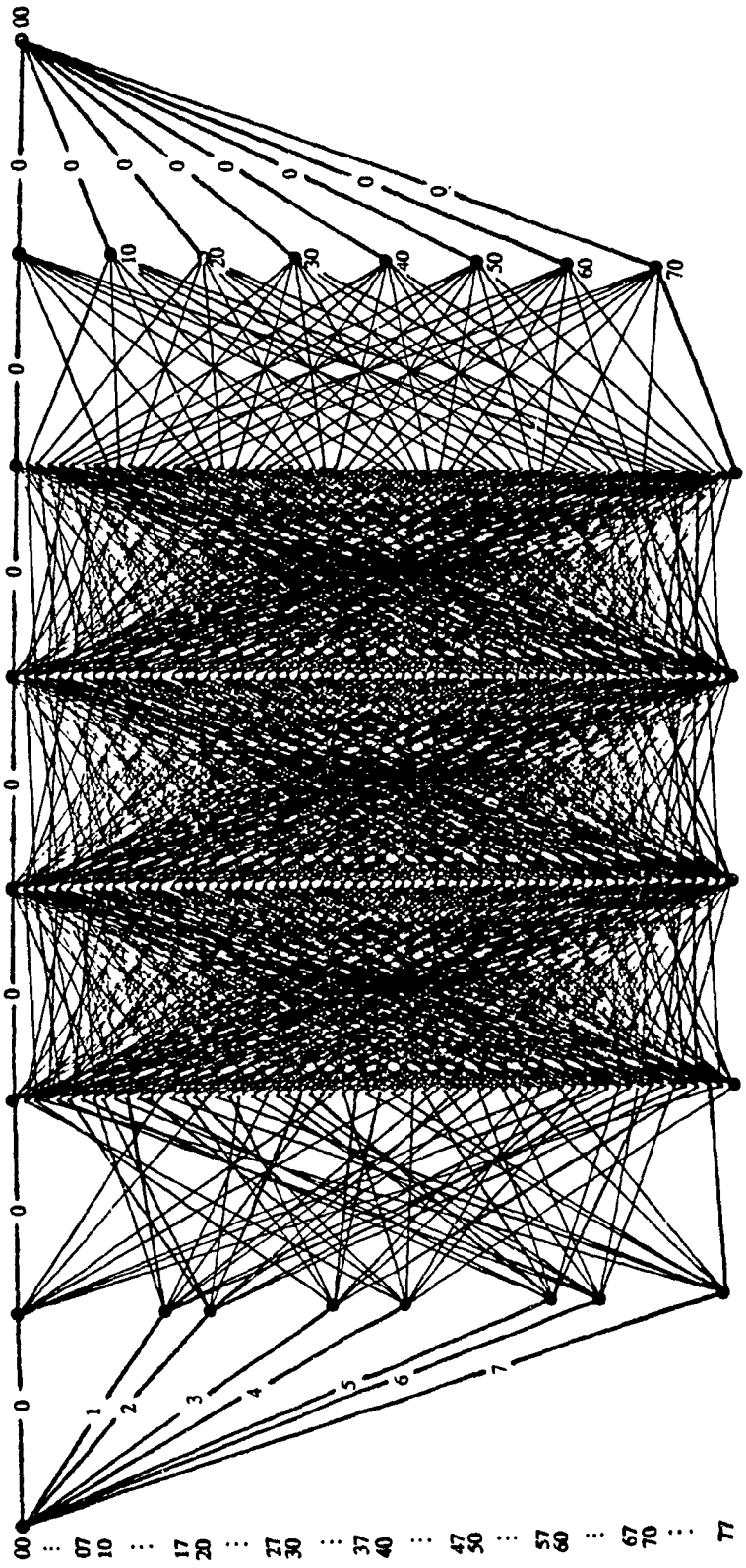

Fig. 6.1. Trellis diagram of RS (7, 5) coded 8PSK.

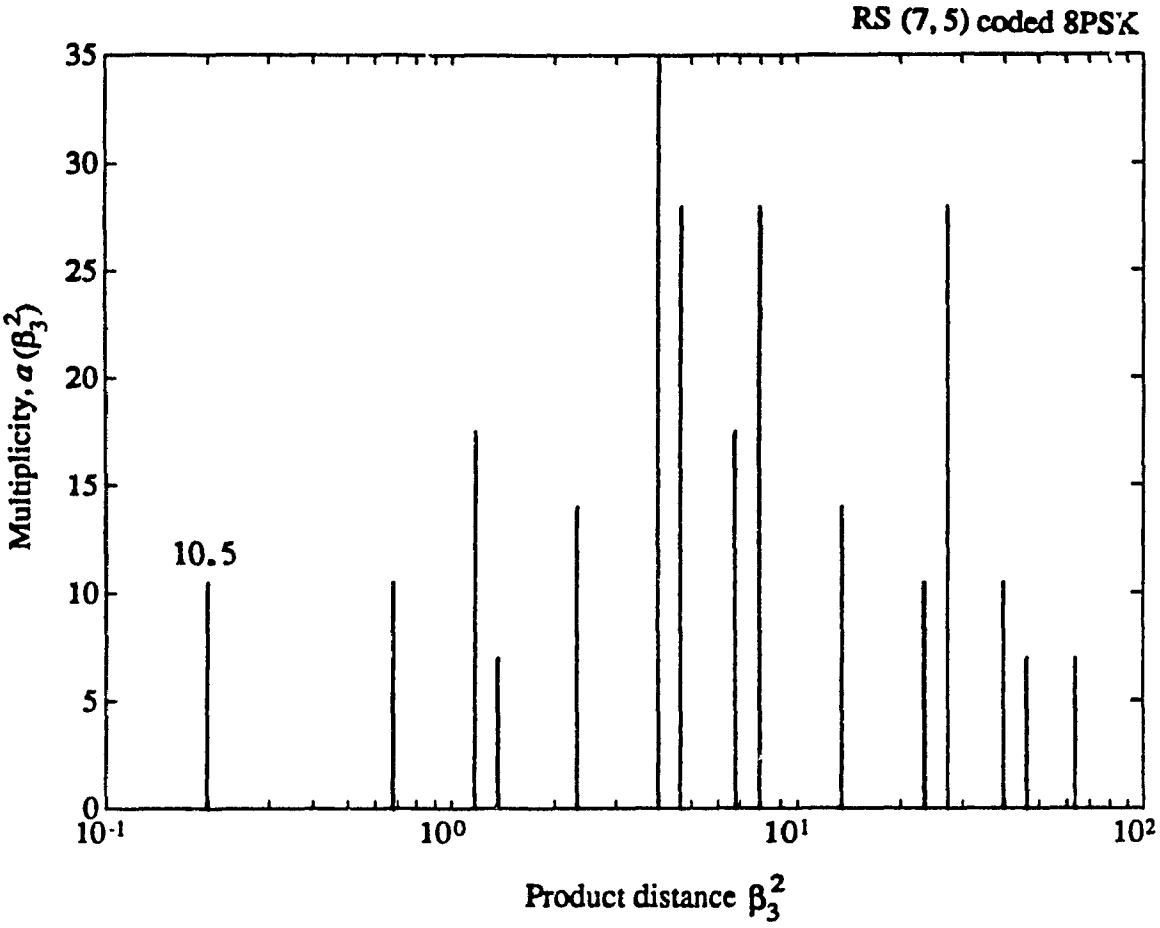

Fig. 6.2. The multiplicity of the product distance β_3^2 for the code words of the RS (7, 5) coded 8PSK scheme with a Hamming distance of 3.

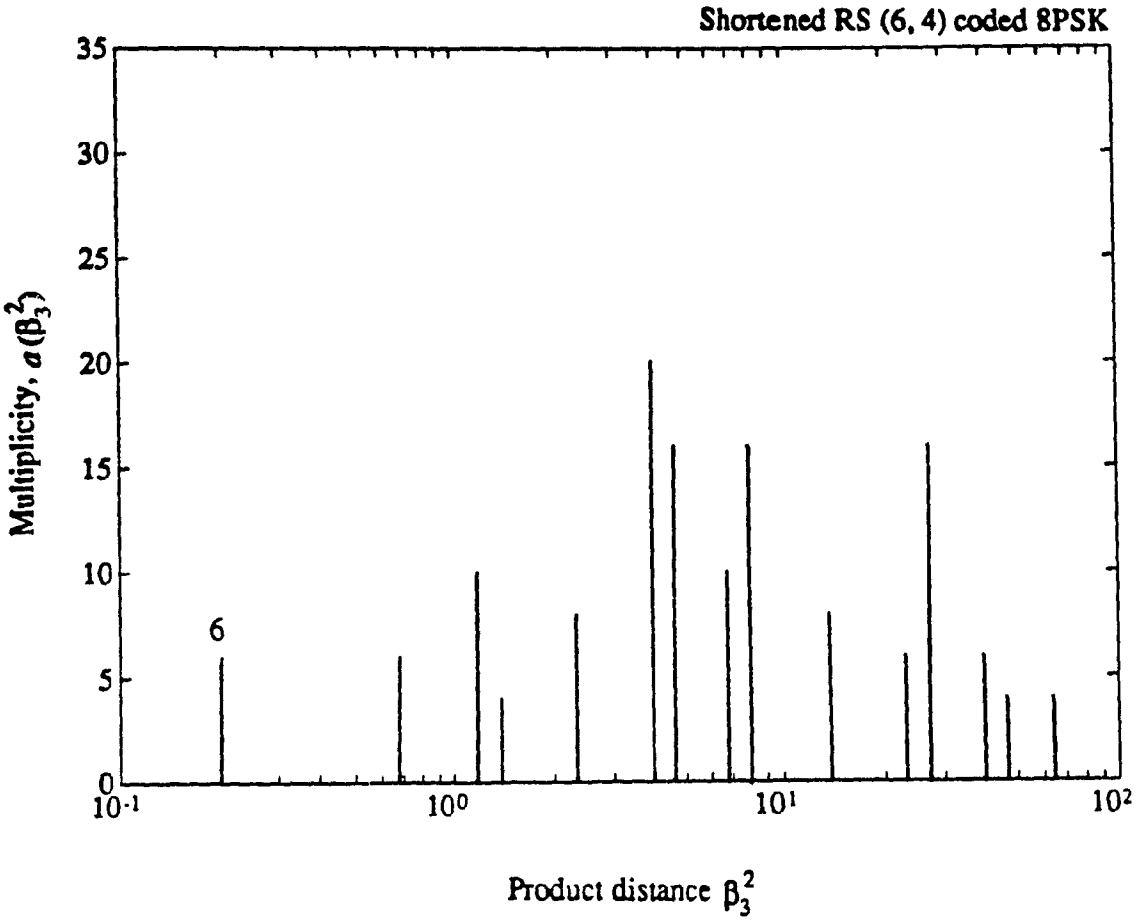

Fig. 6.3. The multiplicity of the product distance β_3^2 for the code words of the shortened RS (6, 4) coded 8PSK scheme with a Hamming distance of 3.

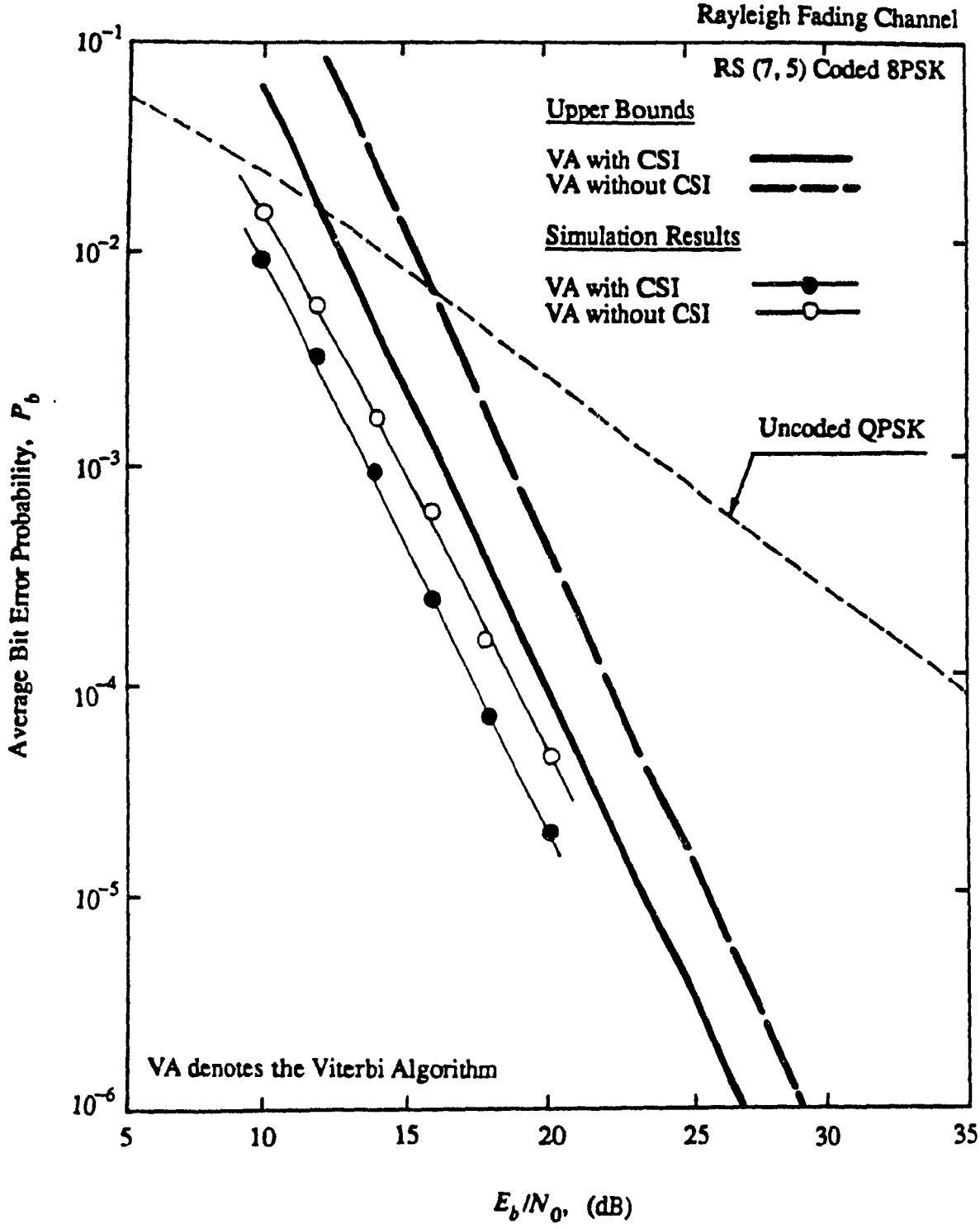

Fig. 6.4. Performance of the RS (7, 5) coded 8PSK scheme, using the VA, in a normalized Rayleigh fading channel.

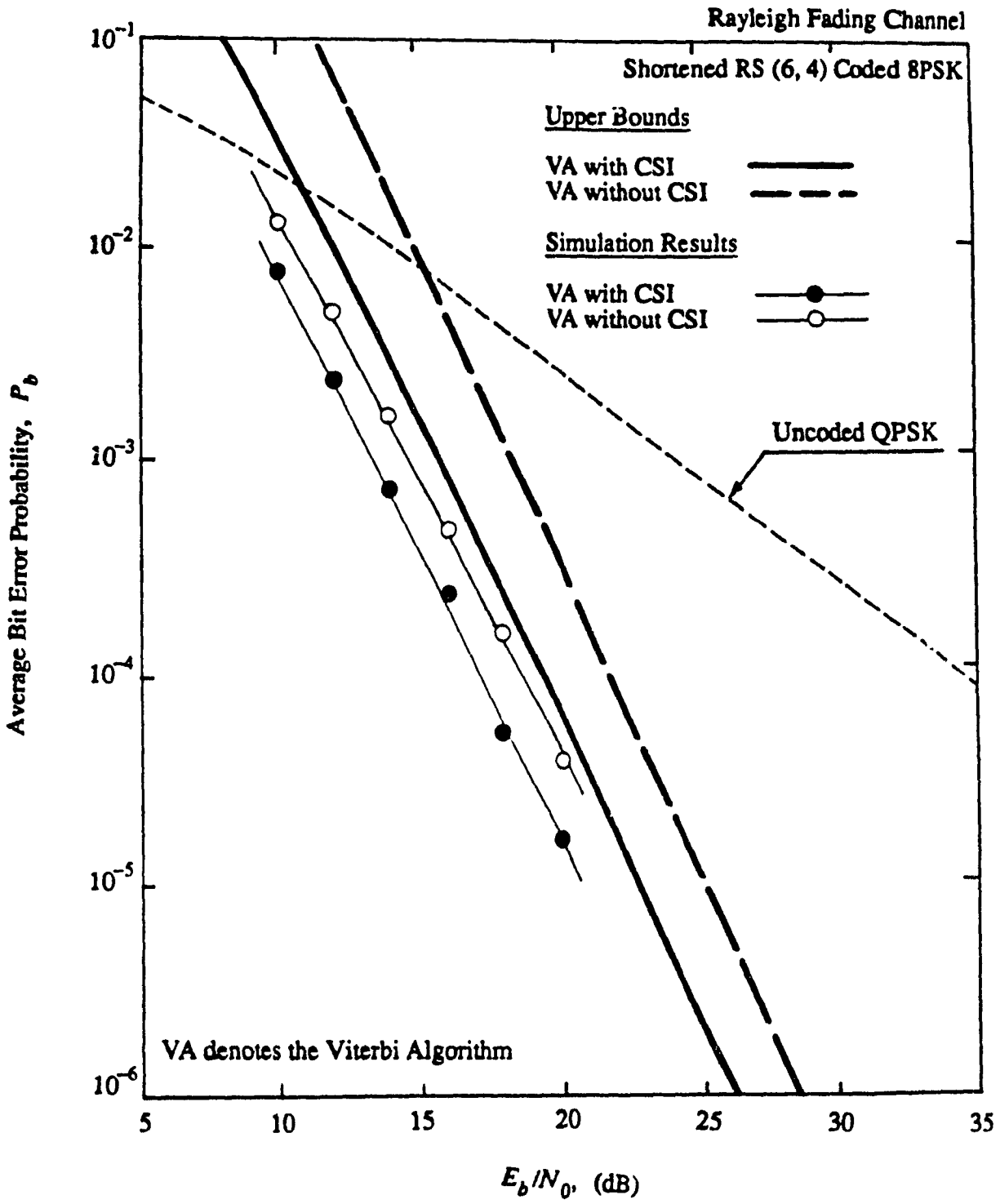

Fig. 6.5. Performance of the shortened RS (6, 4) coded 8PSK scheme, using the VA, in a normalized Rayleigh fading channel.

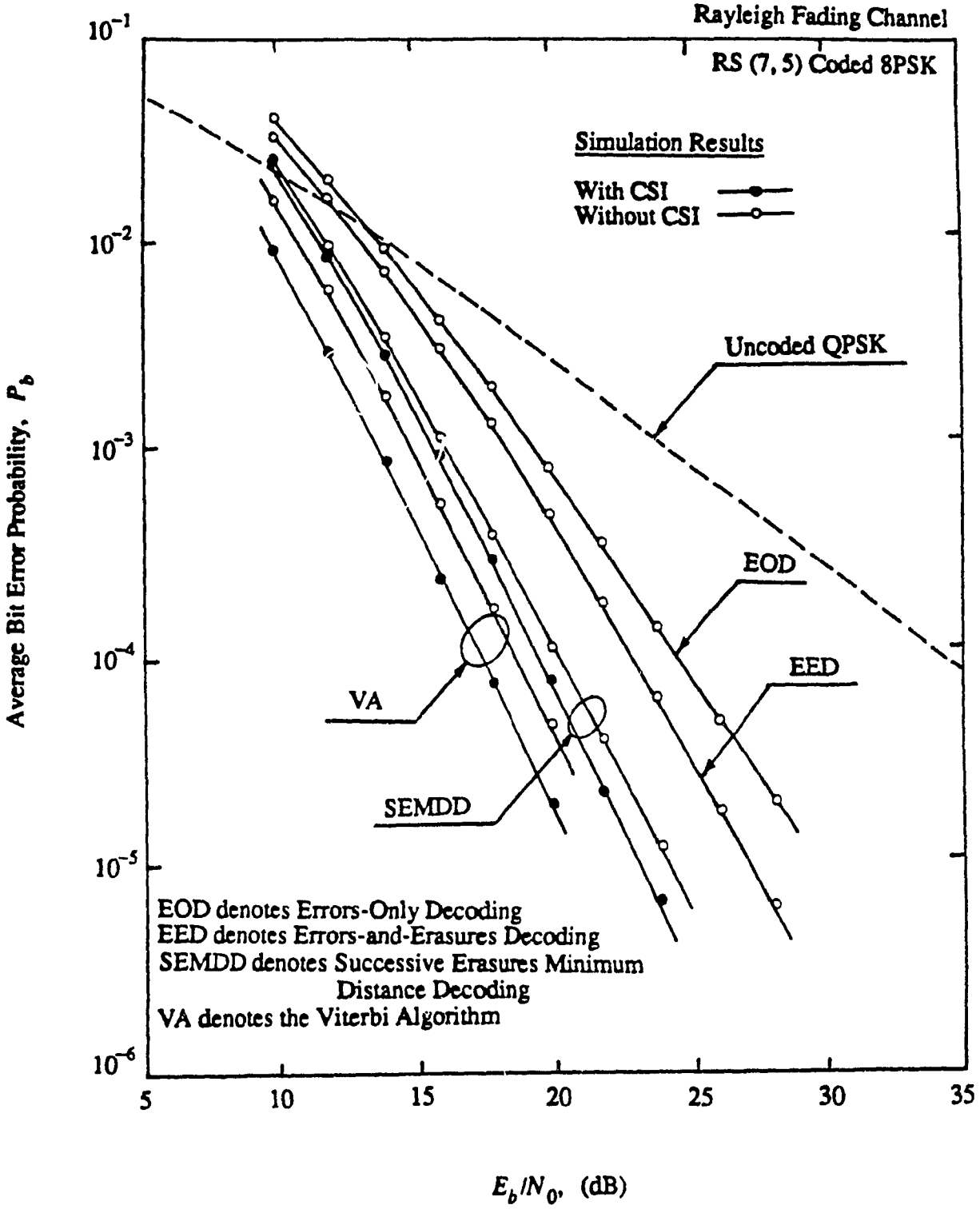

Fig. 6.6. Comparison of the bit error probability of the RS (7, 5) coded 8PSK scheme for different decoding strategies in a normalized Rayleigh fading channel.

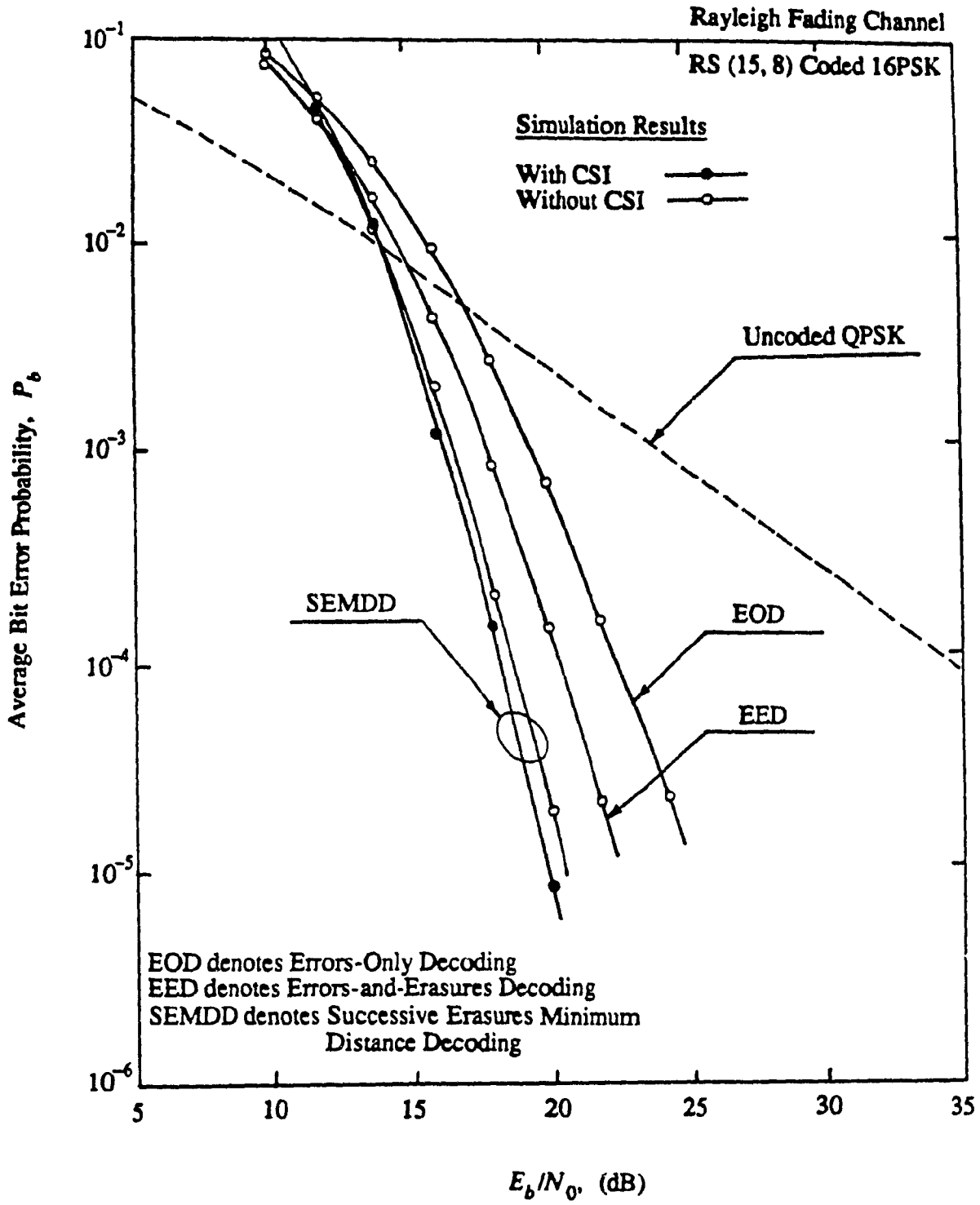

Fig. 6.7. Comparison of the bit error probability of the RS (15, 8) coded 16PSK scheme for different decoding strategies in a normalized Rayleigh fading channel.

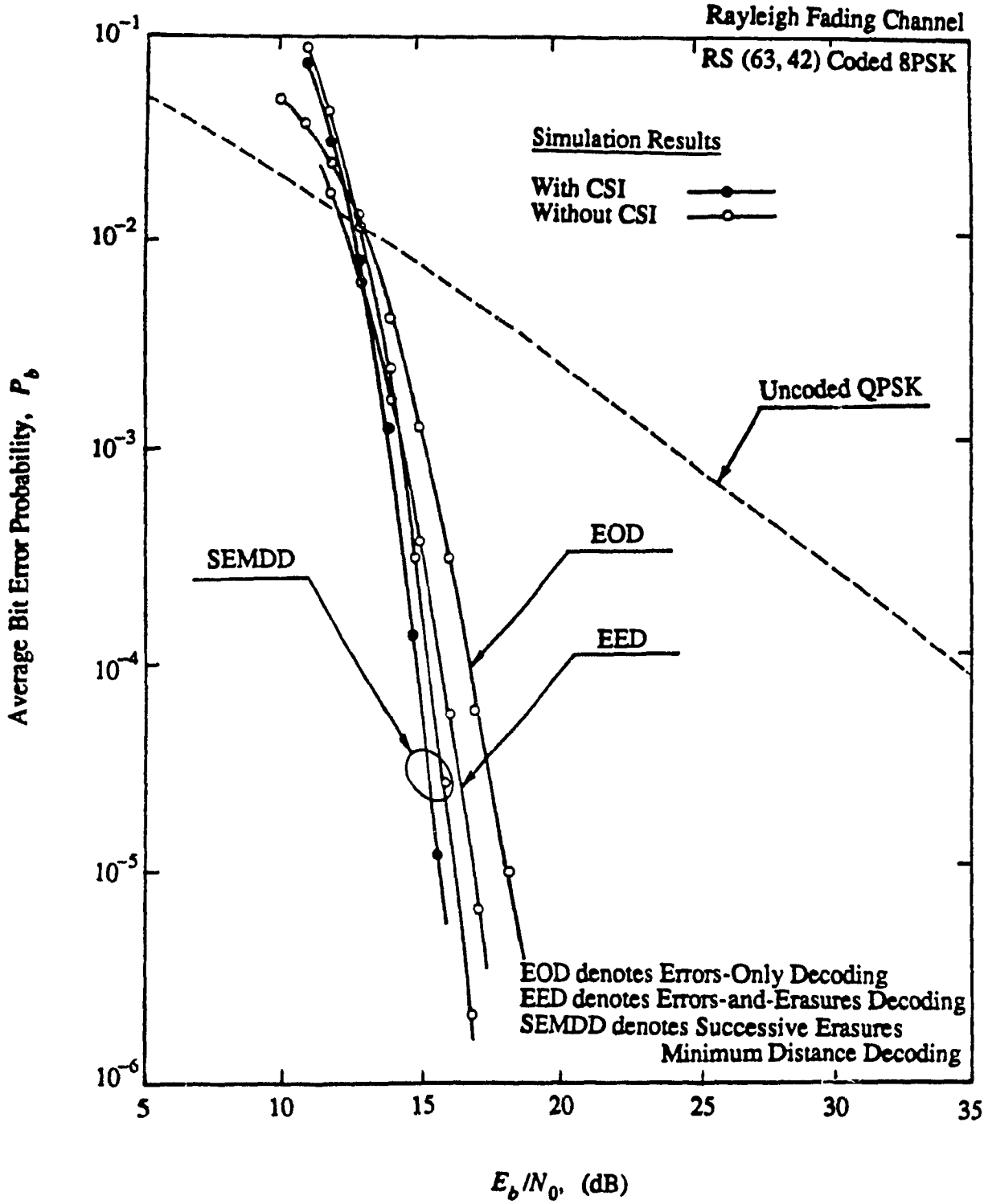

Fig. 6.8. Comparison of the bit error probability of the RS (63, 42) coded 8PSK scheme for different decoding strategies in a normalized Rayleigh fading channel.

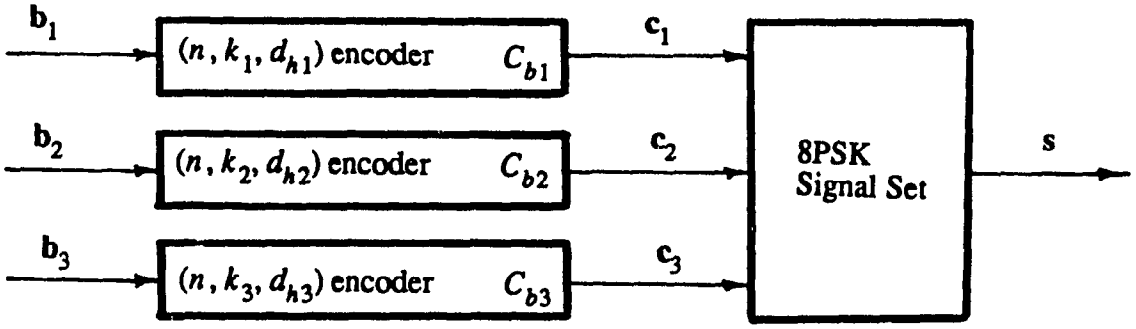

Fig. 6.9. A general encoder for block-coded 8PSK schemes.

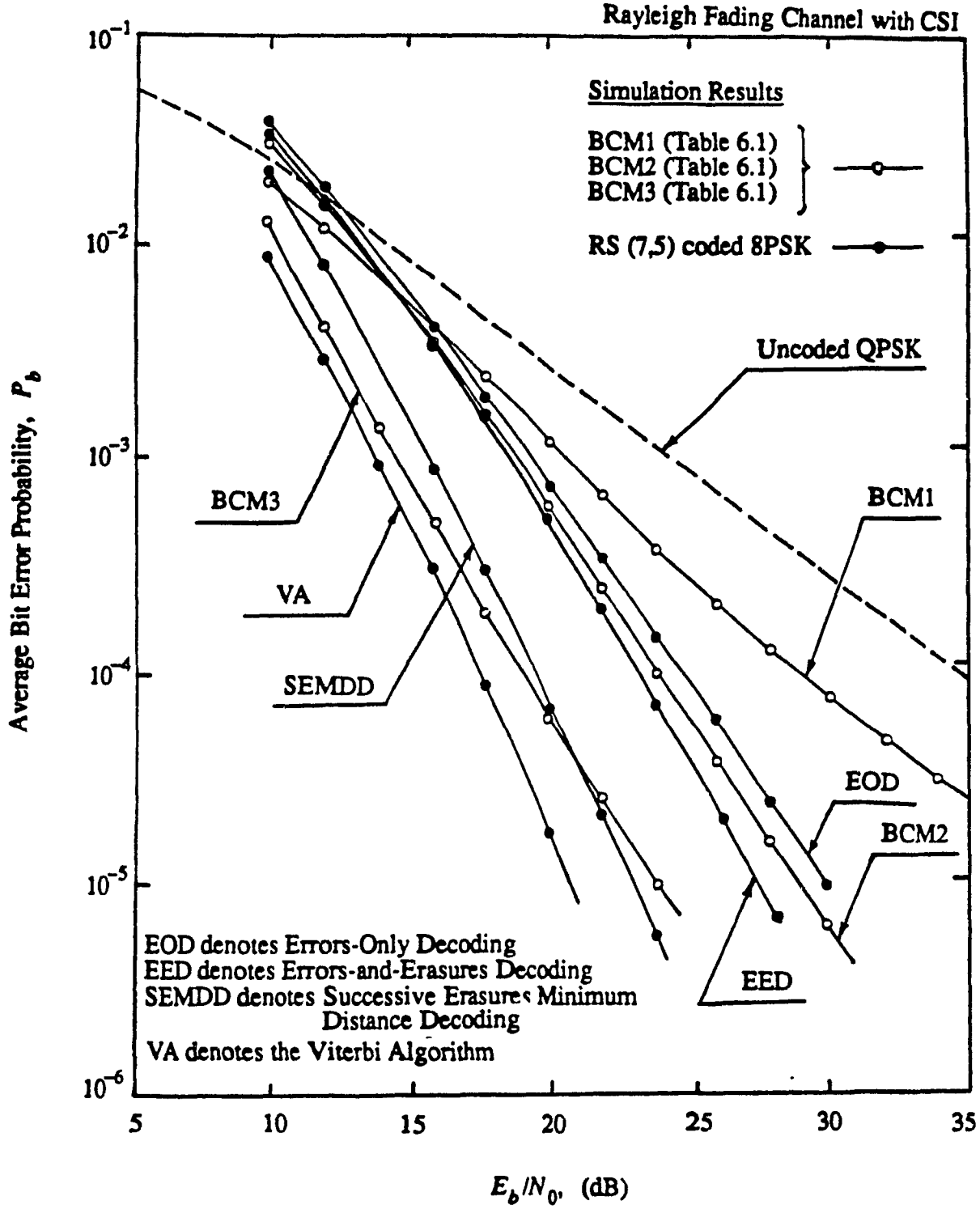

Fig. 6.10. Performance comparison of the RS (7, 5) coded 8PSK scheme with some block-coded 8PSK schemes.

CHAPTER 7

PERFORMANCE OF TRELLIS AND BLOCK CODED SCHEMES ON SHADOWED RICIAN FADING CHANNELS

In preceding chapters, two class of bandwidth-efficient coded-modulation schemes, namely, TCM and BCM schemes were presented. The performance of these schemes was evaluated for a Rayleigh fading channel. The purpose of this chapter is to evaluate the performance of these schemes on a shadowed Rician fading channel and compare them based on the obtained results. With this objective in mind, we first introduce the shadowed Rician fading model and its related parameters. Then the performance of the coded schemes will be evaluated based on the assumption of the ideal interleaving. We will also study the effect of the imperfect interleaving on the performance degradation of the coded schemes. It will be shown that block-coded schemes are less sensitive to the change of fading bandwidth than the trellis-coded ones. Based on this observation and other results a comparison will be carried out between these two class of coded-modulation schemes.

7.1. DESCRIPTION OF THE CHANNEL MODEL

In mobile radio channels, although the statistics of the received signal envelope is Rayleigh distributed, the *shadowing* of the radio signal by buildings and hills leads to gradual changes in local means as the vehicle moves. A suitable model for these channels assumes that [74] the received signal is the sum of a line-of-sight component, γ, which is log-normally distributed because of shadowing, and a Rayleigh distributed multipath

component. If the line-of-sight component is temporarily kept constant, then the conditional probability density function of the fading envelope, a_i, can be shown as

$$p_{A|\Gamma}(a_i|\gamma) = \frac{a_i}{\sigma_a^2} \cdot e^{-\frac{a_i^2+\gamma^2}{2\sigma_a^2}} \cdot I_0\left(\frac{a_i\gamma}{\sigma_a^2}\right), \tag{7.1.1a}$$

where σ_a^2 is the average of the scattered power due to multipath, and $I_0(.)$ represents the zero-order modified Bessel function of the first kind. The probability density function (pdf) of the fading envelope a_i is obtained by averaging the conditional pdf of (7.1.1a) with respect to the log-normally distributed process γ. The pdf of γ is

$$p_\Gamma(\gamma) = \frac{1}{\sqrt{2\pi}\sigma_\gamma \cdot \gamma} \cdot e^{-\frac{(\ln\gamma - m_\gamma)^2}{2\sigma_\gamma^2}}, \tag{7.1.1b}$$

where σ_γ and m_γ are the standard deviation and mean, respectively. Thus,

$$\begin{aligned} p_A(a_i) &= \int_0^\infty p_{A|\Gamma}(a_i|\gamma) \cdot p_\Gamma(\gamma) \cdot d\gamma \\ &= \frac{a_i}{\sqrt{2\pi}\sigma_a^2 \cdot \sigma_\gamma} \int_0^\infty \frac{1}{\gamma} \cdot e^{-\left[\frac{(\ln\gamma - m_\gamma)^2}{2\sigma_\gamma^2} + \frac{(a_i^2+\gamma^2)}{2\sigma_a^2}\right]} \cdot I_0\left(\frac{a_i\gamma}{\sigma_a^2}\right) \cdot d\gamma. \end{aligned} \tag{7.1.1c}$$

The parameter σ_a, σ_γ, and m_γ determine the degree of shadowing. The values of these parameters are given in Table 7.1 for different degrees of shadowing for the Canadian Mobile Satellite (MSAT) Communication channel [75], as an example.

In mobile radio channels the fading amplitudes, a_i's, are correlated due to the Doppler shift associated with relative motion of the transmitter and receiver antennas. The Doppler shift depends upon the mobile speed, the carrier frequency, and the angle between propagation vector and mobile vector [76]. For reasonable bit rates and mobile velocity, the fading varies slowly compared to the bit rate. This results in a channel with memory where the errors occur in bursts. The error bursts degrade the performance of the

coded schemes. To transform the bursts into statistically independent errors, interleaving/de-interleaving is commonly applied. Sufficiently large interleaving destroys the memory of the channel. In the following the error bounds for coded schemes on a shadowed Rician channel are evaluated for zero channel memory (perfect interleaving). The use of the Channel State Information (CSI) by the receiver is assumed.

7.2. UPPER BOUNDS WITH VITERBI DECODING

In determining the upper bound on bit error probability of trellis coded schemes and the Viterbi Algorithm (VA), it is useful to recall the state diagram and the associated generating function approach described in Chapter 4. The pairwise error probability, conditioned on the fading amplitude, is easily shown to be upper bounded by [35]

$$P_2(\mathbf{s}, \hat{\mathbf{s}}|\mathbf{a}) \le \exp\left[-E_s/4N_0 \sum_{i \in \eta} a_i^2 |s_i - \hat{s}_i|^2\right], \tag{7.2.1}$$

where η is the set of all i for which $s_i \neq \hat{s}_i$. The unconditional pairwise error upper bound can then be determined by averaging over the fading amplitude $\mathbf{a}$, with the result

$$P_2(\mathbf{s}, \hat{\mathbf{s}}) \le E_{\mathbf{a}}\left[\exp\left[-E_s/4N_0 \sum_{i \in \eta} a_i^2 |s_i - \hat{s}_i|^2\right]\right], \tag{7.2.2}$$

where $E_{\mathbf{a}}$ denotes the statistical averaging with respect to $\mathbf{a}$. Recall that a union bound on the bit error probability can be obtained by summing the pairwise error probabilities weighted by the number of nonzero information bits along the corresponding incorrect path. This information for a TCM scheme is implicit in the generating function $T(D, I)$ associated with the error state diagram (see Chapter 4).

To evaluate the unconditional pairwise error probability (7.2.2) we consider the *time-varying* fading. We refer time-varying fading to the fading channel with zero memory. This is achieved by assuming suitably large interleaving. Because of ideal interleaving, the fading amplitude, although constant within a signaling interval, is

independent from interval-to-interval. In this case (7.2.2) can be written as

$$P_2(s, \hat{s}) \le \prod_{i \in \eta} E_{a_i}\left[\exp\left[-E_s/4N_0\, a_i^2 |s_i - \hat{s}_i|^2\right]\right], \tag{7.2.3a}$$

where

$$E_{a_i}\left[\exp(-a_i^2 . \delta_i^2 . \gamma_s/4)\right] = \frac{1}{\sqrt{2\pi}\sigma_a^2 . \sigma_\gamma} \int_0^\infty \frac{1}{\gamma} . e^{-\left[\frac{(\ln\gamma - m_\gamma)^2}{2\sigma_\gamma^2} + \frac{(a_i^2 + \gamma^2)}{2\sigma_a^2}\right]}$$

$$. \left(\int_0^\infty a_i e^{-\frac{a_i^2(1 + 2\sigma_a^2 . \delta_i^2 . \gamma_s/4)}{2\sigma_a^2}} . I_0\left(\frac{a_i\gamma}{\sigma_a^2}\right) . da_i\right) . d\gamma. \tag{7.2.3b}$$

In (7.2.3b), γ_s and δ_i^2 denote E_s/N_0 and $|s_i - \hat{s}_i|^2$, respectively. The second integral can be simplified using [77, p.717]

$$\int_0^\infty t e^{-\alpha t^2} J_0(\beta t) . dt = \frac{1}{2\alpha} e^{\left(-\frac{\beta^2}{4\alpha}\right)}, \tag{7.2.4a}$$

where [77, p. 952]

$$J_0(jt) = I_0(t). \tag{7.2.4b}$$

Using (7.2.4) in (7.2.3b), after some mathematical manipulations we obtain

$$E_{a_i}\left[\exp(-a_i^2 . \delta_i^2 . \gamma_s/4)\right] \equiv E_{a_i}[D^{a_i^2\delta_i^2}] = \frac{1}{(1 + \sigma_a^2 . \delta_i^2 . \gamma_s/2)\sqrt{\pi}}$$

$$. \int_{-\infty}^\infty e^{-t^2 - \frac{\delta_i^2 . \gamma_s/4}{1 + \sigma_a^2 . \delta_i^2 . \gamma_s/2} e^{2(\sqrt{2}\sigma_\gamma t + m_\gamma)}} . dt. \tag{7.2.5a}$$

where for high signal-to-noise ratios, i.e., $\gamma_s \gg 2/(\sigma_a^2 . \delta_i^2)$, can be simplified as

$$E_{a_i}[D^{a_i^2\delta_i^2}] = \frac{1}{\sqrt{2\pi\sigma_a^2}\cdot\delta_i^2\cdot\gamma_s/4}\int_{-\infty}^{\infty} e^{-t^2-\frac{1}{2\sigma_a^2}\cdot e^{2(\sqrt{2}\alpha_i t+m_i)}}\,dt. \qquad (7.2.5b)$$

Using (4.2.5) an upper bound on the bit error probability is given by

$$P_b \le \frac{1}{m}\frac{\partial \bar{T}(D,I)}{\partial I}\Big|_{I=1,\,D=\exp(-E_s/4N_0)}, \qquad (7.2.6)$$

where the transfer function $\bar{T}(D,I)$ is obtained from that of the no fading case replacing the branch label factor $D^{\delta_i^2}$ by (7.2.5b).

Similar upper bounds are obtained for RS coded schemes using the analytical approach of Chapter 6. For a time-varying fading channel, the upper bound on bit error probability is determined as

$$P_b \le \sum_{\beta_{d_h}} \frac{d_h}{mn}\cdot\frac{a(\beta_{d_h})}{\beta_{d_h}}\cdot\left[\frac{E_{a_i}[D^{a_i^2\delta_i^2}]}{E_s/4N_0}\right]^{d_h}, \qquad (7.2.7)$$

where $E_{a_i}[D^{a_i^2\delta_i^2}]$ is given by (7.2.5) and the other parameters are defined in Section 6.2.1.

The upper bounds for three rate 2/3 trellis coded 8PSK schemes, namely, Ungerboeck's 4-state scheme (4U), New 4-state scheme (4N), and Ungerboeck's 8-state scheme (8U) are shown in Fig.'s 7.1-7.3 for light, average, heavy shadowed Rician fading channels, respectively. The upper bounds for the Viterbi decoding of the RS (7, 5) coded 8PSK scheme are also included. The simulation results are provided in these figures for examining the tightness of the upper bounds.

It is observed that these bounds become tight for higher signal-to-noise ratios. However, the tightness of the upper bounds depends on the degree of shadowing. For the heavy shadowed Rician channel the upper bounds are weaker than the other two channels. The problem is essentially that the conditional bound given by (7.2.1) is weak for

can assume small values unless there is a strong line-of-sight component. Since for the heavy shadowed channel the line-of-sight component is weak, the upper bound on the bit error probability in this channel is less tighter than the other two channels.

7.3. LOWER BOUNDS WITH HARD-DECISION DECODING

To evaluate the performance of the RS coded schemes on shadowed Rician fading channels for errors-only and errors-and-erasures decoding the lower bounds on the bit error probability of (5.3.10) and (5.3.25) are utilized. The associated probabilities with these lower bounds, however, can no longer be expressed as closed forms, as was in the Rayleigh fading. In this case, these probabilities are obtained by numerical integration.

The lower bounds for RS (7, 5) coded 8PSK, as an example, for different degrees of shadowing are represented in Fig.'s 7.4-7.6. The simulation results for different decoding strategies, i.e., errors-only, errors-and-erasures, and SEMDD, are also included in these figures.

The lower bounds of the post decoding bit error rate for the errors-and-erasures decoding technique have been found by optimizing the fading amplitude threshold, a_T, for each value of E_b/N_0. Fig. 7.7 represents the optimized fading amplitude threshold a_T versus E_b/N_0 for three different shadowed channels. The optimum threshold decreases with increasing signal-to-noise ratio, E_b/N_0. A comparison between optimum threshold values for different channels shows that this value for the light shadowed channel is higher than the other ones. However, the slope of the optimum threshold variation of the heavy shadowed channel is smaller than the light and average shadowed channels.

To study the effect of the erasure threshold a_T on the bit error probability this probability is evaluated for different threshold values. The signal-to-noise ratio is chosen to yield $P_b = 10^{-5}$ for optimum threshold decoding. Fig. 7.8 represents the bit error probability as a function of the threshold value a_T for different degrees of shadowing. It is observed that for values below and above the optimum threshold the bit error probability

increases. This can be explained as follows. For the threshold values below the optimum one, the decoder ignores too many erroneous symbols as erasures and hence P_b increases. On the other hand, for values above the optimum threshold the decoder erases too many correct symbols which again increases P_b. It is intersting to note that the performance improvement due to errors-and-erasures decoding depends upon the degree of shadowing. This can be seen from Fig. 7.8. In this figure the intersection of the curves with $a_T = 0$ denotes the bit error probability corresponding to the errors-only decoding. It is observed that this value becomes higher when the degree of shadowing increases. Hence, the use of errors-and-erasures decoding in heavy shadowed channel results in more improvement.

7.4. THE EFFECT OF FADING BANDWIDTH ON THE PERFORMANCE OF THE CODED SCHEMES

The preceding sections have been concerned with the evaluation of the performance of the coded schemes in time-vaing shadowed Rician fading channels under the assumption of ideal interleaving/de-interleaving. The present section will be concerned with the effect of limited interleaving/de-interleaving. In order to study the performance degradation of the coded schemes due to the imperfect interleaving, we only change the normalized bandwidth of the fading process. With this approach the effect of interleaving is taken into account by considering the results for higher fading bandwidth to be equivalent to those when the actual fading bandwidth is low and interleaving is utilized.

The performance in this case is not amenable to analytical evaluation so that resort has been made to computer simulations only. Before presenting the simulation results a brief description of the simulated channel is required.

To simulate a shadowed Rician channel with limited fading bandwidth the components of the line-of-sight and multipath fading are filtered to provide the desired Doppler bandwidth. The block diagram of the simulated channel is shown in Fig. 7.9.

The complex channel gain $A = a \cdot e^{j\theta}$ is generated by three independent Gaussian Random Variables (GRV) [39], [45]. This random variables are filtered by a third-order Butterworth filter of 3 dB normalized bandwidth $B_D T_s$, where B_D is the Doppler frequency of the channel and T_s denotes the symbol interval. The parameters σ_a^2, m_γ and σ_γ^2 determine the degree of shadowing. In this study we use the light shadowed channel with the parameters of Table 7.1. The parameter ρ depends on the bandwidth of the fading process and its value for different normalized bandwidth $B_D T_s$ is given in [45].

The effect of fading bandwidth on the performance of 4-state and 8-state TCM schemes as well as RS (7,5) coded 8PSK and RS (63, 42) coded 8PSK, on the light shadowed Rician fading channel, are shown in Fig.'s 7.10-7.14, respectively. For RS (7, 5) coded 8PSK the results are given for both hard-decision and soft-decision decoding techniques, while for RS (63, 42) coded 8PSK only the errors-only decoding is considered.

As one would expect the performance of the coded schemes gets better as the fading bandwidth increases; that is, when the channel errors become more bursty. Indeed, for small normalized fading bandwidth the fading is slow enough to be considered as approximately constant over a number of symbol intervals in a decoding span. Using the *slow-fading* model the pairwise error probability (7.2.2) is written as

$$P_2(\mathbf{s}, \hat{\mathbf{s}}) \le E_a \left[\exp\left[-E_s/4N_0 \, a^2 |\mathbf{s} - \hat{\mathbf{s}}|^2 \right] \right], \qquad (7.4.1a)$$

which can be simplified, using (7.2.4), as

$$P_2(\mathbf{s}, \hat{\mathbf{s}}) \le \frac{1}{\sqrt{2\pi}\sigma_a^2 \cdot d_E^2(\mathbf{s},\hat{\mathbf{s}}) \cdot E_s/4N_0} \int_{-\infty}^{\infty} e^{-t^2 - 1/\sigma_a^2 \cdot e^{2(\sqrt{2}\sigma_\gamma t + m_\gamma)}} \cdot dt, \qquad (7.4.1b)$$

where $d_E(\mathbf{s},\hat{\mathbf{s}})$ shows the Euclidean distance between sequences $\mathbf{s}$ and $\hat{\mathbf{s}}$. Eq. (7.4.1b) shows that the pairwise error probability varies inversely with E_s/N_0, and hence, the coded scheme only provides time diversity of order one. This is in contrast with the time-varying fading case where the time diversity of the coded scheme depends upon the

length of the shortest error event path. Considering that the uncoded schemes also provide time diversity of order one, we may find that the coded schemes on slow-fading channel perform worse than the uncoded one (see, for example, Fig.'s 7.10-12). To get benefit of coding in fading channels with memory, therefore, the use of sufficient interleaving is required.

It is observed that the performance degradation of RS (63, 42) coded 8PSK is much less than that of RS (7, 5) coded 8PSK. In the former case, for $B_D T_s \geq 0.2$ there is little difference from the limiting random channel, i.e., $B_D T_s = \infty$. One might expect this by considering the high error correction capability of this code. Also, because of its structure this coded scheme treats burst errors of two channel symbols as one error. Of interest is also the difference between performance degradation of the RS (7,5) coded 8PSK scheme for different decoding strategies. The sensitivity of the Viterbi decoding to the variations of fading bandwidth (imperfect interleaving) is more than the errors-only decoding technique.

Here we compare the effect of the channel fading bandwidth on TCM and RS coded schemes. The average bit error probability, for different coded schemes, in terms of the normalized fading bandwidth is plotted in Fig. 7.15. These results are given for $E_b/N_0 = 10$ dB. It is observed that, in general, the RS coded MPSK schemes are less sensitive to the variation of fading bandwidth than TCM schemes. For example, for RS (63, 42) coded 8PSK the bit error rate (BER) degradation for the fading bandwidth range of 0.1-0.3 is less than 2 times, while this degradation for an 8-state TCM is about 10 times.

The performance degradation of TCM schemes is due to the sensitivity of the Viterbi decoding to bursty errors. This algorithm contributes in degradation of the performance in two ways. First, its error propagation nature which is more effective when the fading bandwidth is small and channel creates burst errors. Second, its non-optimum metric when the samples of the fading process are correlated. Recall that in applying the Viterbi algorithm it is assumed that the channel is memory-less, therefore, the maximum

likelihood rule results in an equivalent Euclidean distance as an additive metric. For the channels with memory the use of such a metric may not be the optimum choice. Note that in the Viterbi decoding of the RS codes since each block is decoded independently the error propagation does not exist, while the second problem can be considered as a source of degradation.

7.5. DISCUSSIONS

To show the efficiency of the RS coded schemes, the performance of these schemes are compared with some rate 2/3 TCM schemes on the light shadowed Rician fading channel. Fig. 7.16 shows the simulation results for the New 4-state (4N) and Ungerboeck's 8-state rate 2/3 trellis coded 8PSK schemes over such a channel with the use of CSI. The simulation results for errors-only decoding and SEMDD of RS (7, 5) coded 8PSK and RS (63,42) coded 8PSK are also included.

It is observed that the performance of RS (7, 5) coded 8PSK, using hard-decision decoding, is inferior to both TCM schemes. However, this scheme with soft-decision decoding, the VA or SEMDD, outperforms the 4-state TCM. The performance of RS (63, 42) coded 8PSK is superior to the TCM schemes at high SNR's. This concludes that the use of RS coded MPSK schemes becomes interesting only for large values of SNR where they begin to outperform trellis codes.

To compare the performance of different decoding strategies for the RS coded schemes over shadowed Rician fading channels, the results of Fig. 7.1-7.3 are summarized in Table 7.2 for the RS (7,5) coded 8PSK scheme. In this table the additional improvement in coding gain compared to the errors-only decoding technique is given at bit error rate of 10^{-5}.

We see that there is only a small difference between errors-only and errors-and-erasures decoding performances. Considering Fig. 7.8 it is also observed that the performance of the errors-and-erasures decoding quickly deteriorates if the threshold is not

optimal. In view of this and difficulty to estimate the fading amplitude errors-and-erasures decoding seems an unattractive solution. Instead, SEMDD promises a remarkable coding gain with some increase in the complexity.

Among the different decoding strategies, the soft-decision decoding is the most effective one. Note that for such channels the use of soft-decision decoding results in a SNR improvement considerably larger than 3dB, the value typically obtained for the AWGN channel. In hard-decision error correction decoding of block codes, errors can occur when the number of errors exceeds the minimum distance of the code, and hence, the effective order of diversity is half the minimum distance of the code. On the other hand, in soft-decision decoding the effective order of diversity corresponds to the minimum distance of the code. In the case of RS (7, 5) coded 8PSK, soft-decision decoding changes the effective diversity order of code from 2 to 3. This increases the slope of the BER curve and causes a significant coding gain which increases with SNR. However, this is achieved by increasing the complexity of the decoder.

The complexity of the soft-decision decoding, using the VA, is measured by the number of the states in the trellis diagram. Hence, the complexity of the soft-decision decoding of the RS(7,5) coded 8PSK scheme, for example, is compared with a 64-states trellis decoder. However, the *decision depth* and the *decoding delay* in this case is much less than that of an equivalent 64-state trellis code. For a 64-state trellis code the decision depth is at least 5×6 = 30 channel symbols, while this delay for the RS (7,5) coded 8PSK scheme is 7 channel symbols. The lower decision delay can be considered as a privilege for this scheme when the overall transmission delay is limited. This allows one to increase the size of the interleaver/de-interleaver and improve the performance of the coded system for burst error channels.

It is also interesting to note that the improvement in SNR for a given bit error rate depends on the degree of shadowing. Table 7.2 shows that this improvement increases with the degree of shadowing. In fact, in heavy shadowed channels the line-of-sight com-

ponent of the received signal experiences more shadowing, hence, the use of the channel measurement information in the decoding process will result in a larger SNR improvement.

Table 7.1. Channel Model Parameters For a Mobile Shadowed Rician Fading Channel

Degree of Shadowing	σ_a^2	m_γ	σ_γ
Light	0.158	0.115	0.115
Average	0.126	-0.115	0.161
Heavy	0.0631	-3.91	0.806

Table 7.2. Additional Coding Gain of Different Decoding Strategies Compared to Errors-Only Decoding Technique at a Bit Error Rate of 10^{-5}, for RS (7, 5) Coded 8PSK

Decoding Strategy / Degree of Shadowing	EED	Soft-Decision (VA)	
		Without CSI	With CSI
Light	1 dB	5.5 dB	6.5 dB
Average	1.5 dB	≈6 dB	≈7 dB
Heavy	2 dB	≈7 dB	≈8.5 dB

EED: Denotes Errors-and-Erasures Decoding

VA: Denotes the Viterbi Algorithm

CSI: Denotes the Channel State Information

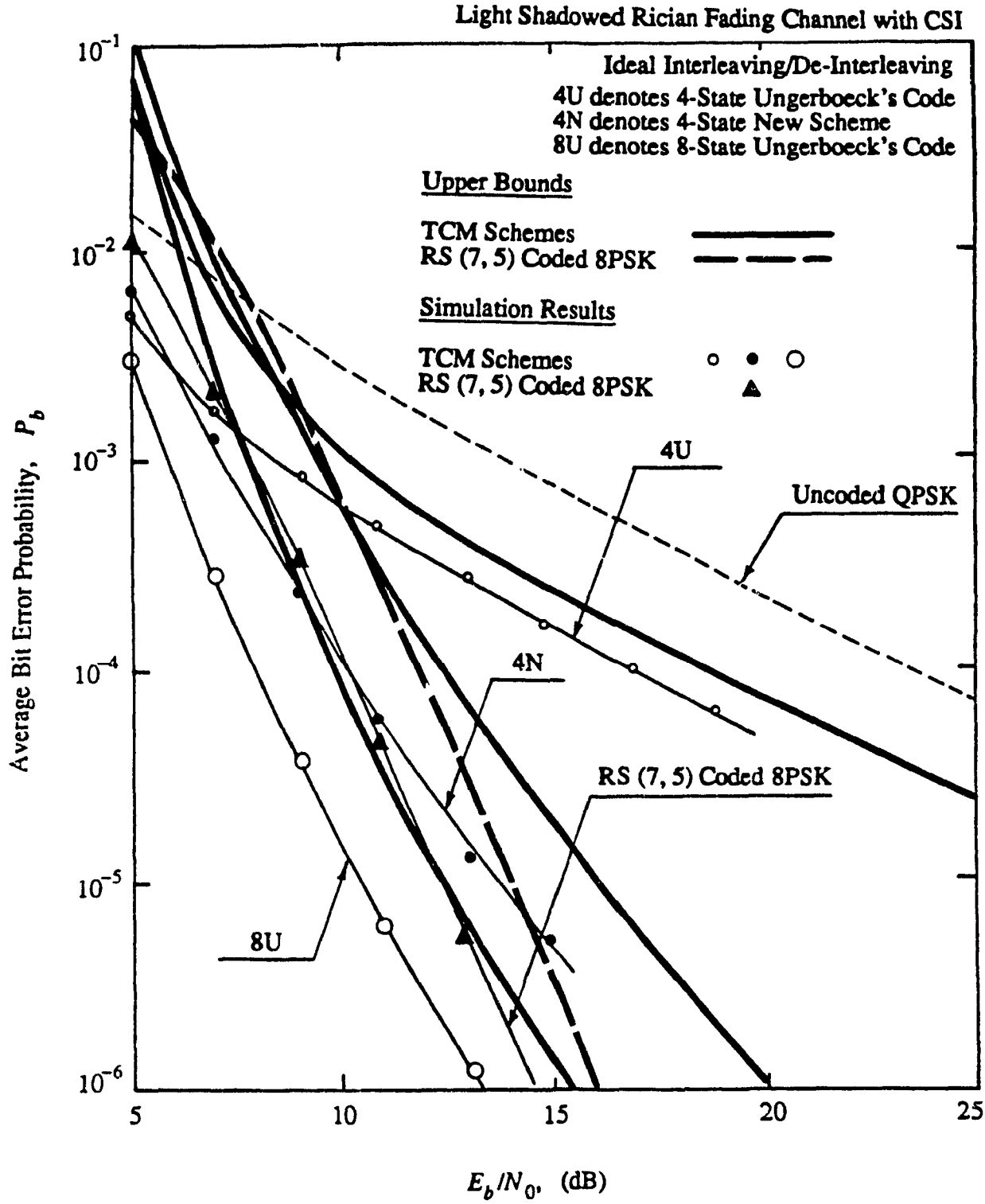

Fig. 7.1. Performance of some trellis-coded 8PSK schemes and the RS (7, 5) coded 8PSK scheme over the light shadowed Rician fading channel.

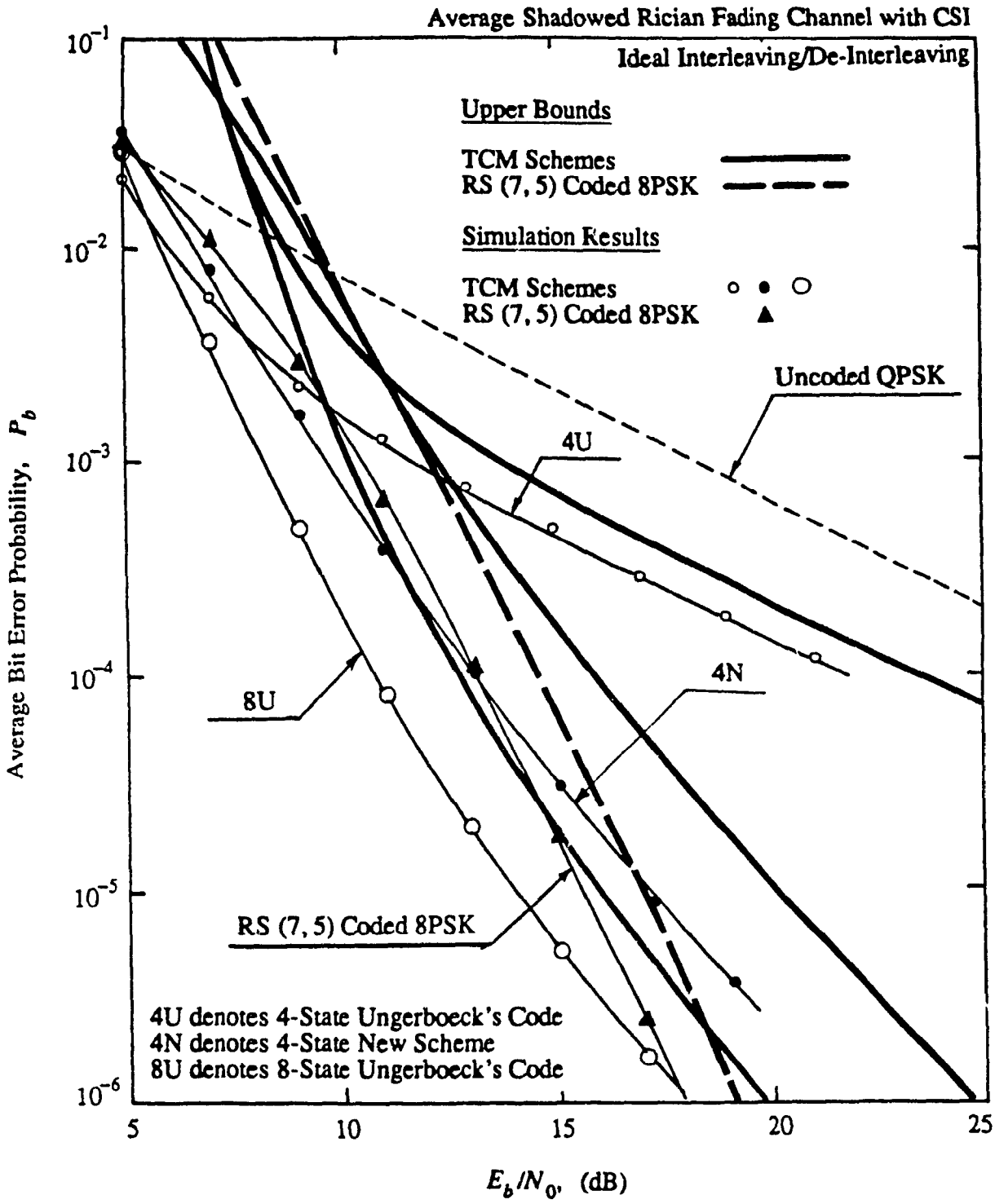

Fig. 7.2. Performance of some trellis-coded 8PSK schemes and the RS (7, 5) coded 8PSK scheme over the average shadowed Rician fading channel.

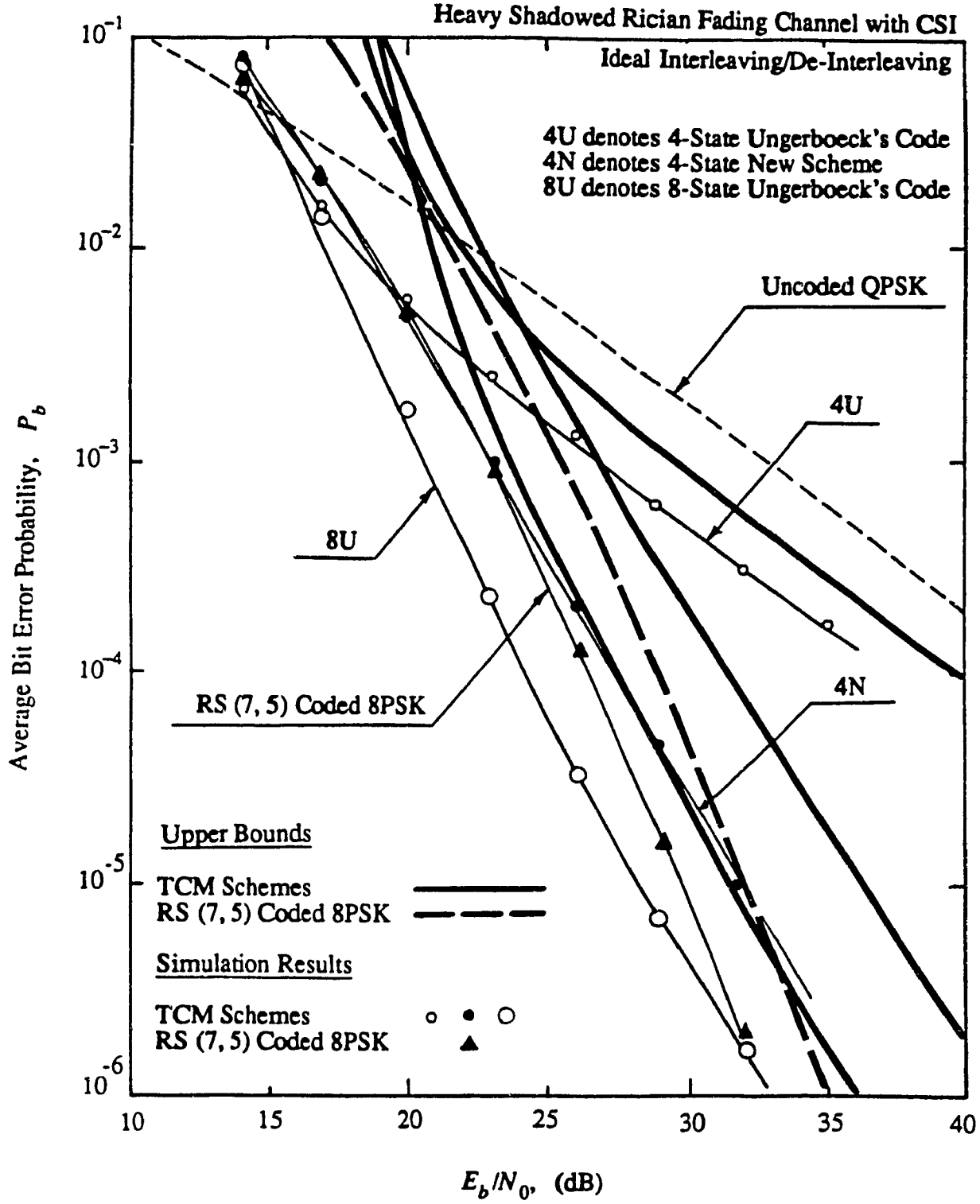

Fig. 7.3. Performance of some trellis-coded 8PSK schemes and the RS (7, 5) coded 8PSK scheme over the heavy shadowed Rician fading channel.

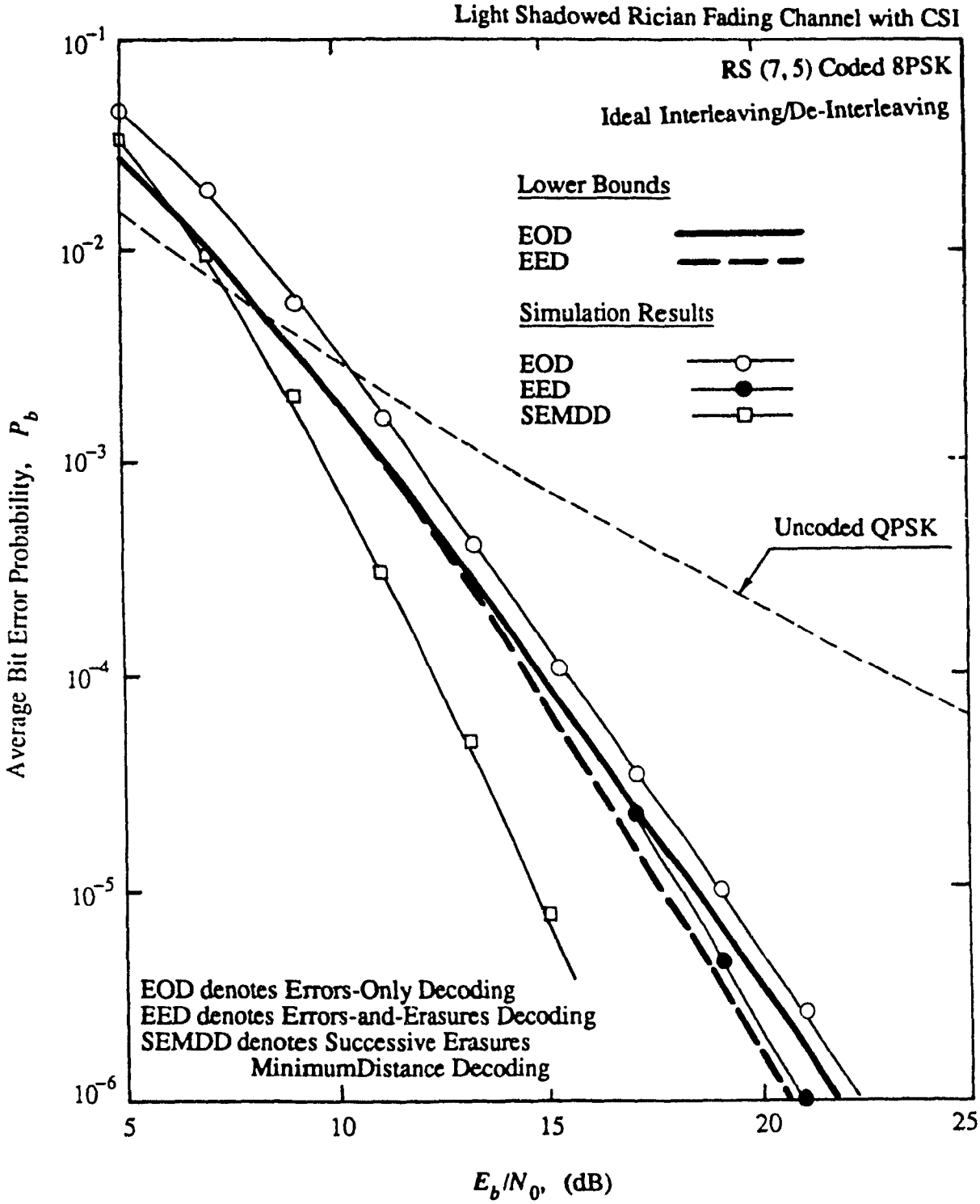

Fig. 7.4. Comparison of the bit error probability of RS (7, 5) coded 8PSK for different decoding strategies over the light shadowed Rician fading channel.

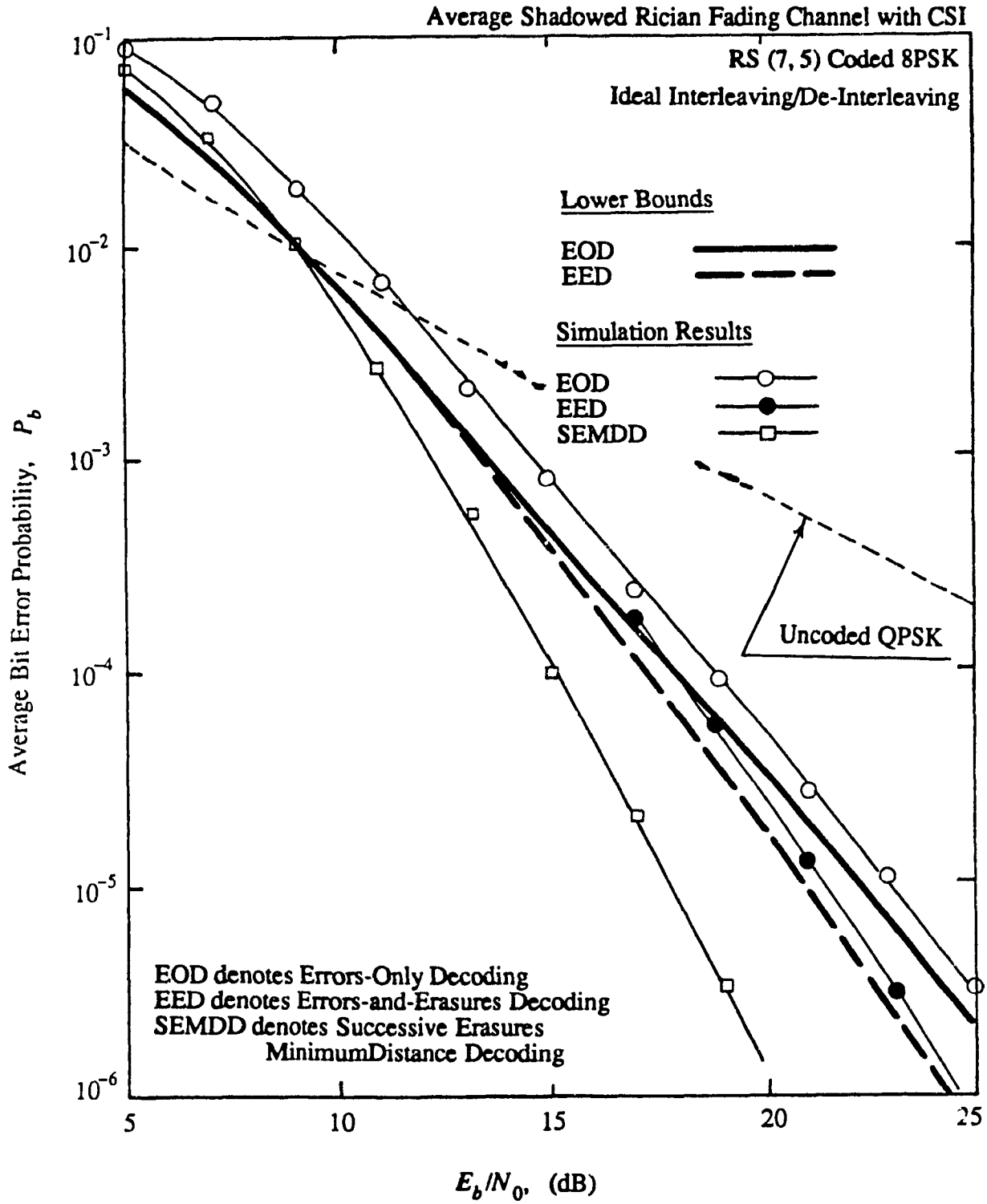

Fig. 7.5. Comparison of the bit error probability of RS (7, 5) coded 8PSK for different decoding strategies over the average shadowed Rician fading channel.

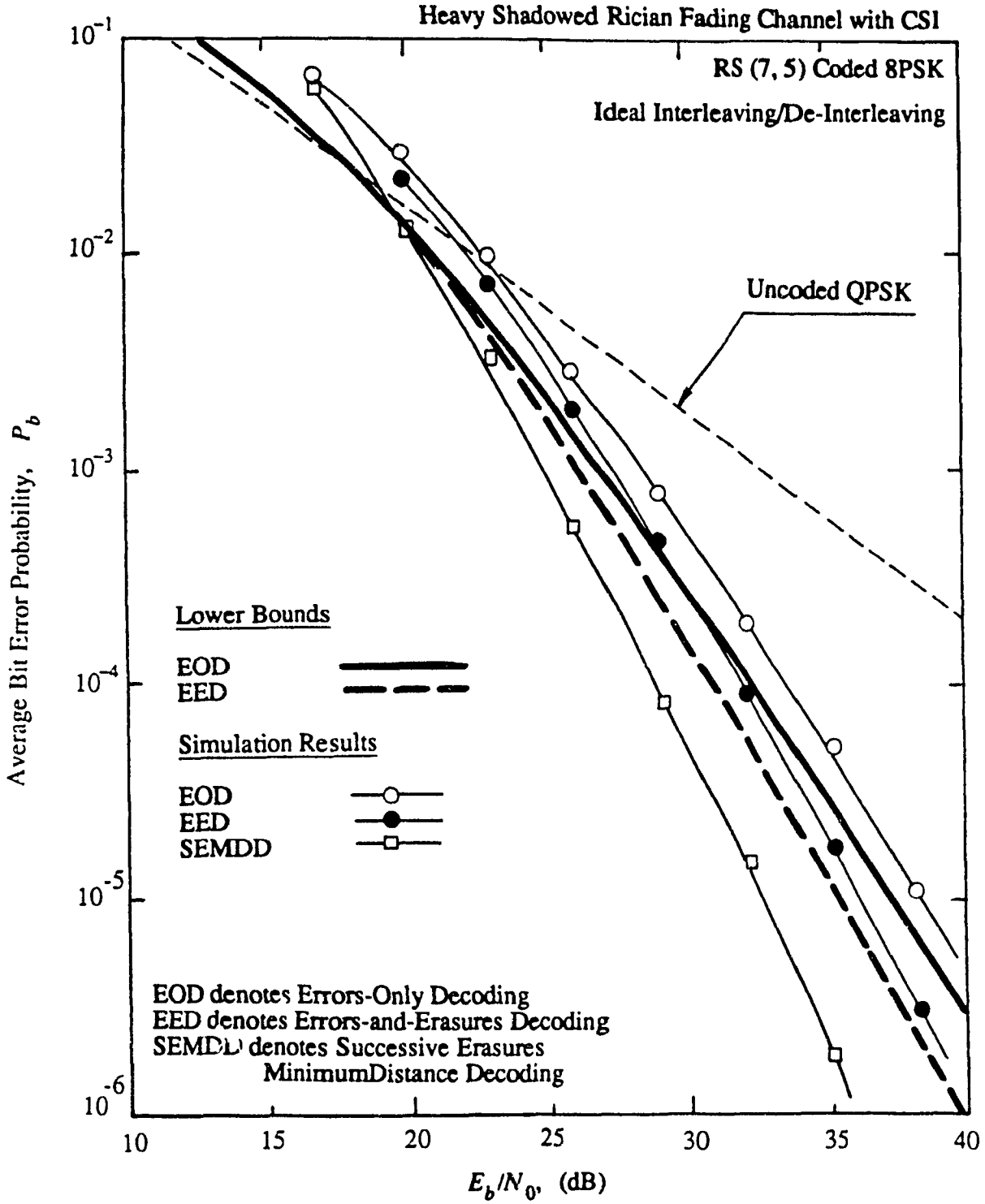

Fig. 7.6. Comparison of the bit error probability of RS (7, 5) coded 8PSK for different decoding strategies over the heavy shadowed Rician fading channel.

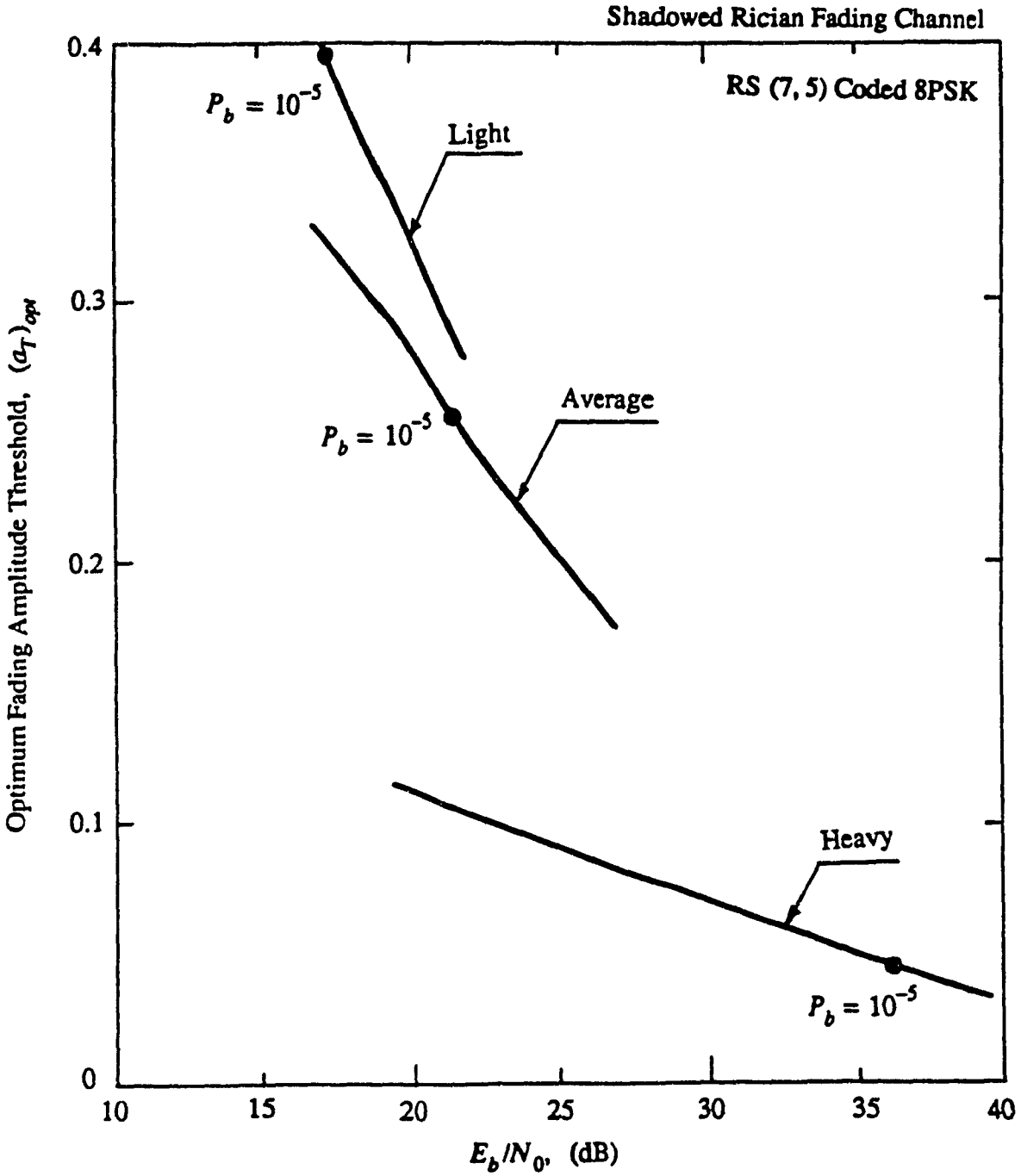

Fig. 7.7. Optimum fading amplitude threshold for errors-and-erasures decoding of the RS (7, 5) coded 8PSK scheme for three different shadowed Rician fading channels.

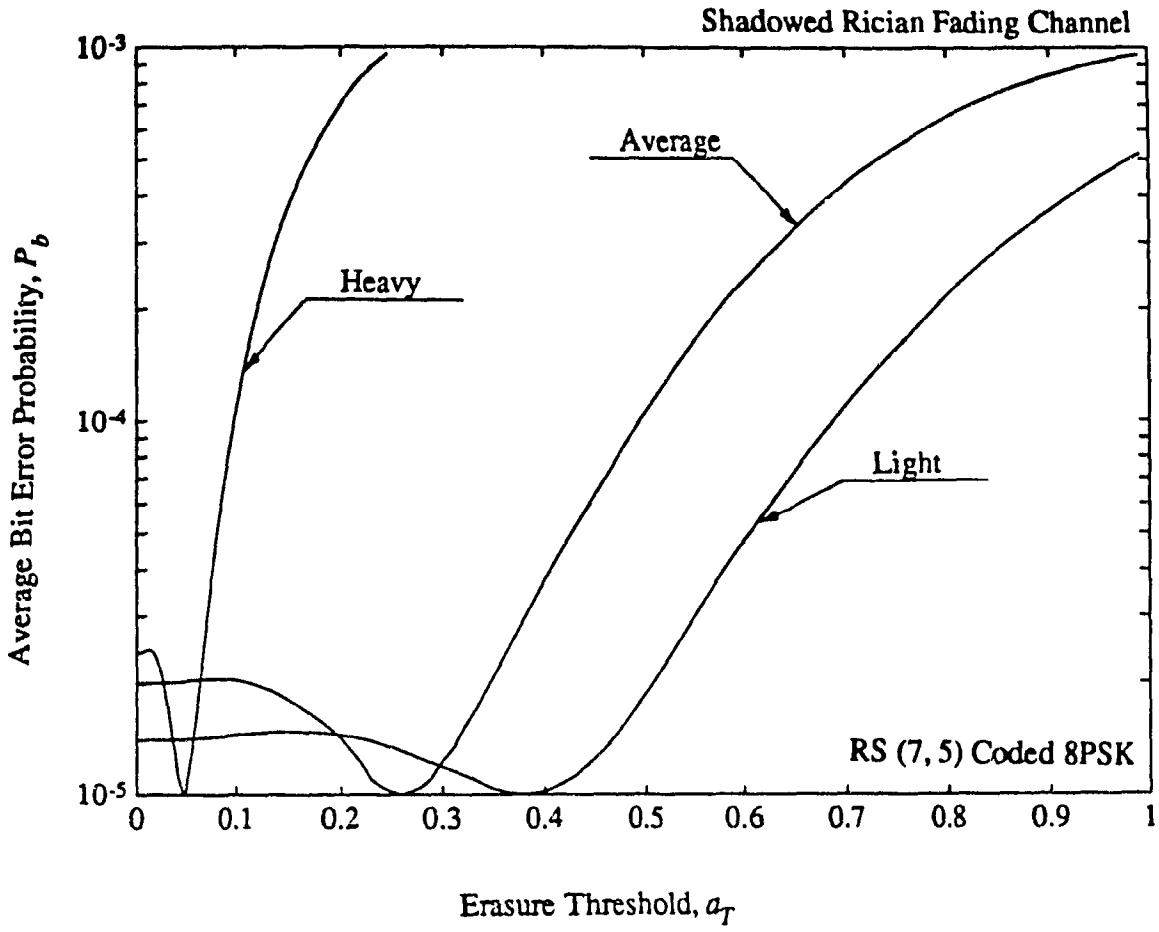

Fig. 7.8. Bit error probability of RS (7, 5) coded 8PSK as a function of erasure threshold a_T, for different shadowed Rician fading channels.

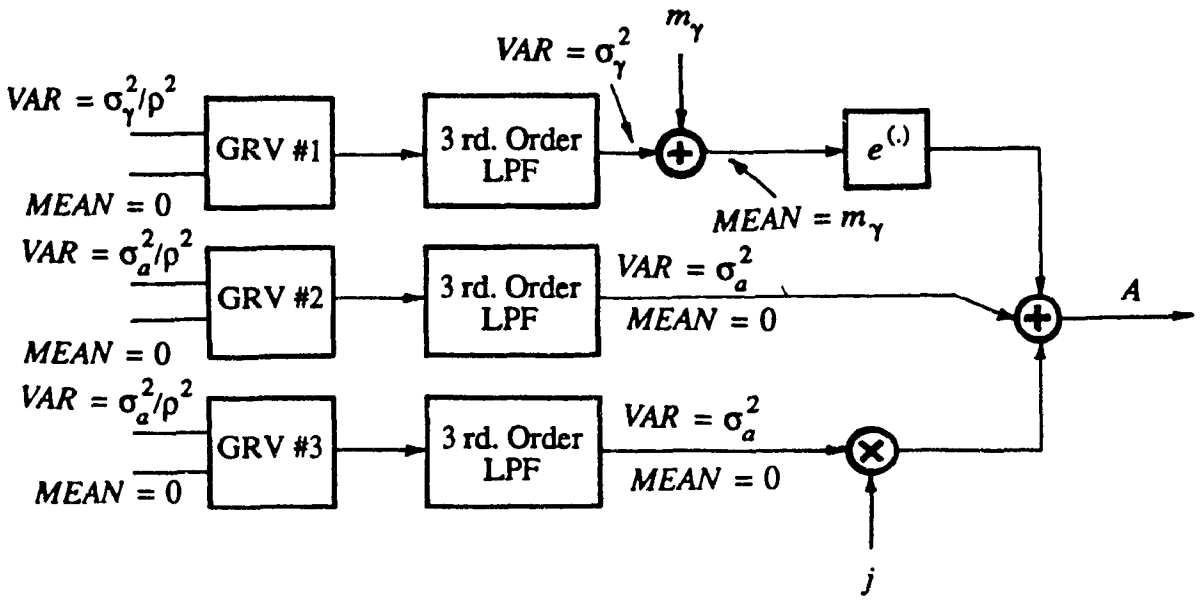

Fig. 7.9. The block diagram of a shadowed Rician fading channel simulator.

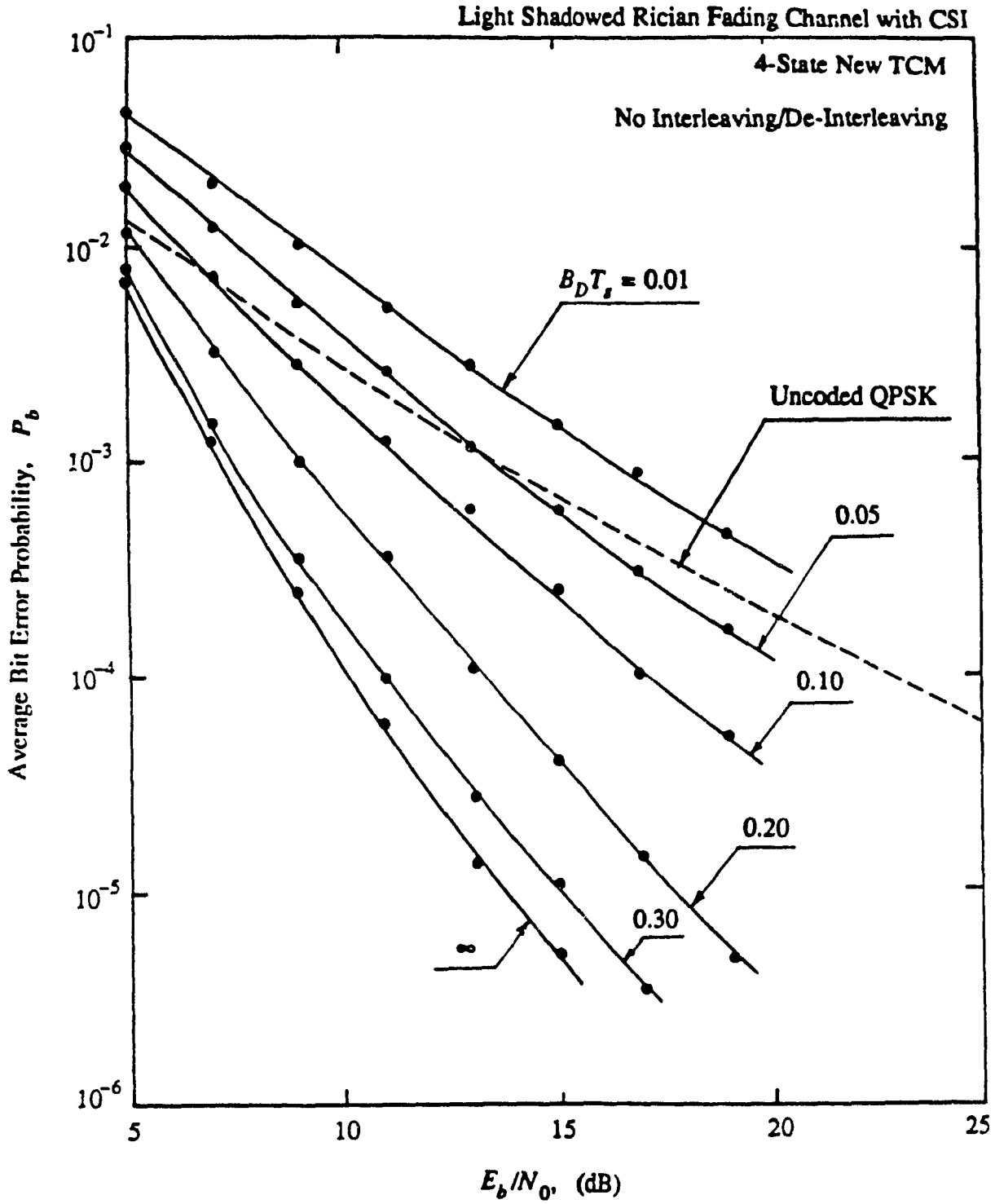

Fig. 7.10. The effect of normalized fading bandwidth on the performance of new 4-state TCM scheme over the light shadowed Rician fading channel.

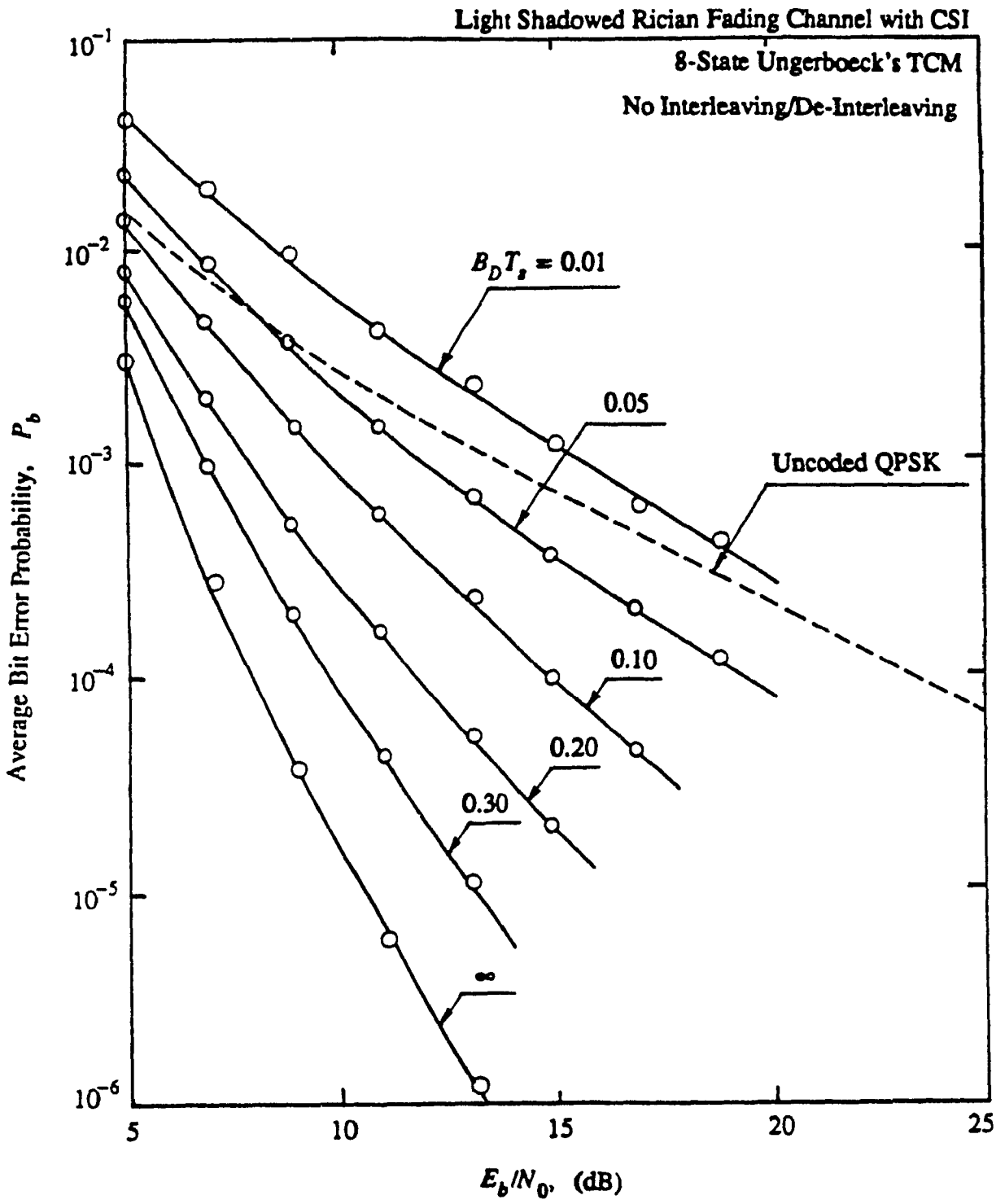

Fig. 7.11. The effect of normalized fading bandwidth on the performance of 8-state Ungerboeck's TCM scheme over the light shadowed Rician fading channel.

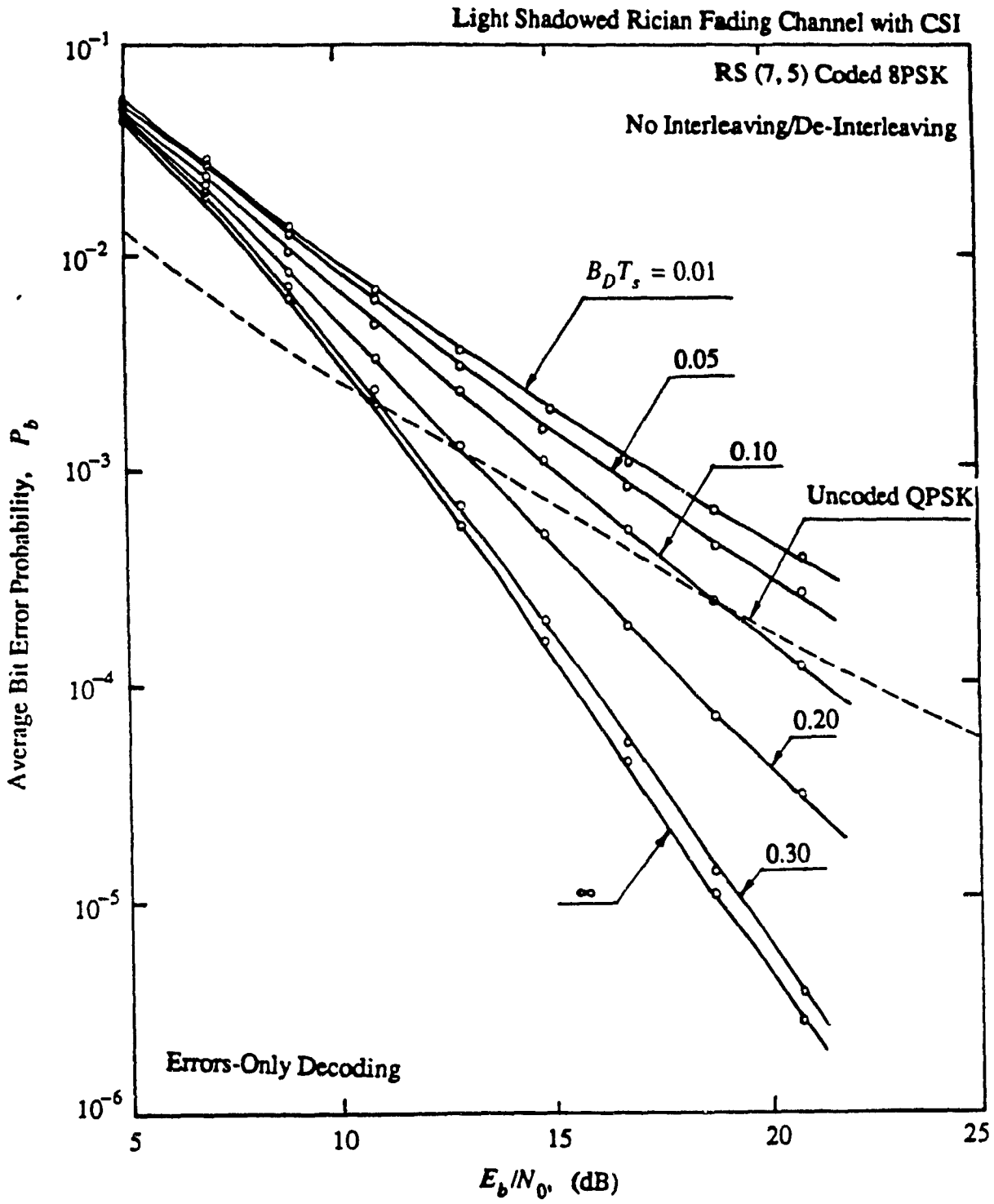

Fig. 7.12. The effect of normalized fading bandwidth on the performance of the RS (7, 5) coded 8PSK scheme over the light shadowed Rician fading channel using errors-only decoding.

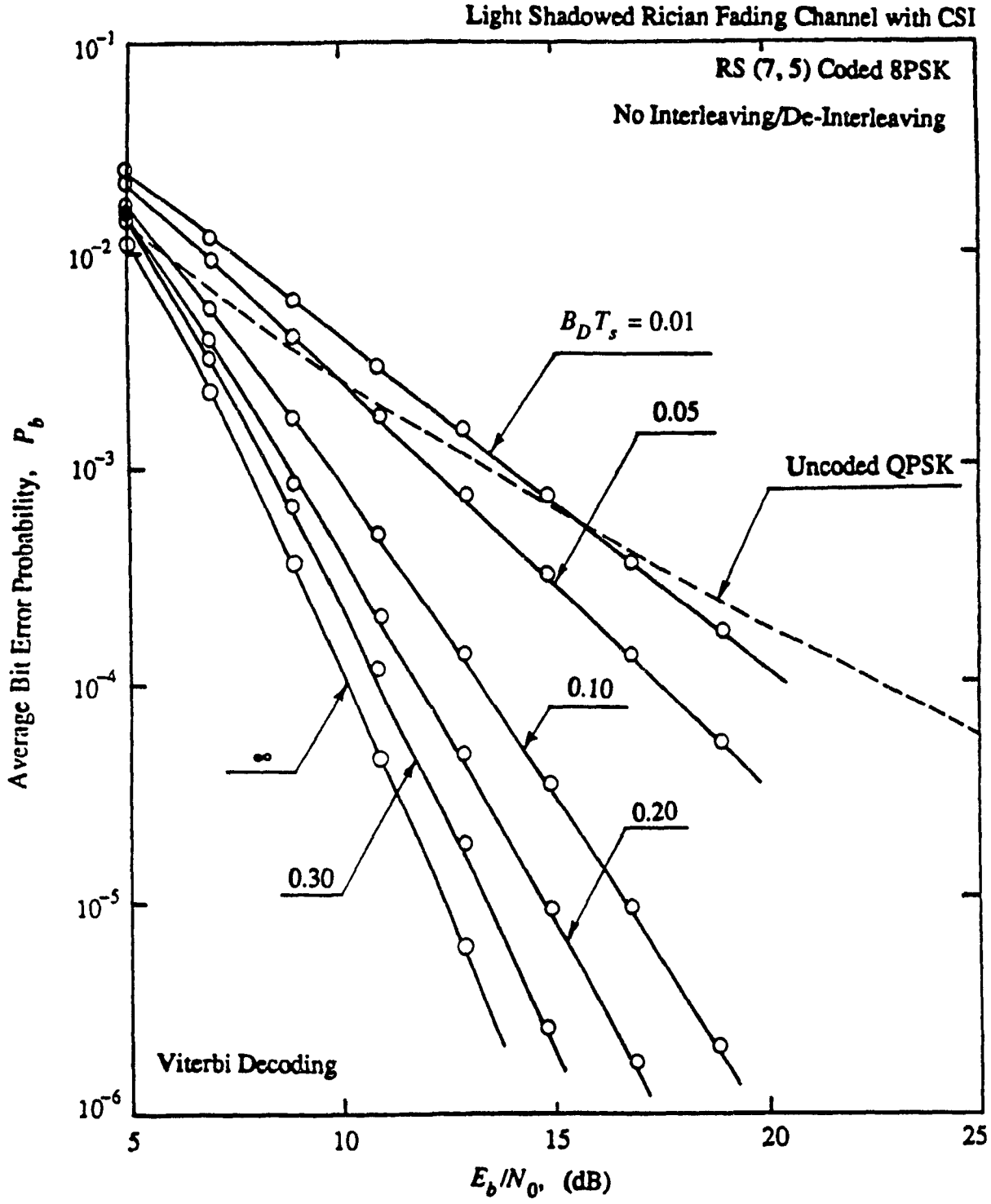

Fig. 7.13. The effect of normalized fading bandwidth on the performance of the RS (7, 5) coded 8PSK scheme over the light shadowed Rician fading channel using Viterbi decoding.

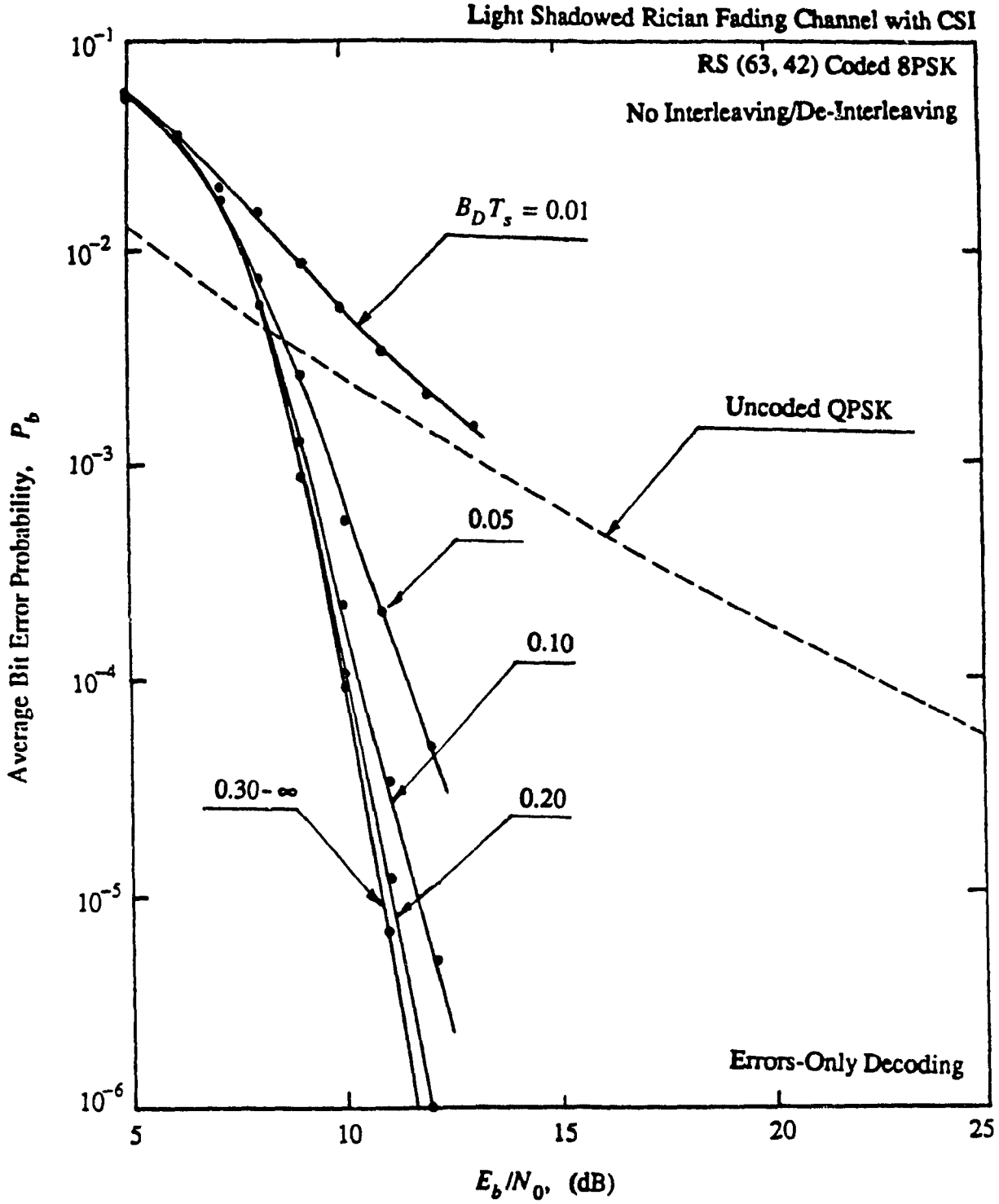

Fig. 7.14. The effect of normalized fading bandwidth on the performance of the RS (63, 42) coded 8PSK scheme over the light shadowed Rician fading channel using errors-only decoding.

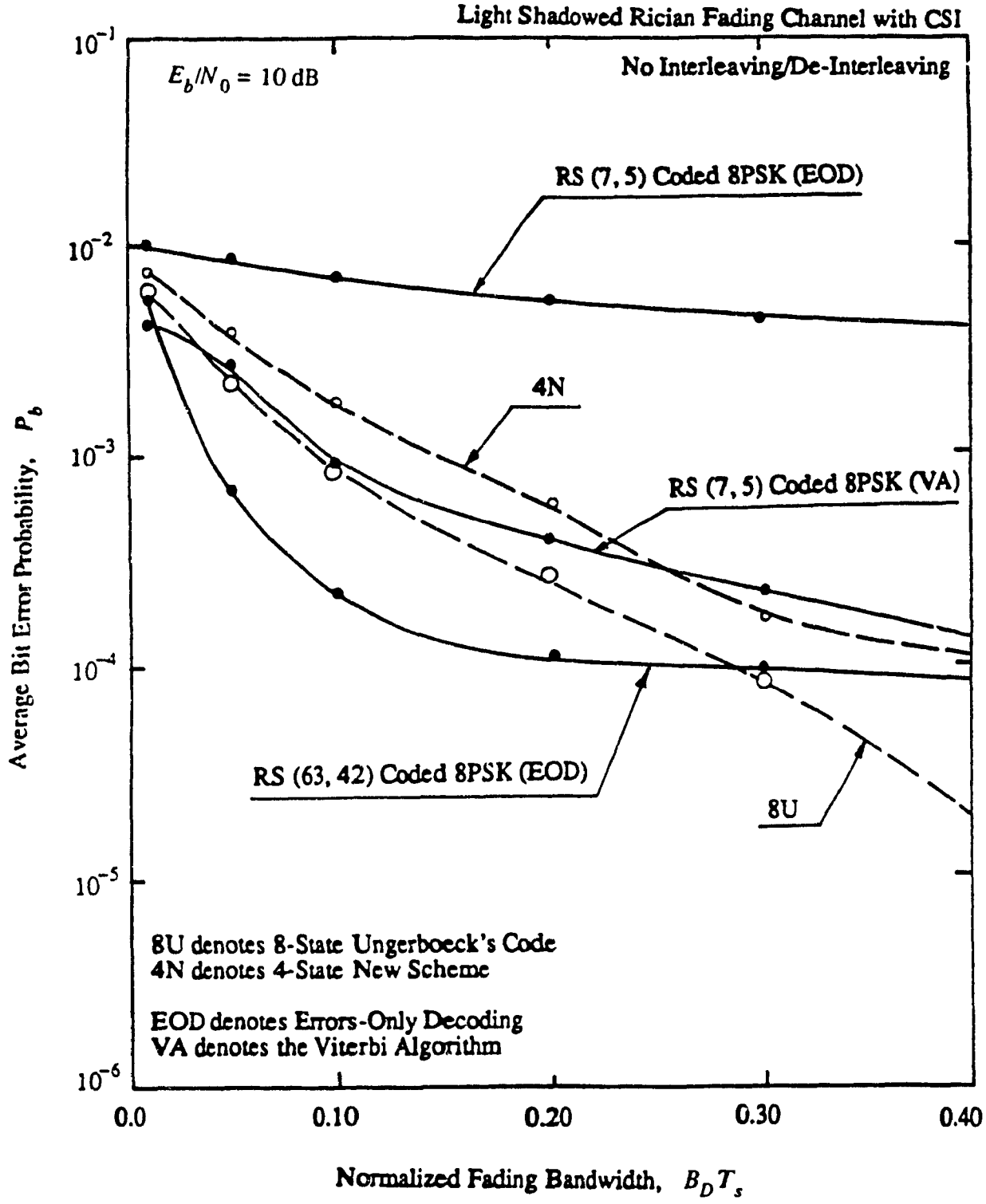

Fig. 7.15. Performance of different coded schemes versus the normalized fading bandwidth for the light shadowed Rician fading channel without interleaving.

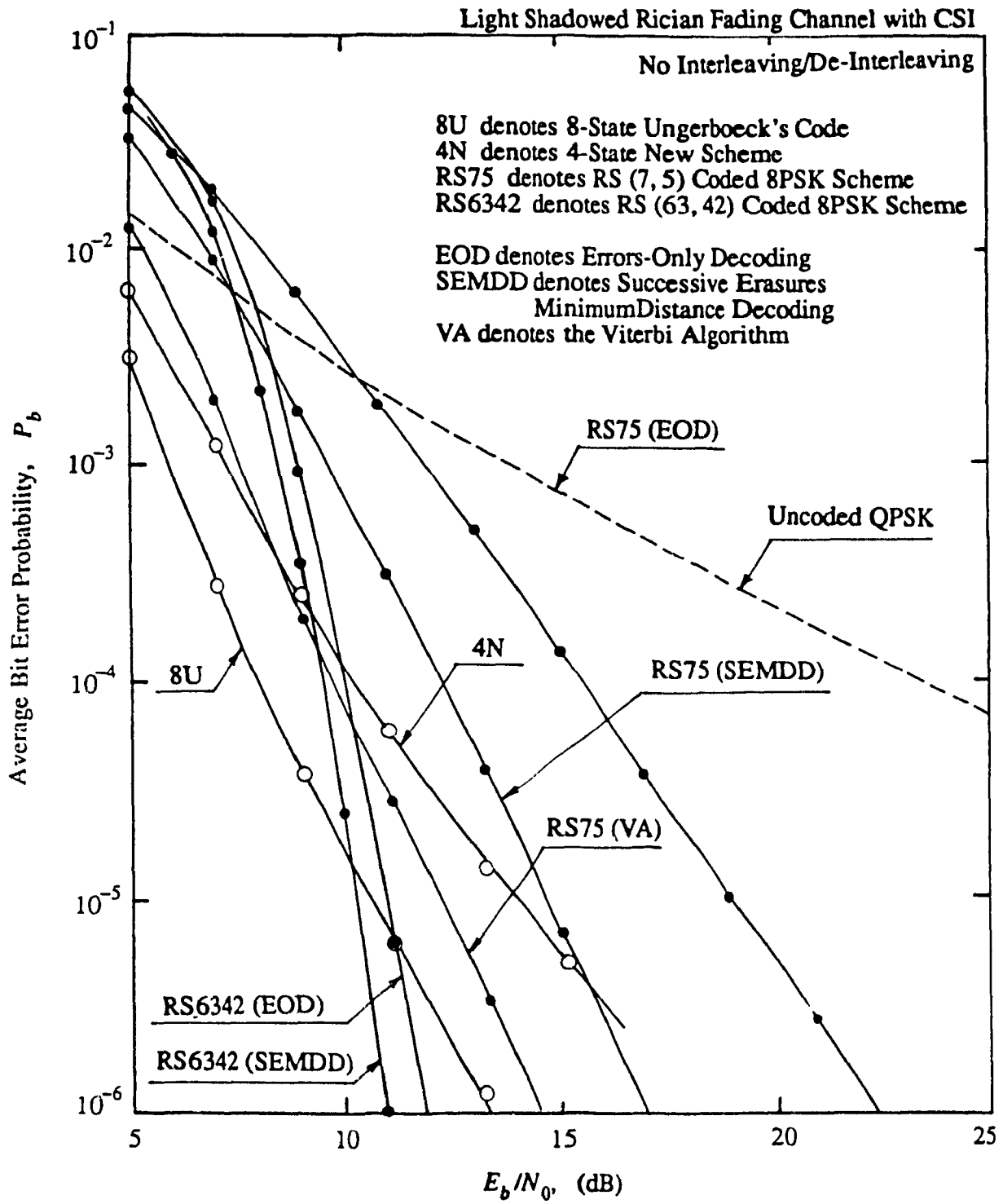

Fig. 7.16. Performance comparison of RS coded 8PSK schemes with some trellis-coded 8PSK schemes over the light shadowed Rician fading channel.

CHAPTER 8

CONCLUSIONS

8.1. CONCLUDING REMARKS

A main goal of this work was to introduce strong bandwidth-efficient coded-modulation for bandwidth-limited fading channels. In Chapter 2, using the random error bounding technique we evaluated the error bounds for an ensemble of coded schemes on fading channels. The cut-off rate was computed for some two-dimensional signalings on a Rayleigh fading channel for different decoding strategies. We observed that using bandwidth-efficient schemes one may expect reduction of 38 dB in SNR at error probability around 10^{-5} without sacrificing bandwidth efficiency. This improvement comes from using the redundancy of an expanded signal set. Also, it was shown that the reduction in SNR due to the use of soft-decision decoding in fading channels is more significant than that in the AWGN channel.

Next, in Chapter 3, we presented a brief background on the aspects of trellis-coded modulation and evaluated the performance of these schemes on a Rayleigh fading channel. We observed that the performance of the coded schemes on fading channel is determined by their time diversity and minimum product distances. In contrary with the AWGN channel, the minimum Euclidean distance has secondary importance in fading channels, particularly at high SNR's.

Chapter 4 was devoted to the design of a new 4-state rate 2/3 8PSK TCM scheme based on maximizing the time diversity and the minimum product distance. Three design rules were introduced to avoid exhaustive computer search. The performance of the new

scheme was compared with two other 4-state rate 2/3 8PSK TCM schemes by means of upper bound analysis and simulation. This comparison showed the superiority of the new scheme compared to the other ones.

We extended the design of the coded-modulation schemes to block codes in Chapter 5. In this context RS codes were chosen as a class of nonbinary block codes and combined with MPSK signaling. The RS coded MPSK schemes were constructed by either using the same symbol size for RS code and MPSK signal set, or concatenating two MPSK symbols to form an RS code symbol. The second approach yields low rate codes which provide higher time diversities. The lower bounds on the bit error probability of some examples of RS coded schemes were evaluated for a Rayleigh fading channel. In this evaluation we considered errors-only decoding as well as errors-and-erasures decoding. The effect of channel state information on the erasure generation strategy was also studied. It was shown that this information does not affect the performance of the coded schemes at high signal-to-noise ratios. The tightness of the evaluated lower bounds were confirmed by the simulation results.

The issue of soft-decision decoding of RS coded MPSK schemes was addressed in Chapter 6. Unlike convolutional codes, in general, there is no low complex solution such as the Viterbi algorithm for soft-decision decoding of block codes. This issue was treated separately for short high rate and long low rate RS coded schemes. Introducing a trellis structure for the former codes the Viterbi algorithm was utilized for soft-decision decoding. The upper bound analysis as well as the simulation results showed that the improvement due to soft-decision decoding is considerable. For long low rate RS coded schemes successive erasure minimum distance decoding was applied. We observed that although the performance of this algorithm is inferior to the maximum likelihood decoding, it can be implemented with lower complexity.

Finally, in Chapter 7, we applied the obtained results in the preceding chapters to a shadowed Rician fading channel with the parameters of the Canadian Mobile Satellite

(MSAT) Communication channel. The performance of TCM schemes as well as RS coded schemes was evaluated. We also studied the effect of imperfect interleaving on the performance of the coded schemes by changing the normalized fading bandwidth and observed that the RS coded schemes are less sensitive to the fading bandwidth than TCM codes.

To summarize our achievement in introducing the bandwidth-efficient coded-modulation schemes, we tabulate the coding gain of some coded schemes, constructed in the thesis, compared to the uncoded QPSK, in Table 8.1. These coding gains are evaluated at $P_b = 10^{-5}$. As a benchmark, the reduction in SNR due to use of bandwidth-efficient coded schemes predicted by cut-off rate discussion of Chapter 2 is also included.

8.2. SUGGESTIONS FOR FURTHER RESEARCH

There are several directions, related to this work, which can be the subject of further exploration in the future. We may classify some of the most important ones as follows.

8.2.1. Rotationally-Invariant Coded Schemes

In coherent detection, the receiver extracts the frequency and phase knowledge of the reference carrier from the received signal by means of carrier recovery circuits. In this case, a rotation in the phase of the received sequence can cause errors in the subsequently detected data symbols. These errors last until the end of message and may therefor severely degrade the performance of the system. The remedy for this problem in the uncoded schemes is using the *differential* coding technique. However, this may not be applied directly to the coded schemes. For, in general, the coded sequences are not *transparent* to the phase rotations and hence they are not differentially decodable. This difficulty can be removed by designing the coded scheme in such a way that a rotated version of a given coded sequence is a valid code word. This imposes a constraint in the code design procedure and may degrade the performance of the coded scheme. The

design of the rotationally-invariant TCM schemes for AWGN channels are well treated in the literature. However, it has not been extended to fading channels. Thus, constructing rotationally-invariant TCM and BCM schemes for fading channels needs further investigations.

8.2.2. Soft-Decision Decoding of Block Codes

The lack of low complex soft-decision decoding of block codes can be considered as a drawback of these schemes compared to convolutional ones. This issue can be important particularly on fading channels when the use of soft-decision information of the channel promises a significant improvement compared to the hard-decision one. On the other hand some features of the block codes make them a good candidate for constructing bandwidth-efficient coded schemes on fading channels. For example, it seems that binary cyclic codes can be used in designing the rotationally-invariant coded MPSK schemes because of their cyclic shift property. Although in the past this issue has been the subject of extensive research, we feel that further effort can be devoted to this problem regarding to the evolution of the technology and advanced processing techniques.

8.2.3. The Effect of Imperfect Carrier Synchronization and Differential Detection on the Performance of the Coded Schemes

Throughout the thesis the performance of the suggested coded schemes was evaluated under the assumption of ideal coherent detection. The results derived from such evaluation only reflects the effect of the fading amplitude. However, in practice it is difficult to maintain the phase coherency and the performance of the coded schemes may degrade if the imperfect synchronization effects are taken into consideration. Additional investigations therefore should be made to study the effect of imperfect carrier synchronization on the performance degradation of the coded schemes.

The performance analysis of the coded schemes can also be extended to multilevel *differential* phase shift keying systems. Although differential detection degrades the per-

formance of the system, it has an important advantage over coherent reception in that a means for extracting a carrier demodulation reference does not have to be provided.

8.2.4. Tighter Upper Bounds

We used the Chernoff bound technique in the upper bound analysis of soft-decision decoding of the coded schemes on fading channels. The simulation results show that this bound is weak on fading channels unless there is a strong line-of-sight component in the received signal. Developing the improved bounds can be considered as a future work.

Table 8.1. Coding Gain of some TCM and BCM Schemes, Constructed in the Thesis, Compared to the Uncoded QPSK at Bit Error Probability $P_b = 10^{-5}$

Coded Scheme	EOD dB	EED dB	SEMDD wo/CSI dB	SEMDD w/CSI dB	VA wo/CSI dB	VA w/CSI dB	Cut-Off Rate Prediction dB
4S-N					22.0	23.7	38.0
RS75-8	17.6	20.0	22.6	23.4	24.0	25.4	38.0
RS158-16	21.0	24.0	26.0	26.6			38.5
RS6342-8	28.0	29.6	30.4	31.0			38.0

EOD: Denotes Errors-Only Decoding

EED: Denotes Errors-and-Erasures Decoding

SEMDD: Denotes Successive Erasures Minimum Distance Decoding

VA: Denotes the Viterbi Algorithm

wo/CSI: Denotes without Channel State Information

w/CSI: Denotes with Channel State Information

4S-N: Denotes 4 State New TCM Scheme

RS75-8: Denotes RS (7, 5) Coded 8PSK Scheme

RS158-16: Denotes RS (15, 8) Coded 16PSK Scheme

RS6342-8: Denotes RS (63, 42) Coded 8PSK Scheme

APPENDIX A

CALCULATION OF THE CHERNOFF FACTORS FOR RICIAN AND RAYLEIGH FADING CHANNELS

In this appendix the Chernoff factors are derived for Rician and Rayleigh fading channels with and without the channel state information.

A.1. FADING CHANNEL WITH CSI

Assume that the channel state information is available at the receiver as $\mathbf{a} = (a_0, a_1, ..., a_{N-1})$ for the transmitted sequence $\mathbf{s} = (s_0, s_1, ..., s_{N-1})$ and the received one $\mathbf{r} = (r_0, r_1, ..., r_{N-1})$. For two-dimensional signals the components of the vectors **a**, **s**, and **r** are represented as complex numbers. Using (2.2.9), the ML metric of (2.3.9a) can be written as

$$m(\mathbf{r}, \mathbf{s}, \mathbf{a}) = -|\mathbf{r} - \mathbf{a} \,.\, \mathbf{s}|^2, \tag{A.1}$$

where, for simplicity, the factor $(E_s/\pi N_0)^{N/2}$ is ignored, since it would be absorbed in the Chernoff bound parameter λ anyway.

Using this metric, the Chernoff bound between the code words **s** and $\hat{\mathbf{s}}$, defined in (2.3.12c), is written as

$$\begin{aligned} C(\mathbf{s}, \hat{\mathbf{s}}, \lambda) &= E_{\mathbf{a}}\left[E_{\mathbf{r}|\mathbf{s}}\left[\exp\left(\lambda(|\mathbf{r} - \mathbf{a} \,.\, \mathbf{s}|^2 - |\mathbf{r} - \mathbf{a} \,.\, \hat{\mathbf{s}}|^2)\right) \right] \right], \\ &= \prod_{j=0}^{N-1} E_{a_j}\left[E_{n_j}\left[\exp(\lambda(|r_j - a_j s_j|^2 - |r_j - a_j \hat{s}_j|^2)) \right] \right], \end{aligned} \tag{A.2}$$

where a_j and n_j are the fading amplitude and the additive noise components in signal

interval j and are assumed to be independent to the corresponding components of the other intervals. Recalling that

$$\mathbf{r} = \mathbf{a} \,.\, \mathbf{s} + \mathbf{n}, \tag{A.3}$$

after some simplifications, (A.2) can be written as

$$C(\mathbf{s}, \hat{\mathbf{s}}, \lambda) = \prod_{j=0}^{N-1} E_{a_j}\left[\exp(-\lambda a_j^2 |s_j - \hat{s}_j|^2) E_{n_j}\left[\exp(-2\lambda a_j \mathrm{Re}\{n_j (s_j - \hat{s}_j)^*\}\right]\right], \tag{A.4}$$

where Re and * denote the real part and complex conjugate of a complex number, respectively. The statistical expectation with respect to the complex Gaussian random variable can be simplified as

$$E_{n_j}\left[\exp(-2\lambda a_j \mathrm{Re}\{n_j (s_j - \hat{s}_j)^*\})\right] = \exp(-\lambda a_j^2 (1 - \frac{N_0}{E_s}\lambda)|s_j - \hat{s}_j|^2). \tag{A.5}$$

Substituting (A.5) into (A.4) yields

$$C(\mathbf{s}, \hat{\mathbf{s}}, \lambda) = \prod_{j=0}^{N-1} E_{a_j}\left[\exp(-\lambda a_j^2 ((1 - \frac{N_0}{E_s}\lambda)|s_j - \hat{s}_j|^2))\right]. \tag{A.6}$$

The above bound is minimized by setting

$$\lambda = \lambda_{opt} = \frac{E_s}{2N_0}, \tag{A.7}$$

which, when substituted in (A.6), results in

$$\begin{aligned} C(\mathbf{s}, \hat{\mathbf{s}}, \lambda) &= \prod_{j=0}^{N-1} E_{a_j}\left[\exp(-\frac{E_s}{4N_0} \,.\, a_j^2 \,.\, |s_j - \hat{s}_j|^2)\right], \\ &= \prod_{j=0}^{N-1} C(s_j, \hat{s}_j). \end{aligned} \tag{A.8}$$

Dropping the subscript j, for simplicity, the Chernoff factor of signals s and $\hat{s}$ can be written as

$$C(s,\hat{s}) = E_a\left[\exp(-\frac{E_s}{4N_0}a^2|s-\hat{s}|^2)\right],$$

$$= \int_0^\infty p_A(a)\,.\,\exp(-\frac{E_s}{4N_0}a^2|s-\hat{s}|^2)\,.\,da, \qquad (A.9)$$

where $p_A(a)$ is the pdf of the fading amplitude. Now, consider a Rician fading channel with the pdf given in (2.1.8). Abbreviating $|s-\hat{s}|^2E_s/4N_0$ by δ^2 in (A.9), we proceed as

$$C(s,\hat{s}) = \int_0^\infty 2a(1+K)e^{-[K+a^2(1+K)-a\delta^2]}I_0(2a\sqrt{K(K+1)})\,.\,da. \qquad (A.10)$$

This integral can be evaluated using [77, p.717]

$$\int_0^\infty te^{-\alpha t^2}\,.\,J_0(\beta t)\,.\,dt = \frac{1}{2\alpha}e^{-\beta^2/4\alpha}, \qquad (A.11a)$$

where [77, p. 952]

$$J_0(jt) = I_0(t), \qquad (A.11b)$$

as

$$C(s,\hat{s}) = \frac{1+K}{1+K+E_s/4N_0|s-\hat{s}|^2}\exp\left[-\frac{KE_s/4N_0|s-\hat{s}|^2}{1+K+E_s/4N_0|s-\hat{s}|^2}\right]. \qquad (A.12a)$$

The Chernoff factor for a Rayleigh fading channel can be simplified as

$$C(s,\hat{s}) = \frac{1}{i+E_s/4N_0|s-\hat{s}|^2}, \qquad (A.12b)$$

by substituting $K = 0$ in (A.12a).

A.2. FADING CHANNEL WITHOUT CSI

The ML metric for the case of decoding without the channel state information is given by

$$m(\mathbf{r}, \mathbf{s}) = -|\mathbf{r} - \mathbf{s}|^2. \tag{A.13}$$

In such a case, the Chernoff bound between code words s and ŝ is expressed as

$$\begin{aligned} C(\mathbf{s}, \hat{\mathbf{s}}, \lambda) &= E_{\underset{N-1}{\mathbf{a}}}\left[E_{\mathbf{r}|\mathbf{s}}\left[\exp\left(\lambda(|\mathbf{r}-\mathbf{s}|^2 - |\mathbf{r}-\hat{\mathbf{s}}|^2)\right)\right]\right], \\ &= \prod_{j=0} E_{a_j}\left[E_{n_j}\left[\exp(\lambda(|r_j - s_j|^2 - |r_j - \hat{s}_j|^2))\right]\right], \end{aligned} \tag{A.14}$$

which simplifies to

$$\begin{aligned} C(\mathbf{s}, \hat{\mathbf{s}}, \lambda) = &\prod_{j=0}^{N-1} \exp(\lambda(|s_j|^2 - |\hat{s}_j|^2) \cdot \\ &E_{a_j}\left[\exp(-2\lambda a_j(|s_j|^2 - \mathrm{Re}\{s_j \hat{s}_j^*\}))\, E_{n_j}\left[\exp(-2\lambda(\mathrm{Re}\{n_j(\hat{s}_j^* - s_j^*)\}))\right]\right] \end{aligned} \tag{A.15}$$

Following the same procedure as the case with CSI, the above expression can be further simplified as

$$\begin{aligned} C(\mathbf{s}, \hat{\mathbf{s}}, \lambda) = &\prod_{j=0}^{N-1} \exp\left(\lambda(|s_j|^2 - |\hat{s}_j|^2 + \lambda\frac{N_0}{E_s}|s_j - \hat{s}_j|^2)\right) \\ &\cdot E_{a_j}\left[\exp\left(a_j\lambda(|s_j|^2 - |\hat{s}_j|^2 + |s_j - \hat{s}_j|^2)\right)\right] \end{aligned} \tag{A.16}$$

Unlike the case with CSI, (A.16) cannot be optimized over λ to yield a constant value for this parameter. The optimization procedure should be done after averaging over the fading amplitude distribution. Therefore, replacing the Chernoff parameter λ by $\lambda E_s/N_0$ (renormalization), the Chernoff factor of signals s and $\hat{s}$ is obtained as

$$C(s,\hat{s},\lambda) = \exp(\lambda\frac{E_s}{N_0}(|s|^2 - |\hat{s}|^2 + \lambda|s-\hat{s}|^2))$$
$$. E_a\left[exp(\lambda\frac{E_s}{N_0}a(|s|^2 - |\hat{s}|^2 + |s-\hat{s}|^2)) \right] \qquad (A.17)$$

The above expression cannot be evaluated in a closed form for a Rician fading channel. In such a case, similar to [2.10], this is expressed as

$$C(s,\hat{s},\lambda) = \exp(\lambda\frac{E_s}{N_0}(|s|^2 - |\hat{s}|^2 + \lambda|s-\hat{s}|^2))$$
$$. \frac{e^{-K}}{\pi}\int_0^{\pi}(1 - \sqrt{\pi}erfc(\nu)e^{\nu^2}\nu) . d\theta, \qquad (A.18a)$$

where

$$\nu = \frac{\lambda E_s/2N_0(|s|^2 - |\hat{s}|^2 + |s-\hat{s}|^2)}{\sqrt{1+K}} - \sqrt{K}\cos(\theta). \qquad (A.18b)$$

For a Rayleigh fading channel $C(s,\hat{s},\lambda)$ is expressed in a closed form. For $K = 0$ the integral in (A.18a) is evaluated as

$$\int_0^{\pi}(1 - \sqrt{\pi}erfc(\nu)e^{\nu^2}\nu) . d\theta = 1 - \sqrt{\pi}\, erfc(\beta) . e^{\beta^2} . \beta, \qquad (A.19a)$$

where

$$\beta = \frac{\lambda E_s}{2N_0}(|s|^2 - |\hat{s}|^2 + |s-\hat{s}|^2), \qquad (A.19b)$$

and

$$C(s,\hat{s},\lambda) = \exp(\lambda\frac{E_s}{N_0}(|s|^2 - |\hat{s}|^2 + \lambda|s-\hat{s}|^2))$$
$$. (1 - \sqrt{\pi}\, erfc(\beta) . e^{\beta^2} . \beta). \qquad (A.19c)$$

APPENDIX B

CALCULATION OF THE TRANSITION PROBABILITIES FOR THE MPSK SIGNAL SET OVER A RAYLEIGH FADING CHANNEL

In this appendix the transition probabilities for an MPSK signal set over a Rayleigh fading channel are derived.

The decision regions for an MPSK signal set, in general, are shown in Fig. 2.7, which include a null zone for the erasure decoding. Due to the symmetry of the MPSK signal set the transition probabilities $\{q_{li}\}$ are independent of the i-th signal. Thus, dropping the subscript i, these probabilities are evaluated for signal s_0. Then q_l is defined as

$$q_l = E_a \left[\int_{\Lambda_l} p(r \mid s_0, a) \, . \, dr \right]; \qquad l = 0, 1, ..., q-1. \tag{B.1}$$

where Λ_l shows the l-th decision region. Recalling that r, n, and s_0 are complex numbers and using (2.2.9), (B.1) can be written as

$$\begin{aligned} q_l &= E_a \left[\int\int_{\Lambda_l} \frac{E_s}{\pi N_0} e^{-\frac{E_s}{N_0}[(r_1 - a s_1)^2 + (r_2 - a s_2)^2]} \, . \, dr_1 \, . \, dr_2 \right], \\ &= E_a \left[\int\int_{\Lambda_l} \frac{E_s}{\pi N_0} e^{-\frac{E_s}{N_0}[r_1^2 + r_2^2 - 2a(s_1 r_1 + s_2 r_2) + a^2(s_1^2 + s_2^2)]} \, . \, dr_1 \, . \, dr_2 \right], \\ &= E_a \left[\int\int_{\Lambda_l} \frac{E_s}{\pi N_0} e^{-\frac{E_s}{N_0}[r_1^2 + r_2^2 - 2a r_1 + a^2]} \, . \, dr_1 \, . \, dr_2 \right], \end{aligned} \tag{B.2}$$

where $r = r_1 + jr_2$ and $s_0 = s_1 + js_2 = 1$. Introducing the polar coordinates as

$$\begin{aligned} r_1 &= \rho \,.\, \cos\theta, \\ r_2 &= \rho \,.\, \sin\theta, \\ dr_1 \,.\, dr_2 &= \rho \,.\, d\rho \,.\, d\theta, \end{aligned} \tag{B.3}$$

(B.2) can be simplified as

$$q_l = E_a \left[\int_{a_T}^{\infty} \int_{\alpha_1}^{\alpha_2} \frac{E_s}{\pi N_0} e^{-\frac{E_s}{N_0}[\rho^2 - 2a\rho\cos\theta + a^2]} \,.\, \rho \,.\, d\theta \,.\, d\rho \right],$$

$$= \int_0^{\infty} \left(2ae^{-a^2} \int_{a_T}^{\infty} \int_{\alpha_1}^{\alpha_2} \frac{E_s}{\pi N_0} e^{-\frac{E_s}{N_0}[\rho^2 - 2a\rho\cos\theta + a^2]} \,.\, \rho \,.\, d\theta \,.\, d\rho \right) .\, da, \tag{B.4}$$

where $\alpha_1 = (2l - 1)\pi/M$ and $\alpha_2 = (2l + 1)\pi/M$. Interchanging the order of integrations and after some simplifications, (B.4) can be written as

$$q_l = \frac{2E_s}{\pi N_0} \int_{\alpha_1}^{\alpha_2} \left(\int_{a_T}^{\infty} \rho e^{-E_s/N_0 \rho^2} \left(\int_0^{\infty} ae^{-(1 + E_s/N_0)[a^2 - \frac{2a\rho E_s/N_0}{1 + E_s/N_0}\cos\theta]} \right) da \right) d\rho \right) d\theta, \tag{B.5}$$

The integration with respect to a can be expressed as

$$\int_0^{\infty} ae^{-(1 + E_s/N_0)[a^2 - \frac{2a\rho E_s/N_0}{1 + E_s/N_0}\cos\theta]} da = \frac{1}{2(1 + E_s/N_0)} \left[1 + \frac{\rho E_s/N_0 \sqrt{\pi}\cos\theta}{\sqrt{1 + E_s/N_0}} \right.$$

$$\left. .\, e^{\frac{\rho^2 (E_s/N_0)^2 \cos^2\theta}{1 + E_s/N_0}} erfc\left(-\frac{\rho E_s/N_0 \cos\theta}{\sqrt{1 + E_s/N_0}}\right) \right]. \tag{B.6}$$

Substituting (B.6) into (B.5) results in

$$q_l = \frac{E_s/N_0}{\pi(1+E_s/N_0)}\left(\frac{\pi}{ME_s/N_0}e^{-E_s a_T^2/N_0} + \int_{(2l-1)\pi/M}^{(2l+1)\pi/M} d\theta \left(\int_{a_T}^{\infty} \rho^2 \frac{E_s}{N_0}\sqrt{\pi}\cos\theta \right.\right.$$

$$\left.\left. \cdot e^{-E_s\rho^2/N_0 + \frac{\rho^2(E_s/N_0)^2\cos^2\theta}{1+E_s/N_0}} erfc\left(\frac{-\rho E_s/N_0\cos\theta}{\sqrt{1+E_s/N_0}}\right) d\rho \right) \right). \qquad \text{(B.7)}$$

The probability of the received signal being in the null zone can be obtained from $\{q_l\}$ as

$$q_e = 1 - \sum_{l=0}^{q-1} q_l. \qquad \text{(B.8)}$$

Note that the transitions probabilities for hard-decision decoding can be simply obtained from (B.7) by setting $a_T = 0$. It is obvious that in this case $q_e = 0$.

APPENDIX C

C.1. CALCULATION OF THE PROBABILITY OF CORRECT DECISION OF A RELIABLE MPSK SYMBOL

The probability of the correct decision of a reliable MPSK symbol, $Q_i^{\bar{E}}$, is defined as (5.3.15). For the equiprobable transmitted MPSK symbols this probability is independent of the ith signal. Hence, dropping the subscript i, the probability of correct decision of a reliable MPSK signal is evaluated for the decision region Λ_0. This evaluation can be simplified by interchanging the integration and averaging operations. Further simplification can be obtained by introducing the polar coordinates ρ and θ related to r_1 and r_2 as

$$\begin{aligned} r_1 &= \rho \,.\, \cos\theta, \\ r_2 &= \rho \,.\, \sin\theta, \\ dr_1 \,.\, dr_2 &= \rho \,.\, d\rho \,.\, d\theta. \end{aligned} \tag{C.1}$$

Representing the radius of the erasure region by ρ_T (see Fig. 2.7), after some mathematical manipulation (5.3.15) can be written as

$$Q^{\bar{E}} = \frac{e^{-\rho_T^2/2\sigma^2}}{M(1+\gamma_s)} + \frac{\sqrt{2\gamma_s}}{2\pi\sigma^3(1+\gamma_s)^{3/2}} \int_{\rho_T}^{\infty} \rho^2 \,.\, e^{-\frac{\rho^2}{2\sigma^2(1+\gamma_s)}} \times \left[\int_{-\pi/M}^{\pi/M} \cos\theta \,.\, e^{-\frac{\gamma_s \rho^2 \sin^2\theta}{2\sigma^2(1+\gamma_s)}} \,.\, \int_{-\frac{\sqrt{\gamma_s}}{\sqrt{2\sigma^2(1+\gamma_s)}}}^{\infty} e^{-x^2} \,.\, d\theta \right] \,.\, d\rho, \tag{C.2}$$

where $\gamma_s \equiv E_s/N_0$ is symbol energy-to-noise ratio and $\sigma^2 = N_0/2$. In general, this expression should be calculated numerically. However, applying the approximation

$$erfc(x) \equiv \frac{2}{\pi}\int_x^{\infty} e^{-t^2}\,.\,dt \approx \frac{2}{\sqrt{\pi}x}e^{-x^2}, \tag{C.3}$$

the expression inside the parentheses in (C.2) can be simplified as

$$\int_{-\pi/M}^{\pi/M} \cos\theta\,.\,e^{-\frac{\gamma_s\rho^2\sin^2\theta}{2\sigma^2(1+\gamma_s)}}\,.\int_{-\frac{\sqrt{\gamma_s}\rho\cos\theta}{\sqrt{2\sigma^2(1+\gamma_s)}}}^{\infty} e^{-x^2}\,.\,d\theta =$$

$$= \frac{\sigma\pi\sqrt{2(1+\gamma_s)}}{\rho\sqrt{\gamma_s}}\,.\left[1 - erfc\left(\frac{\sqrt{\gamma_s}\rho\sin(\pi/M)}{\sqrt{2\sigma^2(1+\gamma_s)}}\right)\right] - \frac{2\pi\sigma\sqrt{1+\gamma_s}}{\rho M\sqrt{2\gamma_s}}\,.\,e^{-\frac{\gamma_s\rho^2}{2\sigma^2(1+\gamma_s)}}. \tag{C.4}$$

Substituting (C.4) into (C.3) and performing some calculations yields

$$Q^{\bar{E}} = e^{-\frac{\rho_T^2}{2\sigma^2(1+\gamma_s)}} - \frac{1}{\sigma^2(1+\gamma_s)}\int_{\rho_T}^{\infty} \rho\,.\,e^{-\frac{\rho^2}{2\sigma^2(1+\gamma_s)}}\,erfc\left(\frac{\sqrt{\gamma_s}\rho\sin(\pi/M)}{\sqrt{2\sigma^2(1+\gamma_s)}}\right).d\rho. \tag{C.5}$$

Using integral by parts the integral part of (C.5) can be evaluated as

$$\int_{\rho_T}^{\infty} \rho\,.\,e^{-\frac{\rho^2}{2\sigma^2(1+\gamma_s)}}\,erfc\left(\frac{\sqrt{\gamma_s}\rho\sin(\pi/M)}{\sqrt{2\sigma^2(1+\gamma_s)}}\right).d\rho$$

$$= \frac{1}{2}\sigma^2(1+\gamma_s)e^{-\frac{\rho_T^2}{2\sigma^2(1+\gamma_s)}}\,erfc\left(\frac{\sqrt{\gamma_s}\rho_T\sin(\pi/M)}{\sqrt{2\sigma^2(1+\gamma_s)}}\right)$$

$$- \frac{\sqrt{\gamma_s}\sigma^2(1+\gamma_s)\sin(\pi/M)}{2\sqrt{1+\gamma_s\sin^2(\pi/M)}}\,erfc\left(\frac{\rho_T\sqrt{1+\gamma_s\sin^2(\pi/M)}}{\sqrt{2\sigma^2(1+\gamma_s)}}\right). \tag{C.6}$$

The final result can be obtained by substituting (C.6) into (C.5) as

$$Q^{\bar{E}} = e^{-\frac{\rho_T^2}{2\sigma^2(1+\gamma_s)}} + \frac{\sqrt{\gamma_s}\sin(\pi/M)}{\sqrt{1+\gamma_s\sin^2(\pi/M)}} \cdot erfc\left(\frac{\rho_T\sqrt{1+\gamma_s\sin^2(\pi/M)}}{\sqrt{2\sigma^2(1+\gamma_s)}}\right)$$
$$- e^{-\frac{\rho_T^2}{2\sigma^2(1+\gamma_s)}} \cdot erfc\left(\frac{\rho_T\sqrt{\gamma_s}\sin(\pi/M)}{\sqrt{2\sigma^2(1+\gamma_s)}}\right). \qquad (C.7)$$

Defining the normalized erasure threshold region radius ρ_{T_n} as $\rho_{T_n} \equiv \rho_T/\sqrt{E_s}$ and using the approximation $\gamma_s \simeq \gamma_s + 1$ at high signal-to-noise ratios, (C.7) can be written as

$$Q^{\bar{E}} = e^{-\rho_{T_n}^2} + \frac{\sqrt{\gamma_s}\sin(\pi/M)}{\sqrt{1+\gamma_s\sin^2(\pi/M)}} \cdot erfc\left(\sqrt{1+\gamma_s\sin^2(\pi/M)}\rho_{T_n}\right)$$
$$- e^{-\rho_{T_n}^2} erfc\left(\sqrt{\gamma_s}\rho_{T_n}\sin(\pi/M)\right). \qquad (C.8)$$

C.2. CALCULATION OF THE PROBABILITY OF CORRECT DECISION OF AN UNRELIABLE MPSK SYMBOL

To find the probability of correct decision of MPSK symbol when the received signal falls into the erasure region we may follow the same steps as previous part. In this case the integration with respect to r in (C.2) should be carried out from 0 to ρ_T. Following the approach of section I the probability of correct decision of an unreliable MPSK symbol, Q^E, at high signal-to-noise ratios, is found to be

$$Q^E = e^{-\rho_{T_n}^2} erfc\left(\sqrt{\gamma_s}\rho_{T_n}\sin(\pi/M)\right) + \frac{\sqrt{\gamma_s}\sin(\pi/M)}{\sqrt{1+\gamma_s\sin^2(\pi/M)}} - e^{-\rho_{T_n}^2}$$
$$- \frac{\sqrt{\gamma_s}\sin(\pi/M)}{\sqrt{1+\gamma_s\sin^2(\pi/M)}} \cdot erfc\left(\sqrt{1+\gamma_s\sin^2(\pi/M)}\rho_{T_n}\right). \qquad (C.9)$$

C.3. CALCULATION OF THE PROBABILITY OF A RELIABLE MPSK SYMBOL

To find the conditional probabilities $P_{SM|\bar{E}}$ and $P_{SM|E}$ the integration in (5.3.17) has to be evaluated. To avoid numerical integration using some approximation is necessary. Interchanging the integration and averaging operations in (5.3.17) and introducing the polar coordinates as (C.1) this equation can be written as

$$P_{\bar{E}M} = \int_{\rho_T}^{\infty} \int_{-\pi/2}^{3\pi/2} \left(\frac{1}{2\pi\sigma^2(1+\gamma_s)} e^{-\frac{\rho^2}{2\sigma^2}} + \frac{\sqrt{2\gamma_s}\rho^2\cos\theta}{2\pi\sigma^3(1+\gamma_s)^{3/2}} e^{-\frac{\rho^2}{2\sigma^2} + \frac{\gamma_s\rho^2\cos^2\theta}{2\sigma^2(1+\gamma_s)}} \right.$$

$$\left. \times \int_{-\sqrt{\gamma_s}\rho\cos\theta/\sqrt{2\sigma^2(1+\gamma_s)}}^{\infty} e^{-x^2} dx \right) . \rho . d\rho . d\theta. \qquad \text{(C.10)}$$

The interval of the integration with respect to phase, i.e., $(-\pi/2, 3\pi/2)$ can be divided into two intervals $(-\pi/2, \pi/2)$ and $(\pi/2, 3\pi/2)$. After some mathematical manipulations the following expression results

$$P_{\bar{E}M} = \frac{1}{1+\gamma_s} e^{-\frac{\rho_T^2}{2\sigma^2}} + \sqrt{\pi} \int_{\rho_T}^{\infty} \frac{\rho^2\sqrt{2\gamma_s}}{2\pi\sigma^3(1+\gamma_s)^{3/2}} e^{-\frac{\rho^2}{2\sigma^2} + \frac{\gamma_s\rho^2}{2\sigma^2(1+\gamma_s)}}$$

$$\times \int_{-\pi/2}^{\pi/2} \cos\theta . e^{-\frac{\gamma_s\rho^2\sin^2\theta}{2\sigma^2(1+\gamma_s)}} \left(1 - erfc\left(\frac{\cos\theta}{\sigma\sqrt{1+\gamma_s}}\right)\right) . d\theta . d\rho. \qquad \text{(C.11)}$$

Using the approximation of (C.3) and ignoring 1 with respect to γ_s at high signal-to-noise ratios, (C.11) can be simplified as

$$P_{\bar{E}M} = e^{-\rho_{T_n}^2} \left(1 - erfc\left(\sqrt{mR\gamma_b}\rho_{T_n}\right)\right) + erfc\left(\sqrt{mR\gamma_b}\rho_{T_n}\right). \qquad \text{(C.12)}$$

The probability of being in unreliable (erasure) region, P_{EM} is obtained as

$$P_{EM} = 1 - P_{\bar{E}M}. \qquad \text{(C.13)}$$

REFERENCES

[1] J. G. Proakis, *Digital Communications*. New York: McGraw-Hill, 1983.

[2] J. M. Wozencraft and I. M. Jacobs, *Principles of Communication Engineering*. New York: John Wiley & Sons, 1965.

[3] S. Stein, "Fading channel issues in system engineering," *IEEE J. Select. Areas Commun.*, vol. SAC-5, no. 2, pp. 68-89, Feb. 1987.

[4] G. L. Grisdale, J. G. Morris, and D. S. Palmer, "Fading of long-distance radio signals and a comparison of spaced- and polarization-diversity reception in the 6-18 Mc/s range," *Proc. Inst. Elec. Eng.*, vol. 104, pt. B, pp. 39-51, Jan. 1957.

[5] R. W. E. McNicole, "The fading of radio waves of medium and high frequencies," *Proc. Inst. Elec. Eng.*, vol. 96, pt. III, pp. 517-524, Nov. 1949.

[6] R. J. C. Bultitude, "Measurements, characterization and modeling of indoor 800/900 MHz radio channels for digital communication," *IEEE Commun. Magazine*, vol. 25, no. 6, pp. 5-12, June 1987.

[7] K. Brayer, editor, *Data Communication via Fading Channels*. New York: IEEE Press, 1975.

[8] J.L. Massey, "Coding and modulation in digital communications," *Proc. 1974 Int. Zurich Seminar on Digital Commun.*, Zurich, Switzerland, pp. E2(1)-(4), March 1974.

[9] G. Ungerboeck, "Channel coding with multilevel/phase signals," *IEEE Trans. Inform. Theory*, vol. IT-28, no. 1, pp. 55-67, Jan. 1982.

[10] G. Ungerboeck, "Trellis-coded modulation with redundant signal sets Part I: Introduction," *IEEE Commun. Magazine*, vol. 25, no. 2, pp. 5-11, Feb. 1987.

[11] G. Ungerboeck, "Trellis-coded modulation with redundant signal sets Part II: State

of the art," *IEEE Commun. Magazine*, vol. 25, no. 2, pp. 12-21, Feb. 1987.

[12] G. D. Forney, Jr., R. G. Gallager, G. R. Lang, F. M. Longstaff, and S. U. Qureshi, "Efficient modulation for band-limited channels," *IEEE J. Select. Areas Commun.*, vol. SAC-2, no. 5, pp. 632-647, Sept. 1984.

[13] R. Calderbank, and J. E. Mazo, "A new description of trellis codes," *IEEE Trans. Inform. Theory*, vol. IT-30, no. 6, pp. 784-791, Nov. 1984.

[14] A. R. Calderbank and N. J. A. Sloane, "Four-dimensional modulation with an eight-state trellis codes," *AT&T Tech. J.*, vol. 64, pp. 1005-1018, 1985.

[15] A. R. Calderbank and N. J. A. Sloane, "An eight-dimensional trellis codes," *Proc. IEEE*, vol. 74, pp. 757-759, 1987.

[16] A. R. Calderbank, and N. J. A. Sloane, "New trellis coded based on lattices and cosets," *IEEE Trans. Inform. Theory*, vol. IT-33, no. 2, pp. 177-195, March 1987.

[17] L. Wei, "Trellis-coded modulation with multidimensional constellations," *IEEE Trans. Inform Theory*, vol. IT-33, no. 4, pp. 483-501, July 1987.

[18] G. D. Forney, Jr., "Coset codes - Part I: Introduction and geometrical classification," *IEEE Trans. Inform. Theory*, vol. 34, no. 5, pp. 1123-1151, Sept. 1988.

[19] G. D. Forney, Jr., "Coset codes - Part II: Binary lattices and related codes," *IEEE Trans. Inform. Theory*, vol. 34, no. 5, pp. 1152-1187, Sept. 1988.

[20] G. D. Forney, Jr. and L.-F. Wei, "Multidimensional constellation - Part I: Introduction, figures of merit, and generalized cross constellations," *IEEE J. Select. Areas Commun.*, vol. 7, no. 6, pp. 877-892, Aug. 1989.

[21] G. D. Forney, Jr., "Multidimensional constellation - Part II: Voroni constellations," *IEEE J. Select. Areas Commun.*, vol. 7, no. 6, pp. 941-958, Aug. 1989.

[22] D. Divsalar and M. K. Simon, "Multiple trellis coded modulation (MTCM)," *IEEE Trans. on Commun.*, vol. 36, no. 4, pp. 410-419, April 1988.

[23] D. Divsalar and M. K. Simon, "Multiple trellis coded modulation (MTCM)," *IEEE Global Telecommun. Conf. Rec.*, Houston, TX, pp. 30.8.1-30.8.7, Dec. 1986.

[24] D. Divsalar and M. K. Simon, "Multiple trellis coded modulation (MTCM)," *IEEE Global Telecommun. Conf. Rec.*, Tokyo, Japan, pp. 43.8.1-43.8.6, Nov. 1987.

[25] D. Divsalar and J. H. Yuen, "Asymmetric MPSK for trellis codes," *IEEE Global Telecommun. Conf. Rec.*, Atlanta, GA, pp. 20.6.1-20.6.8, Nov. 1984.

[26] D. Divsalar, M. K. Simon, and J. H. Yuen, "Trellis coding with asymmetric modulations," *IEEE Trans. on Commun.*, vol. COM-35, no. 2, pp. 130-141, Feb. 1987.

[27] L. Wei, "Rotationally invariant convolutional channel coding with expanded signal space--Part I:180," *IEEE J. Select. Areas Commun.*, vol. SAC-2, no. 5, pp. 659-671, Sept. 1984.

[28] L. Wei, "Rotationally invariant convolutional channel coding with expanded signal space--Part II: Nonlinear codes," *IEEE J. Select. Areas Commun.*, vol. SAC-2, no. 5, pp. 672-686, Sept. 1984.

[29] CCITT Study Group XVII, " Recommendation V.32 for a Family of 2-Wire, Duplex Modems Operating at Data Signaling Rates of up to 9600 bit/s for Use on the General Switched Telephone Network and on Leased Telephone-Type Circuits," Document AP VIII-43-E, May 1984. pp. 724-744, July 1978.

[30] S. Bendetto, M. Ajmon Marsan, G. Albertengo, and E. Giachin, "Combined coding and modulation: Theory and applications," *IEEE Trans. Inform. Theory*, vol. 34, no. 2, pp. 223-236, March 1988.

[31] M. K. Simon and D. Divsalar, "The performance of trellis coded modulation DPSK on a fading mobile satellite channel," *ICC'87 Conf. Rec.*, Seattle, WA, pp. 21.2.1-21.2.7, June 1987.

[32] D. Divsalar, and M. K. Simon, "Trellis coded modulation for 4800-9600 bits/s transmission over a fading mobile satellite channel," *IEEE J. Select. Areas Com-*

mun., vol. SAC-5, no. 2, pp. 162-175, Feb. 1987.

[33] M. K. Simon and D. Divsalar, " The performance of trellis coded multilevel DPSK on a fading mobile satellite channel," *IEEE Trans. on Vehic. Technol.*, vol. 37, no. 2, pp. 78-91, May 1988.

[34] D. Divsalar and M. K. Simon,"The design of trellis coded MPSK for fading channels : performance criteria," *IEEE Trans. on Commun.*, vol. 36, no. 9, pp. 1004-1012, Sept. 1988.

[35] D. Divsalar and M. K. Simon, "The design of trellis coded MPSK for fading channels : set partitioning for optimum code design," *IEEE Trans. on Commun.*, vol. 36, no. 9, pp. 1013-1021, Sept. 1988.

[36] D. Divsalar and M. K. Simon, "Performance of trellis coded MDPSK on fast fading channels," *ICC'89 Conf. Rec.*, pp. 9.1.1-9.1.7, 1989.

[37] S. G. Wilson and Y. S. Leung, "Trellis-coded phase modulation on Rayleigh channels," *ICC'87 Conf. Rec.*, Seattle, W. A., pp. 21.3.1-21.3.5, June 1987.

[38] P. J. McLane, P. H. Wittke, P. K. -M. Ho and C. Loo, "PSK and DPSK trellis coded for fast fading, shadowed mobile satellite communication channels," *ICC'87 Conf. Rec.*, Seattle, W. A., pp. 21.1.1-21.1.6, June 1987.

[39] P. J. McLane, P. H. Wittke, P. K. -M. Ho and C. Loo, "PSK and DPSK trellis coded for fast fading, shadowed mobile satellite communication channels," *IEEE Trans. on Commun.*, vol. 36, no. 11, pp. 1242-1246, Nov. 1988.

[40] R. G. McKay, P. J. McLane and E. Biglieri, "Analytical performance bound on average bit error probability for trellis coded PSK transmitted over fading channels," *ICC'89 Conf. Rec.*, pp. 9.2.1-9.2.7, 1989.

[41] J. H. Lodge and M. L. Moher, "Time diversity for mobile satellite channels using trellis coded modulations," *IEEE Global Telecommun. Conf. Rec.*, Tokyo, Japan, pp. 8.7.1-8.7.5, Nov. 1987.

[42] J. H. Lodge and M. L. Moher, "TCMP- A modulation and coding strategy for Rician fading channels," *IEEE J. Select. Areas Commun.*, vol. SAC-7, no 9, pp. 1347-1355, Dec. 1989.

[43] Y. Wu and P. Ho, "Multiple trellis codes for mobile fading channels," *Canadian Conf. on Elec. and Comput. Eng.*, Vancouver, B. C., Canada, pp. 417-420, Nov. 1988.

[44] C. Schlegel, and D. J. Costello, Jr., "Bandwidth efficient coding for fading channels: code construction and performance analysis," *IEEE J. Select. Areas Commun.*, vol. SAC-7, no. 9, pp. 1356-1368, Dec. 1989.

[45] S. H. Jamali, T. Le-Ngoc, "A new 4-state 8PSK TCM scheme for fast fading, shadowed mobile radio channels," *IEEE Trans on Vehic. Technol.*, vol. 40, no. 1, pp. 216-222, Feb. 1991.

[46] E. L. Cusack, "Error control codes for QAM signaling," *Electron. lett.*, vol. 20, pp. 62-63, Jan. 1984.

[47] S. I. Sayegh, "A class of optimum block codes in signal space," *IEEE Trans. on Commun.*, vol. COM-34, no. 10, pp. 1043-1045, Oct. 1986.

[48] A. Gersho and V. B. Lawrence, "Multidimensional signal constellation for voiceband data transmission," *IEEE J. Select. Areas Commun.*, vol. SAC-2, no. 5, pp. 687-702, Sept. 1984.

[49] F. R. Kschischang, P. G. du Buda, and S. Pasupathy, "Block coset codes for M-ary phase shift keying," *IEEE J. Select. Areas Commun.*, vol. SAC-7, no. 9, pp. 900-913, Aug. 1989.

[50] A. Chouly and H. Sari, "A class of block-coded modulation schemes based on one-step partitioning of the signal alphabet," *ICC'89 Conf. Rec.*, Seattle, WA, pp. 18.6.1-18 6.6, 1989.

[51] M. Isaksson, and L. H. Zetterberg, "A class of block codes with redundant signal-set

for PSK-modulation," *1990 IEEE International Symposium on Inform. Theory,* San Diago 1990.

[52] CODEX CORP., "A simplified 8-space block coding method for V.AA," Contribution to CCITT SG XVII rapporteur group on V.AA, April 1983.

[53] A. J. Viterbi and J. K. Omura, *Principles of Digital Communication and Coding.* New York: McGraw-Hill, 1979.

[54] C. E. Shannon, "A mathematical theory of communication," *Bell System Tech. J.,* vol. 27, (pt. I), pp. 379-423 (pt. II), pp. 623-656, 1948. Reprinted in book form with postscript by W. Weaver, Univ. of Illinois Press, Urbana, 1949.

[55] R. G. Gallager, *Information Theory and Reliable Communications.* New York: Wiley, 1968.

[56] G. D. Forney, Jr., "Generalized minimum distance decoding," *IEEE Trans. Inform. Theory,* vol. IT-12, no. 2, pp. 125-131, April 1966.

[57] S. Lin, and D. J. Costello, Jr., *Error Control Coding: Fundamentals and Applications,* Prentice Hall, 1982.

[58] A. J. Viterbi, "Convolutional codes and their performance in communication systems," *IEEE Trans. Commun. Technol.,* vol. COM-19, pp. 751-772, Nov. 1971.

[59] J. K. Omura, "Generalized transfer function bounds," *ICC'81 Conf. Rec.,* Denver, CO, June 1981.

[60] D. Divsalar, "Performance of mismatched receivers on bandlimited channels", Ph.D. dissertation, Univ. of California, Los Angeles, 1978.

[61] E. Biglieri and P. J. McLane, "Uniform distance and error probability properties of TCM schemes," *IEEE Trans. Commun.,* vol. COM-39, no. 1, pp. 41-53, Jan. 1991.

[62] M.K. Simon and D. Divsalar, *A New Description of Combined Trellis Coding with Asymmetric Modulation.* Pasadena, CA: JPL Publication 85-45, July 15, 1985. vol. SAC-7, pp. 1356-1368, Dec. 1989.

[63] J. M. Turgeon and P. J. McLane, "Minimal transmitter complexity design of analytically described trellis codes," *IEEE Trans. Commun.*, vol. 38, no. 9, pp. 1352-1358, Sept. 1990.

[64] E. Zehavi and J. K. Wolf, "On the performance evaluation of trellis codes," *IEEE Trans. Inform. Theory*, vol. IT-33, no. 2, pp. 196-202, March 1987.

[65] L. Zhang, and B. Vucetic, "Block coded modulation on AWGN and fading channels," Presented in 1990 *IEEE Int. Symposium on Inform. Theory*, San Diago 1990.

[66] S. H. Jamali, T. Le-Ngoc, "On the performance of bandwidth efficient RS coded MPSK signaling over a Rayleigh fading channel," *ICC'91 Conf. Rec.*, Denver, CO., pp. 34.4.1-34.4 5, June 1991.

[67] S. H. Jamali, T. Le-Ngoc, "Bandwidth efficient communication via a Rayleigh fading channel using RS coded multi-phase signaling," Submitted to *IEEE Trans. Commun.* Jan. 1991.

[68] R. E. Blahut, *Theory and Practice of Error Control Codes.* Reading, MA: Addison-Wesley, 1983.

[69] J. Hagenauer, and E. Lutz, "Forward error correction coding for fading compensation in mobile satellite channels," *IEEE J. Select. Areas Commun.* vol. SAC-5, no. 2, pp. 215-225, Feb. 1987.

[70] D. Chase, "A class of algorithms for decoding block codes with channel measurement information," *IEEE Trans. Inform. Theory*, vol. IT-18, no. 1, pp. 170-182, Jan. 1972.

[71] J. K. Wolf, "Efficient maximum likelihood decoding of linear block codes using a trellis," *IEEE Trans. Inform. Theory*, vol. IT-24, no. 1, pp. 76-80, Jan. 1978.

[72] G. D. Forney, Jr., *Concatenated Codes.* Cambridge, MA: MIT, 1966.

[73] G. Einarsson and C. E. Sundberg, "A note on soft decision decoding with successive erasures," *IEEE Trans. Inform. Theory*, vol. IT-22, pp. 88-96, Jan. 1976.

[74] C. Loo, "A statistical model for a land mobile satellite link," *IEEE Trans. Vehic. Technol.*, vol. 34, pp. 122-127, Aug 1985.

[75] C. Loo, E. E. Matt, J. S. Butterworth, and M. Dufour, "Measurements and modeling of land-mobile satellite signal statistics," *1986 Vehic. Technol. Conf*, Dallas, TX, May 20-22, 1986.

[76] S. C. Gupta, R. Viswanathan, and R. Muammar, "Land mobile radio system- a tutorial exposition," *IEEE Commun. Magazine*, vol. 23, no. 6, pp. 43-45, June 1985.

[77] I. S. Gradshteyn and I. M. Ryzhik, *Tables of Integrals, Series, and Products*. Academic Press, 1980.

[78] A. C. Lee and P. J. McLane, "Convolutional interleaved PSK and DPSK trellis codes for shadowed, fast fading mobile satellite communication channels", *IEEE Trans. Vehic. Technol.*, vol. 39, no. 1, pp. 37-47, Feb. 1990.